PLASTIC HINGE LENGTH IN HIGH-RISE CONCRETE SHEAR WALLS

by

ALFREDO GUILLERMO BOHL ARBULU

B.Sc., Universidad Peruana de Ciencias Aplicadas, Peru, 2003

A THESIS SUBMITTED IN PARTIAL FULFILLMENT OF
THE REQUIREMENTS FOR THE DEGREE OF

MASTER OF APPLIED SCIENCE

in

THE FACULTY OF GRADUATE STUDIES

(Civil Engineering)

THE UNIVERSITY OF BRITISH COLUMBIA

November 2006

ABSTRACT

The flexural displacement capacity of a concrete shear wall depends on the length of the plastic hinge. Typical building codes and several researchers recommend the use of an equivalent plastic hinge length at the base equal to half the wall length. However, the plastic hinge length is also influenced by parameters other than the wall length. There are currently no recommendations on what should be the plastic hinge length for parallel walls of different lengths in a high-rise building.

A parametric study was conducted to investigate the parameters that affect the length of the plastic hinge in concrete walls. The walls were analyzed using program VecTor2. The analytical model was validated with tests results performed on wall specimens.

The results obtained show that the inelastic curvatures vary linearly over the plastic hinge length. The shape of the strain profile in slender walls after cracking depends on the amount of reinforcement. Longer walls have larger plastic hinge lengths than shorter walls. Compressive axial loads reduce the plastic hinge length, tensile axial loads have the opposite effect. A simple shear model was proposed to estimate the increase in plastic hinge length when the shear stresses are high.

Walls of different lengths interconnected by rigid slabs at various levels have different curvature distributions and plastic hinge lengths. The curvatures in the longer wall do not change whether it is alone or combined with a wall of shorter length. The shorter length wall is subjected to larger curvatures at the base when it is combined. A simple model was proposed to predict the maximum curvature in the shorter wall.

TABLE OF CONTENTS

LIST OF TABLES

LIST OF FIGURES

LIST OF SYMBOLS

- A_g: Gross area of cross-section
- A_c: Area of concrete
- A_s: Area of reinforcement
- A_{sc}: Area of compression reinforcement
- A_{st}: Area of tension reinforcement
- a: Maximum aggregate size
- a_{sl}: Zero-one variable in Equation 2.46 and 2.47
- b: Width of member
- b_w: Web thickness of wall
- C: Cohesion
- C_d: Compression softening strain softening factor, defined in Equation 3.10
- C_s: Compression softening shear slip factor in Equation 3.9
- c: Neutral axis depth at ultimate moment
- c_a: Averaging factor, defined in Equation 3.5
- c_b: Coefficient used to reflect bar spacing in Equation 3.43
- c_t: Coefficient that incorporates the influence of reinforcement bond characteristics, defined in Equation 3.19
- d: Effective depth of member
- d_b: Bar diameter of the tension reinforcement
- d_v: Lever arm of tensile force in the longitudinal reinforcement
- E_c: Concrete initial tangent stiffness
- E_s: Initial tangent stiffness or elastic modulus of reinforcement
- E_{sec}: Concrete secant stiffness
- E_{sh}: Strain hardening modulus
- F: Lateral force
- f'_c: Concrete cylinder uniaxial compressive strength
- f_{c1}: Average net concrete axial stress in the principal tensile direction
- f_{c1}^a: Average concrete tensile stress due to tension stiffening
- f_{c1}^b: Average concrete tensile stress due to tension softening
- f_{c2}: Average net concrete axial stress in the principal compressive direction
- f_{c2}^a: Average concrete compressive stress contribution of unconfined concrete
- f_{c2}^b: Average concrete compressive stress contribution of confined concrete
- f_{cc}: Concrete cube strength

- f_{cr}: Concrete cracking stress
- f_{cru}: Defined in Equation 3.24
- f_p: Peak concrete compressive stress
- f_s: Reinforcement stress
- f_t: Tensile strength of steel
- f'_t: Concrete uniaxial tensile strength
- f_u: Ultimate strength of reinforcement
- f_y: Yield stress of the tension reinforcement
- f'_y: Yield stress of the compression reinforcement
- G_f: Energy required to form a complete crack of unit area
- H_w: Total height of wall
- h: Depth or height of the cross-section of member
- I_z: Moment of inertia of the reinforcement
- k_1: Factor that considers the influence of the tension reinforcement in Equation 2.12, 2.17 and 2.19
- k_2: Factor that considers the influence of the axial load, defined in Equation 2.13
- k_3: Factor that considers the influence of the concrete strength, defined in Equation 2.14
- k_c: Stiffness of the notional concrete foundation, defined in Equation 3.43
- L: Length of member in the longitudinal direction
- L_p: Plastic hinge length
- $L_{p,i}$: Plastic hinge length in element "i"
- $L_{p,const}$: Plastic hinge length for a constant inelastic curvature
- $L_{p,cy}$: Plastic hinge length for cyclic loading
- $L_{p,lin}$: Plastic hinge length for a linearly varying inelastic curvature
- $L_{p,meas}$: Measured plastic hinge length
- $L_{p,mon}$: Plastic hinge length for monotonic loading
- $L_{p,pred}$: Predicted plastic hinge length
- L_r: Distance over which the crack is assumed to be uniformly distributed
- L_s: Distance from the section of maximum moment to the section of zero moment or shear span
- l_s: Standard length in Equation 2.39 and 2.41
- l_w: Horizontal length of wall section
- M: Total bending moment
- M_f: Moment due to flexure
- M_{max}: Maximum moment in the length of member
- M_u: Ultimate moment
- M_v: Moment due to shear

- M_y: Yield moment
- m: Bond parameter, defined in Equation 3.20
- N_v: Axial compression due to shear
- n: Curve fitting parameter for stress-strain response of concrete in compression, defined in Equation 3.2
- P: Axial load
- P_u: Axial compressive strength of member without any bending moment
- PER: Percentage ratio of volume of stirrups to volume of concrete core measured outside of stirrups
- R_m: Moment ratio, defined in Equation 2.32
- R_ε: Strain ratio, defined in Equation 2.31
- RFT: Defined in Equation 2.43
- r: Ratio of the principal tensile strain to the principal compressive strain
- SPR: Defined in Equation 2.44
- s: Crack spacing
- V: Shear force
- V_c: Shear force in concrete
- V_d: Dowel force
- V_{du}: Ultimate dowel force
- V_s: Shear force in longitudinal reinforcement
- V_z: Shear adjacent to a concentrated load or reaction at the section of maximum moment
- v: Shear stress
- v_{ci}: Local shear stress on the crack
- $v_{ci,max}$: Maximum local shear stress on the crack
- v_{co}: Defined in Equation 3.32
- v_{cr}: Cracking shear stress
- v_d: Shear resistance due to dowel action
- w: Average crack width
- w_z: Uniformly distributed load at the section of maximum moment
- Z_m: Slope of compression post-peak descending curve, defined in Equation 3.8
- α: Calibration parameter in Equation 2.10
- α_1: Model parameter in Equation 2.39, 2.40 and 2.41
- α_2: Model parameter in Equation 2.39, 2.40 and 2.41
- β: Calibration parameter in Equation 2.10
- β_d: Softening parameter, defined in Equation 3.9

- β_l: Strength enhancement factor, defined in Equation 3.14
- Δ: Total displacement
- Δ_f: Flexural displacement
- Δ_p: Plastic or inelastic deformation
- Δ_s: Slip displacement
- Δ_u: Ultimate displacement
- Δ_v: Shear displacement
- Δ_y: Yield displacement
- $\Delta\theta_\sigma$: Post-cracking rotation of the principal stress field
- $\Delta\theta_\varepsilon$: Post-cracking rotation of the principal strain field
- δ_s: Shear slip
- δ_s^* : Defined in Equation 3.29
- ε_{c1}: Average net concrete axial strain in the principal tensile direction
- ε_{c2}: Average net concrete axial strain in the principal compressive direction
- ε_{ce}: Concrete strain in the extreme compression fiber at yield curvature
- ε_{ch}: Characteristic strain
- ε_{cr}: Concrete cracking strain
- ε_{cu}: Concrete strain in the extreme compression fiber at ultimate curvature
- ε_o: Concrete compressive strain corresponding to f'_c
- ε_p: Concrete compressive strain corresponding to f_p
- ε_s: Reinforcement strain
- ε_{sh}: Strain at the onset of strain hardening
- ε_u: Reinforcement ultimate strain
- ε_{xx}: Total axial strain in the x-direction
- ε_y: Yield strain
- ε_{yy}: Total axial strain in the y-direction
- Φ: Internal angle of friction
- ϕ: Total curvature
- ϕ_{max}: Maximum curvature
- $\phi_{max,i}$: Maximum curvature in element "i"
- ϕ_p: Plastic or inelastic curvature
- ϕ_u: Ultimate curvature
- ϕ_y: Yield curvature

- $\phi_{y,i}$: Yield curvature in element "i"
- γ_s: Shear slip strain
- γ_s^a: Shear slip strain determined from the stress-based model
- γ_s^b: Shear slip strain determined from the constant rotation lag model
- γ_{xy}: Total shear strain
- λ: Parameter that compares the stiffness of the concrete to the stiffness of the reinforcing bar, defined in Equation 3.42
- θ: Total rotation or slope
- θ_c: Angle of the crack
- θ_i: Total rotation or slope in element "i"
- θ_{ic}: Inclination of the principal stress field at cracking
- θ^l: Rotation lag
- θ_n: Angle between the normal to the crack surface and the longitudinal axis of the reinforcement
- θ_p: Plastic or inelastic rotation or slope
- $\theta_{p,d/2}$: Plastic or inelastic rotation or slope in the length $d/2$
- θ_u: Ultimate rotation or slope
- θ_σ: Inclination of the principal stress field
- ρ: Tension reinforcement ratio
- ρ': Compression reinforcement ratio
- ρ_b: Reinforcement ratio at balanced ultimate strength condition in a member without compression reinforcement
- ρ_s: Reinforcement ratio
- ω: Tension reinforcement index, defined in Equation 2.15
- ω': Compression reinforcement index, defined in Equation 2.16
- ω_b: Tension reinforcement index for balanced ultimate strength condition, defined in Equation 2.24
- ξ: Calibration parameter in Equation 2.10
- ξ_L: Model error term in Equation 2.39, 2.40 and 2.41
- ψ: Defined in Equation 3.30

ACKNOWLEDGEMENTS

I would like to thank my supervisor, Dr. Perry Adebar, for his support and guidance throughout this research.

I also want to thank the Faculty of Graduate Studies, which granted me with a University of BC Graduate Fellowship.

To my parents, Alfredo and Berta

CHAPTER 1: INTRODUCTION

1.1 Research significance

The use of concrete shear walls to provide lateral strength and stiffness in high-rise buildings has become common practice. These walls require enough shear strength capacity and flexural displacement capacity to have an adequate seismic behaviour. The flexural displacement capacity depends on the compression strain capacity of concrete, the neutral axis depth and the length of the plastic hinge.

The inelastic curvatures at the base of the wall are commonly assumed to be constant over a length known as the equivalent plastic hinge length. Different studies done in the past on concrete members have shown that the equivalent plastic hinge length is proportional to the member dimension (e.g.: beam depth, wall length). Building code requirements in ACI 318 2005 and CSA A23.3 2004 for determining confinement requirements at the ends of a concrete wall assume the plastic hinge length is equal to half of the wall length.

Several empirical models have been developed to estimate the length of the plastic hinge in reinforced concrete members based on test results. A large number of these models were calibrated so that they will give the real total displacement or real total rotation at failure. These models consider different parameters and provide significantly different predictions. Most of the research done in the past has focused on the influence of the member dimension, the span of the member and the longitudinal reinforcement properties. The effect of the axial load ratio and the strain hardening has also been studied. It is still not clear which are the most relevant parameters that influence the length of the plastic hinge.

Many of these models consider that the plastic hinge length is proportional to the member dimension only. This is due to the fact that the member dimension is commonly associated with the effect of diagonal cracking, which causes the length of the plastic hinge to increase. If the angle of the crack is considered to be 45°, it will extend to a distance from the support equal to the member dimension. Therefore, longer members have larger plastic hinge lengths. One of the objectives of this thesis will be to investigate in more depth how the member dimension and the plastic hinge length are related.

The increase in the plastic hinge length due to the influence of diagonal cracking is difficult to quantify. A simple shear model will be developed to try to estimate the plastic hinge length when the shear stresses are high.

Previous investigations on plastic hinge length in concrete walls have been done for individual members. To the knowledge of the author, there are no previous studies done on concrete wall systems. It is not known how the interaction of the walls that are part of the same system will affect the length of the plastic hinge of these members.

A system of coupled walls is connected together by very stiff beams (coupling beams). When a system of coupled walls with a high degree of coupling is subjected to lateral loading, the shear forces in the coupling beams induce high axial forces in the walls. Some walls are subjected to high axial tension, and others are subjected to high axial compression. The axial loads in the walls are expected to have a significant effect on the plastic hinge length. Walls subjected to compressive and tensile axial forces will be analyzed to study this effect.

Figure 1.1 System of coupled walls subjected to lateral loading

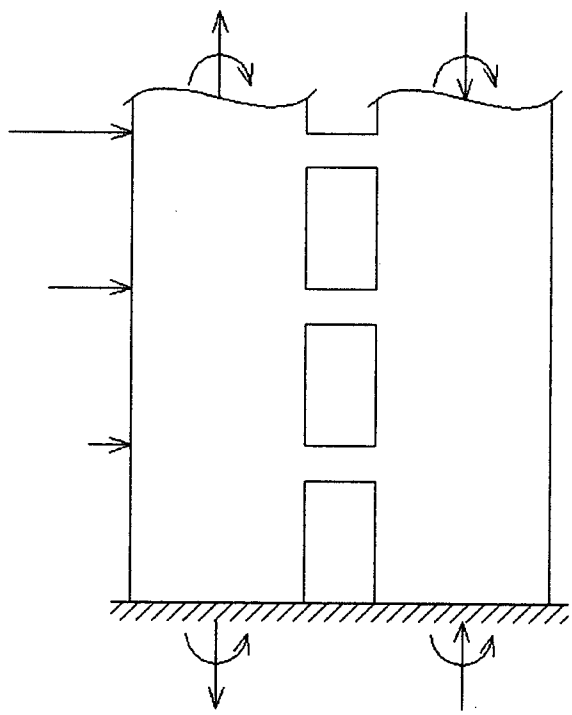

In high-rise buildings, it is common to have systems of walls of different lengths providing lateral resistance in the same direction of lateral loading. These walls are interconnected by rigid slabs at numerous floor levels. As a result, when this system is subjected to lateral loads, the displacement of all these walls is the same at the floor levels.

Figure 1.2 System of walls of different lengths interconnected by rigid slabs

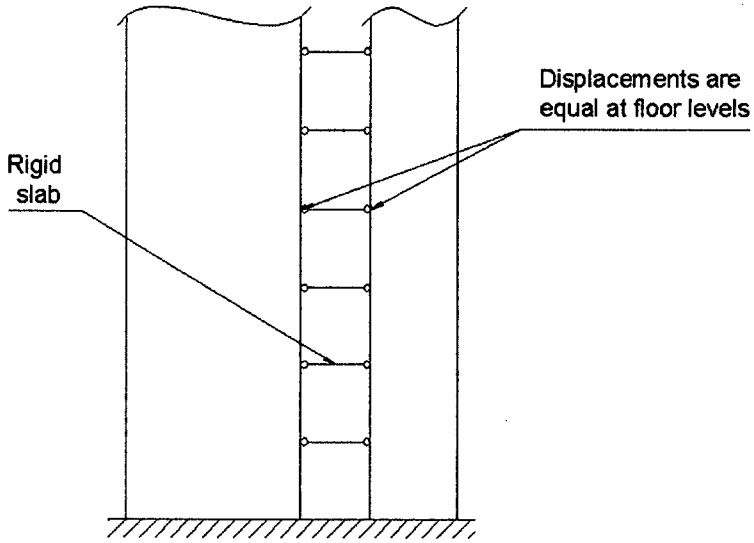

Along with the walls, the gravity columns that do not form part of the lateral force resisting system will also have the same displacement at the floor levels. This tends to increase curvature demand in these elements. The columns must be able to sustain that demand.

An important objective of this thesis will be to analyze walls of different lengths connected together by rigid slabs to study the impact of the connection in the plastic hinge length. The effect on gravity columns will also be studied.

1.2 Objective of the thesis

The main objective of this thesis is to investigate the parameters that affect the length of the plastic hinge in concrete walls, using static nonlinear finite element analysis. The parameters considered in this study were the wall length, the distance from the section of maximum moment to the section of zero moment, diagonal cracking due to shear, and the axial load. This parametric study was first performed for individual walls. Then, walls of different lengths interconnected by rigid slabs at numerous levels were analyzed to investigate how this affects the length of the plastic hinge.

The analysis was performed using program VecTor2. VecTor2 is a computer program developed at the University of Toronto to perform nonlinear finite element analysis of reinforced concrete membrane structures, using the constitutive relationships of the Disturbed Stress Field Model. The program uses low-powered elements to model concrete structures. It considers a variety of effects to accurately predict the response, such as compression softening, tension stiffening, slip distortions and strain hardening.

Prior to the parametric study, analytical predictions made by program VecTor2 were verified with experimental results obtained from previous tests performed on cantilever walls to see how well the program predicts the response of these members. In particular, the curvature distributions along the height and the strain profiles along the wall section were examined and compared.

1.3 Organization of the thesis

The thesis is divided in seven chapters. Chapter 1 is the introduction. It presents the objective of the thesis.

Chapter 2 is the literature review. It first introduces the concept of plastic hinge length and the formulation of classical plastic hinge analysis. The results from 23 previous investigations on plastic hinge length and the models that were developed are presented. A summary of all these investigations, including the type of members studied and the parameters considered, is presented at the end of the chapter.

Chapter 3 presents the analytical methods. It describes the theoretical bases of program VecTor2, as well as its finite element formulation and the description of the material models for concrete and steel. Only the material models used in this thesis are presented. Finally, a brief description of the pre-processor and post-processor for program VecTor2 is presented.

Chapter 4 shows a comparison of analytical predictions from program VecTor2 with isolated wall test results. Two wall specimens were used for the comparison. The first is a high-rise shear wall tested at the University of British Columbia in 2000; the curvature distributions along the height were compared. The second is a rectangular shear wall tested at Clarkson University in 1995; the strain profiles along the wall section were compared.

Chapter 5 presents a parametric study of concrete walls. The factors that affect the length of the plastic hinge were investigated. This study was performed for two individual walls.

Chapter 6 presents the analysis of three systems of walls of different lengths interconnected by rigid slabs at numerous levels. The influence of the connection in the curvature distribution and the plastic hinge length of the walls were studied.

Chapter 7 presents the conclusions of the thesis.

CHAPTER 2: LITERATURE REVIEW

2.1 Concept of plastic hinge length

Consider a slender reinforced concrete cantilever element subjected to a lateral load at the top, like the one in Figure 2.1. The total lateral displacement at the top, Δ, is comprised of three components: the flexural displacement, Δ_f, the shear displacement, Δ_v, and the slip displacement, Δ_s:

Figure 2.1 Displacement components of a reinforced concrete cantilever element

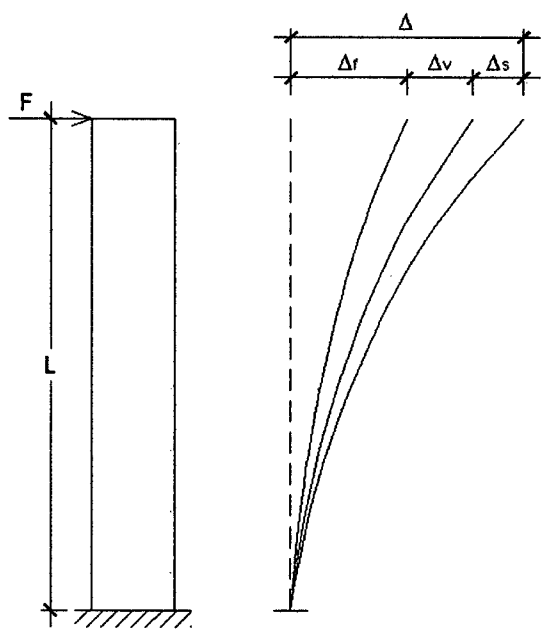

Therefore:

$$\Delta = \Delta_f + \Delta_v + \Delta_s \tag{2.1}$$

The shear and slip displacements are commonly not very important for high-rise buildings. In the classical formulation of plastic hinge analysis, it is considered that the total displacement of a reinforced concrete element after yielding has two components: the yield displacement, Δ_y, and the plastic deformation, Δ_p:

Figure 2.2 Displacement components beyond the yield displacement

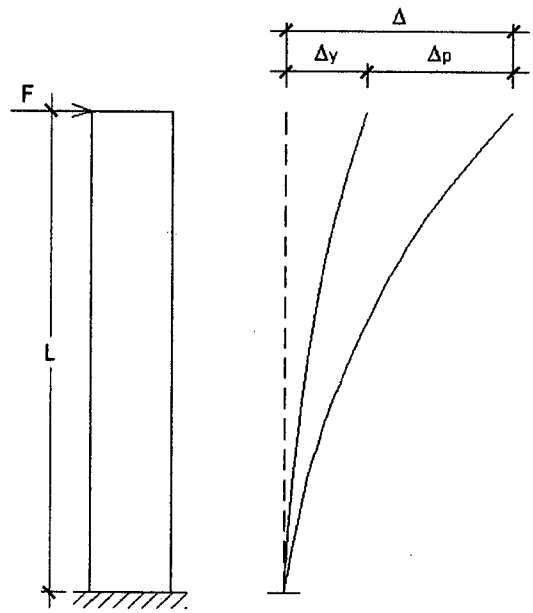

Therefore:

$$\Delta = \Delta_y + \Delta_p \tag{2.2}$$

In practice, it is commonly assumed that the inelastic curvature in the plasticized region, although it has a certain variation, is constant over a length known as the plastic hinge length, L_p. This is shown in the Figure 2.3:

Figure 2.3 Formulation of classical plastic hinge analysis

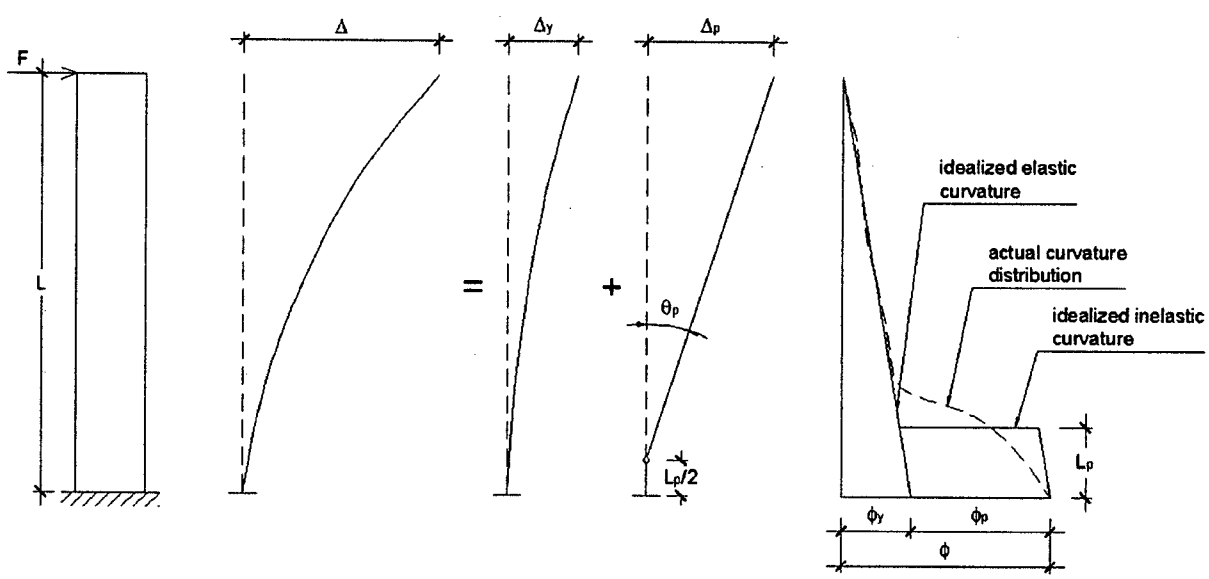

From Figure 2.3, the inelastic curvature, ϕ_p, is calculated from the total curvature, ϕ, by:

$$\phi_p = \phi - \phi_y \tag{2.3}$$

Where ϕ_y is the yield curvature. The inelastic rotation, θ_p, can be determined by integrating the inelastic curvatures:

$$\theta_p = \phi_p L_p \tag{2.4}$$

Considering that the inelastic rotation is concentrated at the centroid of the inelastic curvatures, the inelastic displacement can be expressed as:

$$\Delta_p = \theta_p \left(L - \frac{L_p}{2} \right) = (\phi - \phi_y) L_p \left(L - \frac{L_p}{2} \right) \tag{2.5}$$

Combining Equation 2.2 and 2.5, the total displacement is:

$$\Delta = \Delta_y + (\phi - \phi_y) L_p \left(L - \frac{L_p}{2} \right) \tag{2.6}$$

The yield displacement can be determined by integrating the elastic curvatures, considering a linear variation as shown in Figure 2.3:

$$\Delta_y = \frac{\phi_y L^2}{3} \tag{2.7}$$

Then, the total displacement is:

$$\Delta = \frac{\phi_y L^2}{3} + (\phi - \phi_y) L_p \left(L - \frac{L_p}{2} \right) \tag{2.8}$$

This is the classical formulation of plastic hinge analysis, and it has been used over the years by many researchers to develop models for plastic hinge length. According to this formulation, the plastic hinge length is defined as the equivalent length over which the inelastic curvature is considered to be

constant. In reality, the inelastic curvature has a certain variation. Paulay and Priestly presented the actual curvature distribution of a prismatic reinforced concrete cantilever element, showing that the real spread of plasticity is longer that the equivalent plastic hinge length (Paulay and Priestly 1992: 139).

Classical plastic hinge analysis is based on the assumption of an elasto-plastic behaviour and an equivalent plastic hinge length. The yield curvature used in Equation 2.8 can be determined considering that the moment-curvature relationship in the plastic hinge zone is elasto-plastic (Priestly and Park 1987: 71). This approximation depends on the actual shape of the moment-curvature relationship, which depends on the type of element. Figure 2.4 shows the difference between the equivalent yield curvature for a column and for a shear wall (Adebar and Ibrahim 2002: 408):

Figure 2.4 Bending moment-curvature relationship of different reinforced concrete elements

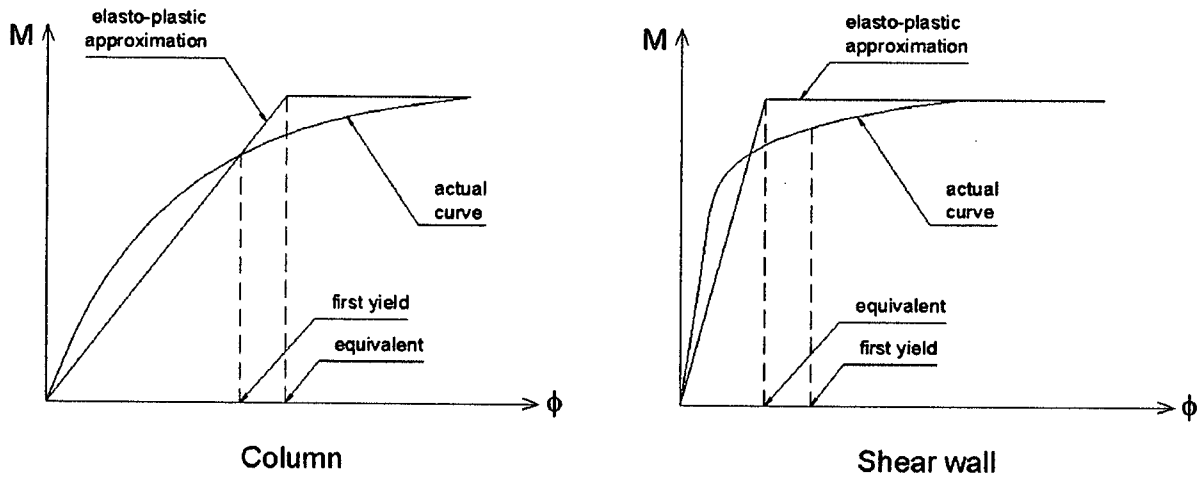

The total displacement at the top can also be determined by calculating the curvature distribution along the length of the member, as shown in Figure 2.5 (Priestly and Park 1987: 71):

Figure 2.5 Curvature distribution along the length of a reinforced concrete cantilever element

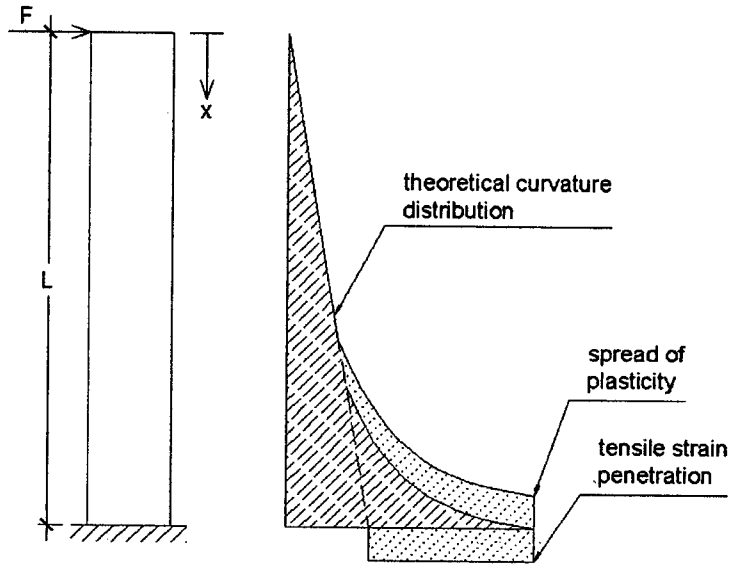

Then:

$$\Delta = \int_0^L \phi(x) x dx \tag{2.9}$$

Equation 2.9 can be used to calculate the total displacement, considering a theoretical curvature distribution like the one in Figure 2.5. However, the actual displacement will be larger than the one calculated with this expression. This is due to the effect of tensile strain penetration and the spread of plasticity due to shear. Tensile strain penetration is the additional rotation in the plastic hinge zone due to the slippage of the longitudinal reinforcement. The extent of the tensile strain penetration depends on the development length of the bar (Paulay and Priestly 1992: 141). The spread of plasticity is caused by the presence of diagonal cracks due to high shear stresses, which produces higher steel strains than the ones due to pure flexure. For a crack angle of 45°, the influence of diagonal cracking is proportional to the depth of the member (Priestly and Park 1987: 71 – 72).

The influence of tensile strain penetration and spread of plasticity can be taken into account in Equation 2.9 by considering a modified curvature distribution, shown in Figure 2.5. However, the most common approach in practice is to use plastic hinge analysis, in which the influence of tensile strain penetration and spread of plasticity is considered implicitly in Equation 2.8 in the parameter L_p, in order to obtain a good estimate of the real displacement (Priestly and Park 1987: 72). Therefore, many of the models developed to determine the equivalent plastic hinge length in reinforced concrete elements were established on the basis that the plastic hinge length is proportional to the length of the member in the

longitudinal direction, the depth of the member, and the longitudinal reinforcement properties; as it is presented in the following expression (Berry and Eberhard 2003: 13):

$$L_p = \alpha L + \beta h + \xi f_y d_b \tag{2.10}$$

- L: Length of the member in the longitudinal direction.
- h: Depth or height of the cross-section of the member.
- f_y: Yield stress of the tension reinforcement.
- d_b: Bar diameter of the tension reinforcement.

In a more general sense, L in Equation 2.10 refers to the distance from the critical section to the point of contraflexure (point of zero moment). For the cantilever element shown in Figure 2.5, this distance is equal to the length of the member. When this is not the case, a different terminology will be used. Also, when referring to walls, the length in the longitudinal dimension (L) will be referred to as the height of the wall (H_w), and the depth of the cross-section (h) will be referred to as the wall length (l_w).

In Equation 2.10, the member length takes into account the curvature distribution along its length, the member depth considers the spread of plasticity, and the longitudinal reinforcement properties consider the effect of tensile strain penetration (Berry and Eberhard 2003: 13). Several researchers have used the form of Equation 2.10 or other similar to it and have calibrated them with experimental results to obtain the values for α, β and ξ.

Most of the studies done in plastic hinge length in reinforced concrete elements have been focused in the parameters presented in Equation 2.10. However, some researchers have also investigated the stress-strain properties of steel and the effect of axial compression, which have a significant influence in the length of the plastic hinge. In the case of walls, when subjected to some axial compression, the length over which the longitudinal reinforcement yields is reduced, and so does the plastic hinge length (Paulay and Uzumeri 1975: 596 – 597).

In this chapter, the models developed by various researchers to determine the plastic hinge length for various kinds of concrete elements will be presented.

2.2 Chan (1955)

Chan performed tests on concrete columns to compare the assumption of plastic hinges concentrated at points with the real spread of plasticity. He also investigated the effect of lateral

confinement in the strain capacity of concrete. He reported the results obtained for 23 columns (Chan 1955: 121 – 132).

Consider the linear bending moment diagram for a reinforced concrete cantilever element subjected to a lateral load at a certain distance from the base, like the one in Figure 2.6:

Figure 2.6 Bending moment diagram for a reinforced concrete cantilever element

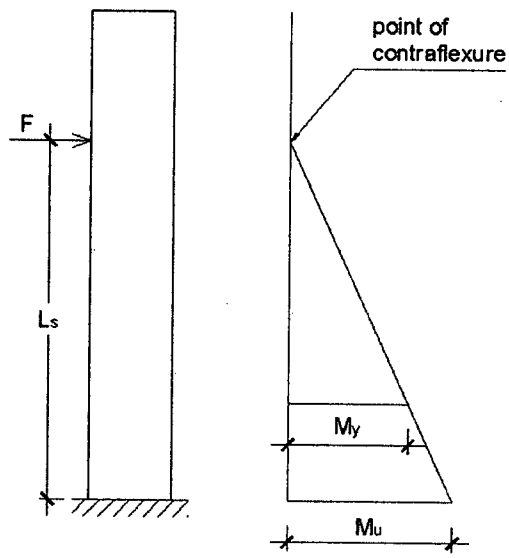

Chan considered the effect of strain hardening to define the length of the plastic hinge. For a linear bending moment diagram like the one shown in Figure 2.6, the length where the yield moment is exceeded is determined by (Chan 1955: 121 – 122):

$$\frac{L_p}{L_s} = 1 - \frac{M_y}{M_u} \tag{2.11}$$

- L_s: Distance from the section of maximum moment to the section of zero moment.
- M_y: Yield moment.
- M_u: Ultimate moment.

Three types of specimens where tested: nine members with bent-in transverse reinforcement, seven members with spiral transverse reinforcement, and seven members with welded transverse reinforcement. The most important variables covered the following range (Chan 1955: 124):

- Depth: 6".

- Width: 3 5/8 and 6".
- Span length: 11 1/2, 12 and 52".
- Diameter of tension reinforcement: 1/2 and 5/8" bars.
- Diameter of compression reinforcement: 1/2 and 5/8" bars.
- Diameter of transverse reinforcement: 1/8, 3/16 and 1/4" bars.
- Eccentricity of axial load: 1/4 and 1/2".
- Concrete cube strength: Between 2.65 and 5.46 ksi.

Each specimen was pin-ended and was loaded until failure. The axial load in the members with bent-in and spiral transverse reinforcement was held constant. The members with welded transverse reinforcement were subjected additionally to a transverse load at the midspan (Chan 1955: 125).

The test results were used to develop stress-strain relationships for unconfined and confined concrete. Then, using these stress-strain curves, an elasto-plastic stress-strain curve for steel, a yield strain of 0.001, and an ultimate strain of 0.0035 for unconfined concrete; the yield moment and ultimate moment were calculated for each of the specimens tested. These values were then used in Equation 2.11 to determine the length of the plastic hinge. For members with low axial loads, the plastic hinge length did not vary significantly with the tension reinforcement ratio, and had a mean value of $0.4L_s$. The plastic hinge length was greater for members with high axial loads, due to concrete spalling. The maximum value was approximately $0.7L_s$ (Chan 1955: 129).

2.3 Baker (1956)

Baker investigated the plastic deformations of hinges and members in concrete frames. He indicated that a safe estimate of the length of the plastic hinge in columns is between $0.5h$ and h (Baker 1956: 27).

2.4 Cohn and Petcu (1963)

Cohn and Petcu performed tests on continuous concrete beams with two spans to investigate the factors that affect the rotational capacity of plastic hinges. The most important factor studied was the percentage of steel. They reported the results obtained for 10 beams (Cohn and Petcu 1963: 282 – 290).

Two series of five concrete beams each were tested. The most important variables covered the following range (Cohn and Petcu 1963: 282 – 284):

- Depth: 8cm.
- Width: 15cm.
- Span length: 1.5m.
- Diameter of longitudinal reinforcement: 6, 8 and 10mm.
- Diameter of stirrups: 6mm.
- Average yield stress of reinforcement: Between 2550 and 3500 kg/cm^2.
- Average tensile strength of reinforcement: Between 3920 and 4900 kg/cm^2.
- Average concrete cube strength: 240 kg/cm^2.

Each beam was loaded with a concentrated load at a certain distance from the central support until failure. This distance was 40cm for one of the series, and 60cm for the other series (Cohn and Petcu 1963: 284).

The test results were used to determine the bending moments at yielding and failure. These were calculated from the measured reactions in the beams using equilibrium equations, considering a linear variation of the bending moment diagram. Then, Equation 2.11 was used to determine the length of the plastic hinge at one side from the central support of the beams (Cohn and Petcu 1963: 284 – 285). The results obtained varied from 30 to 90% of the effective depth of the beam (Cohn and Petcu 1963: 290).

2.5 Baker and Amarakone (1964)

Baker and Amarakone reported tests results on beams and columns that were performed to investigate how the following parameters influenced the moment-curvature relationship of these members: the strength of concrete and steel, percentage of steel, single loads and double loads, axial force, shear force, transverse reinforcement, and percentage of compression reinforcement. They reported the results obtained for 92 specimens (Baker and Amarakone 1964: 85 – 142).

Baker and Amarakone proposed the following expression to determine the plastic hinge length for members with unconfined concrete (Baker and Amarakone 1964: 94):

$$L_p = k_1 k_2 k_3 \left(\frac{L_s}{d}\right)^{1/4} d \tag{2.12}$$

$$k_2 = 1 + 0.5\frac{P}{P_u} \tag{2.13}$$

$$k_3 = 0.9 - \frac{f_{cc} - 13.8}{92} \tag{2.14}$$

- k_1: Factor that considers the influence of the tension reinforcement. It is equal to 0.7 for mild steel or 0.9 for cold-worked steel.
- k_2: Factor that considers the influence of the axial load.
- k_3: Factor that considers the influence of the concrete strength. It is equal to 0.6 for a concrete cube strength of 6 ksi (41.4 MPa) or 0.9 for a concrete cube strength of 2 ksi (13.8 MPa). Linear interpolation may be used between these values, arriving to Equation 2.14.
- d: Effective depth of the member.
- P: Axial load.
- P_u: Axial compressive strength of the member without any bending moment.
- f_{cc}: Concrete cube strength, in MPa units.

They indicated that for values of L/d and L_s/d commonly used in practice, the plastic hinge length is between $0.4d$ and $2.4d$.

Three types of specimens where tested: 32 members with cold-worked steel, 30 members with mild steel, and 32 members subjected to bending and axial load (with both cold-worked and mild steel). The most important variables covered the following range (Baker and Amarakone 1964: 88 – 93):

- Width: 6, 10 and 12".
- Depth: 8 and 11".
- Concrete cylinder strength: Between 2.5 and 6.5 ksi.
- Yield stress of reinforcement: Between 37 and 85 ksi.
- Tension reinforcement index: Between 2.5 and 70.4%.
- Compression reinforcement index: Between 0.96 and 26.3%.
- Transverse reinforcement ratio: Between 0.05 and 1.26%.
- Axial load ratio (in this case, $P/f'_c bd$): Between 0.164 and 1.2.
- Span length: 55, 80, 110 and 117".

The tension and compression reinforcement index, ω and ω', respectively, are given by:

$$\omega = \rho \frac{f_y}{f_c'} \tag{2.15}$$

$$\omega' = \rho' \frac{f_y'}{f_c'} \tag{2.16}$$

- ρ: Tension reinforcement ratio.
- f'_c: Concrete cylinder uniaxial compressive strength.
- ρ': Compression reinforcement ratio.
- f'_y: Yield stress of the compression reinforcement.

The test results were used to compare measured and predicted inelastic rotations. Since concrete behaves differently when it is confined by transverse reinforcement, the authors developed an expression to estimate the inelastic rotation for this case (Baker and Amarakone 1964: 97):

$$\theta_p = 0.8(\varepsilon_{cu} - \varepsilon_{ce})k_1 k_3 \left(\frac{L_s}{d}\right) \tag{2.17}$$

- ε_{cu}: Concrete strain in the extreme compression fiber at ultimate curvature.
- ε_{ce}: Concrete strain in the extreme compression fiber at yield curvature.

Considering that the neutral axis depth at yielding and failure are equal, Equation 2.4 can be expressed as (Baker and Amarakone 1964: 91):

$$\theta_p = \frac{\varepsilon_{cu} - \varepsilon_{ce}}{c} L_p \tag{2.18}$$

Where c is the neutral axis depth at ultimate moment. Therefore, combining Equation 2.17 and 2.18, the plastic hinge length for confined members is:

$$L_p = 0.8 k_1 k_3 \left(\frac{L_s}{d}\right) c \tag{2.19}$$

Although the parameter k_2 is not included in Equation 2.19, the influence of the axial load is considered implicitly in the ratio c/d.

The test results showed that members with cold-worked steel had longer plastic hinge lengths. The ratio L_s/d did not have a significant effect on the plastic hinge lengths (Baker and Amarakone 1964: 116). A considerable scatter was observed for the inelastic rotation, because of the variation of the concrete strain at ultimate curvature. Baker and Amarakone indicated that the neutral axis depth has an important influence in the ultimate strain of confined concrete. Therefore, they plotted the experimental

plastic hinge lengths as a function of the ratio c/d, and found that there is a linear relation between these two parameters (Baker and Amarakone 1964: 95 – 97).

2.6 Sawyer (1964)

Sawyer developed a design methodology for reinforced concrete frames based on a bilinear moment-curvature relationship (Sawyer 1964: 405 – 431). Some of the assumptions made to develop his method were the following:

- The maximum moment at any section is equal to the ultimate moment (Sawyer 1964: 409).
- The ratio M_y/M_u is equal to 0.85. This value was adopted based on previous test results obtained for beams (Sawyer 1964: 415).
- The plasticity spreads $d/4$ past the section in which the bending moment is equal to the yield moment (Sawyer 1964: 422).

An expression to calculate the plastic hinge length can be derived from these assumptions (Mendis 2001: 190 – 191), considering a linear bending moment diagram like the one shown in Figure 2.6. Based on the second assumption, the length where the yield moment is exceeded is $0.15L_s$. The bilinear moment-curvature relationship developed by Sawyer is defined by the points (0, 0), (M_y, ϕ_y) and (M_u, ϕ_u). Based on this, the inelastic rotation at the section of maximum moment can be obtained by integrating the inelastic curvatures over the plastic region:

$$\theta_p = \frac{1}{2}(0.15L_s)(\phi_u - \phi_y) = 0.075L_s\phi_p \tag{2.20}$$

Comparing this equation with Equation 2.4, it can be seen that they are both the same. Therefore:

$$L_p = 0.075L_s \tag{2.21}$$

Including the spread of plasticity (third assumption), the plastic hinge length is given by:

$$L_p = 0.25d + 0.075L_s \tag{2.22}$$

2.7 Mattock (1964)

Mattock performed tests on simply supported beams subjected to a concentrated load at the midspan to investigate how their rotational capacity is influenced by the concrete strength, the effective depth, the distance from the section of maximum moment to the section of zero moment, and the amount and yield stress of the reinforcement. He reported the results obtained for 37 beams (Mattock 1964: 143 – 181).

The most important variables covered the following range (Mattock 1964: 145 – 149):

- Concrete cylinder strength: 4 and 6 ksi.
- Yield stress of tension reinforcement: 47 and 60 ksi.
- Yield stress of compression reinforcement: 50 and 70 ksi.
- Yield stress of stirrups: 50, 60 and 70 ksi.
- Width: 6".
- Effective depth: 10 and 20".
- Span length: 55, 110 and 220".
- Tension reinforcement ratio: Between 1 and 3%.

The test results were used to determine the spread of plasticity of the beam at each side of the midspan. Mattock indicated that a considerable spread of inelastic deformation occurred beyond a distance of half the effective depth, and that it depended on the distance from the section of maximum moment to the section of zero moment (equal to half of the beam length for these beams), the effective depth, and the amount of flexural reinforcement. He used the ratio of the total inelastic rotation in the length L_s, θ_p, to the inelastic rotation in the length $d/2$, $\theta_{p,d/2}$, as a measure of the spread of plasticity (Mattock 1964: 158 – 161).

The total inelastic rotation in each beam was obtained from the plastic deformation at the midspan. The inelastic rotation in the length $d/2$ was obtained from the other measurements made at the midspan.

Mattock plotted the values of $\theta_p/\theta_{p,d/2}$ as a function of the parameters previously indicated. Based on his results, he developed the following expression to determine the spread of plasticity, using a least squares fit:

$$\frac{\theta_p}{\theta_{p,d/2}} = 1 + \left(1.14\sqrt{\frac{L_s}{d}} - 1\right)\left[1 - \left(\frac{\omega - \omega'}{\omega_b}\right)\sqrt{\frac{d}{0.411}}\right] \tag{2.23}$$

$$\omega_b = \rho_b \frac{f_y}{f_c'} \tag{2.24}$$

- L_s: Distance from the section of maximum moment to the section of zero moment, in meters.
- d: Effective depth of the member, in meters.
- ω_b: Tension reinforcement index for balanced ultimate strength condition.
- ρ_b: Reinforcement ratio at balanced ultimate strength condition in a member without compression reinforcement.

Mattock indicated that in Equation 2.23, the ratio of the difference between the tension and compression reinforcement index to the balanced tension reinforcement index is a measure of the strain hardening. As this ratio increases, the amount of strain hardening reduces, and so does the spread of plasticity. As he indicated, this is because the length of the plastic region is proportional to the difference between the yield moment and the ultimate moment, and this difference strongly depends on the amount of strain hardening in the tension reinforcement. This behaviour was also observed in the test results.

The measured inelastic rotations for the tests beams were compared to the inelastic rotations obtained with Equation 2.23. The inelastic rotation in the length $d/2$ was calculated using compatibility and equilibrium equations (Mattock 1964: 163 – 164). The results showed that Equation 2.23 provides a lower bound for most of the beams tested.

The plastic hinge length can be determined by (Mattock 1967: 521):

$$\frac{\theta_{p,d/2}}{d/2} = \frac{\theta_p}{L_p} \tag{2.25}$$

Therefore, combining Equation 2.23 and 2.25, the plastic hinge length is:

$$L_p = \frac{d}{2}\left\{1 + \left(1.14\sqrt{\frac{L_s}{d}} - 1\right)\left[1 - \left(\frac{\omega - \omega'}{\omega_b}\right)\sqrt{\frac{d}{0.411}}\right]\right\} \tag{2.26}$$

2.8 Corley (1966)

Corley performed tests on simply supported beams subjected to a concentrated load at the midspan to investigate the effect of confinement of the concrete in compression and the effect of the size of the member in their rotational capacity. He reported the results obtained for 40 beams, which were an extension of those reported by Mattock in 1964. The size of the specimens in Corley's research extended the range covered by Mattock (Corley 1966: 121 – 146).

The most important variables covered the following range (Corley 1966: 123 – 127):

- Concrete cylinder strength: 4 ksi.
- Yield stress of tension reinforcement: 60 ksi.
- Yield stress of compression reinforcement: 60 ksi.
- Yield stress of stirrups: 50 ksi.
- Width: 3, 9 and 12".
- Effective depth: 5, 10, 24 and 30".
- Span length: 36, 72, 144, 165, 240 and 330".
- Tension reinforcement ratio: Between 1 and 3%.
- Transverse reinforcement ratio: Between 0.3 and 9%.

The test results were used to determine the spread of plasticity of the beam at each side of the midspan. Corley used the ratio $\theta_p/\theta_{p,d/2}$ as a measure of the spread of plasticity, as Mattock did in 1964, and used the same procedure to determine it from the test results. He also investigated the same parameters (Corley 1966: 139 – 141). These are all presented in Section 2.7.

Corley plotted the values of $\theta_p/\theta_{p,d/2}$ as a function of the parameters indicated by Mattock, and found that the amount of flexural reinforcement did not have a significant influence; contrary to what Mattock determined. A pronounced scatter was found for the other variables. Therefore, Corley considered that using a least squares fit was not appropriate. Based on this, he suggested a simpler expression for the spread of plasticity:

$$\frac{\theta_p}{\theta_{p,d/2}} = 1 + \frac{0.064}{\sqrt{d}} \frac{L_s}{d} \tag{2.27}$$

Where L_s and d are in meters. The measured inelastic rotations for the tests beams reported by Corley and Mattock were compared to the inelastic rotations obtained with Equation 2.27. The inelastic

rotation in the length $d/2$ was calculated using compatibility and equilibrium equations (Corley 1966: 143 – 144). The results showed that Equation 2.27 provides a lower bound for most of the beams tested.

Combining Equation 2.25 and 2.27, the plastic hinge length is:

$$L_p = 0.5d + 0.032\frac{L_s}{\sqrt{d}} \tag{2.28}$$

2.9 Mattock (1967)

Mattock, in his discussion of Corley's paper, used the measured values of the total inelastic rotation and the inelastic rotation in the length $d/2$ that he and Corley determined, to calculate the plastic hinge length, using Equation 2.25 (Mattock 1967: 519 – 522). He plotted these values as a function of the distance from the section of maximum moment to the section of zero moment. Although the results showed a considerable scatter, Mattock proposed the following equation, which represents reasonably the measured data:

$$L_p = 0.5d + 0.05L_s \tag{2.29}$$

2.10 ACI-ASCE Committee 428 (1968)

The ACI-ASCE Committee 428, on their progress report on code clauses for "Limit Design", proposed lower and upper bounds for the plastic hinge length in beams and frames (ACI-ASCE Committee 428 1968: 713 – 715). The plastic hinge length is between the following limits:

$$Min\left[R_\varepsilon\left(\frac{d}{4} + 0.03L_sR_m\right), R_\varepsilon d\right] < L_p < R_\varepsilon\left(\frac{d}{2} + 0.10L_sR_m\right) \tag{2.30}$$

In which:

$$R_\varepsilon = \frac{0.004 - \varepsilon_{ce}}{\varepsilon_{cu} - \varepsilon_{ce}} \tag{2.31}$$

$$R_m = \frac{M_{\max} - M_y}{M_u - M_y} \tag{2.32}$$

- R_ε: Strain ratio.
- R_m: Moment ratio.
- ε_{ce}: Concrete strain in the extreme compression fiber at yield curvature; either calculated, or assumed between 0.001 and 0.002.
- ε_{cu}: Concrete strain in the extreme compression fiber at ultimate curvature, neglecting effects of confinement, loading rate and strain gradients. It is assigned a value between 0.003 and 0.004.
- M_{max}: Maximum moment in the length of the member.

The following expression was proposed to calculate the distance from the section of maximum moment to the section of zero moment for members subjected to uniformly distributed load:

$$L_s = \frac{4M_{\max}}{4V_z + \sqrt{w_z M_{\max} R_m}} \tag{2.33}$$

- V_z: Shear adjacent to a concentrated load or reaction at the section of maximum moment.
- w_z: Uniformly distributed load at the section of maximum moment.

2.11 Priestly, Park and Potangaroa (1981)

Priestly, Park and Potangaroa performed tests on spirally-confined concrete columns to study their behaviour under seismic loading. The effect of confinement reinforcement on the ductility of column plastic hinges was investigated. They reported the results obtained for five columns (Priestly, Park and Potangaroa 1981: 181 – 202).

The five column specimens were of octagonal shape with the same dimensions: 600mm diameter, a height of 3.3m, and longitudinal reinforcement of 16-24mm bars equally spaced around the circle (Priestly, Park and Potangaroa 1981: 184 – 187).

The most important variables covered the following range:

- Concrete cylinder strength: Between 26.6 and 32.9 MPa.
- Axial load: Between 1920 and 6770 kN.
- Axial load ratio (P/f'_cA_g): Between 0.237 and 0.737.
- Yield stress of longitudinal reinforcement: 303 and 307 MPa.
- Diameter of spiral reinforcement: 10, 12 and 16mm.
- Spiral reinforcement volumetric ratio: Between 0.75 and 2.61.

- Yield stress of spiral reinforcement: Between 280 and 423 MPa.

The columns were tested as pin-ended vertical members. A cyclic lateral load was applied to a heavily reinforced central stub located in the middle of the column span to produce a linear bending moment diagram above and below the point of application. A constant axial load was applied during the test. The tests continued until failure.

The test results were used to compare experimental plastic hinge lengths with the values obtained using the expressions proposed by Baker and Amarakone (Equation 2.19) and Corley (Equation 2.28). The experimental plastic hinge lengths were obtained from the curvature distributions over the plastic region (Priestly, Park and Potangaroa 1981: 190 – 192).

The experimental plastic hinge lengths were calculated by solving Equation 2.5 for L_p; setting $\phi = \phi_u$, where ϕ_u is ultimate curvature, which for the tests is the average curvature measured on either side of the central stub. An equivalent yield curvature and yield displacement was estimated from the test results. The plastic deformation was determined using Equation 2.2, subtracting the yield displacement from the measured total displacement.

The results showed that the axial load level had very little influence on the experimental plastic hinge lengths. The models proposed by Baker and Amarakone and by Corley predict larger values than the ones measured. In order for the curvatures to be conservatively estimated, the plastic hinge length has to be underestimated (Priestly, Park and Gill 1982: 942). Therefore, these models gave results that were not conservative. For the experimental results, the plastic hinge length had an average value of approximately $0.3h$.

2.12 Park, Priestly and Gill (1982)

Park, Priestly and Gill performed tests on square-confined concrete columns to study their behaviour under seismic loading. This investigation was done in parallel with the experimental study carried by Priestly, Park and Potangaroa in 1981. The effect of confinement reinforcement on the ductility of column plastic hinges was also investigated here. They reported the results obtained for four columns (Priestly, Park and Gill 1982: 929 – 950).

The four column specimens had the same dimensions: cross-sectional area of 550mm^2, a height of 3.3m, longitudinal reinforcement of 12-24mm bars arranged symmetrically around the perimeter, and a longitudinal reinforcement ratio of 1.79% (Priestly, Park and Gill 1982: 932 – 934).

The most important variables covered the following range:

- Concrete cylinder strength: Between 23.1 and 41.4 MPa.
- Axial load: Between 1815 and 4265 kN.
- Axial load ratio: Between 0.214 and 0.6.
- Yield stress of longitudinal reinforcement: 375 MPa.
- Diameter of stirrups: 10 and 12mm.
- Transverse reinforcement ratio: Between 1.5 and 3.5%.
- Yield stress of stirrups: Between 294 and 316 MPa.

The test procedure used for the columns was very similar to the one used by Priestly, Park and Potangaroa in 1981 (Priestly, Park and Gill 1982: 937). It is presented in Section 2.11.

The test results were used to compare experimental plastic hinge lengths with the values obtained using the expressions proposed by Baker and Amarakone (Equation 2.19) and Corley (Equation 2.28), as it was done by the authors in their research from 1981 (Priestly, Park and Gill 1982: 938 – 942). The same procedure was used to determine the experimental plastic hinge lengths.

The results showed that the axial load level had very little influence on the experimental plastic hinge lengths; the mean value for these was $0.42h$. The models proposed by Baker and Amarakone and by Corley predict larger values than the ones measured, so they were not conservative (as in the research in 1981). Corley's equation was more accurate than Baker and Amarakone's equation, because it does not consider the axial load, which is in agreement with the results of this investigation. On the other hand, Baker and Amarakone research suggested that the plastic hinge length depended on the axial load. For the experimental results, the plastic hinge length can be conservatively estimated as $0.4h$.

2.13 Oesterle, Aristizabal-Ochoa, Shiu and Corley (1984)

Oesterle, Aristizabal-Ochoa, Shiu and Corley conducted tests of isolated reinforced concrete structural walls subjected to inelastic load reversals to study their web crushing strength. In this study, they considered a plastic hinge length equal to the horizontal length of the wall section, l_w, (Oesterle, Aristizabal-Ochoa, Shiu and Corley 1984: 233).

2.14 Paulay (1986)

Paulay presented design procedures for ductile reinforced concrete walls for earthquake resistance. He indicated that the plastic hinge length was primarily a function of the wall length. Based on this, he suggested that the length of the plastic hinge is between $0.5l_w$ and l_w (Paulay 1986: 801 – 802).

2.15 Zahn, Park and Priestly (1986)

Zahn, Park and Priestly performed tests on reinforced concrete bridge columns with different cross-sections subjected to combined axial load and bending to study their strength and ductility. As part of their work, they tested the validity of an equation derived by Priestly and Park to calculate the plastic hinge length (Equation 2.36, presented in Section 2.16). This equation was also derived from tests on concrete bridge columns, and did not take into account the axial load, since it did not have a significant effect according to the results obtained. They reported the results obtained for 14 columns (Zahn, Park and Priestly 1986).

Four types of section shapes were studied: two square sections with face loading, four square sections with diagonal loading, two octagonal sections with circular reinforcement, and six circular hollow sections. The length of all the test units was 3.9m, and the depth (or diameter) of all the cross-sections was 0.4m (Zahn, Park and Priestly 1986: 62 – 63).

The most important variables covered the following range (Zahn, Park and Priestly 1986: 211 – 212):

- Internal diameter of hollow sections: 212, 252 and 292mm.
- Concrete cylinder strength: Between 27 and 40.1 MPa.
- Axial load ratio: Between 0.08 and 0.43.
- Yield stress of longitudinal reinforcement: Between 306, 337, 423 and 440 MPa.
- Longitudinal reinforcement ratio: Between 1.51 and 5.48%.
- Yield stress of stirrups: Between 318, 340 and 466 MPa.
- Transverse reinforcement ratio: Between 0.61 and 3.52%.

The test procedure used for the columns was very similar to the one used by Priestly, Park and Potangaroa in 1981 (Zahn, Park and Priestly 1986: 66 – 67). It is presented in Section 2.11.

The test results were used to develop an expression to calculate the equivalent plastic hinge length. The experimental plastic hinge lengths were determined separately above and below the central stub, in both directions of loading. These were determined the same way as it was done by the authors in their research from 1981 (Zahn, Park and Priestly 1986: 71 – 72).

The test observations showed that the inelastic curvatures spread over a longer portion of the column when the axial load was high, due to concrete spalling. Therefore, the authors concluded that the plastic hinge length is a function of this parameter. There was a tendency for the plastic hinge length to be smaller for axial loads ratios lower than 0.3. Based on this, the following expression was proposed to predict the plastic hinge length (Zahn, Park and Priestly 1986: 238 – 240):

$$L_p = \begin{cases} (0.08L_s + 6d_b)\left(0.5 + 1.67\dfrac{P}{f_c' A_g}\right) & ; \ \dfrac{P}{f_c' A_g} < 0.3 \\ 0.08L_s + 6d_b & ; \ \dfrac{P}{f_c' A_g} \geq 0.3 \end{cases} \tag{2.34}$$

For circular hollow columns with one ring of reinforcement and no confinement, the following equation was recommended:

$$L_p = 0.06L_s + 4.5d_b \tag{2.35}$$

2.16 Priestly and Park (1987)

Priestly and Park performed tests on concrete bridge columns with different cross-sections subjected to combined axial load and bending to study their strength and ductility. The influence of the following variables in the seismic behaviour of concrete bridge columns was investigated: the axial load, the amount and yield strength of the transverse reinforcement, and the aspect ratio (Priestly and Park 1987: 61 – 76).

The section shapes tested were square (face and diagonally loaded), octagon with circular reinforcement (solid or hollow) and hollow square (Priestly and Park 1987: 61). In addition to these, smaller octagonal and rectangular sections were also tested (Priestly and Park 1987: 64).

The most important variables covered the following range (Priestly and Park 1987: 61):

- Depth: Between 400 and 750mm.
- Thickness of hollow sections: 120mm.

Two different tests were performed, one for squat columns (with an aspect ratio of two) and one for slender columns (with an aspect ratio of four). Members with square and octagonal sections were tested as squat columns. The test procedure used for these was very similar to the one used by Priestly, Park and Potangaroa in 1981. It is presented in Section 2.11. The hollow-section columns were tested as cantilever elements, a constant axial load and a cyclic lateral load at the top were applied to these (Priestly and Park 1987: 64 – 66).

The test results were used to develop an expression to calculate the equivalent plastic hinge length. The experimental plastic hinge lengths were determined the same way as it was done by the authors in their research from 1981. These values were correlated with the column parameters, arriving to the following expression (Priestly and Park 1987: 71 – 73):

$$L_p = 0.08L_s + 6d_b \tag{2.36}$$

This equation was used to compute plastic hinge lengths for columns with different aspect ratios that were tested by other researchers (including the ones tested by the authors in 1981 and 1982), and were compared with the experimental plastic hinge lengths obtained in these tests. There was a good agreement between the experimental and predicted values for most cases. The average value for all tests was approximately $0.5h$. The test results in this research also indicated that the plastic hinge length did not have any significant dependence on the axial load ratio, the longitudinal reinforcement ratio, and the yield stress of longitudinal reinforcement.

2.17 Paulay and Priestly (1992)

Paulay and Priestly proposed the following expression to estimate the plastic hinge length (Priestly, Seible and Calvi 1996: 308 – 309):

$$L_p = 0.08L_s + 0.022f_y d_b \geq 0.044f_y d_b \tag{2.37}$$

Where f_y is in MPa units. The authors indicated that for commonly used beam and column dimensions, Equation 2.37 gives plastic hinge lengths of approximately $0.5h$. They also indicated that the plastic region where special detailing requirements must be provided to have sufficient rotational capacity

is larger than the calculated equivalent plastic hinge length (Paulay and Priestly 1992: 141 – 142). For f_y = 275 MPa, Equation 2.37 becomes the same as Equation 2.36.

2.18 Wallace and Moehle (1992)

Wallace and Moehle presented an analytical procedure to determine the need of confined boundaries in concrete walls subjected to earthquake loading. They stated that the plastic hinge length is usually between $0.5l_w$ and l_w (Wallace and Moehle 1992: 1633 – 1634).

2.19 Moehle (1992)

Moehle indicated that the equivalent plastic hinge length in reinforced concrete columns depends on the section depth, aspect ratio, bar diameter, and the axial and shear force. He stated that good correlation with experimental results may be obtained if a plastic hinge length equal to $0.5h$ is used (Moehle 1992: 411 – 412).

2.20 Paulay and Priestly (1993)

Paulay and Priestly reported tests on ductile concrete walls of rectangular shape subjected to seismic loading to study out-of-plane buckling. In this study, they used the following expression to calculate the plastic hinge length (Paulay and Priestly 1993: 386 – 387):

$$L_p = 0.2l_w + 0.044H_w \tag{2.38}$$

Where H_w is the total height of the wall. The authors indicated that Equation 2.38 predicts conservatively the plastic hinge length, so that the curvature ductility demands are not underestimated; and that it gives a good approximation of the portion of the height of the wall over which out-of-plane buckling can occur.

2.21 Sasani and Der Kiureghian (2001)

Sasani and Der Kiureghian developed probabilistic displacement capacity and demand models for reinforced concrete walls. They derived a model for the plastic hinge length in concrete walls, using the test results reported by Corley in 1966 (Section 2.8) and Mattock in 1967 (Section 2.9). From the 40 beams tested back then, they selected 29 of them with effective depths greater than 0.5m. This data was

used to estimate the parameters of the following two equations, which are normalized versions of Equation 2.28 and 2.29, respectively (Sasani and Der Kiureghian 2001: 220 – 221):

$$\frac{L_p}{d} = \alpha_1 + \alpha_2 \frac{L_s l_s^{1/2}}{d^{3/2}} + \xi_L \tag{2.39}$$

$$\frac{L_p}{d} = \alpha_1 + \alpha_2 \frac{L_s}{d} + \xi_L \tag{2.40}$$

- l_s: Standard length equal to 1m (39.4"), inserted to make the model parameters dimensionless.
- α_1, α_2: Model parameters.
- ξ_L: Model error term.

For the 29 beams selected, the mean values of α_1 and α_2 for Corley's equation were 0.52 and 0.047, respectively; and for Mattock's equation they were 0.56 and 0.051. These results were used in Equation 2.39 and 2.40 to determine plastic hinge lengths as a function of the effective depth and of the distance from the section of maximum moment to the section of zero moment. The results obtained for both models overestimated the plastic hinge length for large values of the effective depth, which are representative of concrete walls. Therefore, the authors explored several different models, and finally arrived to the following expression:

$$\frac{L_p}{d} = \alpha_1 + \alpha_2 \frac{\sqrt{L_s} l_s^{3/2}}{d^2} + \xi_L \tag{2.41}$$

The mean values of α_1 and α_2 for this equation were now 0.427 and 0.077, respectively. These results were used in Equation 2.41 to determine plastic hinge lengths as a function of the effective depth and of the distance from the section of maximum moment to the section of zero moment. The results obtained showed that Equation 2.41 provides a better fit to the data, specially for large values of the effective depth.

2.22 Mendis (2001)

Mendis performed tests on simply supported beams subjected to a concentrated load at the midspan to investigate how the plastic hinge length is influenced by the amount of tension, compression and transverse reinforcement, and shear and axial forces. He reported the results obtained for 13 beams (Mendis 2001: 189 – 195).

The most important variables covered the following range (Mendis 2001: 192 – 193):

- Span length: 630, 750 and 938mm.
- Width: 60mm.
- Depth: 164mm.
- Axial load: 0, 50, 100 and 175 kN.
- Stirrup spacing: 30, 50, 75 and 150mm.
- Amount of tension reinforcement: 3Y12 and 4Y12 bars.
- Amount of compression reinforcement: 2Y12 and 3Y12 bars.
- Concrete cylinder strength: Between 37.4 and 57.9 MPa.

The test results were used to compare experimental plastic hinge lengths with the values obtained using the expressions proposed by Baker and Amarakone (Equation 2.12 and 2.19), Sawyer (Equation 2.22), Mattock (Equation 2.26 and 2.29), Corley (Equation 2.28), ACI-ASCE Committee 428 (Equation 2.30), and Park, Priestly and Gill (who suggested a value of $0.4h$). Most of the experimental results were between the ACI-ASCE bounds.

The experimental results showed that the plastic hinge length increased with the length, the shear-span ratio (M/Vh) and the longitudinal reinforcement ratio; and decreased with the transverse reinforcement ratio. For the specimens tested with axial loads, the plastic hinge length was approximately $0.4d$, meaning that it was independent of the axial load (Mendis 2001: 193). Park, Priestly and Gill arrived to this same conclusion from their research in 1982 (see Section 2.12).

Comparisons between the experimental and predicted results showed that the expression of Baker and Amarakone for unconfined concrete (Equation 2.12) overestimated the plastic hinge length by a small margin, while their equation for confined concrete (Equation 2.19) underestimated it. The equations proposed by Mattock and Corley significantly overestimated the plastic hinge length. Sawyer's equation also overestimated the plastic hinge length for many specimens. The value recommended by Park, Priestly and Gill gave good predictions for beams with axial loads.

The test results were used to derive an equation to calculate the plastic hinge length for beams without axial loads (Mendis 2001: 193 – 194):

$$L_p = 0.25d\frac{RFT^{0.2}SPR^{0.5}}{PER^{0.2}} \tag{2.42}$$

$$RFT = \left(\frac{A_{st} - A_{sc}}{bd} \right) \times 100 \tag{2.43}$$

$$SPR = \frac{L_s}{d} \tag{2.44}$$

- *PER*: Percentage ratio of volume of stirrups to volume of concrete core measured outside of stirrups.
- A_{st}: Area of tension reinforcement.
- A_{sc}: Area of compression reinforcement.
- b: Width of the member.

For members with the same amount of tension and compression reinforcement (like symmetrical columns or walls), Equation 2.42 gives a plastic hinge length of zero, so it is not applicable for these cases.

Mendis also reported measured plastic hinge lengths obtained from tests on high-strength concrete (up to 80 MPa) beams and columns with low axial load that were performed by other researchers, and compared these results with the ACI-ASCE bounds. Most of the experimental results were between these bounds, the author recommended their use to estimate the plastic hinge length for normal and high-strength concrete beams and columns with low axial loads.

2.23 Panagiotakos and Fardis (2001)

Panagiotakos and Fardis reported tests on reinforced concrete members subjected to uniaxial bending, with and without axial loads, to derive expressions for deformations at yielding and failure, in terms of the member geometric and mechanical properties. These members are representative of beams, columns and walls. They reported the results obtained for 1012 specimens (Panagiotakos and Fardis 2001: 135 – 148).

The experimental database used in this research was the following (Panagiotakos and Fardis 2001: 136 – 139):

- 266 specimens were representative of beams, they had unsymmetrical reinforcement and were not subjected to axial loads. All the specimens had rectangular cross-sections, except for two of them, which had T-sections. Beams with and without closely spaced stirrups were tested.

- 682 specimens were representative of columns, they had symmetrically reinforced square or rectangular cross-sections, subjected or not to axial load. Columns with and without closely spaced stirrups were tested.
- 61 specimens were representative of walls, with rectangular, barbelled or T-sections. Walls with and without confined boundaries were tested.
- 23 column specimens had diagonal reinforcement, combined or not with longitudinal bars.
- 824 specimens used hot-rolled steel, 129 specimens used heat-treated steel, and 59 specimens used brittle cold-worked steel.

The most important variables covered the following range:

- Concrete cylinder strength: Between 15 and 120 MPa.
- Axial load ratio: Between 0 and 0.95.
- Shear-span ratio: Between 1 and 6.5.
- Diagonal reinforcement ratio: Between 0 and 1.125%.
- Hardening ratio (f_t/f_y): Between 1.1 and 1.5 (where f_t is the tensile strength of steel).
- Steel strain at peak stress: Between 4 and 15%.

Most of the specimens were tested as simple or double cantilevers, and others were tested as simply supported beams with a concentrated load applied at the midspan. They were subjected to monotonic and cyclic loading. Most tests continued until failure (Panagiotakos and Fardis 2001: 136).

The test results were used to compare measured and predicted total rotations. The results for 875 specimens subjected to monotonic or cyclic loading, for which the values of the rotations at failure were measured and where failure was due to bending, were used for the comparison. From the data used, 242 were monotonic tests and 633 were cyclic tests. All 61 walls specimens were used. There was some slippage of the longitudinal reinforcement for 703 of these tests, most of them for cyclic loading (Panagiotakos and Fardis 2001: 140).

An approach used by the authors to determine the total rotation at failure was through plastic hinge analysis (Panagiotakos and Fardis 2001: 144 – 147). This was done by rearranging Equation 2.8. Setting $L = L_s$ and $\phi = \phi_u$, and dividing Equation 2.8 by L_s, an expression for the total rotation at failure is obtained:

$$\theta_u = \frac{\phi_y L_s}{3} + (\phi_u - \phi_y) L_p \left(1 - \frac{L_p}{2L_s}\right) \tag{2.45}$$

Equation 2.45 requires knowing the yield and ultimate curvature, and the plastic hinge length. The yield and ultimate curvature were determined from expressions based on basic principles of mechanics, since these expressions predicted the measured curvatures well on average, although with a large scatter. With expressions for the yield and ultimate curvature combined with Equation 2.45, the total rotations at failure for the 875 tests considered were used to arrive for expressions for the plastic hinge length that provided the best fit to this data. For this, the authors decided to use the same form of the expression proposed by Paulay and Priestly in 1992 (Equation 2.37), since the parameters included in this expression were the most significant. They developed the following expressions to determine the plastic hinge length:

For cyclic loading:

$$L_{p,cy} = 0.12L_s + 0.014a_{sl}d_b f_y \tag{2.46}$$

For monotonic loading:

$$L_{p,mon} = 1.5L_{p,cy} = 0.18L_s + 0.021a_{sl}d_b f_y \tag{2.47}$$

- $L_{p,cy}$: Plastic hinge length for cyclic loading.
- $L_{p,mon}$: Plastic hinge length for monotonic loading.
- a_{sl}: Zero-one variable. It is equal to one if slippage of the longitudinal reinforcement is possible, and zero if it is not possible.
- f_y: Yield stress of the tension reinforcement, in MPa units.

Equation 2.46 and 2.47 were used in conjunction with Equation 2.45 to calculate the total rotation at failure for the 875 tests considered. Equation 2.37 of Paulay and Priestly was also used with Equation 2.45 to calculate the total rotations at failure. These predictions were compared with the experimental results. The quality of the predictions was very similar for these three equations, meaning that the predictions of Equation 2.45 were not very sensitive to the expression used to calculate the plastic hinge length. A considerable scatter of the results was observed.

2.24 Thomsen and Wallace (2004)

Thomsen and Wallace conducted tests of slender reinforced concrete walls with rectangular-shaped and T-shaped cross-sections with moderate amounts of transverse reinforcement in the boundaries

to evaluate the simplified displacement-based design approach in ACI 318 1999. The premises on which displacement-based design is founded on were verified with the experimental results. They reported the results obtained for four walls (Thomsen and Wallace 2004: 618 – 630).

The four wall specimens included two with rectangular sections (named RW1 and RW2) and two with T-sections (named TW1 and TW2). All had an aspect ratio of three and were considered as four-storey walls. The walls were 4" thick, 48" long and 144" high. Additionally, the flanges in the T-shaped walls were 4" thick and 48" long, and floor slabs were provided every 36" over the height for these walls (Thomsen and Wallace 2004: 618 – 619).

The most important variables covered the following range (Thomsen and Wallace 2004: 621 – 622):

- Average concrete cylinder strength at first storey: 4.6, 4.9, 6.3 and 6.1 ksi.
- Average concrete strain at peak stress: 0.002.
- Concrete rupture strength: Between 13 and 14% of concrete cylinder strength.
- Diameter of boundary longitudinal reinforcement: #3 bars.
- Diameter of boundary transverse reinforcement: 3/16" smooth wire.
- Diameter of distributed horizontal and vertical web reinforcement: #2 bars.
- Average axial load ratio: 0.1.

The wall specimens were tested as cantilever elements. They were subjected to cyclic lateral displacements applied at the top, and a constant compressive axial load (Thomsen and Wallace 2004: 622 – 623).

The test results were used to verify the premises on which displacement-based design for slender concrete walls is based on (Thomsen and Wallace 2004: 626 – 629). Some of these premises are:

- The normal strain profile along the wall length at the critical section is linear.
- The yield curvature is equal to $0.003/l_w$.
- The plastic hinge length is equal to $0.5l_w$.

The experimental strain profiles were obtained from measurements made along the length of the wall. The analytical strain profiles were determined using a simplified version of Equation 2.8. Setting $L = H_w$, and considering that the plastic hinge length is very small compared to the height of the wall, Equation 2.8 becomes:

$$\Delta = \frac{\phi_y H_w^2}{3} + (\phi - \phi_y) L_p H_w \tag{2.48}$$

Considering a yield curvature of $0.003/l_w$ and a plastic hinge length of $0.5l_w$, and solving Equation 2.48 for the total curvature, the following expression can be derived:

$$\phi = \left(\frac{\Delta}{H_w} - 0.001\frac{H_w}{l_w} + 0.0015 \right)\left(\frac{2}{l_w} \right) \tag{2.49}$$

Then, the strain profile along the length of the wall is given by multiplying this curvature by the distance to the neutral axis. The strain profiles were computed for different drift levels (Δ/H_w). The curvature was computed for each drift level, and the neutral axis depth associated to that curvature was obtained from a moment-curvature analysis.

The sensitivity of the strain profile to the assumed yield curvature and plastic hinge length was then analyzed. This was done using the same procedure as before: consider different values for these parameters, plug them into Equation 2.48, consider a drift level, solve for the curvature, determine the neutral axis depth, and calculate the strain profile. Variation of the yield curvature from $0.0025/l_w$ to $0.0035/l_w$ had a negligible impact on the strain profiles. However, the plastic hinge length had a very significant influence. The authors compared the experimental and analytical strain profiles, considering plastic hinge lengths of $0.33l_w$, $0.5l_w$ and $0.67l_w$; and determined that plastic hinge lengths between $0.33l_w$ and $0.5l_w$ produced the best agreement between results. For the specimen RW2, the best agreement was found for $0.33l_w$.

The experimental results also showed that the strain profiles are not linear, although the walls are slender. The greater difference between the experimental and analytical strain profiles was in the tension zone; the authors indicated that it was due to the influence of concrete cracking and slippage of the reinforcement.

2.25 Summary

An extensive review of the models used to calculate the equivalent plastic hinge length has been presented. These models were developed for beams, columns and walls. Details on the tests performed to arrive at these expressions have been described.

In classical plastic hinge analysis, the plastic hinge length is defined as the equivalent length over which the inelastic curvature is considered to be constant. This definition has been used by most of researchers cited to derive their models. The influence of phenomena like tensile strain penetration and spread of plasticity is considered implicitly through the plastic hinge length.

The plastic hinge length is a function of several parameters. One of the most important is the depth of the member, as it has been included in most of the models presented. Other important parameters are the span of the member, the longitudinal reinforcement properties, the axial load ratio and the strain hardening. However, most researchers have not included the same parameters in their models, due to the characteristics of the specimens tested.

Chan (1955), Cohn and Petcu (1963), Sawyer (1964) and the ACI-ASCE Committee 428 (1968) considered the effect of strain hardening. Mattock (1964) also considered this parameter along with the reinforcement properties. However, Corley (1966) found that these two parameters did not have a significant influence, based on additional test results. Mattock (1967) proposed a new expression that did not include these parameters.

Sawyer (1964), Corley (1966), Mattock (1967) and Sasani and Der Kiureghian (2001) did not include the longitudinal reinforcement properties. On the other hand, Baker and Amarakone (1964), Zahn, Park and Priestly (1986), Priestly and Park (1987), Paulay and Priestly (1992), Mendis (2001) and Panagiotakos and Fardis (2001) considered that these were important parameters.

Baker and Amarakone (1964) included the influence of the type of steel and the concrete strength. They also considered the effect of the axial load, which had a direct relation with the plastic hinge length according to the results of their research. Zahn, Park and Priestly (1986) also considered that the effect of the axial load and concrete strength was important. However, Priestly, Park and Potangaroa (1981), Park, Priestly and Gill (1982), Priestly and Park (1987), Mendis (2001) and Panagiotakos and Fardis (2001) conducted tests for members subjected to axial load and found no significant dependence between this parameter and the plastic hinge length.

The ACI-ASCE Committee 428 (1968) proposed lower and upper bounds for the plastic hinge length, instead of a one equation.

Many researchers arrived to the conclusion that a safe (lower bound) approximation for the plastic hinge length is $0.5h$ or $0.5l_w$. This is the value given in many concrete codes, including CSA A23.3.

Most of the research done in plastic hinge length has been more focused in beams and columns. Some models have been developed for walls, but have certain limitations. Oesterle, Aristizabal-Ochoa, Shiu and Corley (1984), Paulay (1986) and Wallace and Moehle (1992) suggested values for plastic hinge length between $0.5l_w$ and l_w. Paulay and Priestly (1993) proposed an equation for the plastic hinge length applicable to walls, which provides conservative predictions of the curvature ductility demand. Sasani and Der Kiureghian (2001) developed plastic hinge length models for reinforced concrete walls using the test results reported by Corley (1966) and Mattock (1967). However, these tests were performed on beams, which have a different behaviour compared to walls. Panagiotakos and Fardis (2001) derived expressions for the plastic hinge length for monotonic and cyclic loading using the results obtained for 875 specimens. Only 61 of these were walls, so these models may not be representative of this type of members. Thomsen and Wallace (2004) obtained an approximation of the plastic hinge length by comparing experimental and analytical strain profiles. The best agreement was found for values between $0.33l_w$ and $0.5l_w$.

Table 2.1 summarizes all the studies previously done on plastic hinge length presented in this chapter, including the type of members studied and the parameters considered by the authors to develop their models:

Table 2.1 Summary of previous research done on plastic hinge length

Researchers reference	Members studied	Parameters considered
Chan (1955)	Columns	Span, strain hardening
Baker (1956)	Beams and columns	Depth
Cohn and Petcu (1963)	Beams	Depth, strain hardening
Baker and Amarakone (1964)	Beams and columns	Depth, span, reinforcement properties, axial load ratio
Sawyer (1964)	Beams and columns	Depth, span, strain hardening
Mattock (1964)	Beams	Depth, span, reinforcement properties, strain hardening
Corley (1966)	Beams	Depth, span
Mattock (1967)	Beams	Depth, span
ACI-ASCE Committee 428 (1968)	Beams and columns	Depth, span, strain hardening
Priestly, Park and Potangaroa (1981)	Columns	Depth
Park, Priestly and Gill (1982)	Columns	Depth
Oesterle, Aristizabal-Ochoa, Shiu and Corley (1984)	Walls	Depth
Paulay (1986)	Walls	Depth
Zahn, Park and Priestly (1986)	Columns	Span, reinforcement properties, axial load ratio
Priestly and Park (1987)	Columns	Depth, span, reinforcement properties
Paulay and Priestly (1992)	Beams and columns	Depth, span, reinforcement properties
Wallace and Moehle (1992)	Walls	Depth
Moehle (1992)	Columns	Depth
Paulay and Priestly (1993)	Walls	Depth, span
Sasani and Der Kiureghian (2001)	Beams $d > 0.5$m	Depth, span
Mendis (2001)	Beams and columns	Depth, span, reinforcement properties
Panagiotakos and Fardis (2001)	Beams, columns and walls	Span, reinforcement properties
Thomsen and Wallace (2004)	Walls	Depth

The models presented in this chapter will be used to determine the equivalent plastic hinge length for a test specimen representative of a shear wall in a high-rise building, in order to compare the results obtained. These results are presented in Chapter 4 (see Section 4.2.8).

CHAPTER 3: ANALYTICAL METHODS

3.1 Introduction to program VecTor2

Program VecTor2 will be the analysis tool used in this research. VecTor2 is a computer program developed to perform nonlinear finite element analysis of two-dimensional reinforced concrete membrane structures subjected to quasi-static loading. This program has been developed by researchers from the University of Toronto. In this chapter, a general overview of program VecTor2 will be presented, focusing basically on the models used in this research. The information presented in this chapter comes directly from the *VecTor2 and FormWorks User's Manual* (Wong and Vecchio 2002) and the VecTor Analysis Group website.

Along with program VecTor2, program FormWorks is used as the pre-processor for the analysis, and program Augustus is used as the post-processor.

3.2 Theoretical bases of program VecTor2

The analysis was performed using the constitutive models of the Disturbed Stress Field Model (Vecchio 2000: 1070 – 1077), which is a refinement of the Modified Compression Field Theory (Vecchio and Collins 1986: 219 – 231). Both analytical models can predict the behaviour of reinforced concrete elements subjected to in-plane normal and shear stresses, modeling cracked concrete as an orthotropic material with smeared, rotating cracks. Constitutive models for a variety of effects, such as compression softening and tension stiffening, are included to accurately predict the response (Wong and Vecchio 2002: 2). Additionally, the Disturbed Stress Field Model can consider different directions of the principal stresses and strains, and takes into account crack shear slip deformations (Wong and Vecchio 2002: 13).

3.3 Finite element formulation

Program VecTor2 uses low-powered finite elements to model the structure. These include the 3-node constant strain triangle (with six degrees of freedom) and the 4-node plane stress rectangle (with eight degrees of freedom) to model concrete, and the 2-node truss bar element (with four degrees of freedom) to model discrete reinforcement. The reinforcement may be modeled as either smeared within concrete elements or as discrete bars. The stresses, strains and material properties are constant within each element (VecTor Analysis Group).

The finite element solution is based on a secant stiffness formulation that uses a total-load iterative procedure (VecTor Analysis Group). At each load step, the element stiffness matrices are calculated from the current stress-strain state and then assembled, and the nodal loads are calculated. The nodal displacements are determined and then used to calculate one strain tensor for each element, and then the principal strains are determined. These are used in the constitutive relationships for concrete and steel to calculate the stress tensor in each element. The secant moduli are then determined from the new stress-strain state, and compared to the secant moduli from the previous stress-strain state. If convergence is satisfactory, the analysis for that load step is completed and then continues to the next load step. If not, the analysis is repeated using the new stress-strain state. Usually, convergence is achieved after 10 to 30 iterations (Selby, Vecchio and Collins 1996: 306 – 307). This procedure continues until the specified force or the target displacement is reached, or until the structure becomes unstable.

3.4 Models for concrete in compression

The compression response of concrete is described through nonlinear functions relating stresses and strains. Different models are used for the ascending and descending branches of the concrete response in uniaxial compression. These curves are then modified to account for second-order effects (Wong and Vecchio 2002: 45).

Figure 3.1 Concrete compression response

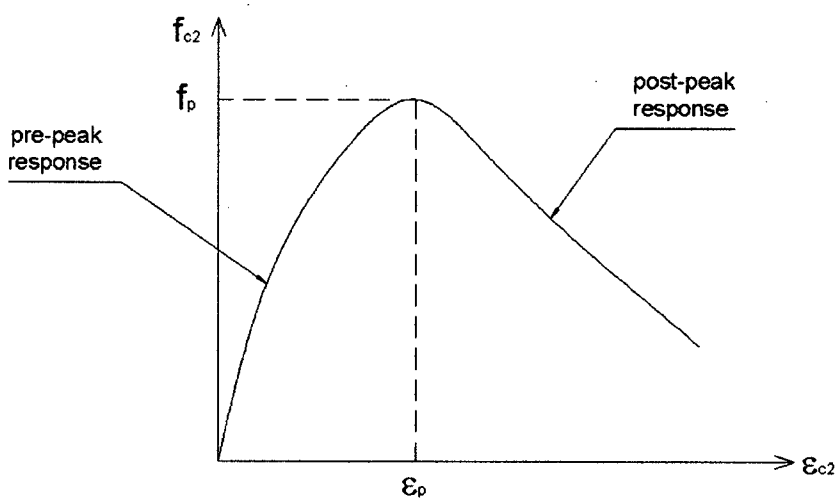

3.4.1 Compression pre-peak response

Compression pre-peak response models compute the principal compressive stresses while the principal compressive strain is less than the strain corresponding to the peak compressive stress. The

model used for the ascending curve for concrete compressive stress is the one proposed by Popovics for normal-strength concrete. The stress-strain curve is described by (Wong and Vecchio 2002: 46 – 47):

$$f_{c2} = -\left(\frac{\varepsilon_{c2}}{\varepsilon_p}\right) f_p \frac{n}{n-1+\left(\varepsilon_{c2}/\varepsilon_p\right)^n} \; ; \; \varepsilon_p < \varepsilon_{c2} < 0 \tag{3.1}$$

$$n = \frac{E_c}{E_c - E_{sec}} \tag{3.2}$$

$$E_{sec} = \frac{f_p}{|\varepsilon_p|} \tag{3.3}$$

- f_{c2}: Average net concrete axial stress in the principal compressive direction.
- ε_{c2}: Average net concrete axial strain in the principal compressive direction.
- ε_p: Concrete compressive strain corresponding to f_p.
- f_p: Peak concrete compressive stress.
- n: Curve fitting parameter for stress-strain response of concrete in compression.
- E_c: Concrete initial tangent stiffness.
- E_{sec}: Concrete secant stiffness.

3.4.2 Compression post-peak response

Compression post-peak response models compute the principal compressive stresses while the principal compressive strain is greater than the strain corresponding to the peak compressive stress. The compressive stresses are computed as follows (Wong and Vecchio 2002: 52):

$$f_{c2} = (1-c_a) f_{c2}^a + c_a f_{c2}^b \; ; \; \varepsilon_{c2} < \varepsilon_p < 0 \tag{3.4}$$

$$c_a = 4\left(\frac{f_p - f_c'}{f_c'}\right) \; ; \; 0 \le c_a \le 1 \tag{3.5}$$

- c_a: Averaging factor.
- f_{c2}^a: Average concrete compressive stress contribution of unconfined concrete.
- f_{c2}^b: Average concrete compressive stress contribution of confined concrete.

The stress contribution of unconfined concrete is determined using the Smith-Young model:

$$f_{c2}^{a} = -f_p\left(\frac{\varepsilon_{c2}}{\varepsilon_p}\right)Exp\left(1-\frac{\varepsilon_{c2}}{\varepsilon_p}\right) \tag{3.6}$$

The stress contribution of confined concrete is determined using the Modified Park-Kent model, in which the stresses decay linearly (Wong and Vecchio 2002: 53 – 54):

$$f_{c2}^{b} = -\left[f_p + Z_m f_p\left(\varepsilon_{c2}-\varepsilon_p\right)\right] < \begin{cases} 0 & ; 0 < f_p < f_c^{'} \\ -0.2f_p & ; 0 < f_c^{'} < f_p \end{cases} \tag{3.7}$$

$$Z_m = \frac{0.5}{\left(\frac{3+0.29\left|f_c^{'}\right|}{145\left|f_c^{'}\right|-1000}\right)\left(\frac{\varepsilon_o}{-0.002}\right)+\left(\frac{\left|f_{c1}\right|}{170}\right)^{0.9}+\varepsilon_p} \tag{3.8}$$

- Z_m: Slope of compression post-peak descending curve.
- f'_c: Concrete cylinder uniaxial compressive strength, in MPa units.
- ε_o: Concrete compressive strain corresponding to f'_c.
- f_{c1}: Average net concrete axial stress in the principal tensile direction.

3.4.3 Compression softening

Compression softening is the reduction of compressive strength and stiffness of concrete due to transverse cracking and tensile straining. In VecTor2, compression softening is included by calculating a softening parameter, β_d, which varies between zero to one. The model used to determine this parameter is the Vecchio 1992-A ($\varepsilon_{c1}/\varepsilon_{c2}$-Form). This factor is then applied to the uniaxial compressive strength and its corresponding strain to obtain the peak compressive strength and its corresponding strain, respectively; used in the compression response models previously described. The following expressions apply (Wong and Vecchio 2002: 58 – 61):

$$\beta_d = \frac{1}{1+C_s C_d} \leq 1 \tag{3.9}$$

$$C_d = \begin{cases} 0 & ; r < 0.28 \\ 0.35(r-0.28)^{0.8} & ; r > 0.28 \end{cases} \tag{3.10}$$

$$r = \frac{-\varepsilon_{c1}}{\varepsilon_{c2}} \leq 400 \tag{3.11}$$

$$f_p = \beta_d \beta_l f_c^{'} \tag{3.12}$$

$$\varepsilon_p = \begin{cases} \beta_d \beta_l \varepsilon_o & ; \beta_d \beta_l \varepsilon_o < \varepsilon_o < 0 \\ \varepsilon_{c2} & ; \varepsilon_o < \varepsilon_{c2} < \beta_d \beta_l \varepsilon_o < 0 \\ \varepsilon_o & ; \varepsilon_{c2} < \varepsilon_o < \beta_d \beta_l \varepsilon_o < 0 \end{cases} \tag{3.13}$$

- C_s: Compression softening shear slip factor. It is assigned a value of one if shear slip is not considered, and 0.55 if it is considered.
- C_d: Compression softening strain softening factor.
- r: Ratio of the principal tensile strain to the principal compressive strain.
- ε_{c1}: Average net concrete axial strain in the principal tensile direction.
- β_l: Strength enhancement factor.

The value of ε_p may be modified in some cases, as shown in Equation 3.13, so that compression response ascends for strains up to ε_o and then descend.

3.4.4 Confinement strength

Confinement increases the compressive strength and ductility of concrete. In VecTor2, the effect of confinement is included by calculating a strength enhancement factor, β_l, which is equal or greater than one. The model used to determine this parameter is the Kupfer-Richart model. This factor is then applied to the uniaxial compressive strength and its corresponding strain, to obtain the peak compressive strength and its corresponding strain, respectively; used in the compression response models previously described (Equations 3.12 and 3.13). For the case of biaxial compression, the strength enhancement factor for the direction of the largest compressive stress, f_{c2}, is determined using the following expression (Wong and Vecchio 2002: 77 – 78):

$$\beta_l = 1 + 0.92\left(\frac{-f_{c1}}{f_c^{'}}\right) - 0.76\left(\frac{-f_{c1}}{f_c^{'}}\right)^2 \geq 1 \; ; \; f_{c2} < f_{c1} < 0 \tag{3.14}$$

The strength enhancement factor for the direction of f_{c1} is determined by interchanging f_{c1} for f_{c2} in Equation 3.14.

3.5 Models for concrete in tension

The tension response of concrete is divided into uncracked and cracked response:

Figure 3.2 Concrete tension response

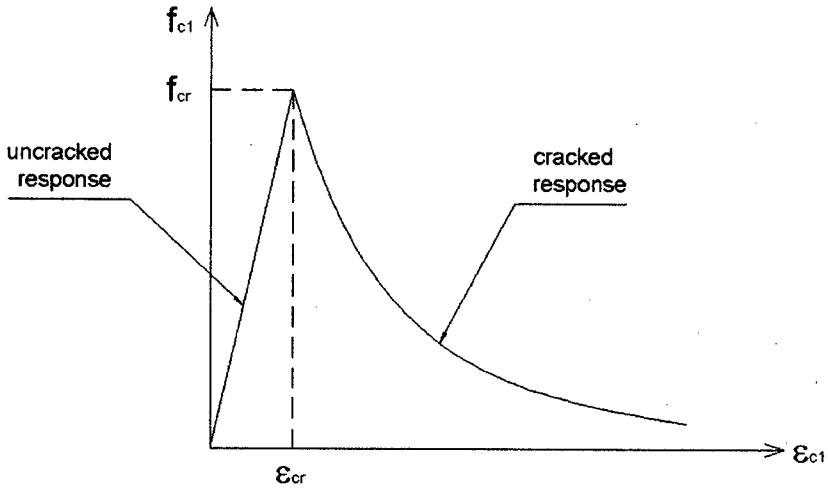

Before cracking, the response is considered linear-elastic (Wong and Vecchio 2002: 64):

$$f_{c1} = E_c \varepsilon_{c1} \; ; \; 0 < \varepsilon_{c1} < \varepsilon_{cr} \tag{3.15}$$

$$\varepsilon_{cr} = \frac{f_{cr}}{E_c} \tag{3.16}$$

- ε_{cr}: Concrete cracking strain.
- f_{cr}: Concrete cracking stress.

After cracking, VecTor2 does two calculations to determine the average concrete tensile stresses, one due to tension stiffening and the other due to tension softening. The larger of the two values is taken as the average post-cracking tensile stress (Wong and Vecchio 2002: 65):

$$f_{c1} = Max\left(f_{c1}^{a}, f_{c1}^{b}\right) \; ; \; 0 < \varepsilon_{cr} < \varepsilon_{c1} \tag{3.17}$$

- f_{c1}^{a}: Average concrete tensile stress due to tension stiffening.
- f_{c1}^{b}: Average concrete tensile stress due to tension softening.

3.5.1 Tension stiffening

Tension stiffening is the presence of post-cracking tensile stresses between cracks in the vicinity of the reinforcement. In VecTor2, for discrete reinforcement elements, their tributary area in which the concrete within exhibits tension stiffening is delineated by a distance equal to 7.5 bar diameters from the

reinforcement element (Wong and Vecchio 2002: 64 – 65). Tension stiffening is included by decreasing gradually the average stress-strain response of concrete in tension. The Modified Bentz model is used for this purpose. This model is the same as the Bentz 1999 model when the steel is aligned with the x or y-axis (no skew steel). The concrete tensile stresses decay following these expressions (Wong and Vecchio 2002: 18):

$$f_{c1}^{a} = \frac{f_{cr}}{1+\sqrt{c_t \varepsilon_{c1}}} \tag{3.18}$$

$$c_t = 2.2m \tag{3.19}$$

$$\frac{1}{m} = \sum_i \frac{4\rho_i}{d_{bi}} |Cos\theta_{ni}| \tag{3.20}$$

- c_t: Coefficient that incorporates the influence of reinforcement bond characteristics.
- m: Bond parameter, in millimetres.
- θ_n: Angle between the normal to the crack surface and the longitudinal axis of the reinforcement.

3.5.2 Tension softening

Tension softening is the presence of post-cracking tensile stresses in plain concrete. It is included by decreasing gradually the average stress-strain response of concrete in tension, as it is done for tension stiffening. The linear model, which does not consider residual tensile stresses, is used for this purpose. The concrete tensile stresses decrease linearly following these expressions (Wong and Vecchio 2002: 70 – 72):

$$\varepsilon_{ch} = \frac{2G_f}{L_r f_{cr}} \; ; \; 1.1\varepsilon_{cr} < \varepsilon_{ch} < 10\varepsilon_{cr} \tag{3.21}$$

$$f_{c1}^{b} = f_{cr}\left(1 - \frac{\varepsilon_{c1} - \varepsilon_{cr}}{\varepsilon_{ch} - \varepsilon_{cr}}\right) \geq 0 \tag{3.22}$$

- ε_{ch}: Characteristic strain.
- G_f: Energy required to form a complete crack of unit area, it is assigned a value of 75 N/m.
- L_r: Distance over which the crack is assumed to be uniformly distributed, it is assigned a value of half the crack spacing.

3.5.3 Cracking criterion

The concrete cracking stress usually decreases as the compressive stresses acting transversely increase, so it does not remain constant and may have a different value from the specified concrete uniaxial tensile strength, f'_t. The Mohr-Coulomb stress model is used to calculate the cracking stress. The following expressions apply (Wong and Vecchio 2002: 80 – 82):

$$C = f'_c \frac{1 - Sin\Phi}{2Cos\Phi} \tag{3.23}$$

$$f_{cru} = 2C \frac{Cos\Phi}{1 + Sin\Phi} \tag{3.24}$$

$$f_{cr} = f_{cru}\left(1 + \frac{f_{c2}}{f'_c}\right) \; ; \; 0.2f'_t \leq f_{cr} \leq f'_t \tag{3.25}$$

- C: Cohesion.
- Φ: Internal angle of friction, it is assigned a value of 37°.

3.6 Models for slip distortions in concrete

VecTor2 can take into account crack shear slip deformations, as it is formulated in the Disturbed Stress Field Model. When crack shear slip deformations are considered, the crack shear check requirement is eliminated (Wong and Vecchio 2002: 13). The model used to calculate the shear slip is the Hybrid-I model, which combines the Lai-Vecchio stress model (a stress-based model) and the constant rotation lag model (Wong and Vecchio 2002: 88). A hybrid model computes the shear slip strains using both the stress-based model and the constant rotation lag model, and takes the greater value:

$$\gamma_s = Max\left(\gamma_s^a, \gamma_s^b\right) \tag{3.26}$$

- γ_s: Shear slip strain.
- γ_s^a: Shear slip strain determined from the stress-based model.
- γ_s^b: Shear slip strain determined from the constant rotation lag model.

3.6.1 Stress-based model

The stress-based models relate the shear slip along the crack to the local shear stress along the crack. The shear slip strain is then computed from the shear slip with the following expression (Wong and Vecchio 2002: 85 – 86):

$$\gamma_s^a = \frac{\delta_s}{s} \tag{3.27}$$

- δ_s: Shear slip.
- s: Crack spacing.

For the Lai-Vecchio stress model, the following expressions used are to calculate the shear slip (Wong and Vecchio 2002: 87):

$$\delta_s = \delta_s^* \sqrt{\frac{\psi}{1-\psi}} \leq 2w \tag{3.28}$$

$$\delta_s^* = \frac{0.5v_{ci,\max} + v_{co}}{1.8w^{-0.8} + \left(0.234w^{-0.707} - 0.2\right)f_{cc}} \tag{3.29}$$

$$\psi = \frac{v_{ci}}{v_{ci,\max}} \tag{3.30}$$

$$v_{ci,\max} = \frac{\sqrt{f_c^{'}}}{0.31 + \frac{24w}{a+16}} \tag{3.31}$$

$$v_{co} = \frac{f_{cc}}{30} \tag{3.32}$$

$$f_{cc} = 1.2f_c^{'} \tag{3.33}$$

- w: Average crack width, in millimetres.
- v_{ci}: Local shear stress on the crack, in MPa units.
- $v_{ci,max}$: Maximum local shear stress on the crack, in MPa units.
- a: Maximum aggregate size, in millimetres.

3.6.2 Constant rotation lag model

The constant rotation lag models relate the post-cracking rotation of the principal stress field to the post-cracking rotation of the principal strain field using a rotation lag (Wong and Vecchio 2002: 86):

$$\Delta\theta_\sigma = \begin{cases} \Delta\theta_\varepsilon & ; |\Delta\theta_\varepsilon| \le \theta^l \\ \Delta\theta_\varepsilon - \theta^l & ; |\Delta\theta_\varepsilon| > \theta^l \end{cases} \tag{3.34}$$

- $\Delta\theta_\sigma$: Post-cracking rotation of the principal stress field.
- $\Delta\theta_\varepsilon$: Post-cracking rotation of the principal strain field.
- θ^l: Specified rotation lag. It is assigned a value of 10° for unreinforced elements, 7.5° for uniaxially reinforced elements and 5° for biaxially reinforced elements.

The shear slip strain is then computed with the following expressions:

$$\theta_\sigma = \theta_{ic} + \Delta\theta_\sigma \tag{3.35}$$

$$\gamma_s^b = \gamma_{xy} Cos2\theta_\sigma + (\varepsilon_{yy} - \varepsilon_{xx}) Sin2\theta_\sigma \tag{3.36}$$

- θ_σ: Inclination of the principal stress field.
- θ_{ic}: Inclination of the principal stress field at cracking.
- γ_{xy}: Total shear strain.
- ε_{xx}: Total axial strain in the x-direction.
- ε_{yy}: Total axial strain in the y-direction.

3.7 Models for reinforcement

The constitutive models for steel use nonlinear functions relating stresses and strains. Effect of strain hardening is considered (Wong and Vecchio 2002: 98).

3.7.1 Stress-strain response

The model used for the monotonic stress-strain response of the reinforcement is the ductile steel reinforcement model. The response is trilinear, consisting of a linear-elastic response, a yield plateau, and a linear strain-hardening phase until rupture:

Figure 3.3 Reinforcement compression and tension response

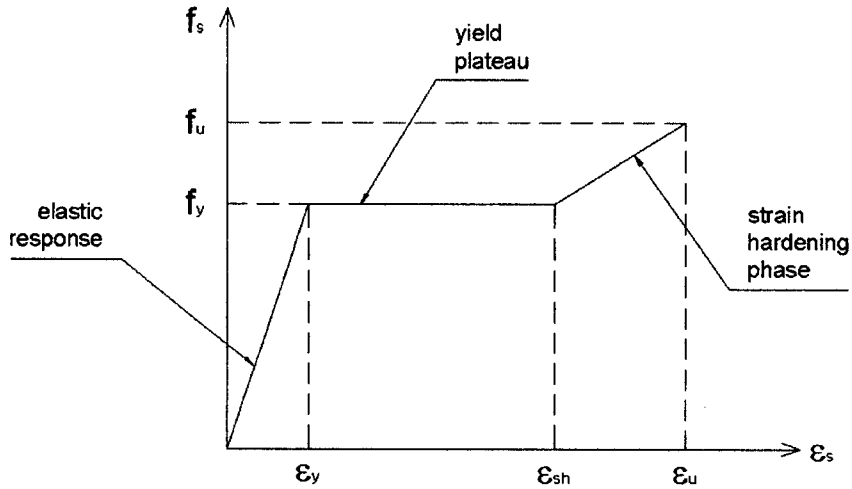

The reinforcement stress, both in tension and compression, is given by the following expression (Wong and Vecchio 2002: 98 – 99):

$$f_s = \begin{cases} E_s \varepsilon_s & ; |\varepsilon_s| \le \varepsilon_y \\ f_y & ; \varepsilon_y < |\varepsilon_s| \le \varepsilon_{sh} \\ f_y + E_{sh}(\varepsilon_s - \varepsilon_{sh}) & ; \varepsilon_{sh} < |\varepsilon_s| \le \varepsilon_u \\ 0 & ; \varepsilon_u < |\varepsilon_s| \end{cases} \tag{3.37}$$

$$\varepsilon_y = \frac{f_y}{E_s} \tag{3.38}$$

$$\varepsilon_u = \varepsilon_{sh} + \frac{f_u - f_y}{E_{sh}} \tag{3.39}$$

- f_s: Reinforcement stress.
- E_s: Initial tangent stiffness or elastic modulus of reinforcement.
- ε_s: Reinforcement strain.
- ε_y: Yield strain.
- ε_{sh}: Strain at the onset of strain hardening.
- E_{sh}: Strain hardening modulus.
- ε_u: Reinforcement ultimate strain.
- f_u: Ultimate strength of reinforcement.

3.7.2 Dowel action

Dowel action is the shear resistance offered by reinforcing bars crossing a crack. In VecTor2, dowel action models are used in conjunction with the stress-based slip distortion models for concrete. The shear resistance due to dowel action is calculated as a function of the shear slip at the crack. This shear resistance is then subtracted from the local shear stress on the crack, which reduces the shear slip. The model used to determine the shear resistance due to dowel action is the Tassios model. The following expressions are used to determine the shear resistance (Wong and Vecchio 2002: 103 – 104):

$$V_d = E_s I_z \lambda^3 \delta_s \leq V_{du} \tag{3.40}$$

$$I_z = \frac{\pi d_b^2}{64} \tag{3.41}$$

$$\lambda = \sqrt[4]{\frac{k_c d_b}{4 E_s I_z}} \tag{3.42}$$

$$k_c = \frac{127 c_b \sqrt{f_c'}}{d_b^{2/3}} \tag{3.43}$$

$$V_{du} = 1.27 d_b^2 \sqrt{f_c' f_y} \tag{3.44}$$

$$v_d = \frac{\rho_s V_d}{A_s} \tag{3.45}$$

- V_d: Dowel force.
- I_z: Moment of inertia of the reinforcement.
- λ: Parameter that compares the stiffness of the concrete to the stiffness of the reinforcing bar.
- V_{du}: Ultimate dowel force.
- k_c: Stiffness of the notional concrete foundation.
- c_b: Coefficient used to reflect bar spacing, it is assigned a value of 0.8.
- v_d: Shear resistance due to dowel action.
- ρ_s: Reinforcement ratio.
- A_s: Area of reinforcement.

CHAPTER 4: COMPARISON OF ANALYTICAL PREDICTIONS WITH ISOLATED WALL TEST RESULTS

4.1 Scope of analysis

Program VecTor2 was used to analyze isolated walls specimens that have been previously tested. The analytical predictions were compared with the test results available in order to see how well VecTor2 predicts the response of these members. In particular, the curvature distribution and the strain profile at critical sections were examined, since these results were then used to estimate plastic hinge lengths. The objective of this analysis was to test the validity of the results provided by VecTor2, so that the program can then be used to perform a parametric study of concrete walls. Also, the actual curvature distributions and strain profiles were investigated.

Two wall specimens were analyzed. The first is a high-rise shear wall tested at the University of British Columbia in 2000 (Adebar, Ibrahim and Bryson 2004). The second is one of the rectangular shear walls tested at Clarkson University in 1995 (Thomsen and Wallace 1995); the wall analyzed is the rectangular specimen RW2 (see Section 2.24).

4.2 High-rise shear wall tested at the University of British Columbia

A test was conducted on a large-scale model of a slender reinforced concrete cantilever shear wall from the core of a high-rise building at the University of British Columbia in 2000 by Adebar, Ibrahim and Bryson. The wall had an aspect ratio of 7.2, had a flanged cross-section, had a low amount of vertical reinforcement, and was subjected to a constant compressive axial load. The purpose of this test was to investigate the influence of cracking on the effective stiffness of the wall used for seismic analysis. Extensive concrete strains measurements were made at the faces of the wall over the cracked region (Adebar, Ibrahim and Bryson 2004: 1 – 2).

4.2.1 Description of the wall specimen

The specimen was a 1/4 scale model of a typical wall from a high-rise building. It was 12200mm high and 1625mm long, with a flanged cross-section. The web was 1219mm long and 127mm thick, and the two flanges were 203mm long and 380mm thick (Adebar, Ibrahim and Bryson 2004: 4 – 5).

The reinforcement was arranged symmetrically. The vertical reinforcement in the two flanges consisted of 5-10M reinforcing bars enclosed by 10M ties, spaced at 64mm in the lower 3m of the wall

and then spaced at 152mm over the remaining height of the wall. The vertical reinforcement in each flange was arranged in two layers, the exterior layer had three bars and the other layer had two bars. The clear cover of the ties was 6mm. The web had 10M reinforcing bars spaced at 305mm, vertically and horizontally. A total of four bars were used in the web.

High-rise buildings typically have large perimeter walls below grade that are much larger than the tower walls. These are connected together by diaphragm action of the concrete slabs. Because of this, the section where the maximum bending moment occurs in the tower walls is usually at grade level, and there is no pullout of the vertical reinforcement from the foundation. To simulate this effect, the critical section was located at 426mm from the base, providing additional vertical reinforcement below a construction joint at this location (Adebar, Ibrahim and Bryson 2004: 5).

The wall specimen was tested in a horizontal position because of the limited height of the laboratory. The base of the wall was post-tensioned to the floor to prevent movement during the test (Adebar, Ibrahim and Bryson 2004: 5 – 6).

The average cylinder compressive strength was 49 MPa at the time of testing. The average yield strength of the reinforcing steel was 455 MPa, and the average ultimate strength was 650 MPa. The stress-strain response from four bar samples was measured, the yield plateau was very short (Adebar, Ibrahim and Bryson 2004: 6).

4.2.2 Instrumentation

A cyclic lateral load was applied at the top of the wall by a hydraulic actuator. Dywidag bars were used to apply a uniformly distributed axial compression load. The wall displacement at the top was measured using linear variable differential transducers. Displacement transducers were also provided to measure movement of the base of the wall (Adebar, Ibrahim and Bryson 2004: 6 – 7).

Twelve metal targets were glued to the concrete surface over the lower 5.08m of the wall height along each face to measure average concrete strains. Targets named TE1 to TE12 were located at the east face, and targets named TW1 to TW12 were located at the west face. The relative vertical displacements of the targets were measured with a large digital calliper. On each side of the wall, 10 targets located above the construction joint (TE3 to TE12 and TW3 to TW12) were used to measure strains over the cracked region. Targets TE3 and TW3 were located 59mm above the construction joint, and the rest were spaced at 500mm approximately. The two bottom targets located below the construction joint were more

closely spaced. Targets TE2 and TW2 were located 134mm below the construction joint, and targets TE1 and TW1 were located just above the base (Adebar, Ibrahim and Bryson 2004: 32).

4.2.3 Test procedure

A constant compressive axial load of $0.1A_g f'_c$, equal to 1500 kN, was applied to the wall during the test. This load was applied through two hydraulic actuators located below the base of the wall that pulled the Dywidag bars.

The cyclic lateral load at the top was applied at 11.76m from the base of the wall; that is, 11.33m from the construction joint. The wall was subjected to 13 displacement levels, which varied from 15 to 300mm. East was considered the positive direction of loading, and west the negative direction of loading. At each displacement level, four complete displacement cycles (zero, then maximum positive, then maximum negative, and finally zero) were performed (Adebar, Ibrahim and Bryson 2004: 6 – 7).

4.2.4 Test results

The test results were used to determine curvature distributions along the height of the wall for different lateral displacement levels. The curvatures were determined from the axial strains at the faces of the wall, which were determined from the measured relative axial displacements of the targets. The lateral displacements were corrected so that they did not include the effect of the base rotation. Although the authors determined experimental curvatures for the wall, the curvatures presented in this section were recalculated from the original measured data, and differ from the results reported by the authors.

During the test, some rotation at the base of the wall was measured. The total displacements included the lateral displacement component (wall displacement) and the rigid body motion of the wall due to base rotation (Adebar, Ibrahim and Bryson 2004: 8). Measurements from displacement transducers at the base were used to determine displacements due to base rotation to separate these two components. For each total displacement level, the corresponding wall displacement in each direction of loading was different (Adebar, Ibrahim and Bryson 2004: 27).

The first cracking in the wall occurred at a wall displacement of 21mm (total displacement of 30mm) in the positive direction, and yielding of the vertical reinforcement at the construction joint occurred at a wall displacement of 46mm (total displacement of 60mm) in the positive direction (Adebar, Ibrahim and Bryson 2004: 9). The maximum wall displacement was 281mm (total displacement of 300mm) in the positive direction (Adebar, Ibrahim and Bryson 2004: 11).

The relative axial displacements of the targets in the compression and tension face of the wall were measured at the peak displacement of the first cycle for each wall displacement level. The difference between the vertical distance between targets at a particular displacement level and the initial vertical distance between targets (zero reading), divided by this initial distance, gives the average axial strain over that length at the faces of the wall for that displacement level. Then, the difference between the compression and tension strain, divided by the wall length between the two faces, gives the average curvature over the length between targets (Adebar, Ibrahim and Bryson 2004: 12 – 13). This procedure was used to calculate the curvature distribution at total displacement levels of 120, 150 and 200mm; for which the corresponding wall displacement levels were the following:

- Wall displacements of 105, 132 and 182mm, respectively; in the east (positive) direction of loading.
- Wall displacements of 104, 138 and 187mm, respectively; in the west (negative) direction of loading.

A significant portion of the concrete cover fell off at a total displacement level of 300mm and some targets were lost, so the curvature distribution could not be determined for this displacement level (Adebar, Ibrahim and Bryson 2004: 14).

Regarding the zero readings, several target measurements were made before and after the axial compression was applied. The average of all these readings was taken as the zero reading used in the calculations. Measurements that were significantly out of range were neglected to determine the zero readings.

Figure 4.1 shows the experimental curvature distributions for the wall displacement levels mentioned in the east direction:

Figure 4.1 Experimental curvatures (pushing east) for different wall displacement levels

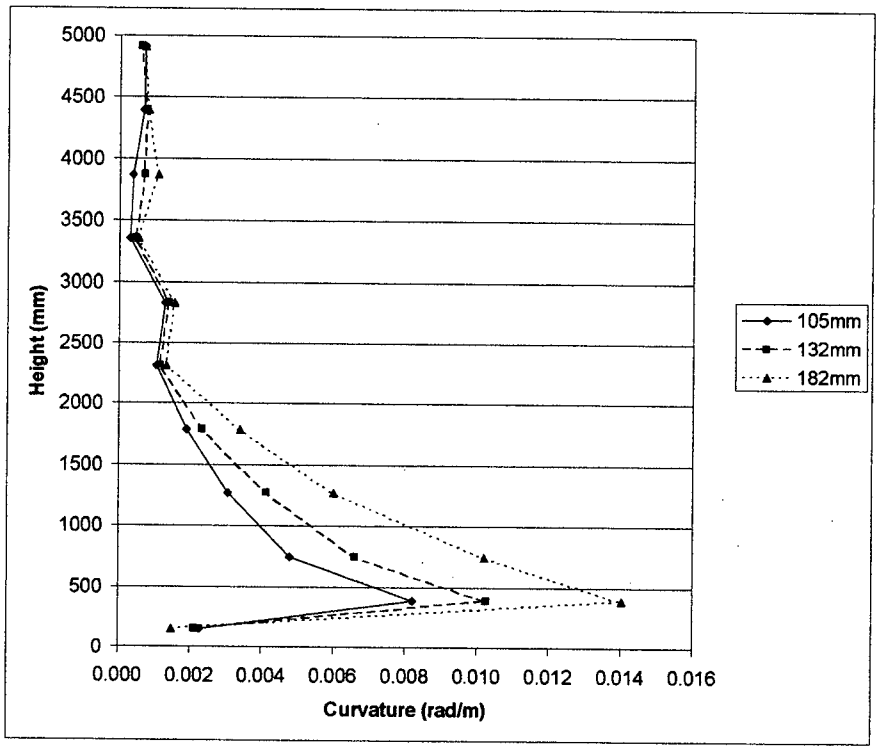

Figure 4.2 shows the experimental curvature distributions for the wall displacement levels mentioned in the west direction:

Figure 4.2 Experimental curvatures (pushing west) for different wall displacement levels

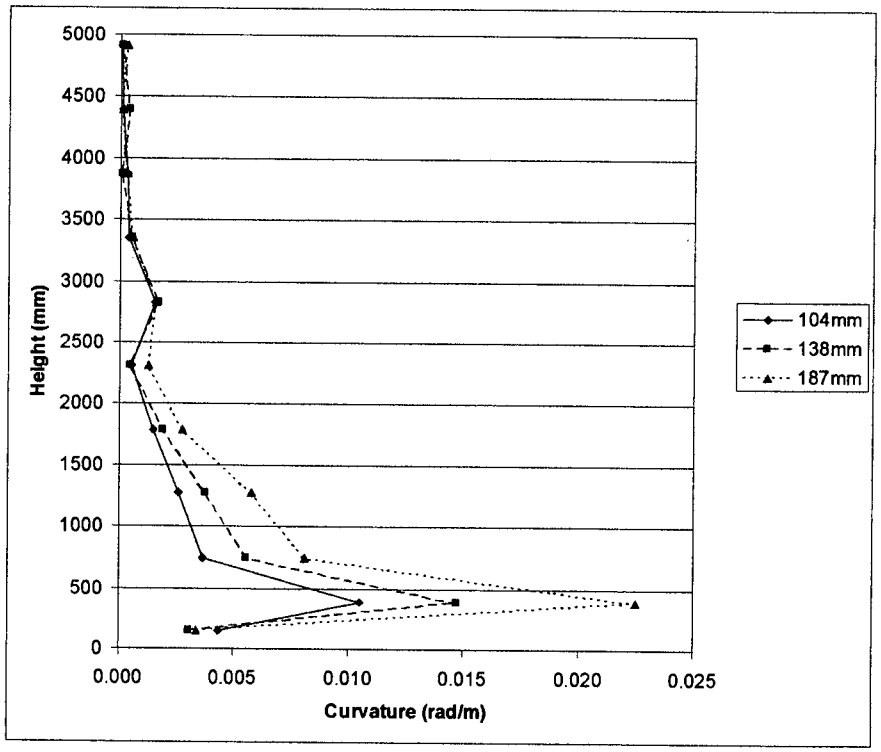

As expected, the maximum curvature is located at the construction joint; that is, at approximately 426mm from the base. There were differences between the curvatures for both directions of loading; these become very significant near the construction joint for the higher displacement levels. This is because the wall was first pushed to the east and then to the west, so the crack pattern was not symmetrical (Adebar, Ibrahim and Bryson 2004: 10).

An experimental moment-curvature relationship for the wall was developed by the authors, in order to estimate the yield curvature. The yield curvature was taken as the curvature prior to the yield plateau, which was approximately equal to 0.002 rad/m (Adebar, Ibrahim and Bryson 2004: 15).

4.2.5 Analytical model of the wall specimen

The prototype wall was modeled and analyzed using program VecTor2. The purpose of this analysis is to predict the curvature distribution along the height of the wall and compare these predictions with the experimental results. The strain profile along the length of the wall was also studied. Low-powered rectangular and triangular elements were used to model the concrete, with smeared steel to account for the presence of reinforcement. The constitutive models for concrete and steel described in Chapter 3 were used in the analysis.

Three different material types were used to represent various regions of the wall in the finite element model:

- The first material type was used to represent the flanges in the lower 3m of the wall, in which the ties were spaced at 64mm.
- The second material type was used to represent the web of the wall.
- The third material type was used to represent the flanges over the remaining height of the wall, in which the ties were spaced at 152mm.

As described in Section 4.2.1, the wall had a construction joint at 426mm from the base; and the maximum curvature occurs at this location, as shown in Figure 4.1 and 4.2. For this reason, the wall was modeled from the construction joint upwards. The horizontal and vertical displacements at the bottom in the analytical model were restrained.

The finite element mesh was more refined near the base (critical section), in order to have a good representation of the strain profile along the length of the wall. The mesh was refined in such a way that the position of certain nodes coincides with the position of the targets. Meshes of 68×59, 68×87, 87×59

and 87×87 rectangular elements were used; 20 elements (21 nodes) were used in the transverse direction of the wall. This level of refinement was maintained up to approximately half the height of the wall. Up from this point, 16 elements (17 nodes) were used in the transverse direction, and then it was further reduced to eight elements (nine nodes) up to the top of the wall. The transitions were made using triangular elements. All nodes and elements were numbered in the horizontal (short) direction. The complete mesh consisted of 1487 nodes, 1360 rectangular elements and 60 triangular elements.

The material properties used in the analysis were those reported in the description of the wall specimen, presented in Section 4.2.1. For the material properties that were not measured during the test, the values given by default in program VecTor2 were used. For the concrete properties, VecTor2 uses the following expressions to determine the tensile strength, the initial tangent elastic modulus and the cylinder strain at f'_c (Wong and Vecchio 2002: 146):

$$f'_t = 0.33\sqrt{f'_c} \tag{4.1}$$

$$E_c = 5500\sqrt{f'_c} \tag{4.2}$$

$$\varepsilon_o = 1.8 + 0.0075 f'_c \tag{4.3}$$

Where f'_c, f'_t and E_c are in MPa units, and ε_o is in mm/m. The maximum aggregate size given by default is 10mm. For the reinforcement properties, a modulus of elasticity of 200000 MPa was considered; while the strain hardening modulus and the strain at the onset of strain hardening were determined from the measured stress-strain curve.

A monotonic lateral load was applied at the top of the wall. This load was applied in a displacement-control mode, in increments of 0.2mm. Although the actual wall was subjected to cyclic loading, applying a monotonic load seems reasonable, since the envelopes for the monotonic and cyclic response were almost the same. Additionally, the constant axial load of 1500 kN was applied; this load was equally distributed among all the nine nodes at the top. The self-weight of the wall was not considered.

Figure 4.3 shows the finite element model of the wall specimen, created in the pre-processor FormWorks:

Figure 4.3 Finite element model of UBC wall in FormWorks

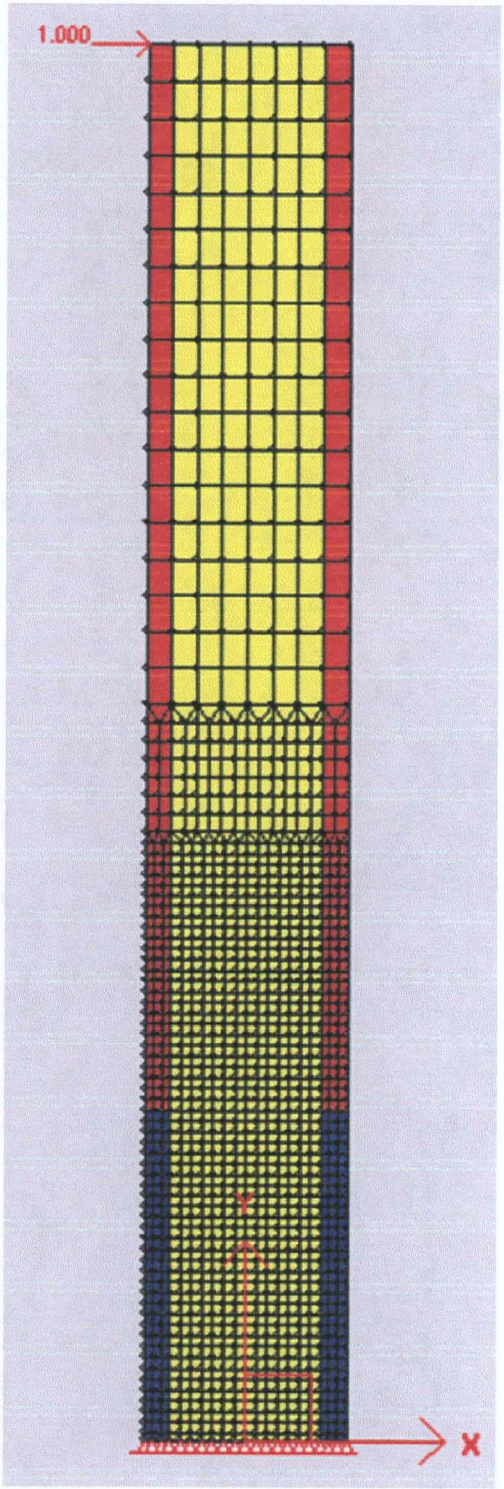

Table 4.1 shows the material properties in the different regions of the wall:

Table 4.1 Material properties of UBC wall model

Concrete properties	**Material 1**		**Material 2**		**Material 3**	
Color						
Thickness (mm)	380		127		380	
Cylinder compressive strength (MPa)	49		49		49	
Reinforcement component properties	***x*-direction**	***y*-direction**	***x*-direction**	***y*-direction**	***x*-direction**	***y*-direction**
Reinforcement ratio (%)	0.831	0.65	0.259	0.259	0.346	0.65
Reinforcement diameter (mm)	10	10	10	10	10	10
Yield strength (MPa)	455	455	455	455	455	455
Ultimate strength (MPa)	650	650	650	650	650	650
Elastic modulus (MPa)	200000	200000	200000	200000	200000	200000
Strain hardening modulus (MPa)	4875	4875	4875	4875	4875	4875
Strain hardening strain (mm/m)	10	10	10	10	10	10

4.2.6 Analytical results

The analytical predictions obtained from program VecTor2 were used to determine curvature distributions along the height of the wall for different lateral displacement levels. The curvatures were determined the same way as it was done for the experimental results in order to make comparisons, using the vertical nodal displacements at the faces of the wall obtained from the analysis. Since the model of the wall was fixed at the base, the total displacement and wall displacement are the same.

As previously described, the position of certain nodes at the faces of the wall coincides with the position of the targets. The vertical nodal displacements at these particular nodes were used to calculate the curvatures. The difference in vertical displacements between two consecutive nodes at the face, divided by the vertical distance between these nodes, gives the average axial strain over that length. Then, the difference between the compression and tension strain, divided by the wall length between the two faces, gives the average curvature over the length between nodes. The curvature distribution was determined for the following wall displacement levels:

- Wall displacements of 105, 132 and 182mm; to be compared with experimental curvatures when the wall is pushed in the east direction.
- Wall displacements of 104, 138 and 187mm; to be compared with experimental curvatures when the wall is pushed in the west direction.

This way, the experimental and analytical average curvatures were calculated over the same lengths. The only exception is near the construction joint, due to the fact that for the analysis, the wall was modeled from the construction joint upwards. Therefore, the analytical curvature at this location was calculated for a shorter length than for the experimental curvature; this length goes from the location of the construction joint to the location of targets TE3 and TW3, located 59mm above the construction joint.

4.2.7 Comparison of experimental and analytical results

Figure 4.4 to 4.9 show comparisons between the experimental and analytical curvature distributions for the wall displacement levels mentioned. Note that the vertical axis shows the distance from the construction joint, not the height of the wall:

Figure 4.4 Experimental (pushing east) and analytical curvatures for a wall displacement of 105mm

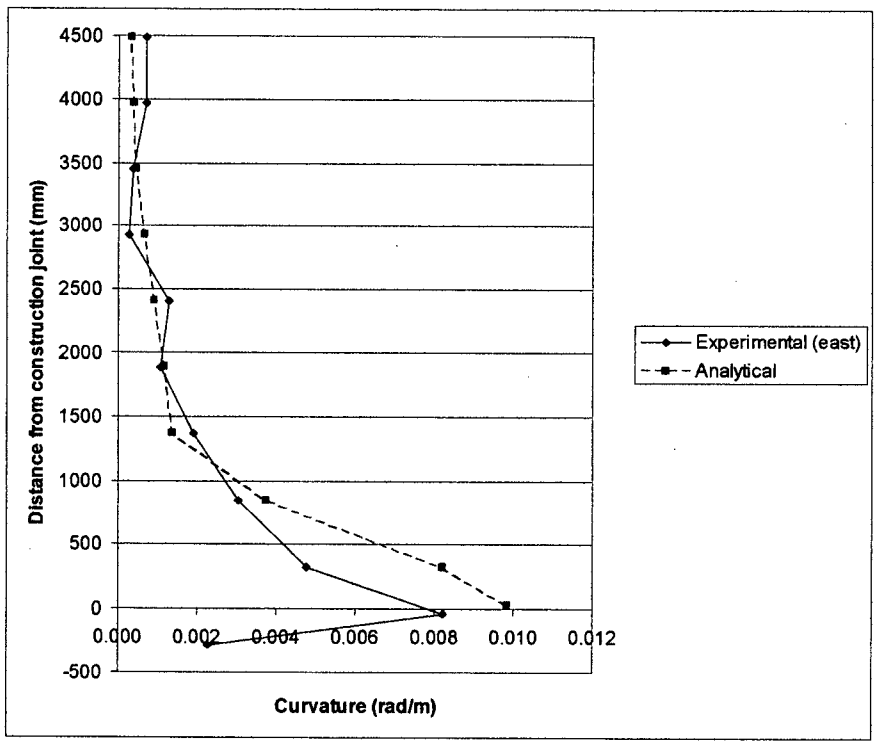

Figure 4.5 Experimental (pushing west) and analytical curvatures for a wall displacement of 104mm

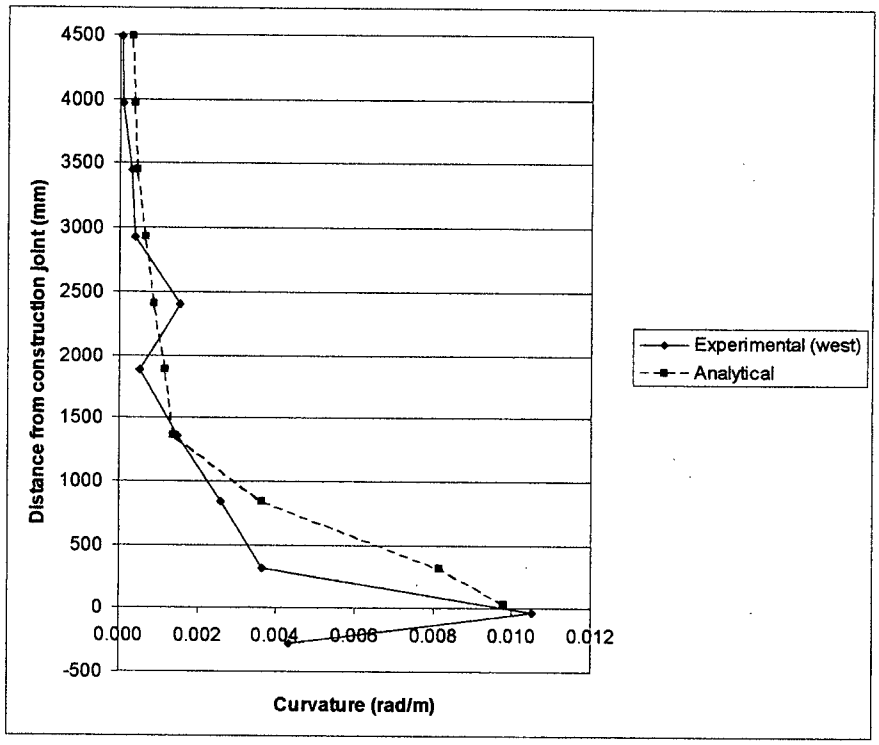

Figure 4.6 Experimental (pushing east) and analytical curvatures for a wall displacement of 132mm

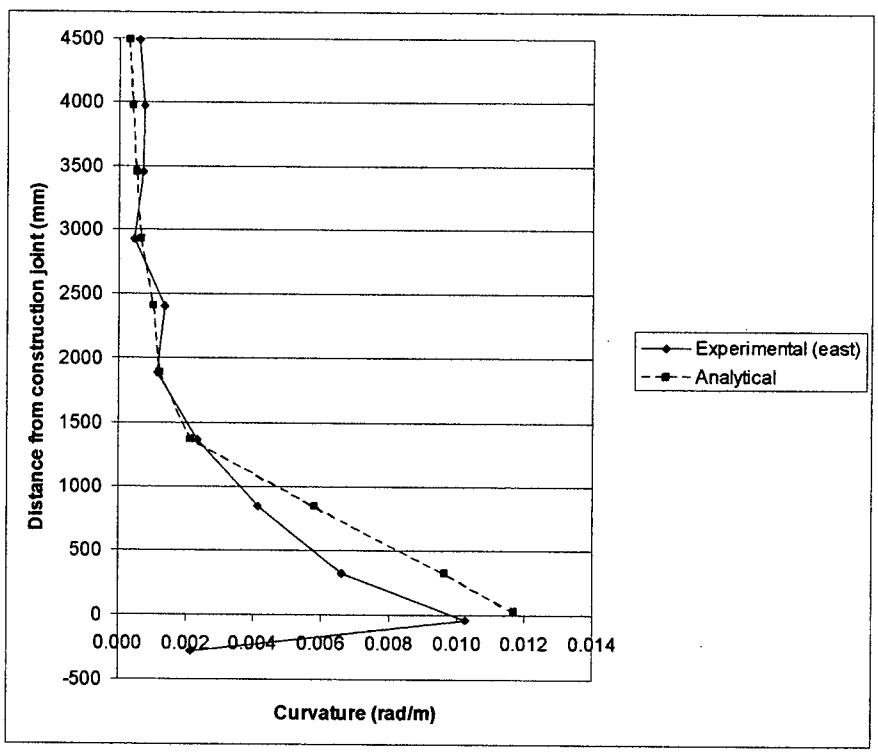

Figure 4.7 Experimental (pushing west) and analytical curvatures for a wall displacement of 138mm

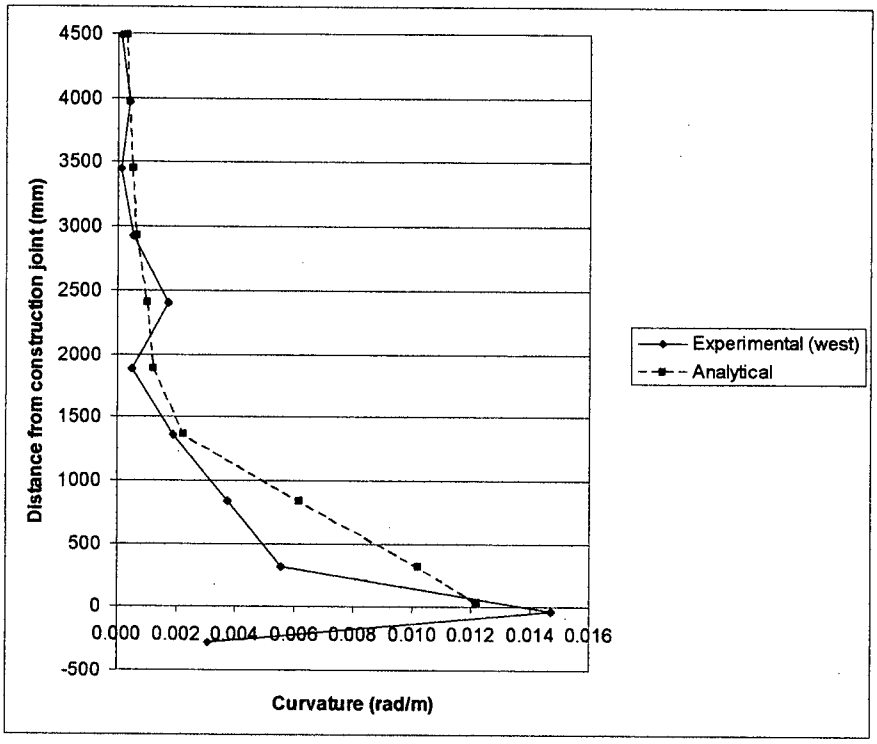

Figure 4.8 Experimental (pushing east) and analytical curvatures for a wall displacement of 182mm

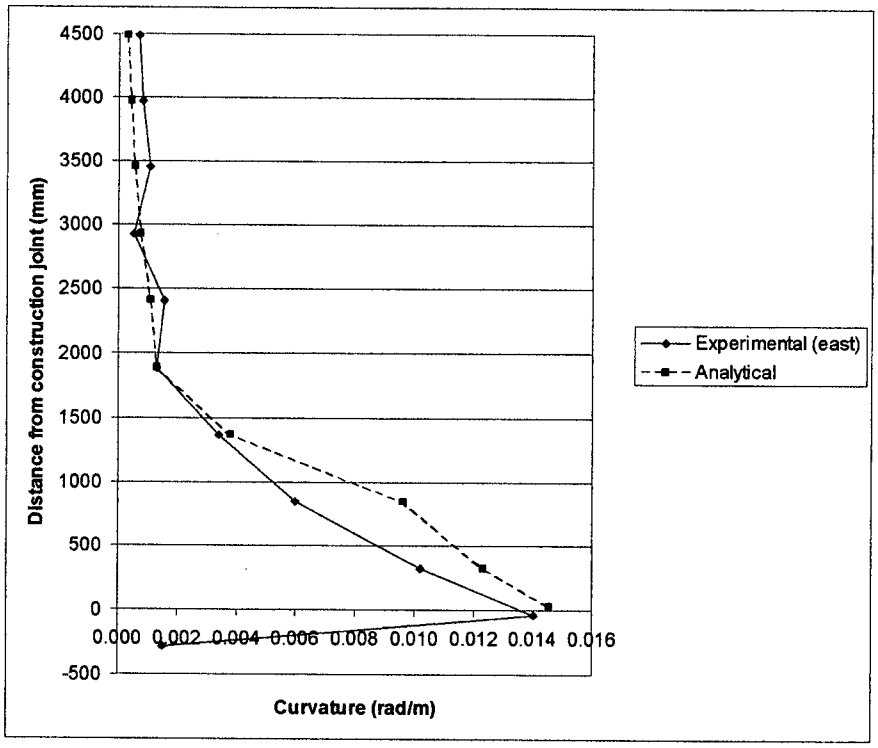

Figure 4.9 Experimental (pushing west) and analytical curvatures for a wall displacement of 187mm

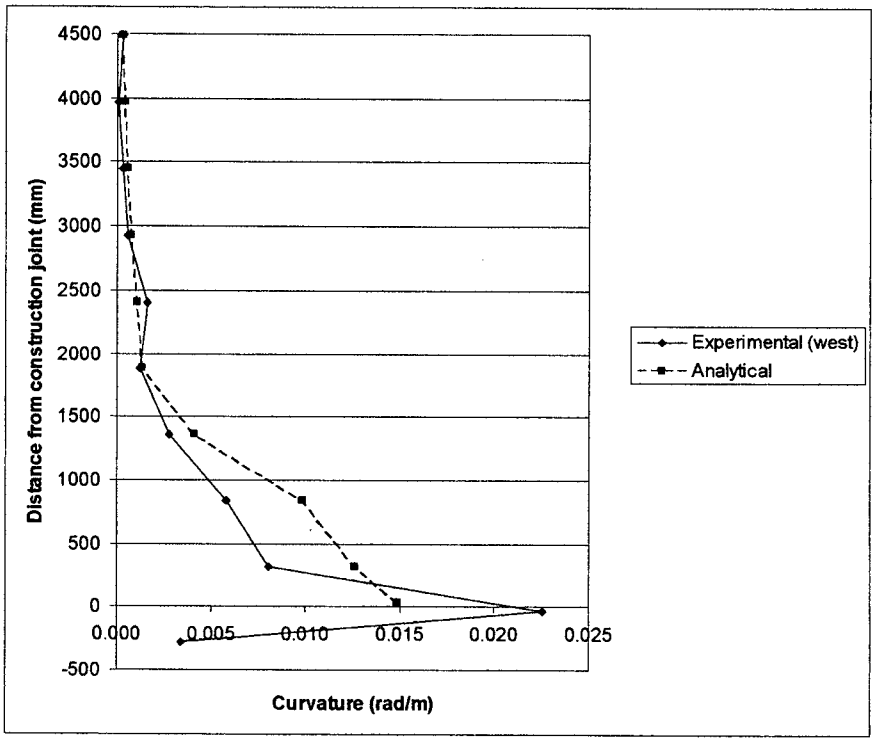

There is a good agreement between the experimental and analytical curvatures prior to yielding for most wall displacement levels. For the higher wall displacement levels, there is a better agreement between the analytical curvatures and the experimental curvatures in the east direction, than with the experimental curvatures in the west direction. A reason for these discrepancies is that the model was constructed from the construction joint upwards and it was fixed at the base, so it is stiffer than the actual wall. Despite these differences, the analytical model seems to predict reasonably well the curvature distribution of the wall.

4.2.8 Equivalent plastic hinge length

The models presented in Chapter 2 will be used to compute the equivalent plastic hinge length for the test wall, in order to compare the results obtained and see how accurate these models are. The relevant wall parameters required for these calculations are shown in Table 4.2:

Table 4.2 UBC wall parameters

Parameter	Symbol	Value
Height of wall (m)	$L_s = H_w$	11.33
Horizontal length of wall (m)	$h = l_w$	1.625
Bar diameter of tension reinforcement (mm)	d_b	10
Yield stress of tension reinforcement (MPa)	f_y	455
Concrete cylinder compressive strength (MPa)	f'_c	49
Axial load (kN)	P	1500
Gross area of cross-section (mm^2)	A_g	309093

Baker and Amarakone's equation for unconfined concrete was used (Equation 2.12). Regarding Mattock's equation (Equation 2.26), the second term in parenthesis was neglected, since the wall has the same amount of reinforcement in both flanges ($\rho = \rho'$). Regarding the bounds proposed by the ACI-ASCE Committee 428 (Equation 2.30), since the plastic hinge length is being calculated at failure, the maximum moment is equal to the ultimate moment ($R_m = 1$). In the equation proposed by Sasani and Der Kiureghian (Equation 2.41), the mean values of the model parameters were used, and the model error term was not included ($\xi_L = 0$). Panagiotakos and Fardis' equation for cyclic loading was used (Equation 2.46), and the second term in the equation was neglected, as it was considered that no significant slippage occurred ($a_{sl} = 0$). Other required parameters in the calculations are presented in Table 4.3:

Table 4.3 Parameters required in plastic hinge length models

Parameter	Symbol	Value	Comments
Effective depth (m)	d	1.3	Calculated as $0.8l_w$, according to CSA A23.3
Area of reinforcement (mm^2)	A_s	1400	14-10M bars in the wall
Area of concrete (mm^2)	A_c	307693	
Axial compressive strength without bending moment (kN)	P_u	15714	Calculated without using strength reduction factors
Concrete cube strength (MPa)	f_{cc}	58.8	Calculated with equation 3.33
Tension reinforcement factor (Baker and Amarakone's equation)	k_1	0.7	Mild steel
Axial load factor (Baker and Amarakone's equation)	k_2	1.048	Calculated with equation 2.13
Concrete strength factor (Baker and Amarakone's equation)	k_3	0.411	Calculated with equation 2.14
Concrete strain in extreme compression fiber at yield curvature	ε_{ce}	0.0015	Average of recommended values
Concrete strain in extreme compression fiber at ultimate curvature	ε_{cu}	0.0035	According to CSA A23.3
Strain ratio (ACI-ASCE equation)	R_ε	1.25	Calculated with equation 2.31

The equivalent plastic hinge length can also be determined experimentally from the test results available. Although the authors determined experimental plastic hinge lengths, the one presented in this

section was recalculated from the measured data, and differs from the results reported by the authors. In Equation 2.6, setting $L = H_w$, $\Delta = \Delta_u$ and $\phi = \phi_u$, this equation becomes:

$$\Delta_u = \Delta_y + (\phi_u - \phi_y) L_p \left(H_w - \frac{L_p}{2} \right) \tag{4.4}$$

Solving Equation 4.4 for L_p:

$$L_p = H_w - \sqrt{H_w^2 - 2\left(\frac{\Delta_u - \Delta_y}{\phi_u - \phi_y} \right)} \tag{4.5}$$

As it was mentioned in Section 4.2.4, the maximum wall displacement was 281mm, the wall yield displacement was 46mm, and the yield curvature was 0.002 rad/m. Because some targets were lost at the ultimate displacement level, the ultimate curvature could not be determined experimentally. Therefore, a plane sections analysis of the wall was performed to predict the ultimate curvature. The analysis was done considering an elasto-plastic stress-strain curve for steel, the concrete cylinder strength, a concrete ultimate strain of 0.0035, a compressive axial load of 1500 kN, the CSA A23.3 stress block for concrete in compression, and strength reduction factors of unity. The estimated curvature capacity was 0.0236 rad/m. Using all these values in Equation 4.5, the equivalent plastic hinge length was 1m or $0.62 l_w$.

The predictions obtained are summarized in Table 4.4:

Table 4.4 Comparison of equivalent plastic hinge length models

Researchers reference	Equation	L_p (m)	L_p/l_w
Baker and Amarakone (1964)	Eq. 2.12	0.67	0.41
Sawyer (1964)	Eq. 2.22	1.17	0.72
Mattock (1964)	Eq. 2.26	2.19	1.35
Corley (1966)	Eq. 2.28	0.97	0.60
Mattock (1967)	Eq. 2.29	1.22	0.75
ACI-ASCE lower bound (1968)	Eq. 2.30	0.83	0.51
ACI-ASCE upper bound (1968)		2.23	1.37
Zahn, Park and Priestly (1986)	Eq. 2.34	0.64	0.40
Priestly and Park (1987)	Eq. 2.36	0.97	0.59
Paulay and Priestly (1992)	Eq. 2.37	1.01	0.62
Paulay and Priestly (1993)	Eq. 2.38	2.34	1.44
Sasani and Der Kiureghian (2001)	Eq. 2.41	0.75	0.46
Panagiotakos and Fardis (2001)	Eq. 2.46	1.36	0.84
CSA A23.3		0.81	0.50
Experimental		1.00	0.62

Figure 4.10 shows these results graphically:

Figure 4.10 Comparison of equivalent plastic hinge length models

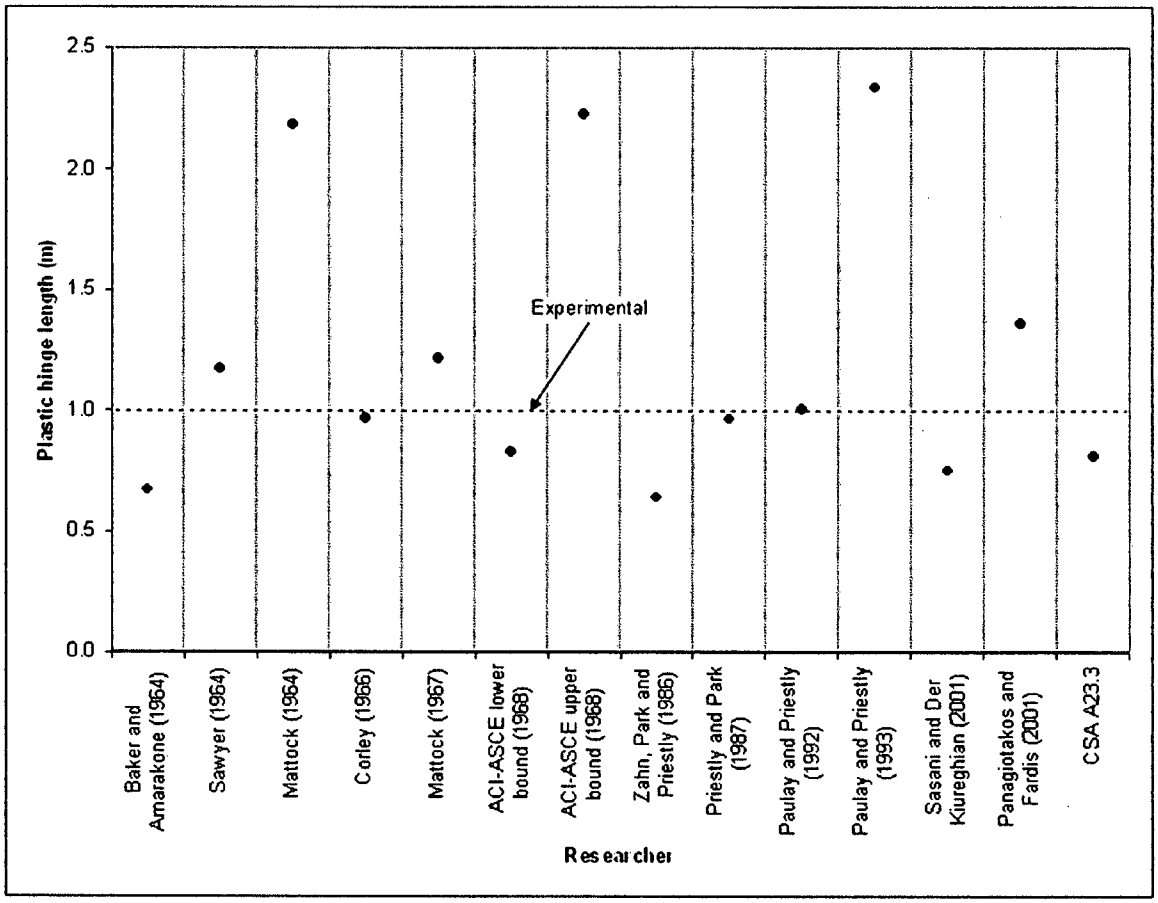

The results obtained using the models for plastic hinge length presented in Table 4.4 vary from $0.4l_w$ to $1.44l_w$. The plastic hinge length given by the code is also presented. Most of these equations estimate a plastic hinge greater than the one given by the code; therefore, the code is conservative compared to most of these. The plastic hinge length obtained experimentally is also larger than the one predicted by the code.

Comparing the experimental and predicted results from Figure 4.10, the equations of Mattock (1964), ACI-ASCE upper bound (1968) and Paulay and Priestly (1993) significantly overestimate the plastic hinge length. The equations of Sawyer (1964), Mattock (1967) and Panagiotakos and Fardis (2001) also overestimate it, but by a smaller margin. The equations of Baker and Amarakone (1964), ACI-ASCE lower bound (1968), Zahn, Park and Priestly (1986) and Sasani and Der Kiureghian (2001) underestimate the plastic hinge length. The best predictions are given by the equations of Corley (1966), Priestly and Park (1987) and Paulay and Priestly (1992).

The experimental plastic hinge length is between the bounds proposed by the ACI-ASCE Committee 428. The lower bound gives a better prediction.

The results provided by all these expressions are significantly different. This is because they have been derived from tests for different types of concrete members and consider different parameters. The last three equations in Table 4.4 (Equation 2.38, 2.41 and 2.46) where derived specifically for walls. These, however, are not providing good predictions compared to other equations.

4.2.9 Distribution of inelastic curvatures

Figure 4.4 to 4.9 show the actual distribution of the inelastic curvatures. Since the elastic portion of the curvature was 0.002 rad/m, the inelastic curvatures can be visualized by shifting the vertical axis by this amount. The resulting curvatures suggest that the inelastic curvature over the plastic hinge length are not uniform, as it is commonly assumed; but have a linear variation over a distance equal to approximately the length of the wall (1625mm) measured from the construction joint, which is the critical section (Adebar, Ibrahim and Bryson 2004: 15 – 16). Both the experimental and analytical results are showing this trend.

As seen in Chapter 2, in the classical formulation of plastic hinge analysis, the inelastic curvature is considered to be constant over the equivalent plastic hinge length. This equivalent length is commonly assumed to be $0.5h$ or $0.5l_w$, according to typical concrete codes and several researchers. However, the actual inelastic curvature has a certain variation. The test results and the analytical predictions from this study are suggesting that this variation may be considered linear over a length of $1.0h$ or $1.0l_w$; that is, twice the length normally considered.

If we consider $L_{p,lin}$ to be the plastic hinge length for a linearly varying inelastic curvature, the resulting inelastic displacement at the top of a cantilever wall can be determined from the following formulation:

Figure 4.11 Linearly varying inelastic curvatures

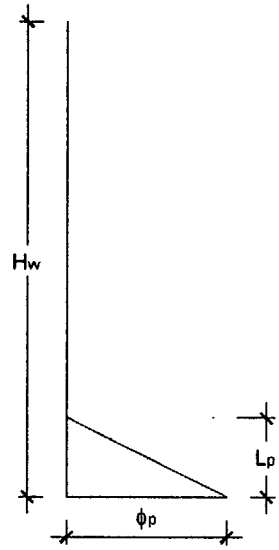

The inelastic rotation can be determined by integrating the inelastic curvatures:

$$\theta_p = \frac{\phi_p L_{p,lin}}{2} \tag{4.6}$$

Considering that the inelastic rotation is concentrated at the centroid of the inelastic curvatures, the inelastic displacement can be expressed as:

$$\Delta_p = \theta_p \left(H_w - \frac{L_{p,lin}}{3} \right) = (\phi - \phi_y) \frac{L_{p,lin}}{2} \left(H_w - \frac{L_{p,lin}}{3} \right) \tag{4.7}$$

If we consider $L_{p,const}$ to be the plastic hinge length for a constant inelastic curvature, and setting $L_{p,lin} = 2L_{p,const}$, Equation 4.7 can be expressed as:

$$\Delta_p = (\phi - \phi_y) L_{p,const} \left(H_w - \frac{2L_{p,const}}{3} \right) \tag{4.8}$$

Compare this inelastic displacement with the one obtained for a uniform inelastic curvature:

$$\Delta_p = (\phi - \phi_y) L_{p,const} \left(H_w - \frac{L_{p,const}}{2} \right) \tag{4.9}$$

If the plastic hinge length is small compared to the height of the wall, both formulations give the same inelastic displacement. However, if this is not the case, the inelastic displacement is greater if a uniform inelastic curvature is considered.

Although many researchers have considered a uniform inelastic curvature to develop their models for plastic hinge length, some have studied the actual curvature distribution in concrete elements. Paulay and Priestly plotted the actual curvature distribution of a prismatic reinforced concrete cantilever element. They showed that the actual extent of plasticity is approximately twice the equivalent plastic hinge length obtained considering a uniform inelastic curvature, and that the actual variation of the inelastic curvature can be reasonably considered as linear; as it was observed in this study (Paulay and Priestly 1992: 139).

In the next chapter, a linearly varying inelastic curvature will be considered to perform a parametric study of concrete walls.

4.2.10 Analysis of strain profiles

So far, the length of the plastic hinge has been obtained from the curvature distribution. The concept of curvature (strain gradient) is based on the hypothesis that plane sections remain plane after bending, which is a widely used engineering assumption. During the test, strain measurements were only made at the faces of the wall, and the curvatures were calculated assuming that the strains along the length of the wall had a linear variation. The analytical curvatures were also determined this way in order to compare results. Since this wall is very slender, it is expected than the actual variation of the strain profile will be close to linear. The average vertical strains in the elements along the length of the wall obtained from program VecTor2 were studied to verify if this assumption is true.

First, we will consider the case where the wall is subjected to a constant compressive axial load only (before applying lateral displacements). It is expected that the strain profile in every cross-section will be constant. Figure 4.12 shows the strain profile at the construction joint:

Figure 4.12 Strain profile at construction joint for the case of no bending

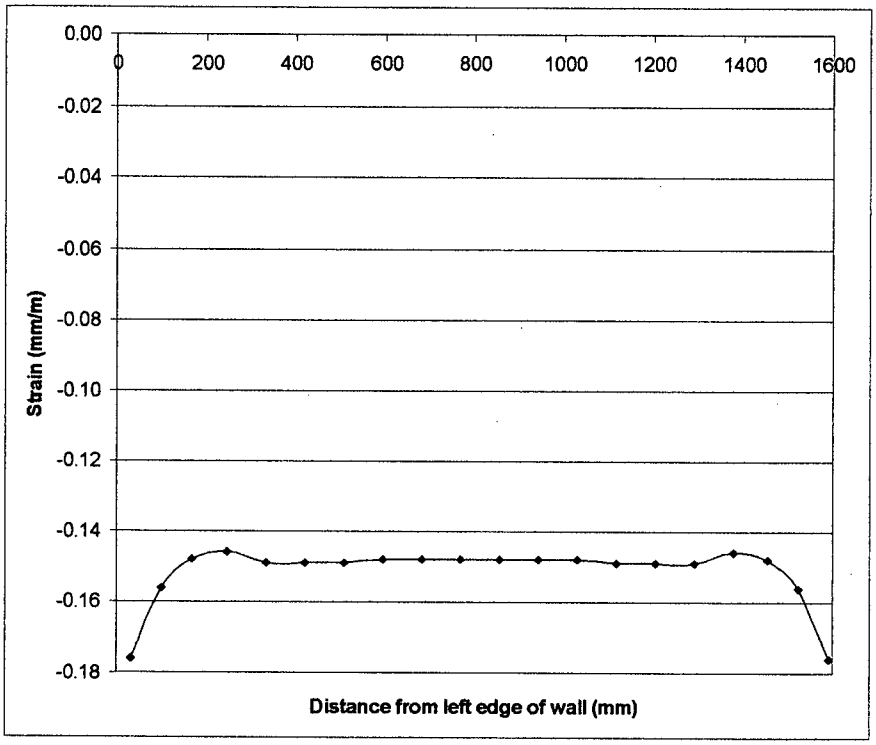

Contrary to what it is expected, the strain profile is not constant. In order to investigate why, the strain profile at a certain distance from the construction joint is shown in Figure 4.13:

Figure 4.13 Strain profile at 319mm from construction joint for the case of no bending

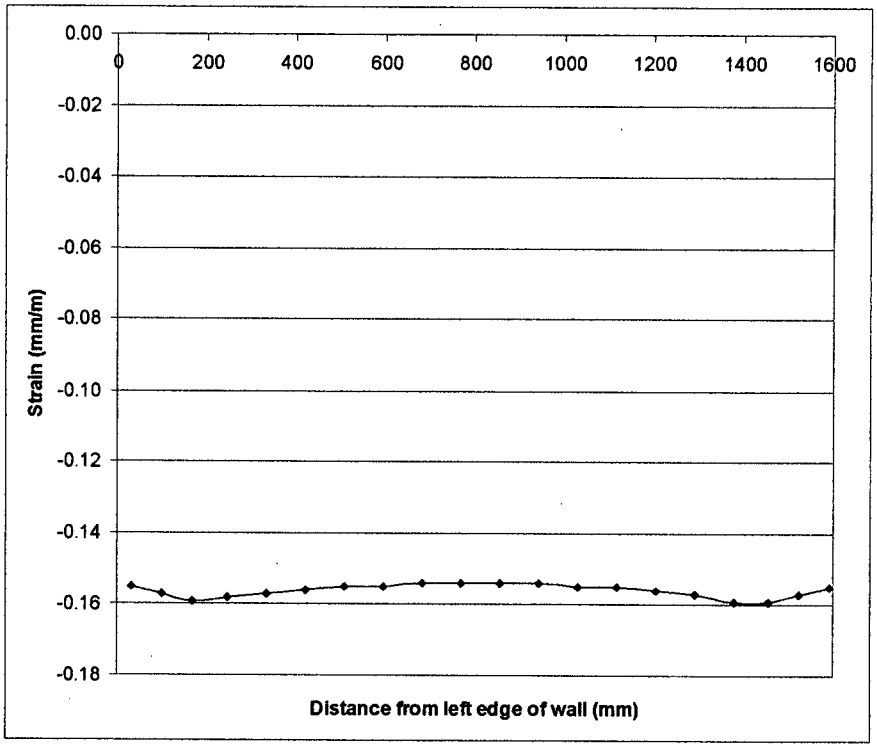

As we get further from the construction joint, the strain profile becomes almost constant. Therefore, the results are distorted near the construction joint due to the boundary conditions of the model.

Figure 4.14 shows the strain profile for a wall displacement of 12.8mm at the construction joint, before cracking occurs:

Figure 4.14 Strain profile at construction joint for a wall displacement of 12.8mm

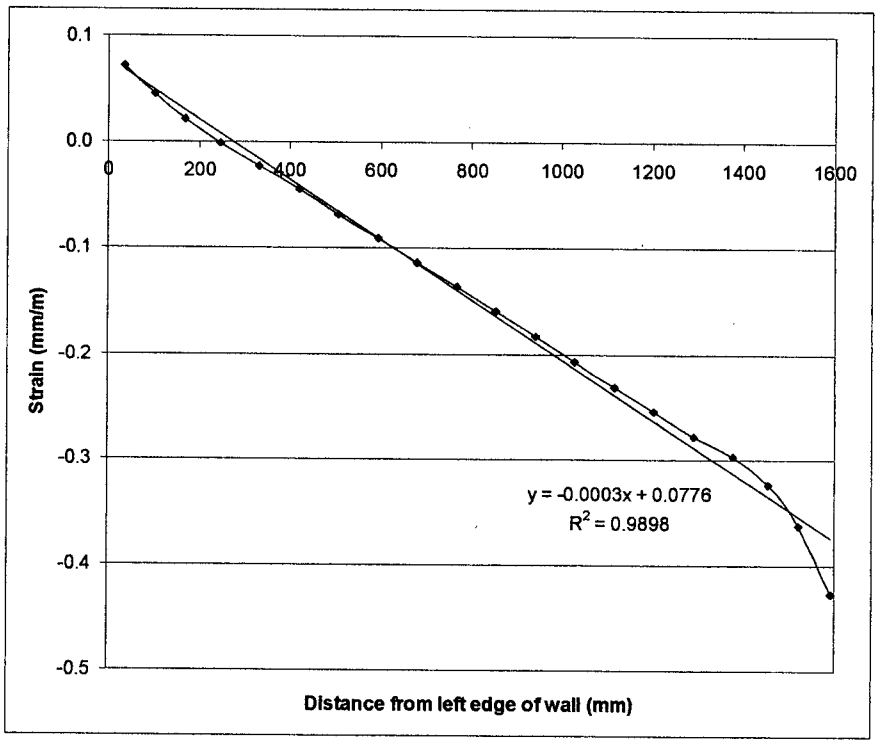

Prior to cracking, the strain profile is almost linear. There are some distortions near the base due to the boundary conditions, as seen previously. A least-squares fit was used to obtain a linear strain profile; the slope of this line is the curvature, in rad/m.

Figure 4.15 shows the strain profile for this wall displacement level at 319mm from the construction joint:

Figure 4.15 Strain profile at 319mm from the construction joint for a wall displacement of 12.8mm

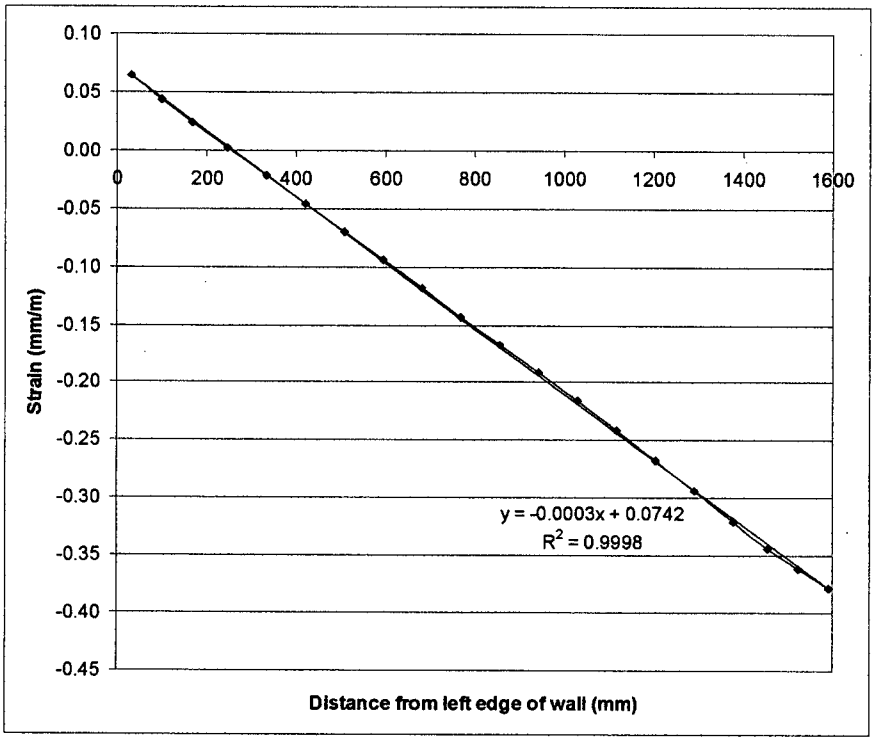

At this distance from the construction joint, the strain profile has practically a perfect linear variation. Therefore, it can be concluded that the strain profiles remain linear before cracking.

Figure 4.16 shows the strain profile for a wall displacement of 25.4mm at the construction joint, after cracking and prior to yielding:

Figure 4.16 Strain profile at construction joint for a wall displacement of 25.4mm

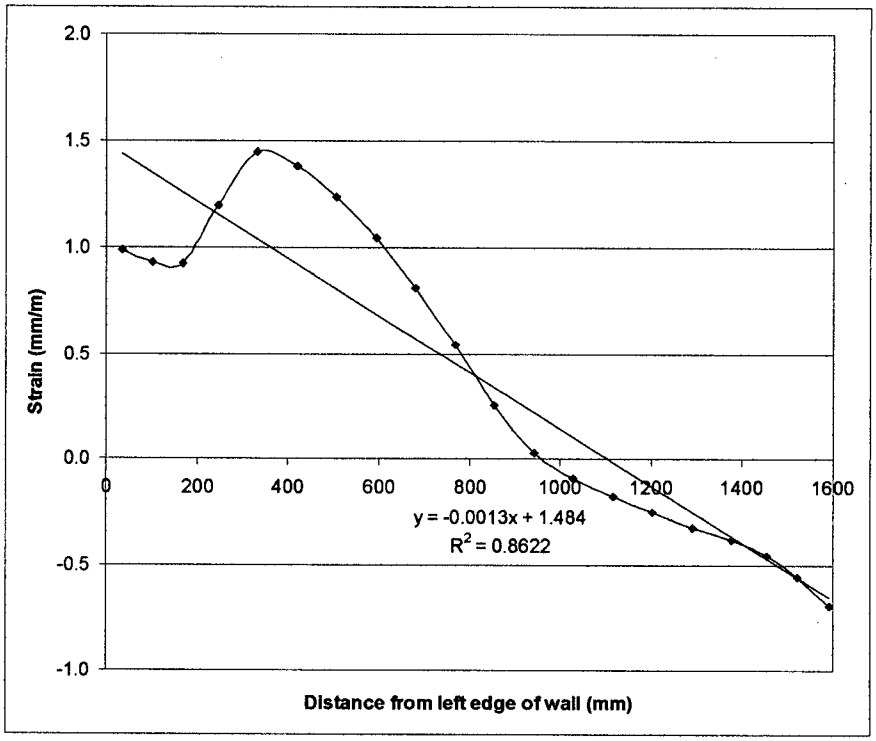

After cracking, the strain profile does not have a linear variation. Note that using a least-squares fit to determine the curvature gives a different result that if we use only the strains at the faces of the wall.

Figure 4.17 shows the strain profile for this wall displacement level at 840mm from the construction joint:

Figure 4.17 Strain profile at 840mm from the construction joint for a wall displacement of 25.4mm

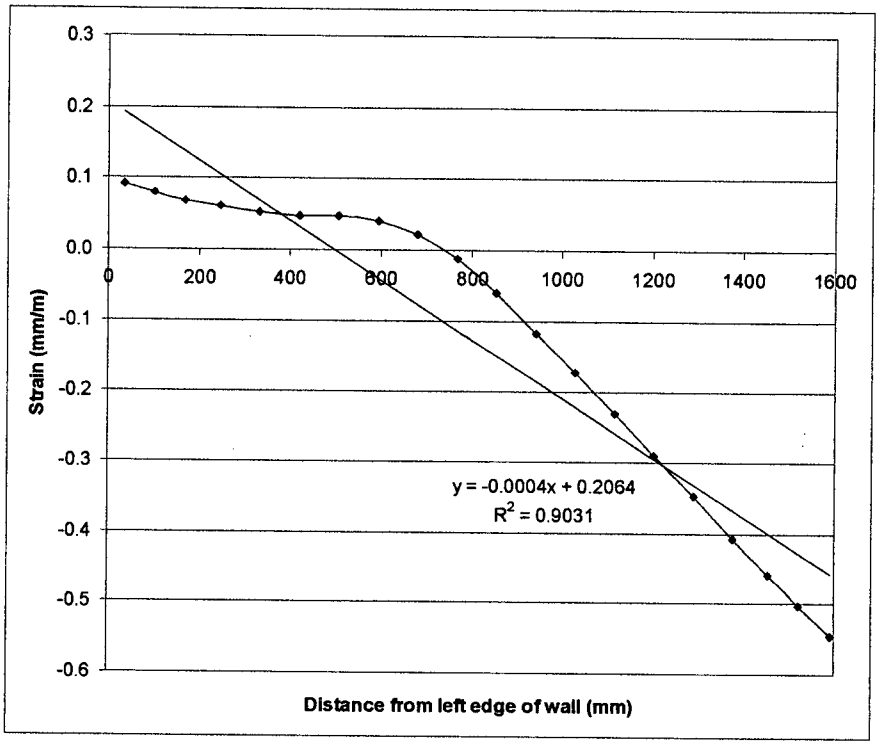

At this distance from the construction joint, the strain profile does not have a linear variation either. The distortions in this case are not due to the boundary conditions. Therefore, it can be concluded that after cracking, the strain profile does not remain linear, even though the wall is slender.

Figure 4.18 shows the strain profile for a wall displacement of 48mm at 840mm from the construction joint, after yielding:

Figure 4.18 Strain profile at 840mm from the construction joint for a wall displacement of 48mm

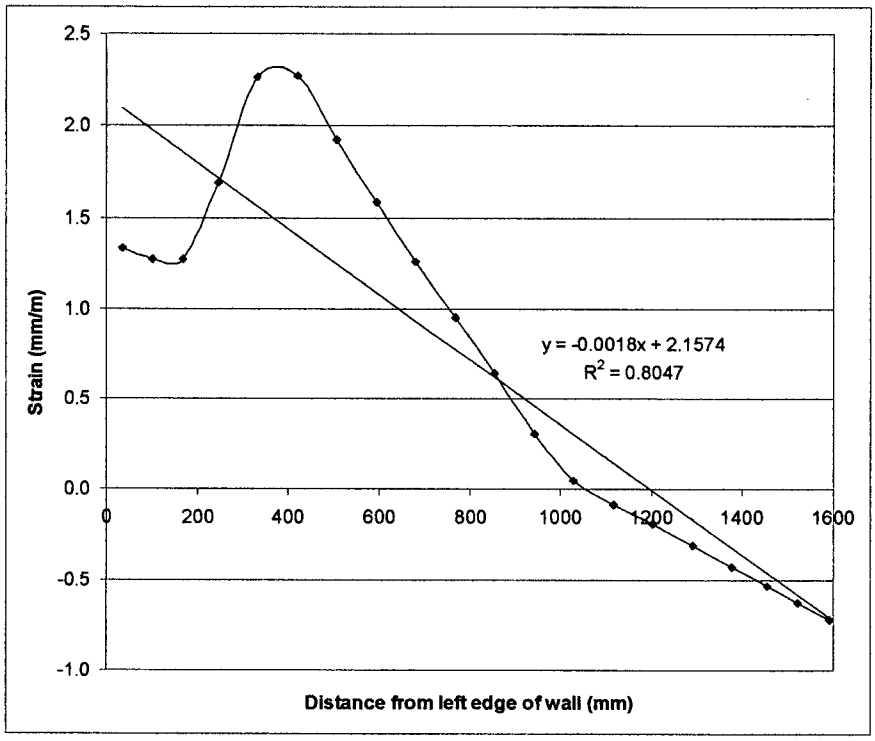

As we get further into the nonlinear range, the strain profile is less close to having a linear variation.

Because these observations contradict the results that were expected, a new analysis was carried to study why the strain profiles do not have a linear variation after cracking. As it was previously described, the wall had a low amount of reinforcement. In order to investigate how the amount of reinforcement influences the shape of the strain profiles, a second finite element analysis of the wall specimen, with an increased amount of reinforcement, was performed using program VecTor2. A new model was constructed for this purpose. This model had the same characteristics as the previous one, described in Section 4.2.5, except for the amount of horizontal and vertical reinforcement. The same loads were also applied. The average vertical strains in the elements along the length of the wall obtained from this analysis were examined.

Table 4.5 shows the material properties in the different regions of this new model of the wall:

Table 4.5 Material properties of UBC wall model with added reinforcement

Concrete properties	**Material 1**		**Material 2**		**Material 3**	
Color						
Thickness (mm)	380		127		380	
Cylinder compressive strength (MPa)	49		49		49	
Reinforcement component properties	***x*-direction**	***y*-direction**	***x*-direction**	***y*-direction**	***x*-direction**	***y*-direction**
Reinforcement ratio (%)	1.5	2.0	0.5	0.5	1.5	2.0
Reinforcement diameter (mm)	10	10	10	10	10	10
Yield strength (MPa)	455	455	455	455	455	455
Ultimate strength (MPa)	650	650	650	650	650	650
Elastic modulus (MPa)	200000	200000	200000	200000	200000	200000
Strain hardening modulus (MPa)	4875	4875	4875	4875	4875	4875
Strain hardening strain (mm/m)	10	10	10	10	10	10

Figure 4.19 shows the strain profile for a wall displacement of 41.4mm at the construction joint for this new analysis, after cracking and prior to yielding:

Figure 4.19 Strain profile at construction joint for a wall displacement of 41.4mm

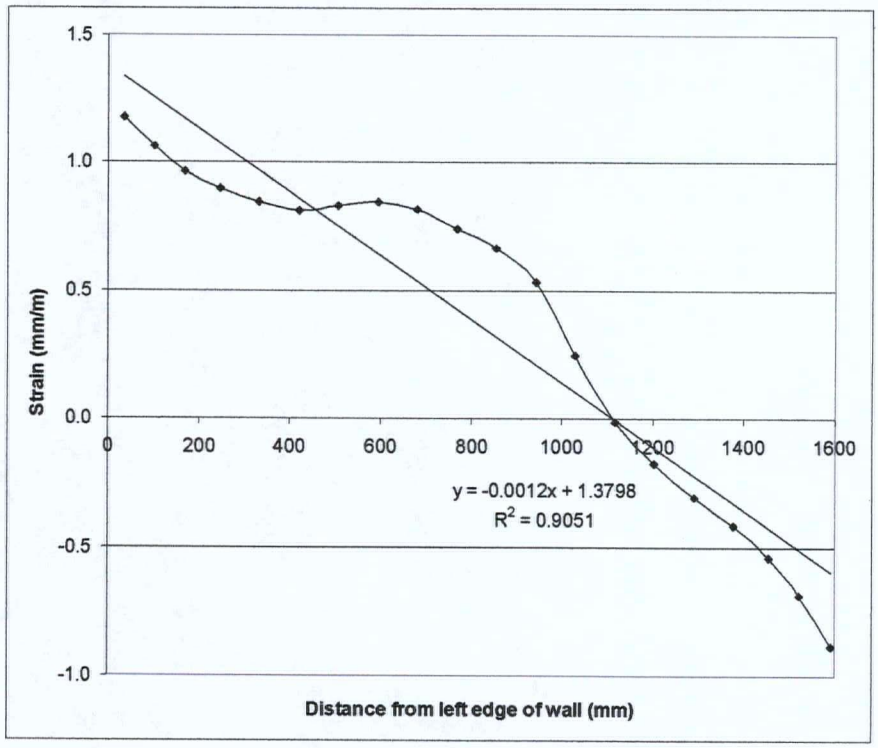

Comparing this figure with Figure 4.16, the variation of the strain profile is more close to linear.

Figure 4.20 shows the strain profile for this wall displacement level at 840mm from the construction joint:

Figure 4.20 Strain profile at 840mm from the construction joint for a wall displacement of 41.4mm

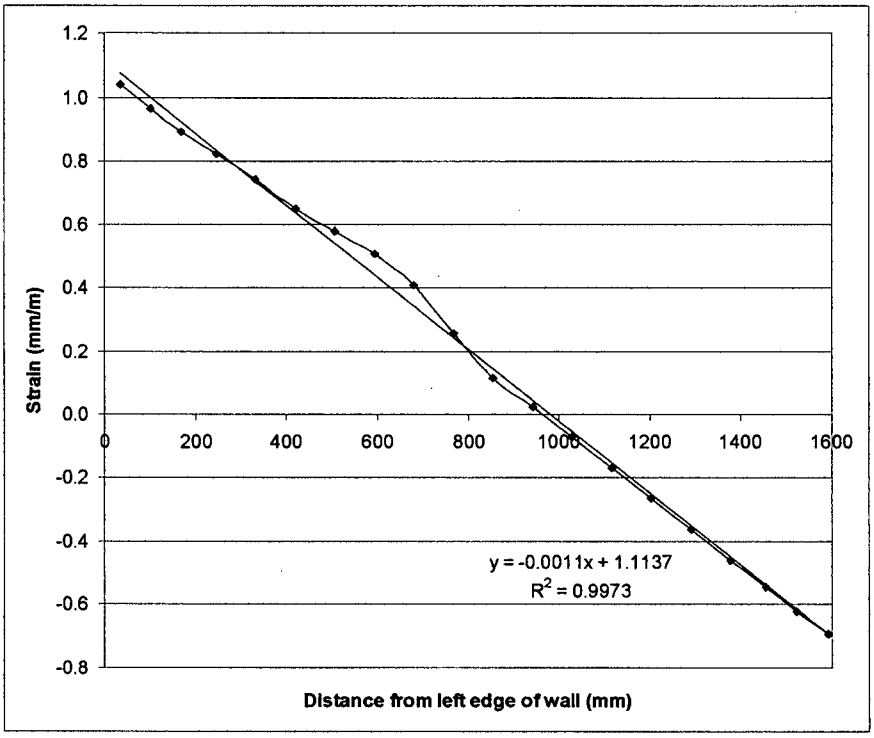

At this distance from the construction joint, the strain profile is very close to linear. The distortions in Figure 4.19 are due to the boundary conditions. Therefore, it can be concluded that the amount of reinforcement in the wall has a very significant impact in the shape of the strain profile after cracking.

With this amount of reinforcement, yielding occurs at a wall displacement of 70mm. Figure 4.21 shows the strain profile for a wall displacement of 105mm at 840mm from the construction joint, after yielding:

Figure 4.21 Strain profile at 840mm from the construction joint for a wall displacement of 105mm

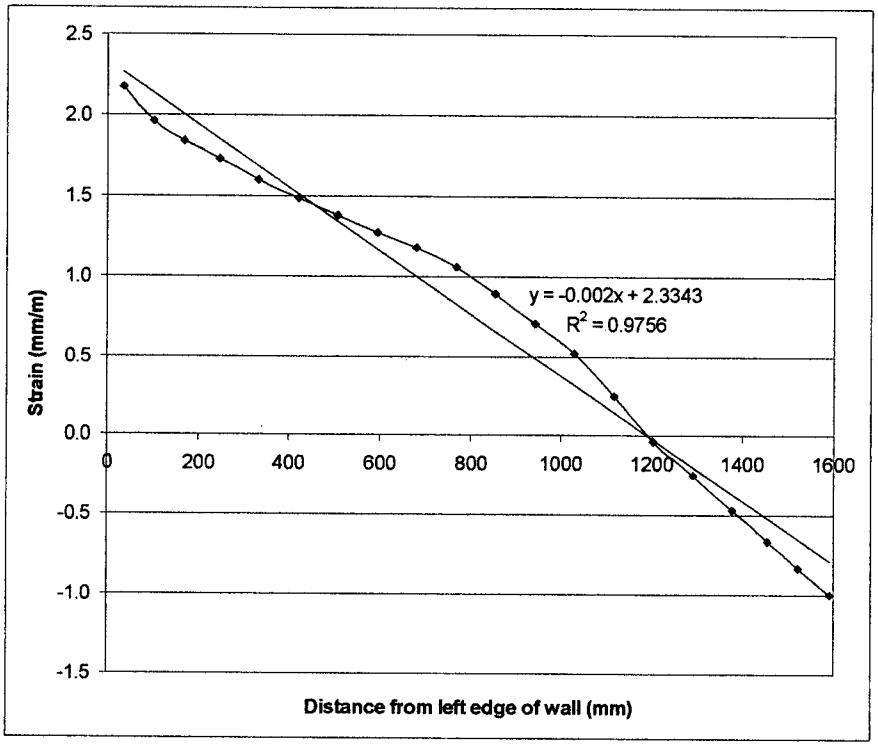

Comparing this figure with Figure 4.18, the variation of the strain profile is more close to linear after yielding at this distance from the construction joint.

Figure 4.22 shows the strain profile for a wall displacement of 281mm at 840mm from the construction joint:

Figure 4.22 Strain profile at 840mm from the construction joint for a wall displacement of 281mm

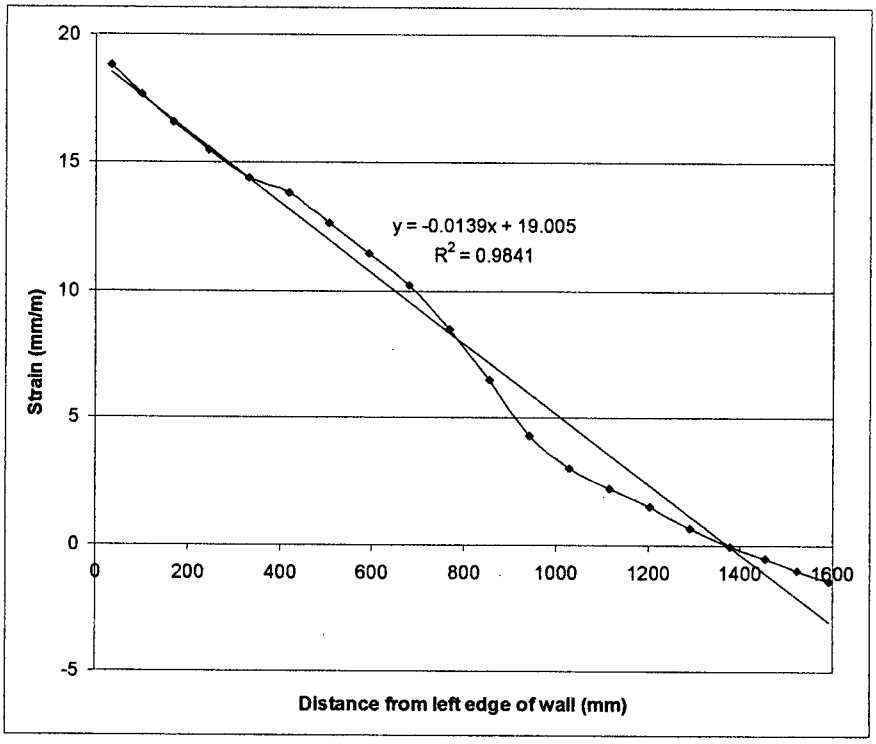

As seen previously in Figure 4.18, as we get further into the nonlinear range, the strain profile is less close to having a linear variation. However, for this case, considering a linear variation is still a fair approximation.

The four main conclusions made from this study can be summarized as the following:

- The boundary conditions of the model distort the shape of the strain profile.
- Before cracking, the strain profile remains linear.
- After cracking, the shape of the strain profile depends on the amount of reinforcement. As the amount of reinforcement is increased, the strain profile is closer to having a linear variation.
- The linearity of the strain profile degrades as the wall goes further into the nonlinear range.

Therefore, considering that the strain profile is linear is not always true. It is important to take this into consideration when we design slender walls with low amounts of reinforcement. For the wall studied, there was no experimental information available regarding the axial strains along the cross-section, so a linear variation had to be assumed to determine the curvatures. Tests results showing the actual variation of axial strains along the cross-section of slender walls will be presented in the next section.

4.3 Rectangular shear wall tested at Clarkson University

A series of tests were conducted at Clarkson University in 1995 on slender reinforced concrete walls with rectangular-shaped and T-shaped cross-sections with moderate amounts of transverse reinforcement by Thomsen and Wallace. The purpose of these tests was to evaluate the simplified displacement-based design approach in ACI 318 1999 (Thomsen and Wallace 2004: 618 – 630). A brief description of the tests and the results obtained has already been given in Section 2.24. These tests are of particular interest because extensive measurements of the concrete strains were made along the length of the wall at the base, so the actual variation of the axial strains was determined. Therefore, these test results can be compared with analytical predictions made with program VecTor2. The wall analyzed for these comparisons was the rectangular specimen RW2. The following sections will be focused on this specimen only; additional information needed for the analysis will be presented.

4.3.1 Description of the wall specimen

The specimen RW2 was a 1/4 scaled model of a wall in an area of high seismicity. It had an aspect ratio of three and was considered as a four-storey wall. The wall was 102mm thick, 1219mm long and 3658mm high (Thomsen and Wallace 2004: 618 – 620).

The reinforcement was arranged symmetrically. The boundary zones were 191mm long each. The vertical reinforcement in the two zones consisted of eight deformed #3 bars enclosed by 3/16" diameter smooth wire hoop and cross-ties spaced at 51mm. The vertical reinforcement in each zone was arranged in four layers (spaced at 51mm) of two bars each. The clear cover of the hoops was 9.5mm. The web had two deformed #2 bars in each layer spaced at 191mm, vertically and horizontally. A total of eight bars were used in the web.

The wall had different concrete strengths at the base and at each of the four storeys at the time of testing. At the first storey, the compressive cylinder strength was 43.7 MPa and the rupture strength was 5.63 MPa. All three types of reinforcing steel used had different properties. The yield strength was 434, 448 and 434 MPa for the #3 bars, #2 bars and 3/16" smooth wires, respectively; and the ultimate strength was 641, 586 and 483 MPa, respectively. The modulus of elasticity was 200000 MPa for all three. The strain at the onset of strain hardening for the #3 bars was 16 mm/m (Thomsen and Wallace 1995: 148 – 150). The stress-strain response of three types of reinforcing steel was measured (Thomsen and Wallace 1995: 182).

4.3.2 Instrumentation

The wall was tested as a cantilever element. It was subjected to cyclic lateral displacements applied at the top by a hydraulic actuator. Additionally, a constant compressive axial load was applied at the top by hydraulic jacks (Thomsen and Wallace 2004: 622 – 623).

Four wire potentiometers were used to measure lateral displacements at 914mm intervals along the height of the wall. Seven linear variable differential transducers were provided along the wall length to measure vertical displacements; these were placed vertically over a gage length of 229mm (Thomsen and Wallace 2004: 624).

4.3.3 Test procedure

During the test, the constant axial load applied to the wall was on average $0.07A_g f'_c$, equal to 378 kN, calculated using the concrete cylinder strength of the first storey. However, the axial load had to be constantly adjusted, resulting in a considerable variation of it. The maximum axial load applied was 436 kN (Thomsen and Wallace 1995: 205).

The lateral displacements applied to the wall consisted of 20 cycles. The drift for the 12 first cycles increased from 0.125 to 1.5%, and for the last eight cycles it increased from 1 to 2.5%. The drifts were increased every two cycles (Thomsen and Wallace 1995: 203).

4.3.4 Test results

The test results were used to determine strain profiles along the length of the wall for different drifts levels. The axial strains were determined from the displacement readings measured with the seven transducers provided along the wall. These readings were divided by the gage length to obtain axial strains. Some of the readings at the surface were not reliable because of concrete spalling (Thomsen and Wallace 2004: 627). The experimental strain profiles were determined for the positive and negative direction of loading (Thomsen and Wallace 1995: 223).

4.3.5 Analytical model of the wall specimen

The wall specimen was modeled and analyzed using program VecTor2. The purpose of this analysis is to predict the strain profile along the length of the wall and compare these predictions with the experimental results obtained by Thomsen and Wallace. Low-powered rectangular elements were used to

model the concrete, with smeared steel to account for the presence of reinforcement. The constitutive models for concrete and steel described in Chapter 3 were used in the analysis.

Two different material types were used to represent various regions of the wall in the finite element model:

- The first material type was used to represent the confined boundaries of the wall.
- The second material type was used to represent the web of the wall.

The analytical model was fixed at the bottom; both the horizontal and vertical displacements were restrained.

The finite element mesh was refined in such a way that the position of certain nodes coincides with the position of the transducers. Meshes of 89×114, 102×114 and 114×114 rectangular elements were used; 12 elements (13 nodes) were used in the transverse direction of the wall. This level of refinement was used to model the whole wall. All nodes and elements were numbered in the horizontal (short) direction. The complete mesh consisted of 429 nodes and 384 rectangular elements.

The material properties used in the analysis were those reported in the description of the wall specimen, presented in Section 4.3.1. The concrete properties from the first storey were considered for the whole wall. The concrete tensile strength was taken as half of the rupture strength, that is, 2.8 MPa. For the material properties that were not measured during the test, the values given by default in program VecTor2 were used. The concrete initial tangent elastic modulus and the cylinder strain at f'_c where determined with Equation 4.2 and 4.3, respectively. The maximum aggregate size was 10mm, given by default. For the reinforcement properties, the strain hardening modulus and the strain at the onset of strain hardening were determined from the measured stress-strain curves; except for the strain at the onset of strain hardening for the deformed #3 bar, which is given in Section 4.3.1.

A monotonic lateral load was applied at the top of the wall. This load was applied in a displacement-control mode, in increments of 0.2mm. Additionally, a constant axial load of 436 kN was applied; this was the maximum axial load applied during the test. This load was equally distributed among all the 13 nodes at the top. The self-weight of the wall was not considered.

Figure 4.23 shows the finite element model of the wall specimen, created in the pre-processor FormWorks:

Figure 4.23 Finite element model of specimen RW2 in FormWorks

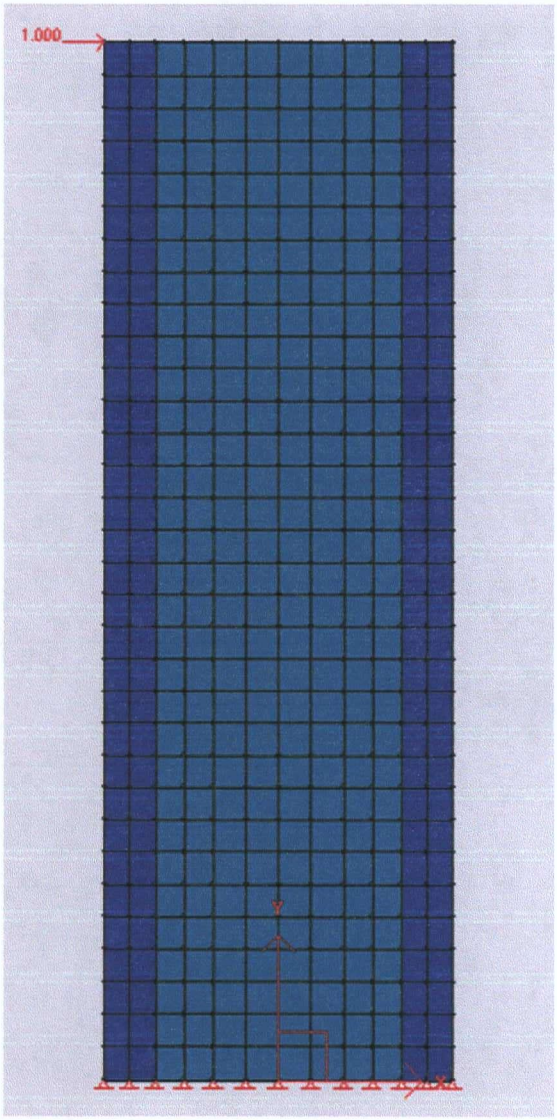

Table 4.6 shows the material properties in the different regions of the wall:

Table 4.6 Material properties of specimen RW2 model

Concrete properties	Material 1		Material 2	
Color				
Thickness (mm)	101.6		101.6	
Cylinder compressive strength (MPa)	43.7		43.7	
Tensile strength (MPa)	2.8		2.8	
Reinforcement component properties	***x*-direction**	***y*-direction**	***x*-direction**	***y*-direction**
Reinforcement ratio (%)	0.69	2.95	0.33	0.33
Reinforcement diameter (mm)	4.75	9.5	6.4	6.4
Yield strength (MPa)	434	434	448	448
Ultimate strength (MPa)	483	641	586	586
Elastic modulus (MPa)	200000	200000	200000	200000
Strain hardening modulus (MPa)	1119	5750	3391	3391
Strain hardening strain (mm/m)	2.2	16	2.3	2.3

4.3.6 Analytical results

The analytical predictions obtained from program VecTor2 were used to determine strain profiles along the length of the wall for different drift levels. The axial strains were determined the same way as it was done for the experimental results in order to make comparisons, using the vertical nodal displacements along the wall length obtained from the analysis.

As previously described, the position of certain nodes along the length of the wall coincides with the position of the transducers. The vertical nodal displacements at these particular nodes were used to calculate the axial strains. The difference in vertical displacements between two nodes in the same position along the wall length, divided by the vertical distance between these nodes, gives the average axial strain over that length at that position. This way, the experimental and analytical axial strains were calculated over the same length. The strain profile was determined for drift levels of 1.5 and 2%.

4.3.7 Comparison of experimental and analytical results

Figure 4.24 and 4.25 show comparisons between the experimental strain profile, in both directions of loading, and the analytical strain profile; for the two drift levels mentioned:

Figure 4.24 Strain profile at base for a drift of 1.5%

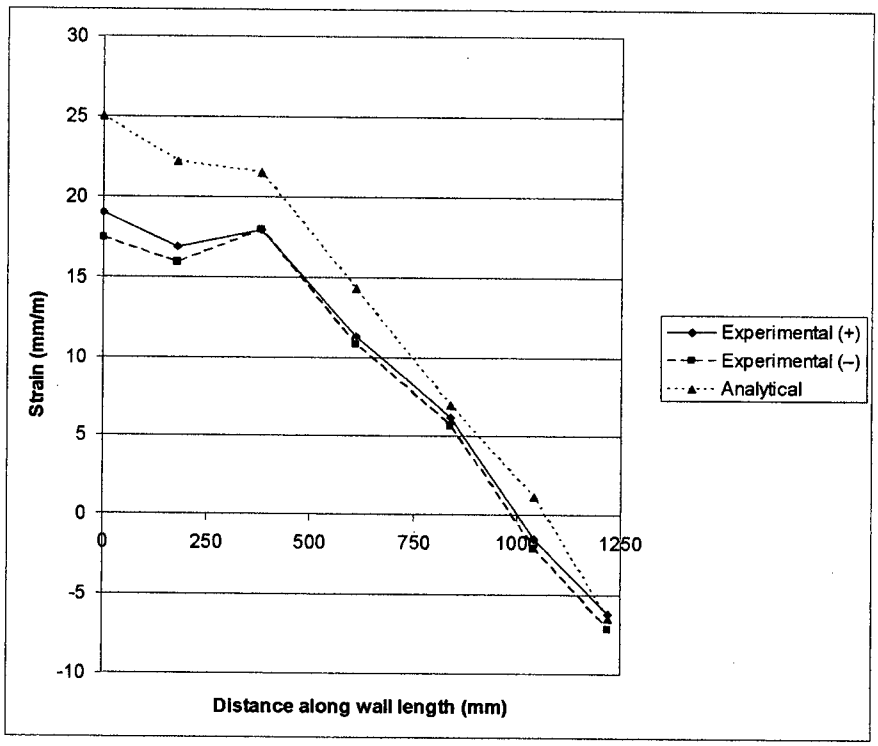

Figure 4.25 Strain profile at base for a drift of 2%

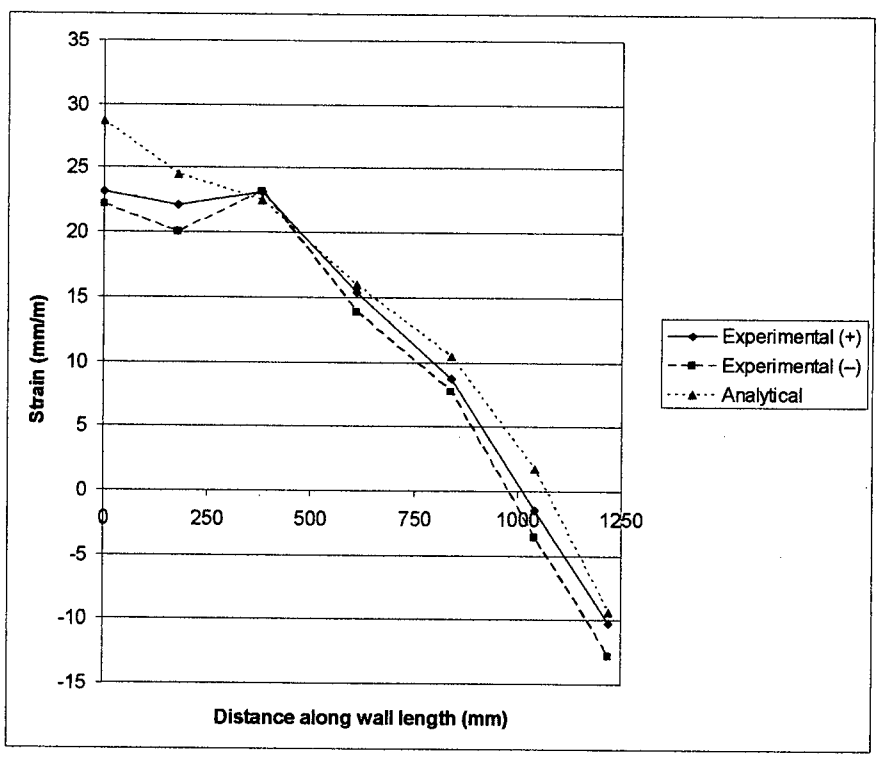

Both the experimental and the analytical results show that the strain profiles are not linear, although the walls are slender; which confirms the results obtained for the UBC wall test. As it was

discussed previously, the nonlinearity of the strain profile is because this wall had a moderate amount of reinforcement.

Although program VecTor2 predicts reasonably well the shape of the strain profiles along the length of the wall, there are differences between the experimental and analytical results, specially in the tension zone. There is a better agreement between the analytical and the experimental strain profiles in the positive direction of loading. The greater differences in the tension zone, as the authors indicated, are due to the influence of concrete cracking and slippage of the reinforcement (Thomsen and Wallace 2004: 628). The differences in the compression zone are due to the very significant damage and spalling of the concrete cover at the wall boundaries during the test (Thomsen and Wallace 2004: 626).

The analytical predictions in the compression zone can be improved if the cover spalling at the wall boundary is considered in the finite element model. For this, only the concrete inside the core was modeled. The area of concrete in the wall boundary considered in the analysis was delimited by the longitudinal axis of the hoops. This is shown in Figure 4.26:

Figure 4.26 Area of concrete considered in the analysis to account for cover spalling

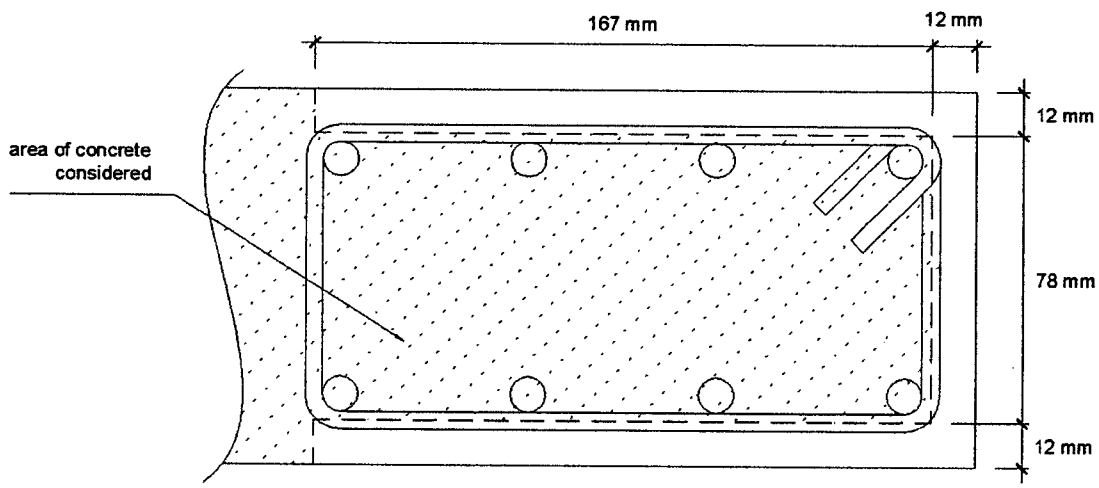

A second finite element analysis of the wall, considering cover spalling, was performed using program VecTor2. A new model was constructed for this purpose. This model had the same characteristics as the previous one, described in Section 4.3.5, except that a new material type was created for the confined boundary of the wall in the compression zone. This material type had a reduced thickness of 78mm to account for cover spalling at the sides, as shown in Figure 4.26. The nodes at the far right in the model were moved 12mm to the left to account for cover spalling at the face of the wall. The same loads were applied for this analysis. The vertical nodal displacements obtained were used to calculate the

axial strains along the length of the wall using the same procedure described in Section 4.3.6, for drift levels of 1.5 and 2%.

Figure 4.27 shows the new finite element model of the wall specimen, created in the pre-processor FormWorks:

Figure 4.27 Finite element model accounting for cover spalling of specimen RW2 in FormWorks

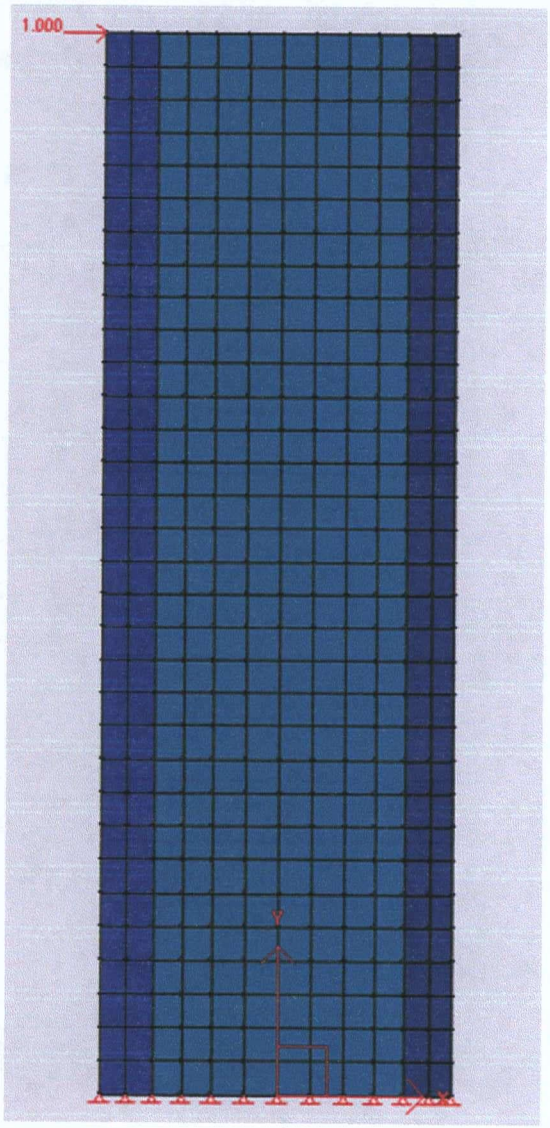

Table 4.7 shows the material properties in the different regions of this new model of the wall:

Table 4.7 Material properties of specimen RW2 model accounting for cover spalling

Concrete properties	Material 1		Material 2		Material 3	
Color						
Thickness (mm)	101.6		101.6		77.75	
Cylinder compressive strength (MPa)	43.7		43.7		43.7	
Tensile strength (MPa)	2.8		2.8		2.8	
Reinforcement component properties	***x*-direction**	***y*-direction**	***x*-direction**	***y*-direction**	***x*-direction**	***y*-direction**
Reinforcement ratio (%)	0.69	2.95	0.33	0.33	0.69	2.95
Reinforcement diameter (mm)	4.75	9.5	6.4	6.4	4.75	9.5
Yield strength (MPa)	434	434	448	448	434	434
Ultimate strength (MPa)	483	641	586	586	483	641
Elastic modulus (MPa)	200000	200000	200000	200000	200000	200000
Strain hardening modulus (MPa)	1119	5750	3391	3391	1119	5750
Strain hardening strain (mm/m)	2.2	16	2.3	2.3	2.2	16

Figure 4.28 and 4.29 show comparisons between the experimental strain profile, in both directions of loading, and the analytical strain profile; for the two drift levels mentioned:

Figure 4.28 Strain profile accounting for cover spalling at base for a drift of 1.5%

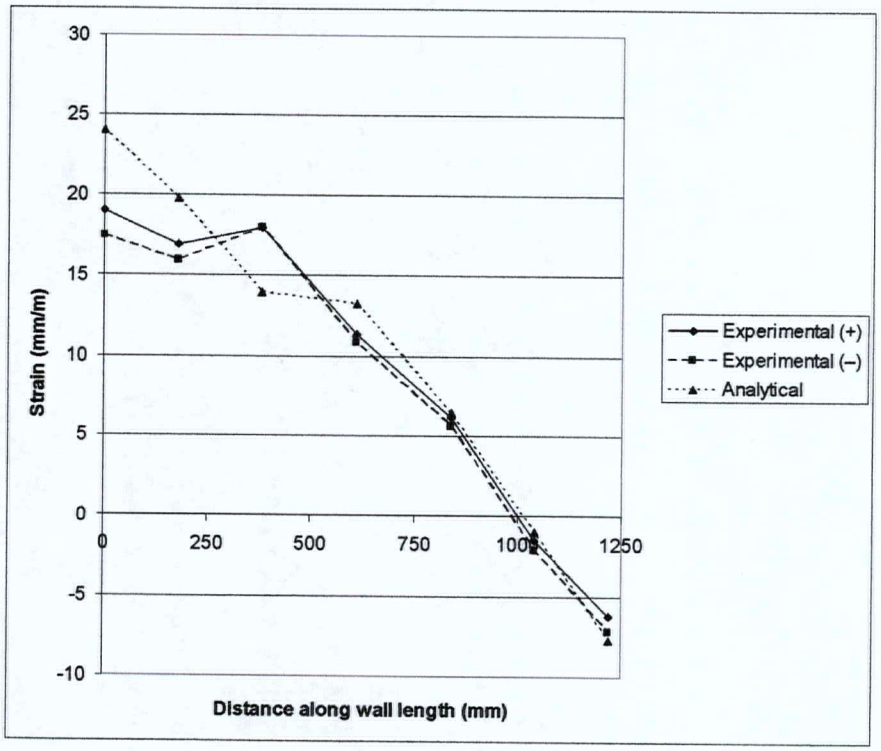

Figure 4.29 Strain profile accounting for cover spalling at base for a drift of 2%

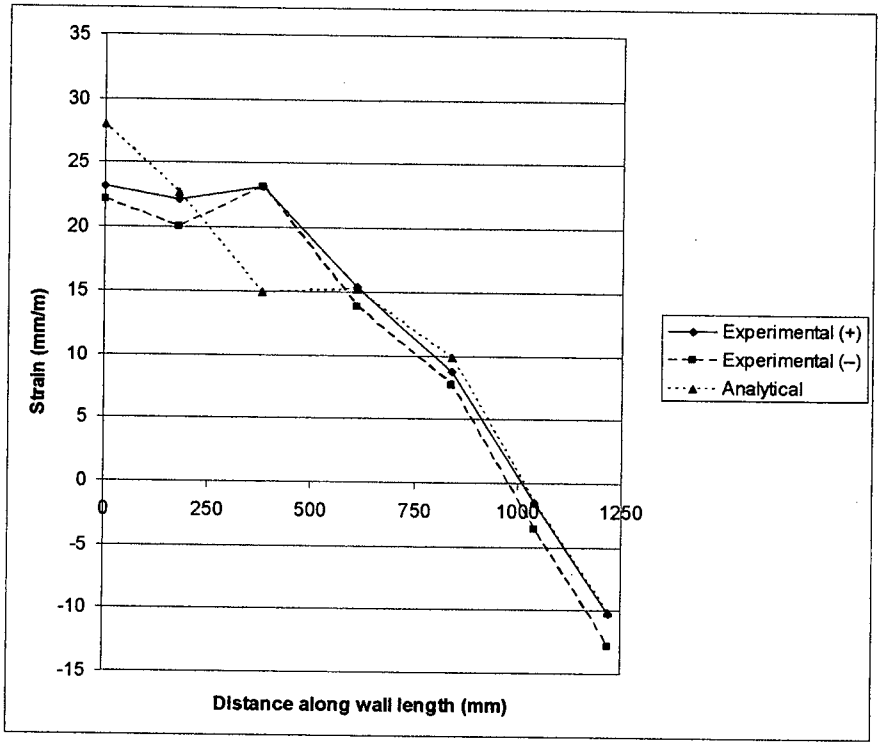

Comparing these figures with Figure 4.24 and 4.25, there is an excellent agreement between the experimental and analytical strain profiles in the compression zone. Despite the discrepancies in the tension zone, the analytical model seems to predict reasonably well the strain profile of the wall.

CHAPTER 5: PARAMETRIC STUDY OF CONCRETE WALLS

5.1 Scope of analysis

Program VecTor2 was used to perform a parametric study of concrete walls. The factors that affect the plastic hinge length were investigated. The parameters considered in this study were the wall length, the distance from the section of maximum moment to the section of zero moment (shear span), the diagonal cracking and the axial load.

5.2 Description of wall models

Two cantilever wall models were considered for this parametric study, which will be referred to as Wall 1 and Wall 2 throughout this chapter. Wall 1 was twice as long as Wall 2. The dimensions and material properties of these walls were typical of high-rise buildings. The two walls had a rectangular cross-section, and they were 54860mm high and 508mm thick.

Wall 1 was 7620mm long. The boundary zones were 1219mm long, the vertical reinforcement in these consisted of 24-25M reinforcing bars enclosed by 15M ties spaced at 100mm. The clear cover of the ties was 40mm. The web had 15M reinforcing bars spaced at 150mm vertically and horizontally. The cross-section of Wall 1 is shown in Figure 5.1:

Figure 5.1 Cross-section details of Wall 1

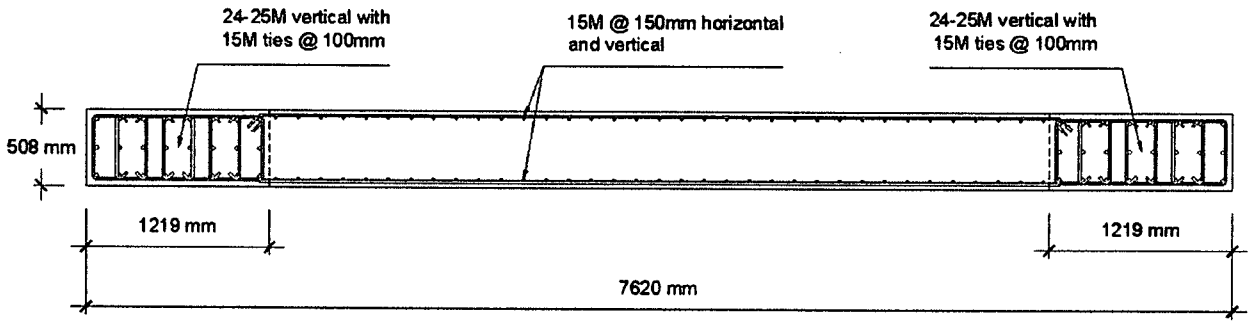

Wall 2 was 3810mm long. The boundary zones were 610mm long, the vertical reinforcement in these consisted of 12-25M reinforcing bars enclosed by 15M ties spaced at 100mm. The clear cover of the ties was 40mm. The web had 15M reinforcing bars spaced at 150mm vertically and horizontally. The cross-section of Wall 2 is shown in Figure 5.2:

Figure 5.2 Cross-section details of Wall 2

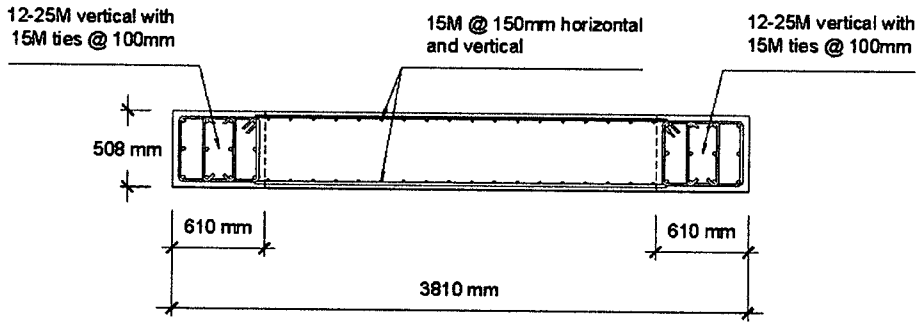

The concrete cylinder compressive strength of both walls was 40 MPa. The stress-strain curve of all the reinforcing bars was assumed to be the same as the one used for the UBC wall test, whose properties are shown in the bottom five rows of Table 4.1, except that the yield strength was taken as 400 MPa.

Both walls were fixed at the base. They were subjected to a monotonically increasing lateral load at the top; as well as a constant compressive axial load of $0.1A_g f'_c$, equal to 15484 kN for Wall 1 and 7742 kN for Wall 2.

Using these two wall models as the base cases, the parametric study was performed by changing the wall parameters and observing how this affects the length of the plastic hinge.

5.3 Analytical model of walls

Wall 1 and 2 were modeled and analyzed using program VecTor2. Each wall was analyzed separately. Low-powered rectangular and triangular elements were used to model the concrete, with smeared steel to account for the presence of reinforcement. The constitutive models for concrete and steel described in Chapter 3 were used in the analysis.

Two different material types were used to represent various regions of the two walls in the finite element model:

- The first material type was used to represent the confined boundaries of the wall.
- The second material type was used to represent the web of the wall.

The analytical model was fixed at the bottom; both the horizontal and vertical displacements were restrained. The finite element mesh was more refined near the base (critical section) in both walls. Also,

the two walls had the same refinement in the vertical direction up to a half of the height, so that the curvatures could be calculated over the same average length.

For Wall 1, meshes of 305×423 and 305×203 rectangular elements were used; 25 elements (26 nodes) were used in the transverse direction of the wall. This level of refinement was maintained up to half the height of the wall. Up from this point, 18 elements (19 nodes) were used in the transverse direction, then it was further reduced to 10 elements (11 nodes), and then to five elements (six nodes) up to the top of the wall. The transitions were made using triangular elements. All nodes and elements were numbered in the horizontal (short) direction. The complete mesh consisted of 2081 nodes, 1927 rectangular elements and 86 triangular elements.

For Wall 2, meshes of 305×423, 305×203, 288×423 and 288×203 rectangular elements were used; 13 elements (14 nodes) were used in the transverse direction of the wall. This level of refinement was maintained up to half the height of the wall. Up from this point, eight elements (nine nodes) were used in the transverse direction, and then it was further reduced to five elements (six nodes) up to the top of the wall. The transitions were made using triangular elements. All nodes and elements were numbered in the horizontal (short) direction. The complete mesh consisted of 1276 nodes, 1139 rectangular elements and 30 triangular elements.

The material properties used in the analysis were those reported in the description of the wall models, presented in Section 5.2. For the material properties not mentioned in that section, the values given by default in program VecTor2 were used. The concrete tensile strength, the initial tangent elastic modulus and the cylinder strain at f'_c where determined with Equation 4.1, 4.2 and 4.3, respectively. The maximum aggregate size was 10mm, given by default. For the reinforcement properties, these were the same as those for the UBC wall test, except for the yield strength, as it was previously mentioned.

A monotonic lateral load was applied at the top of the walls. This load was applied in a displacement-control mode, in increments of 1mm. Additionally, a constant axial load of 15484 kN in Wall 1 and 7742 kN in Wall 2 was applied; these loads were equally distributed among the six nodes at the top of each wall. The self-weight of the walls was not considered.

Figure 5.3 shows the finite element model of Wall 1, created in the pre-processor FormWorks:

Figure 5.3 Finite element model of Wall 1 in FormWorks

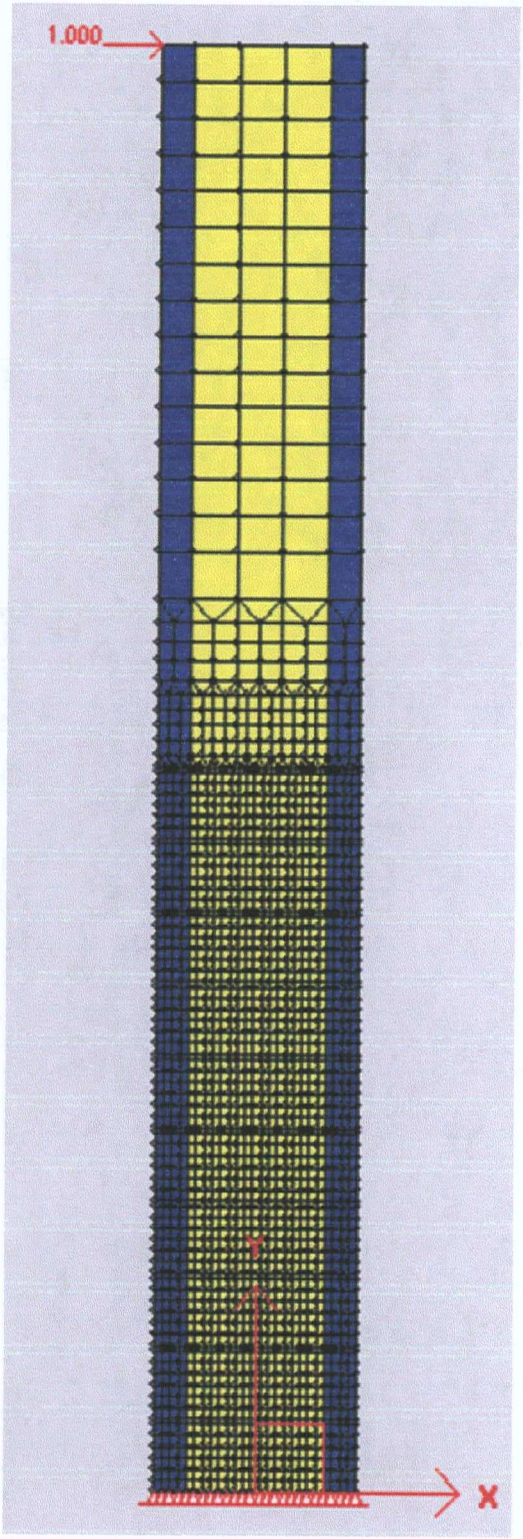

Figure 5.4 shows the finite element model of Wall 2, created in the pre-processor FormWorks:

Figure 5.4 Finite element model of Wall 2 in FormWorks

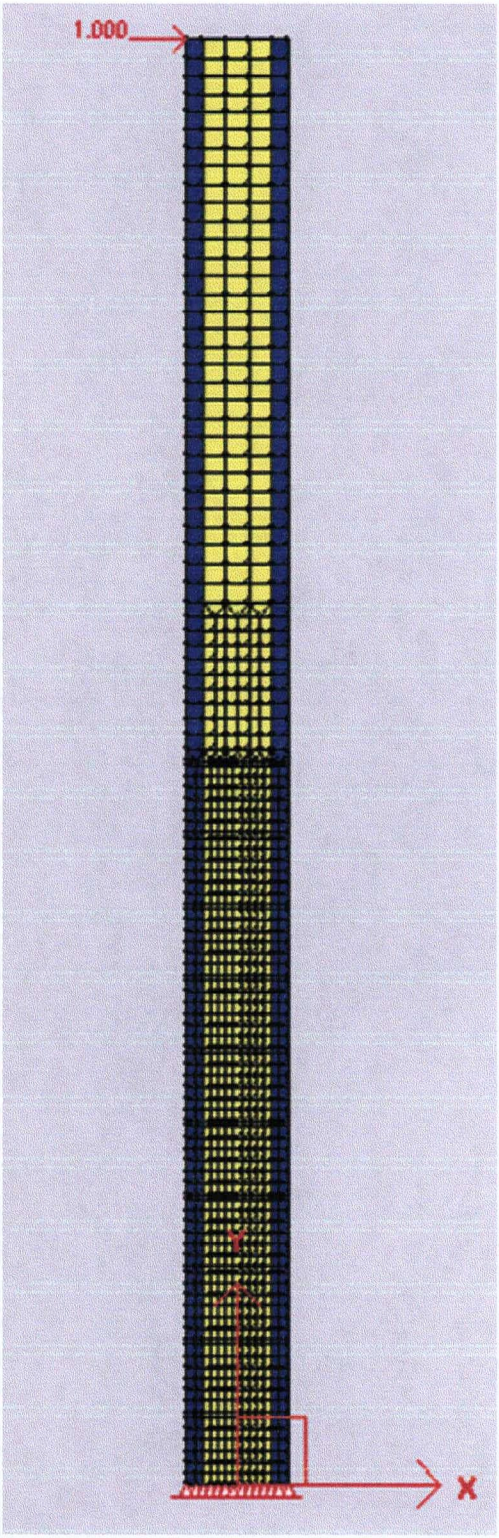

Table 5.1 shows the material properties in the different regions of the two walls:

Table 5.1 Material properties of Wall 1 and 2

Concrete properties	**Material 1**		**Material 2**	
Color				
Thickness (mm)	508		508	
Cylinder compressive strength (MPa)	40		40	
Reinforcement component properties	***x*-direction**	***y*-direction**	***x*-direction**	***y*-direction**
Reinforcement ratio (%)	0.8	2.0	0.5	0.5
Reinforcement diameter (mm)	15	25	15	15
Yield strength (MPa)	400	400	400	400
Ultimate strength (MPa)	650	650	650	650
Elastic modulus (MPa)	200000	200000	200000	200000
Strain hardening modulus (MPa)	4875	4875	4875	4875
Strain hardening strain (mm/m)	10	10	10	10

5.4 Analytical results

The analytical predictions obtained from program VecTor2 were used to determine curvature distributions along the height of the walls for different lateral displacement levels. The vertical nodal displacements at the faces of the walls were used to calculate the curvatures, as it was done for the UBC wall test, which is described in Section 4.2.6. The difference in vertical displacements between two nodes at the face, divided by the vertical distance between these nodes, gives the average axial strain over that length. Then, the difference between the compression and tension strain, divided by the wall length between the two faces, gives the average curvature over the length between nodes. The curvatures were calculated over average lengths of 847 or 1050mm; that is, between every two or three elements.

The strain profile along the length of the two walls was investigated. For slender walls like the ones being studied, with the amount of reinforcement that they have, we expect the strain profile along the wall length to be close to linear, as seen in Section 4.2.10. The average vertical strains in the elements along the length of the walls obtained from program VecTor2 were studied to verify if this assumption is true. The ultimate drift for Wall 1 was 2%. Figure 5.5 shows the strain profile of Wall 1 for this drift at the base:

Figure 5.5 Strain profile of Wall 1 at base for a drift of 2%

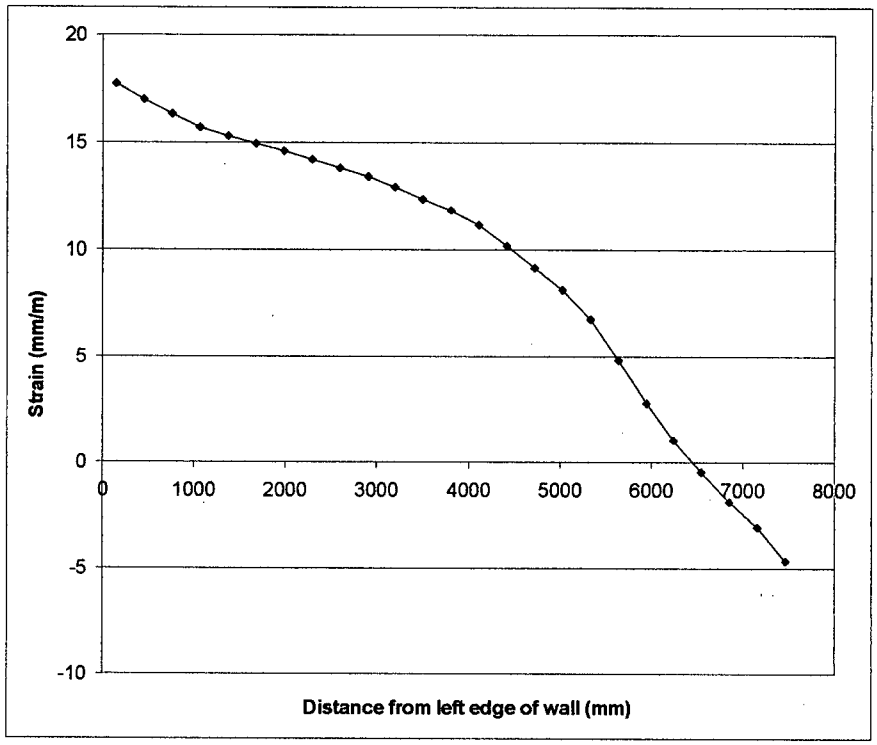

The strain profile is not linear due to the boundary conditions, as seen in Section 4.2.10. Figure 5.6 shows the strain profile of Wall 1 for a 2% drift at 1270mm from the base:

Figure 5.6 Strain profile of Wall 1 at 1270mm from the base for a drift of 2%

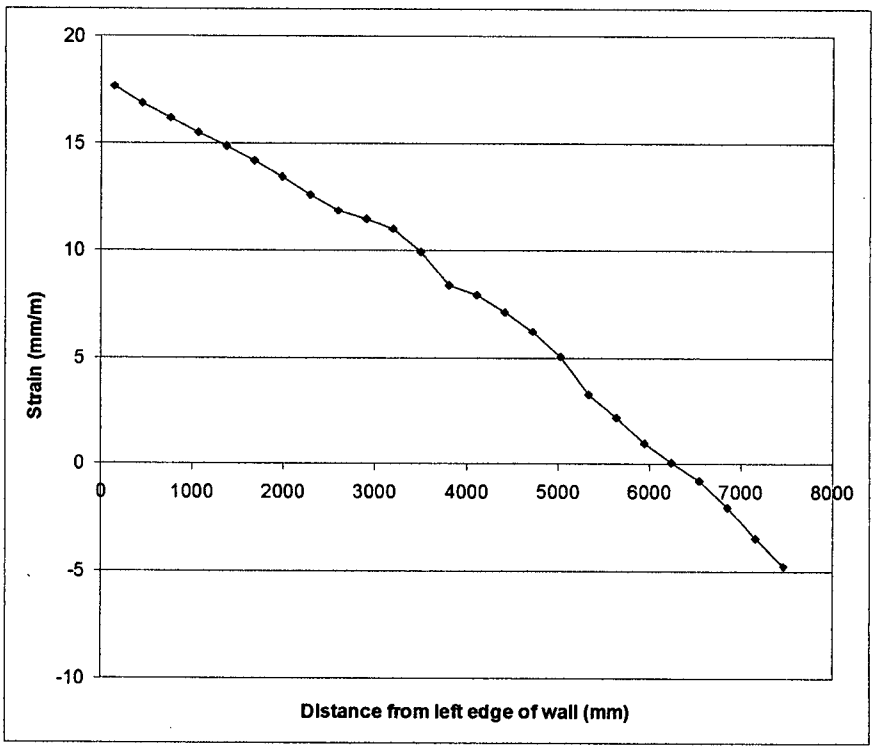

At this distance from the base, the strain profile very close to having a linear variation. Figure 5.7 shows the strain profile of Wall 2 for a 2% drift at the base:

Figure 5.7 Strain profile of Wall 2 at the base for a drift of 2%

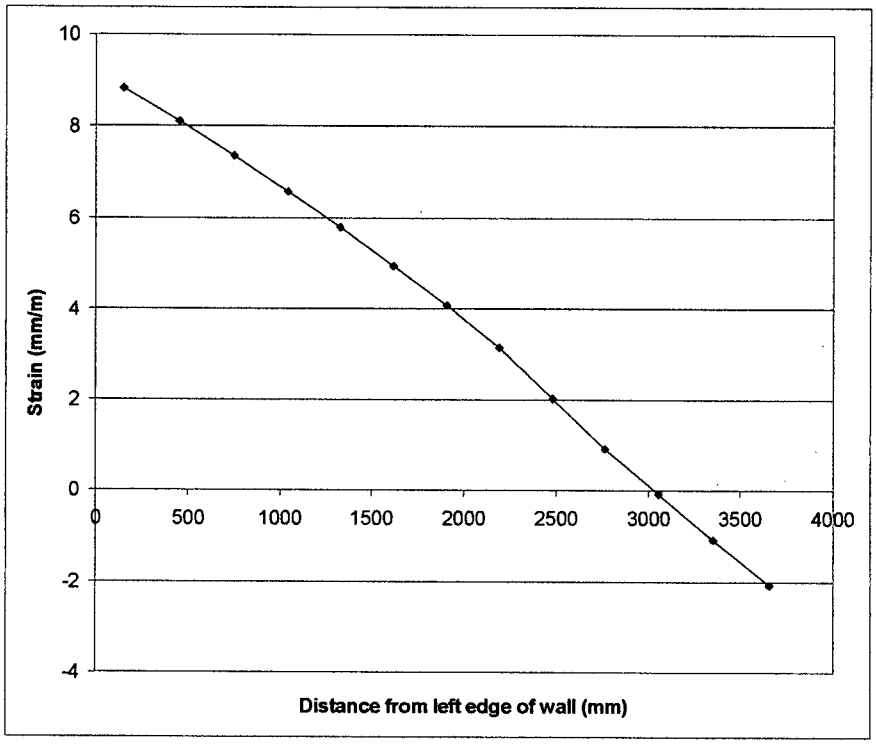

Because Wall 2 is more slender, the strain profile is linear even at the base. From these figures, it can be seen that considering that plane sections remain plane after bending is a reasonable assumption for these two walls. The curvatures were calculated from the strains at the wall faces considering a linear variation. Figure 5.8 shows the curvature distribution up to the mid-height of both walls for a drift of 2%:

Figure 5.8 Curvatures up to the mid-height of Wall 1 and 2 for a drift of 2%

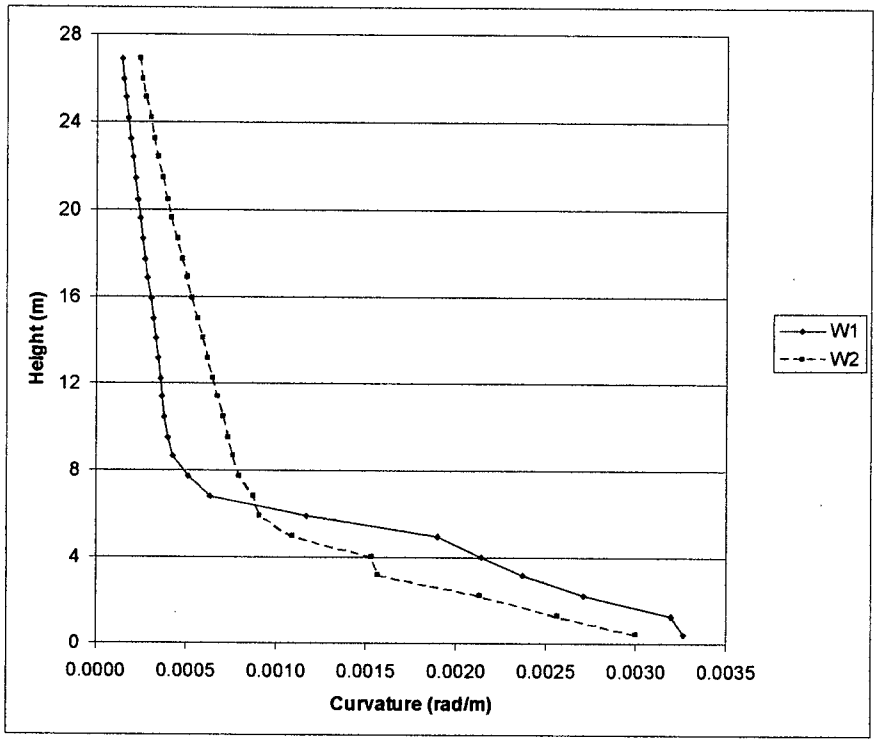

As seen in Section 4.2.9, the inelastic curvatures can be well approximated as linearly varying. Wall 2 has larger elastic curvatures because it is more flexible. In order to determine the plastic hinge length from the curvature distribution, the yield curvature of the walls has to be estimated. Once the yield curvature is determined, the inelastic curvatures can be visualized by shifting the vertical axis by this amount, which defines the length of the plastic hinge for a linearly varying inelastic curvature.

There are two ways to determine the yield curvature. One way is to calculate the curvature just above the base, using the procedure described in this section, for the yield displacement or drift (first yield of the longitudinal reinforcement). The yield drifts were determined by looking at the average vertical steel strains in the elements obtained from program VecTor2. For Wall 1, the steel started to yield at a drift of 0.61%, for which the curvature just above the base was 0.00045 rad/m. For Wall 2, the steel started to yield at a drift of 1.18%, for which the curvature just above the base was 0.0009 rad/m.

A second way to estimate the yield curvature is from the moment-curvature relationships of the walls. To develop this relationship, the bending moment diagram along the height of the wall must be calculated at the same locations where the curvatures in Figure 5.8 were determined. For Wall 1 and 2, since they were subjected to a lateral load at the top, the bending moment diagram was linearly varying and could be easily determined. Figure 5.9 shows the bending moments along the height of both walls for a drift of 2%:

Figure 5.9 Bending moments along the height of Wall 1 and 2 for a drift of 2%

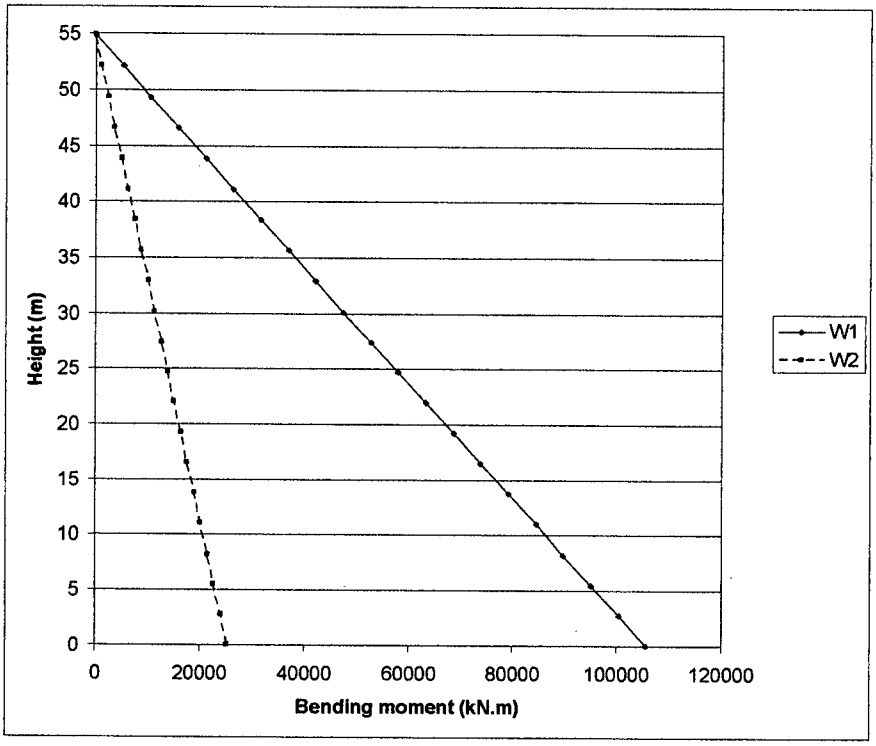

Figure 5.10 shows the moment-curvature relationship of Wall 1:

Figure 5.10 Moment-curvature relationship of Wall 1

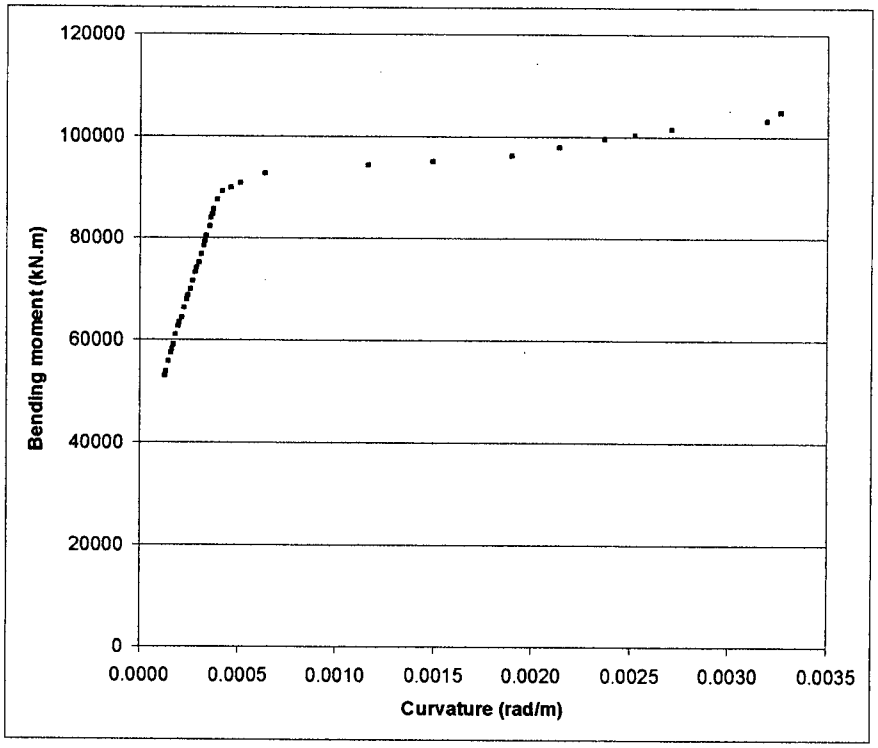

Figure 5.11 shows the moment-curvature relationship of Wall 2:

Figure 5.11 Moment-curvature relationship of Wall 2

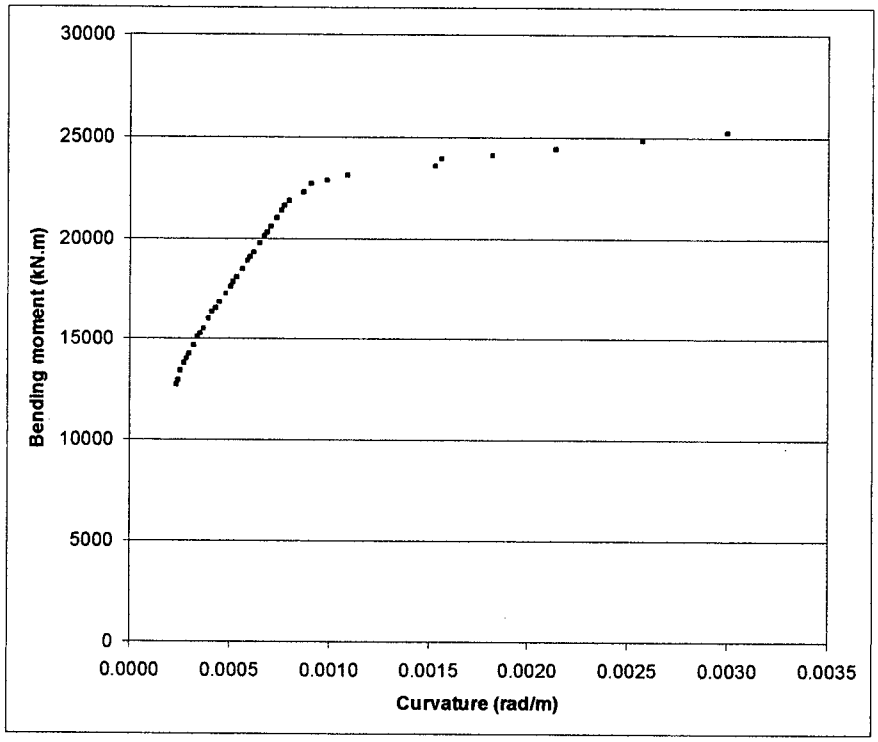

From Figure 5.10 and 5.11, it can be seen that the yield curvature of 0.00045 rad/m for Wall 1 and 0.0009 rad/m for Wall 2 determined previously are approximately the same values estimated from the moment-curvature relationships. Both procedures are giving the same result, so these values were used to estimate the plastic hinge length.

Similarly, the yield moment can be determined using these two procedures. The bending moment just above the base was calculated using the procedure described in this section for the yield drift. For Wall 1, this moment was 90680 kN.m; and for Wall 2, this moment was 22740 kN.m. These were approximately the same values estimated from the moment-curvature relationships shown in Figure 5.10 and 5.11. Therefore, these values were selected as the yield moments.

5.5 Revision of analytical results

The moment-curvature relationships of Wall 1 and 2 were used to check the results obtained from program VecTor2, by comparing these with the moment-curvature relationships obtained from a sectional analysis. Program Response-2000 was used for this purpose. Response-2000 is a computer program developed to perform two-dimensional sectional analysis of concrete members. This program was also

developed at the University of Toronto, by Evan Bentz. More information about the program Response-2000 can be found in the *Response-2000, Shell-2000, Triax-2000, Membrane-2000 User Manual* (Bentz 2001). Response-2000 was used to perform a sectional analysis of Wall 1 and 2 and develop their moment-curvature relationships for pure bending.

To compare the results obtained from VecTor2 and Response-2000, the material models used in both programs have to be the same. Response-2000 uses the Modified Compression Field Theory, and has specific constitutive models incorporated in it to account for effects like compression softening and tension stiffening. These models are different from the ones used in the VecTor2 analysis. Using different constitutive models can significantly change the response. Therefore, a new analysis for both walls was performed in VecTor2, using the same constitutive models as in Response-2000, in order to compare results. The new models used in this analysis are the following, the details of these models can be found in the *VecTor2 and FormWorks User's Manual* (Wong and Vecchio 2002: 45 – 88):

- Compression pre-peak response: Popovics for high-strength concrete.
- Compression post-peak response: Popovics for high-strength concrete.
- Compression softening: Vecchio-Collins 1986.
- Tension stiffening: Bentz 1999.
- Cracking criterion: Unixial cracking stress.
- Crack slip check: Vecchio-Collins 1986 (this check was not done before because it is not required when using the Disturbed Stress Field Model).
- Slip distortions: Not considered (since the Modified Compression Field Theory is being used).

The moment-curvature relationship from the results of VecTor2 was determined using the same procedure described in Section 5.4. Figure 5.12 shows the moment-curvature relationship of Wall 1:

Figure 5.12 Moment-curvature relationship of Wall 1 using Response-2000 constitutive models

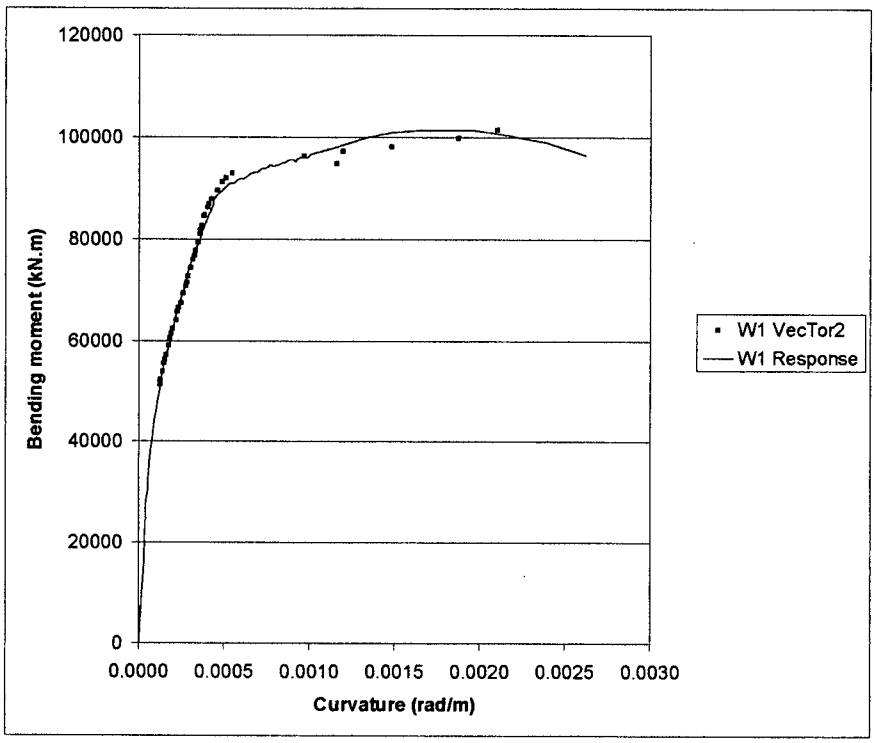

Figure 5.13 shows the moment-curvature relationship of Wall 2:

Figure 5.13 Moment-curvature relationship of Wall 2 using Response-2000 constitutive models

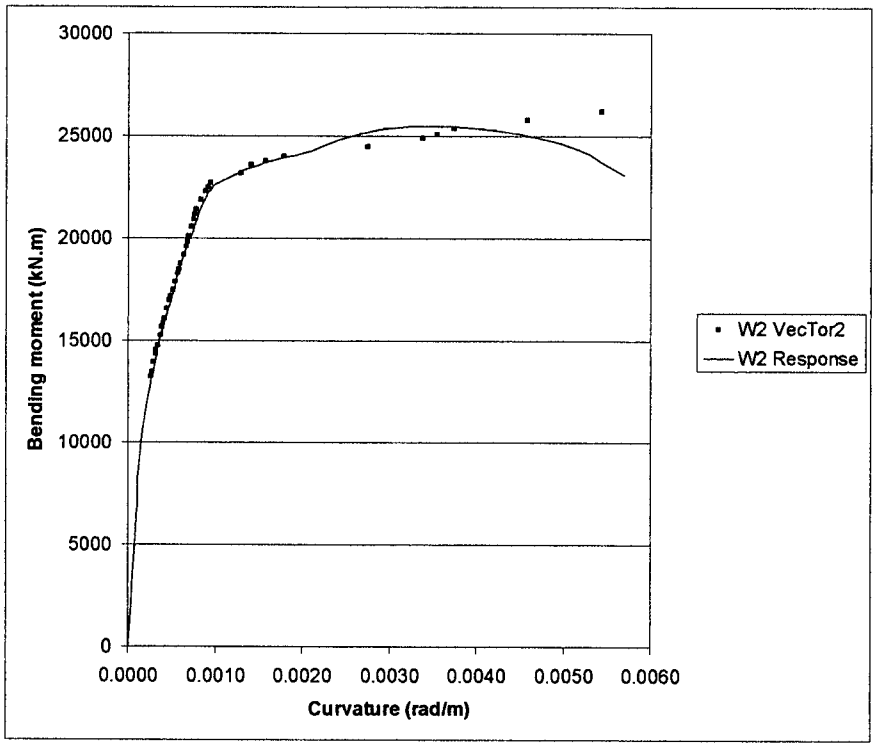

There is a good agreement between the results provided by VecTor2 and Response-2000. This analysis was only performed to check the VecTor2 predictions. The parametric study in this chapter was done using the constitutive models described in Chapter 3, since these models provided the best agreement with the experimental results from the tests described in Chapter 4.

5.6 Influence of wall length

The first parameter studied was the wall length. As it was discussed in Chapter 2, many models developed for plastic hinge length consider that it is proportional to the wall length only, so it is an important parameter to be considered. The results obtained for Wall 1 and 2 will be used to analyze how the plastic hinge length is influenced by the wall length.

As seen in Section 5.4, the yield curvature and yield moment for Wall 1 were 0.00045 rad/m and 90680 kN.m, respectively; and for Wall 2 they were 0.0009 rad/m and 22740 kN.m. The yield curvature was used to measure the plastic hinge length for a drift of 2% from the curvature distribution in Figure 5.8. For Wall 1, the plastic hinge length was 8.39m or $1.10l_w$; and for Wall 2, it was 6.21m or $1.63l_w$. Therefore, predicting the plastic hinge length as a function of the wall length only does not work for these walls.

A different approach to predict the plastic hinge length is by using moments; that is, the yield moment determined from the moment-curvature relationship defines the length of the plastic hinge. For a linear bending moment diagram like the one shown in Figure 2.6, the length where the yield moment is exceeded can be determined from Equation 2.11, repeated here for convenience:

$$\frac{L_p}{L_s} = 1 - \frac{M_y}{M_{\max}} \tag{5.1}$$

From Figure 5.9, the maximum moment in Wall 1 was 105633 kN.m, and for Wall 2 it was 25406 kN.m. Using Equation 5.1, the plastic hinge length for Wall 1 was 7.77m or $1.02l_w$; and for Wall 2, it was 5.76m or $1.51l_w$. This flexural prediction matches well with the measured plastic hinge lengths.

The spread of yielding was larger in Wall 1. To explain why a longer wall has a larger plastic hinge length, the tensile steel strains in the wall were observed. The average vertical steel strains in the elements along the height of the walls obtained from program VecTor2 were studied for this. The steel strains were observed in the exterior and interior steel layer in the boundary zones, shown in Figure 5.14:

Figure 5.14 Exterior and interior steel layers in zones in Wall 1 and 2

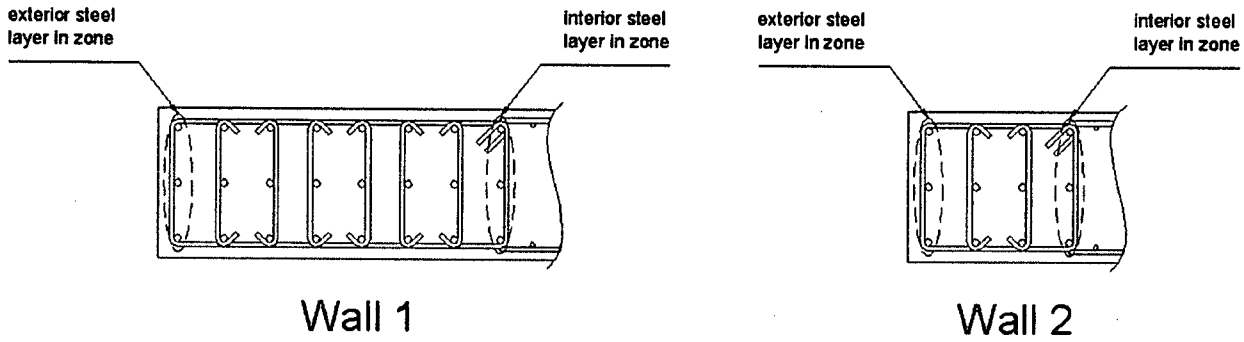

Figure 5.15 shows the steel strains up to the mid-height of both walls for a drift of 2%:

Figure 5.15 Steel strains up to the mid-height of Wall 1 and 2 for a drift of 2%

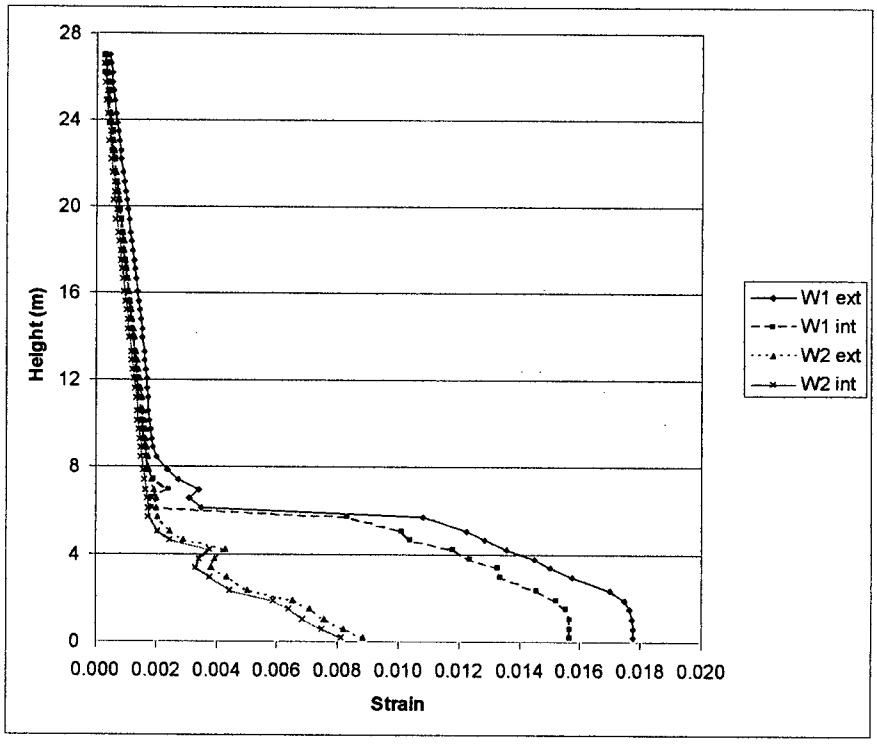

The steel strains exceed the yield strain (0.002 for these walls) at a larger distance from the base in Wall 1, so the spread of yielding was larger in this wall. The reason why the steel strains are larger in Wall 1 can be explained from the curvature distribution in Figure 5.8. At this drift, the curvatures at the base are approximately the same. For the same curvature, the steel strains will be larger in the longer wall; and therefore, it will have a larger spread of yielding.

The reason why a longer wall has a larger plastic hinge length can also be explained by comparing the moment-curvature relationships of both walls. The plastic hinge length increases as the

difference between the yield and ultimate moment increases, which is also reflected in Equation 5.1. By plotting the moment-curvature relationships together, it can be observed that the slope of the post-yielding phase is bigger in Wall 1; therefore, it has a larger plastic hinge length. This is shown in Figure 5.16:

Figure 5.16 Moment-curvature relationships of Wall 1 and 2

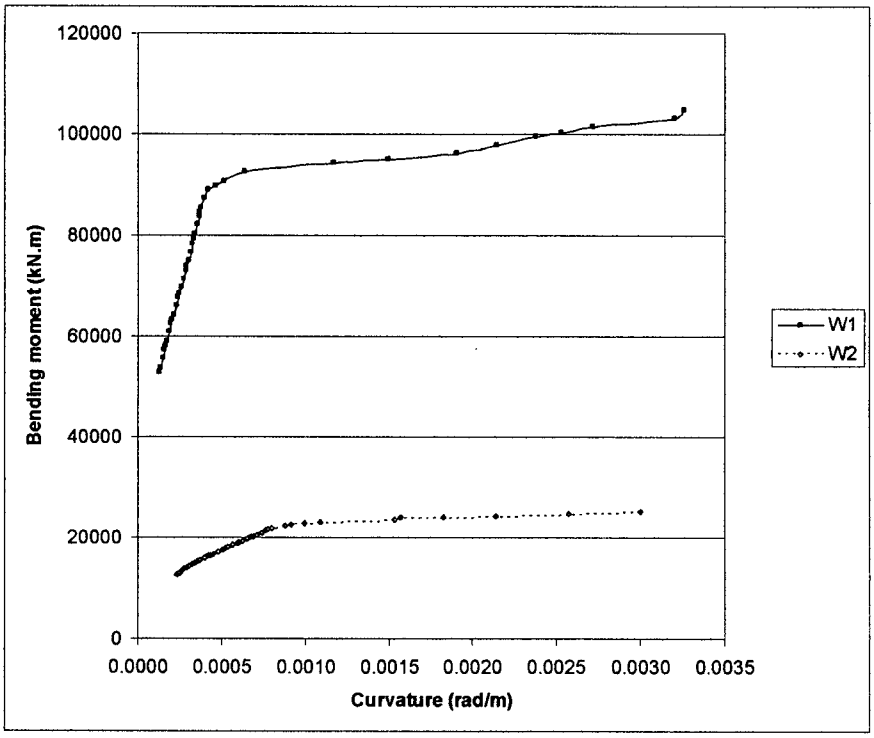

It can be concluded that longer walls have larger plastic hinge lengths because there is a bigger difference between the yield and ultimate moment for these. However, predicting the plastic hinge length as a function of the wall length only does not provide good results. Better predictions can be made by using a flexural prediction, like the one shown in Equation 5.1.

The measured (from curvature distribution) and predicted (using Equation 5.1) plastic hinge lengths were determined for different drift levels, using the same procedure described in Section 5.4 and this section. The results are shown in Table 5.2 and 5.3:

Table 5.2 Predicted and measured plastic hinge lengths for Wall 1

Drift (%)	M_{max} (kN.m)	M_y (kN.m)	L_s (m)	L_p (m)	
				W1 Predicted	W1 Measured
2.0	105632.9	90680.0	54.860	7.77	8.39
1.8	104908.8	90680.0	54.860	7.44	8.08
1.6	104316.3	90680.0	54.860	7.17	7.40
1.4	103345.3	90680.0	54.860	6.72	7.18
1.2	102281.0	90680.0	54.860	6.22	6.53

Table 5.3 Predicted and measured plastic hinge lengths for Wall 2

Drift (%)	M_{max} (kN.m)	M_y (kN.m)	L_s (m)	L_p (m)	
				W2 Predicted	W2 Measured
2.0	25405.7	22740.0	54.860	5.76	6.21
1.8	25136.9	22740.0	54.860	5.23	5.54
1.6	24769.3	22740.0	54.860	4.49	4.56
1.4	24050.6	22740.0	54.860	2.99	3.12
1.2	23079.6	22740.0	54.860	0.81	1.02

The flexural prediction provides good results for all drift levels.

5.7 Influence of shear span

The second parameter studied was the shear span. This parameter has also been included in many models for plastic hinge length presented in Chapter 2, so it has a significant importance.

So far, the analysis for Wall 1 and 2 had been performed for a shear span equal to the wall height. To study the influence of the shear span, three new analyses for each wall were performed in VecTor2 for the following shear spans:

- 35659mm (2/3 of wall height).
- 27430mm (1/2 of wall height).
- 19201mm (1/3 of wall height).

The models used for these analyses had the same characteristics as the previous ones, described in Section 5.3, except that the lateral load was now applied at these heights measured from the base. The results from the analysis were used to determine the curvatures and bending moments for different drift levels, using the same procedure described in Section 5.4 and 5.6.

Table 5.4 to 5.9 show the measured (from curvature distribution) and predicted (using Equation 5.1) plastic hinge lengths for different drift levels. These drifts were measured at the location of the lateral load (Δ/L_s):

Table 5.4 Predicted and measured plastic hinge lengths for Wall 1 for a shear span of 35659mm

Drift (%)	M_{max} (kN.m)	M_y (kN.m)	L_s (m)	L_p (m)	
				W1 Predicted	W1 Measured
1.6	106852.2	90680.0	35.659	5.40	6.06
1.4	106338.7	90680.0	35.659	5.25	5.72
1.2	105650.5	90680.0	35.659	5.05	5.74
1.0	103803.3	90680.0	35.659	4.51	5.01

Table 5.5 Predicted and measured plastic hinge lengths for Wall 2 for a shear span of 35659mm

Drift (%)	M_{max} (kN.m)	M_y (kN.m)	L_s (m)	L_p (m)	
				W2 Predicted	W2 Measured
1.6	25941.9	22740.0	35.659	4.40	4.74
1.4	25774.3	22740.0	35.659	4.20	4.29
1.2	25275.1	22740.0	35.659	3.58	3.61
1.0	24494.2	22740.0	35.659	2.55	2.61

Table 5.6 Predicted and measured plastic hinge lengths for Wall 1 for a shear span of 27430mm

Drift (%)	M_{max} (kN.m)	M_y (kN.m)	L_s (m)	L_p (m)	
				W1 Predicted	W1 Measured
1.6	108123.6	90680.0	27.430	4.43	5.55
1.4	107983.7	90680.0	27.430	4.40	5.37
1.2	106905.7	90680.0	27.430	4.16	5.31
1.0	105764.6	90680.0	27.430	3.91	4.61
0.8	104069.4	90680.0	27.430	3.53	4.00

Table 5.7 Predicted and measured plastic hinge lengths for Wall 2 for a shear span of 27430mm

Drift (%)	M_{max} (kN.m)	M_y (kN.m)	L_s (m)	L_p (m)	
				W2 Predicted	W2 Measured
1.6	26585.2	22740.0	27.430	3.97	4.28
1.4	26288.9	22740.0	27.430	3.70	3.98
1.2	26025.6	22740.0	27.430	3.46	3.50
1.0	25603.2	22740.0	27.430	3.07	3.06
0.8	24610.2	22740.0	27.430	2.08	2.16

Table 5.8 Predicted and measured plastic hinge lengths for Wall 1 for a shear span of 19201mm

Drift (%)	M_{max} (kN.m)	M_y (kN.m)	L_s (m)	L_p (m)	
				W1 Predicted	W1 Measured
1.2	108372.4	90680.0	19.201	3.13	4.45
1.0	107362.4	90680.0	19.201	2.98	4.31
0.8	106567.5	90680.0	19.201	2.86	3.40
0.6	104616.6	90680.0	19.201	2.56	3.01

Table 5.9 Predicted and measured plastic hinge lengths for Wall 2 for a shear span of 19201mm

Drift (%)	M_{max} (kN.m)	M_y (kN.m)	L_s (m)	L_p (m)	
				W2 Predicted	W2 Measured
1.2	26766.2	22740.0	19.201	2.89	3.16
1.0	26282.3	22740.0	19.201	2.59	2.80
0.8	25911.7	22740.0	19.201	2.35	2.47
0.6	24840.3	22740.0	19.201	1.62	1.63

It can be observed that as the shear span gets smaller, the measured plastic hinge length becomes larger than the predicted one; specially for Wall 1 at high drifts. The reason for this is that the shear stress becomes larger as the shear span decreases, because the lateral force required to produce the same maximum moment at the base becomes larger. This produces more diagonal cracking, which increases the tensile forces in the longitudinal reinforcement, and so, the length of the plastic hinge. Therefore, a pure flexural prediction does not work when shear stresses are high. However, for low shear stresses, the prediction is good, independent of the shear span. The influence of the shear span is strongly related to the influence of diagonal cracking, which will be studied in the next section.

5.8 Influence of diagonal cracking

The third parameter studied was the diagonal cracking. As it was discussed in Chapter 2, the reason why many of the models developed for plastic hinge length consider that it is proportional to the wall length is because the longer it is, more significant is the influence of diagonal cracking. Therefore, diagonal cracking was related to the wall length. In this study, diagonal cracking was related to the magnitude of the shear stress.

The results of all the previous analyses made for Wall 1 and 2 were used to study the influence of diagonal cracking. Additionally, two new analyses for each wall were performed in VecTor2, this time reducing the thickness of the web, so that the shear stresses become higher (that is, they were now flanged walls). These new analyses were performed for the following shear spans:

- 27430mm (1/2 of wall height).
- 19201mm (1/3 of wall height).

The models used for these analyses had the same characteristics as the previous ones, described in Section 5.3, with the lateral load being applied at these heights measured from the base. The only difference was that the web thickness was reduced from 508mm to 254mm. The results from the analysis were used to determine the curvatures and bending moments for different drift levels, using the same procedure described in Section 5.4 and 5.6.

Table 5.10 shows the material properties in the different regions of these new models of the two walls:

Table 5.10 Material properties of Wall 1 and 2 with a web thickness of 254mm

Concrete properties	**Material 1**		**Material 2**	
Color				
Thickness (mm)	508		254	
Cylinder compressive strength (MPa)	40		40	
Reinforcement component properties	***x*-direction**	***y*-direction**	***x*-direction**	***y*-direction**
Reinforcement ratio (%)	0.8	2.0	0.5	0.5
Reinforcement diameter (mm)	15	25	15	15
Yield strength (MPa)	400	400	400	400
Ultimate strength (MPa)	650	650	650	650
Elastic modulus (MPa)	200000	200000	200000	200000
Strain hardening modulus (MPa)	4875	4875	4875	4875
Strain hardening strain (mm/m)	10	10	10	10

Since the walls in these new analyses had a different web thickness, the moment-curvature relationship was also different. The yield curvature and yield moment were determined using the same procedures described in Section 5.4. Figure 5.17 shows the moment-curvature relationship for Wall 1 with a web thickness of 254mm:

Figure 5.17 Moment-curvature relationship of Wall 1 with a web thickness of 254mm

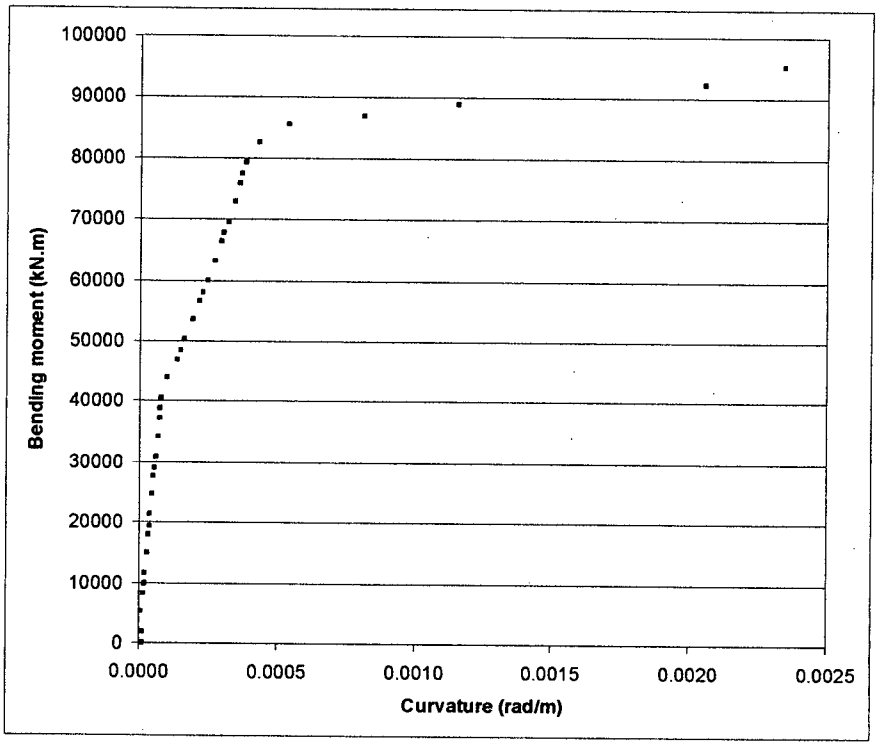

Figure 5.18 shows the moment-curvature relationship for Wall 2 with a web thickness of 254mm:

Figure 5.18 Moment-curvature relationship of Wall 2 with a web thickness of 254mm

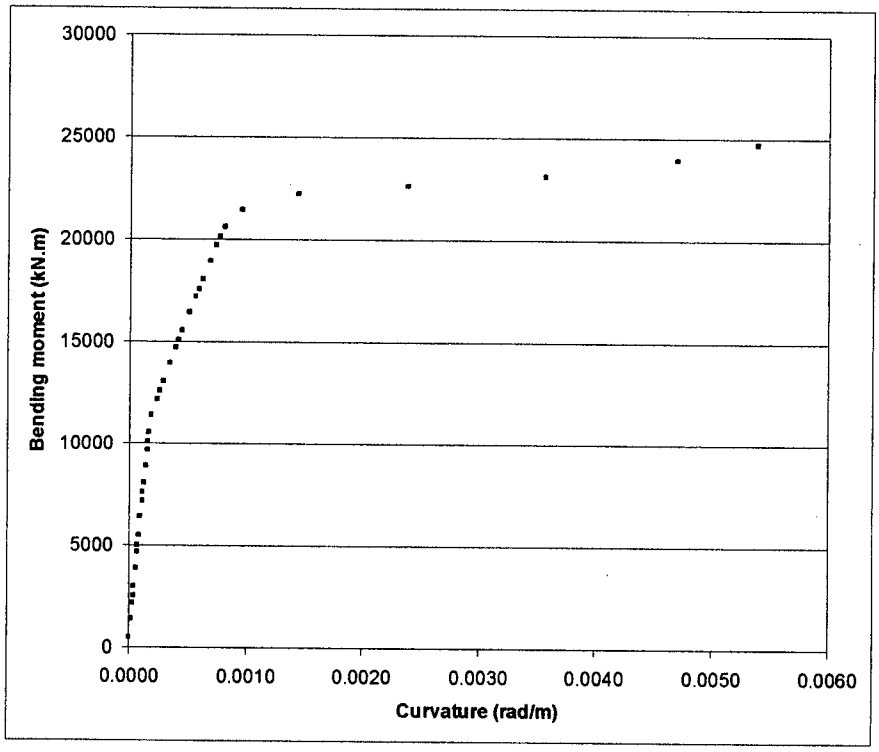

The yield curvature of both walls is approximately the same, and yield moment has decreased. The yield curvature and yield moment for Wall 1 were now 0.00045 rad/m and 84700 kN.m, respectively; and for Wall 2 they were now 0.0009 rad/m and 21420 kN.m. Table 5.11 to 5.14 show the measured (from curvature distribution) and predicted (using Equation 5.1) plastic hinge lengths for different drift levels. Again, these drifts were measured at the location of the lateral load (Δ/L_s):

Table 5.11 Predicted and measured plastic hinge lengths for Wall 1 for a web thickness of 254mm and a shear span of 27430mm

Drift (%)	M_{max} (kN.m)	M_y (kN.m)	L_s (m)	L_p (m)	
				W1 Predicted	W1 Measured
1.8	100292.3	84700.0	27.430	4.26	6.26
1.6	99837.0	84700.0	27.430	4.16	5.83
1.4	97971.7	84700.0	27.430	3.72	5.06
1.2	98202.1	84700.0	27.430	3.77	4.72
1.0	97801.7	84700.0	27.430	3.67	4.35
0.8	96663.3	84700.0	27.430	3.39	3.89

Table 5.12 Predicted and measured plastic hinge lengths for Wall 2 for a web thickness of 254mm and a shear span of 27430mm

Drift (%)	M_{max} (kN.m)	M_y (kN.m)	L_s (m)	L_p (m)	
				W2 Predicted	W2 Measured
1.8	25112.2	21420.0	27.430	4.03	4.42
1.6	24815.9	21420.0	27.430	3.75	4.13
1.4	24431.9	21420.0	27.430	3.38	3.72
1.2	24149.4	21420.0	27.430	3.10	3.30
1.0	23716.0	21420.0	27.430	2.66	2.79
0.8	23161.9	21420.0	27.430	2.06	2.06

Table 5.13 Predicted and measured plastic hinge lengths for Wall 1 for a web thickness of 254mm and a shear span of 19201mm

Drift (%)	M_{max} (kN.m)	M_y (kN.m)	L_s (m)	L_p (m)	
				W1 Predicted	W1 Measured
1.8	101277.6	84700.0	19.201	3.14	5.86
1.6	101004.9	84700.0	19.201	3.10	5.57
1.4	100235.0	84700.0	19.201	2.98	4.98
1.2	99442.0	84700.0	19.201	2.85	4.63
1.0	99117.5	84700.0	19.201	2.79	4.00
0.8	97243.5	84700.0	19.201	2.48	3.55
0.6	96679.0	84700.0	19.201	2.38	3.34

Table 5.14 Predicted and measured plastic hinge lengths for Wall 2 for a web thickness of 254mm and a shear span of 19201mm

Drift (%)	M_{max} (kN.m)	M_y (kN.m)	L_s (m)	L_p (m)	
				W2 Predicted	W2 Measured
1.8	25796.5	21420.0	19.201	3.26	3.68
1.6	25500.8	21420.0	19.201	3.07	3.47
1.4	25376.0	21420.0	19.201	2.99	3.49
1.2	24945.9	21420.0	19.201	2.71	3.16
1.0	24441.0	21420.0	19.201	2.37	2.81
0.8	24108.8	21420.0	19.201	2.14	2.37
0.6	23296.6	21420.0	19.201	1.55	1.63

It is clear from these results that as the shear span decreases and the shear stresses become higher, the plastic hinge length is much larger than the one determined from the pure flexural prediction. To make a better prediction, we have to account for the diagonal cracking. A measure of the diagonal cracking in the walls is the average shear stress, determined by:

$$v = \frac{V}{0.8 l_w b_w} \tag{5.2}$$

- v: Shear stress.
- V: Shear force.
- b_w: Web thickness of wall.

Although the lateral force acting on the walls keeps increasing until they reach their capacity, its increase after yielding is not very large. Therefore, the average shear stress in the walls after yielding remained approximately constant. Table 5.15 shows the average shear stress after yielding in Wall 1 and 2 calculated with Equation 5.2 for the six analyses presented so far in this chapter. The yield drifts (first yield of the longitudinal reinforcement) are also shown; these were determined by looking at the average vertical steel strains in the elements obtained from program VecTor2:

Table 5.15 Yield drifts and shear stresses of Wall 1 and 2

L_s (mm)	b_w (mm)	v (MPa)		Δ_y/L_s (%)	
		Wall 1	Wall 2	Wall 1	Wall 2
54860.0	508.0	0.60	0.30	0.61	1.18
35659.0	508.0	0.95	0.45	0.43	0.79
27430.0	508.0	1.25	0.60	0.35	0.63
19201.0	508.0	1.80	0.85	0.28	0.47
27430.0	254.0	2.30	1.15	0.37	0.65
19201.0	254.0	3.35	1.65	0.30	0.49

The results obtained so far show that the plastic hinge length increases as the lateral displacement or drift increases. This trend is plotted in Figure 5.19, which shows the measured plastic hinge lengths for Wall 1 and 2 as a function of the total drift for the six analyses presented so far in this chapter. The continuous lines show the results for Wall 1, and the discontinuous lines show the results for Wall 2:

Figure 5.19 Measured plastic hinge lengths vs. total drift for Wall 1 and 2

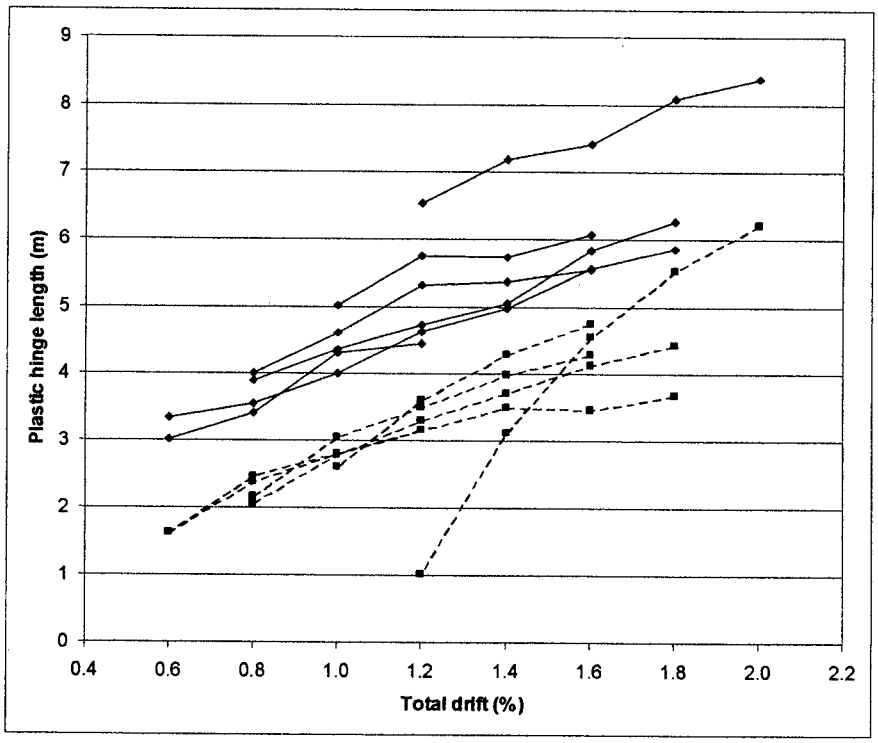

Figure 5.20 shows the measured plastic hinge lengths for Wall 1 and 2 as a function of the plastic drift. The plastic drift was calculated as the difference between the total drift and the yield drift:

Figure 5.20 Measured plastic hinge lengths vs. plastic drift for Wall 1 and 2

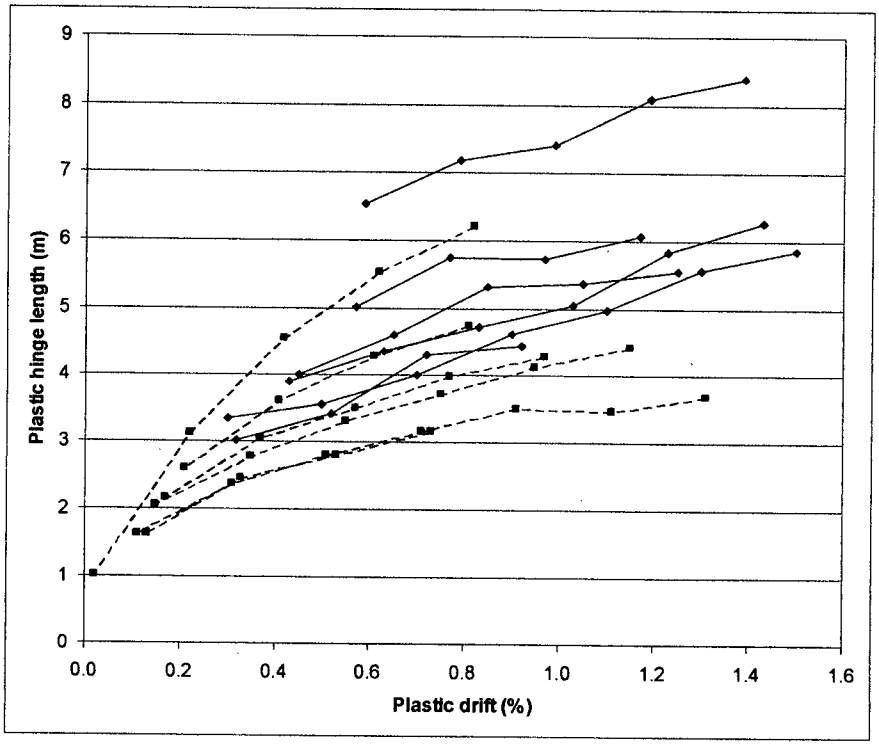

The quality of the predictions was evaluated by plotting the ratio of the measured to predicted plastic hinge length for different drift levels and shear stresses. This is shown in Figure 5.21 and 5.22:

Figure 5.21 Ratio of measured to predicted plastic hinge lengths vs. drift for Wall 1 for different shear stresses without accounting for shear

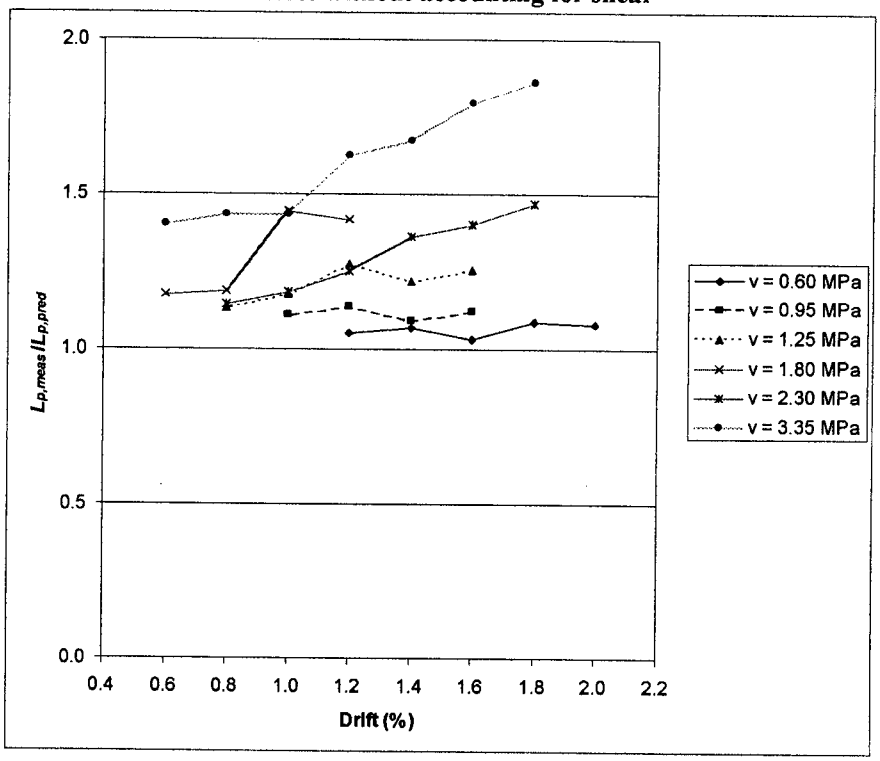

Figure 5.22 Ratio of measured to predicted plastic hinge lengths vs. drift for Wall 2 for different shear stresses without accounting for shear

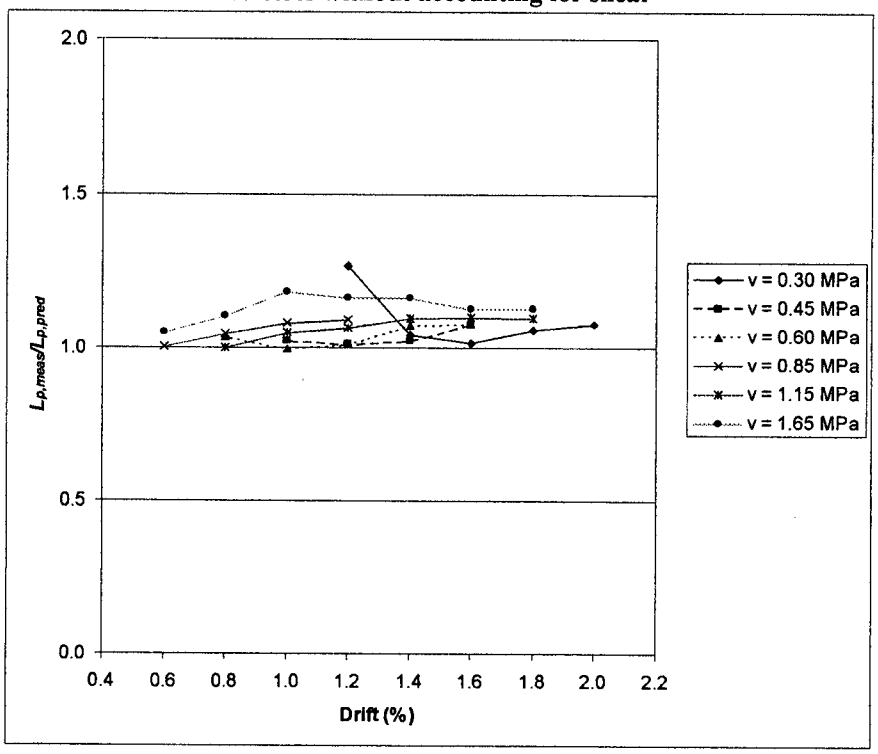

The predictions for Wall 2 are good for all cases because the shear stresses are not very high, since this wall is more slender than Wall 1. For Wall 1, it can be seen that the measured plastic hinge lengths are very large for high shear stresses.

As seen in Section 2.1, diagonal cracking changes the curvature distribution along the height (see Figure 2.5). This has an influence in the moment-curvature relationship. Figure 5.23 shows the moment-curvature relationship for Wall 1 for low and high shear stresses. These relations were developed for the same web thickness but different shear spans (see Table 5.15):

Figure 5.23 Moment-curvature relationships of Wall 1 for different shear stresses

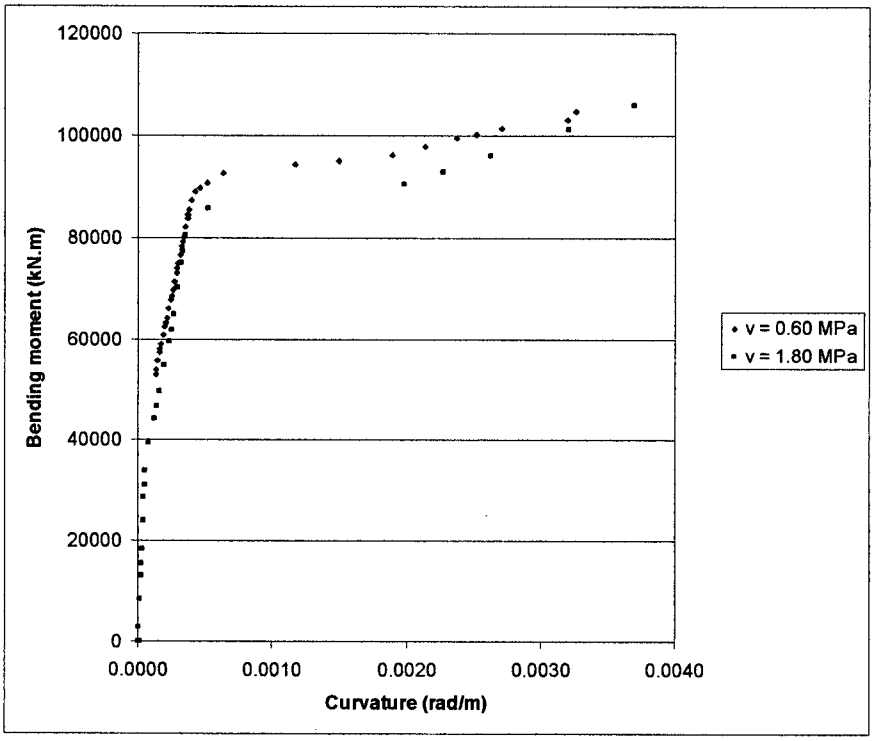

This difference in the moment-curvature relationship is the reason why the pure flexural prediction, which is based on the moment-curvature relationship developed for low shear stresses (pure bending), is not providing good results for Wall 1 for high shear stresses.

In order to improve the predictions for Wall 1, a very simple shear model was developed. As it was mentioned previously, high shear stresses produce more diagonal cracking, which increases the tensile forces in the longitudinal reinforcement. Therefore, we must take into account these additional tensile forces. A simple way to determine the additional tension due to shear (shift) is using the following expression:

$$\frac{N_v}{2} = \frac{V_s}{2} Cot\theta_c + V_c Cot\theta_c \tag{5.3}$$

- N_v: Axial compression due to shear.
- V_s: Shear force in the longitudinal reinforcement.
- θ_c: Angle of the crack.
- V_c: Shear force in the concrete.

It was consider that the total shear force was carried by the reinforcement ($V = V_s$ and $V_c = 0$), because it gives a smaller shift (which is more conservative, since this gives a smaller plastic hinge length). Also, it was assumed that $\theta_c = 45°$. Therefore, the additional tension due to shear is:

$$\frac{N_v}{2} = \frac{V}{2} \tag{5.4}$$

The additional moment due to shear is then given by:

$$M_v = \frac{V}{2} d_v \tag{5.5}$$

- M_v: Moment due to shear.
- d_v: Lever arm of the tensile force in the longitudinal reinforcement.

For these walls, it was considered that:

$$d_v = 0.8 l_w \tag{5.6}$$

So, for high shear stresses, the bending moment diagram is shifted by an amount equal to M_v. The total bending moment at any section is given by:

$$M = M_f + M_v \tag{5.7}$$

Where M_f is the moment due to flexure. This simple model was used to predict the plastic hinge length in Wall 1 for high shear stresses. In typical concrete codes, the following expression is proposed for the cracking shear stress:

$$v_{cr} = 0.17\sqrt{f_c'} \tag{5.8}$$

Where v_{cr} and f'_c are in MPa units. For a concrete cylinder strength of 40 MPa, used for Wall 1 and 2, the cracking shear stress is 1.08 MPa. However, Figure 5.21 for Wall 1 shows that for shear stresses up to 1.25 MPa, the pure flexural prediction provides good results. Also, Figure 5.22 for Wall 2 shows that the pure flexural prediction provides good results in all cases, for which the highest shear stress is 1.65 MPa. Therefore, the shear model should be used for shear stresses that are higher than these.

Figure 5.21 suggests that the influence of diagonal cracking in the plastic hinge length is significant for shear stresses higher or equal than 1.8 MPa; this value is equal to 0.29 times the square root of f'_c. Based on this, the cracking shear stress should be:

$$v_{cr} = 0.3\sqrt{f'_c} \tag{5.9}$$

The following expression was proposed to account for shear stresses:

$$M_v = \begin{cases} 0 & ; \ v < v_{cr} \\ \frac{V}{2} d_v & ; \ v \geq v_{cr} \end{cases} \tag{5.10}$$

Where v_{cr} is calculated with Equation 5.9. The plastic hinge length in Wall 1 was predicted for different drift levels and for shear stresses of 1.8, 2.3 and 3.35 MPa, using this model. For the linear bending moment diagram of Wall 1, since it is now shifted by M_v, the yield moment is located at a larger distance from the base, so the plastic hinge length is longer. The moment due to shear was first calculated with Equation 5.5, and then added to the maximum bending moment at the base. Then, this moment was applied in Equation 5.1 to determine the plastic hinge length. The results are shown in Table 5.16 to 5.18:

Table 5.16 Predicted and measured plastic hinge lengths for Wall 1 for a shear span of 19201mm using shear model

Drift (%)	V (kN)	l_w (mm)	b_w (mm)	v (MPa)	d_v (mm)	M_v (kN.m)
1.2	5644.1	7620.0	508.0	1.82	6096.0	17203.2
1.0	5591.5	7620.0	508.0	1.81	6096.0	17042.9
0.8	5550.1	7620.0	508.0	1.79	6096.0	16916.7
0.6	5448.5	7620.0	508.0	1.76	6096.0	16607.0
Drift (%)	M_f (kN.m)	M_{max} (kN.m)	M_y (kN.m)	L_s (m)	L_p (m)	
					W1 Predicted	W1 Measured
1.2	108372.4	125575.6	90680.0	19.201	5.34	4.45
1.0	107362.4	124405.3	90680.0	19.201	5.21	4.31
0.8	106567.5	123484.2	90680.0	19.201	5.10	3.40
0.6	104616.6	121223.7	90680.0	19.201	4.84	3.01

Table 5.17 Predicted and measured plastic hinge lengths for Wall 1 for a web thickness of 254mm and a shear span of 27430mm using shear model

Drift (%)	V (kN)	l_w (mm)	b_w (mm)	v (MPa)	d_v (mm)	M_v (kN.m)
1.8	3656.3	7620.0	254.0	2.36	6096.0	11144.4
1.6	3639.7	7620.0	254.0	2.35	6096.0	11093.8
1.4	3571.7	7620.0	254.0	2.31	6096.0	10886.5
1.2	3580.1	7620.0	254.0	2.31	6096.0	10912.1
1.0	3565.5	7620.0	254.0	2.30	6096.0	10867.6
0.8	3524.0	7620.0	254.0	2.28	6096.0	10741.2
Drift (%)	M_f (kN.m)	M_{max} (kN.m)	M_y (kN.m)	L_s (m)	L_p (m)	
					W1 Predicted	W1 Measured
1.8	100292.3	111436.7	84700.0	27.430	6.58	6.26
1.6	99837.0	110930.8	84700.0	27.430	6.49	5.83
1.4	97971.7	108858.3	84700.0	27.430	6.09	5.06
1.2	98202.1	109114.3	84700.0	27.430	6.14	4.72
1.0	97801.7	108669.3	84700.0	27.430	6.05	4.35
0.8	96663.3	107404.5	84700.0	27.430	5.80	3.89

Table 5.18 Predicted and measured plastic hinge lengths for Wall 1 for a web thickness of 254mm and a shear span of 19201mm using shear model

Drift (%)	V (kN)	l_w (mm)	b_w (mm)	v (MPa)	d_v (mm)	M_v (kN.m)
1.8	5274.6	7620.0	254.0	3.41	6096.0	16077.0
1.6	5260.4	7620.0	254.0	3.40	6096.0	16033.7
1.4	5220.3	7620.0	254.0	3.37	6096.0	15911.5
1.2	5179.0	7620.0	254.0	3.34	6096.0	15785.6
1.0	5162.1	7620.0	254.0	3.33	6096.0	15734.1
0.8	5064.5	7620.0	254.0	3.27	6096.0	15436.6
0.6	5035.1	7620.0	254.0	3.25	6096.0	15347.0
Drift (%)	M_f (kN.m)	M_{max} (kN.m)	M_y (kN.m)	L_s (m)	L_p (m)	
					W1 Predicted	W1 Measured
1.8	101277.6	117354.6	84700.0	19.201	5.34	5.86
1.6	101004.9	117038.6	84700.0	19.201	5.31	5.57
1.4	100235.0	116146.5	84700.0	19.201	5.20	4.98
1.2	99442.0	115227.6	84700.0	19.201	5.09	4.63
1.0	99117.5	114851.6	84700.0	19.201	5.04	4.00
0.8	97243.5	112680.1	84700.0	19.201	4.77	3.55
0.6	96679.0	112025.9	84700.0	19.201	4.68	3.34

The quality of these predictions was evaluated by plotting the ratio of the measured to predicted plastic hinge length. This is shown in Figure 5.24:

Figure 5.24 Ratio of measured to predicted plastic hinge lengths vs. drift for Wall 1 for different shear stresses using the shear model

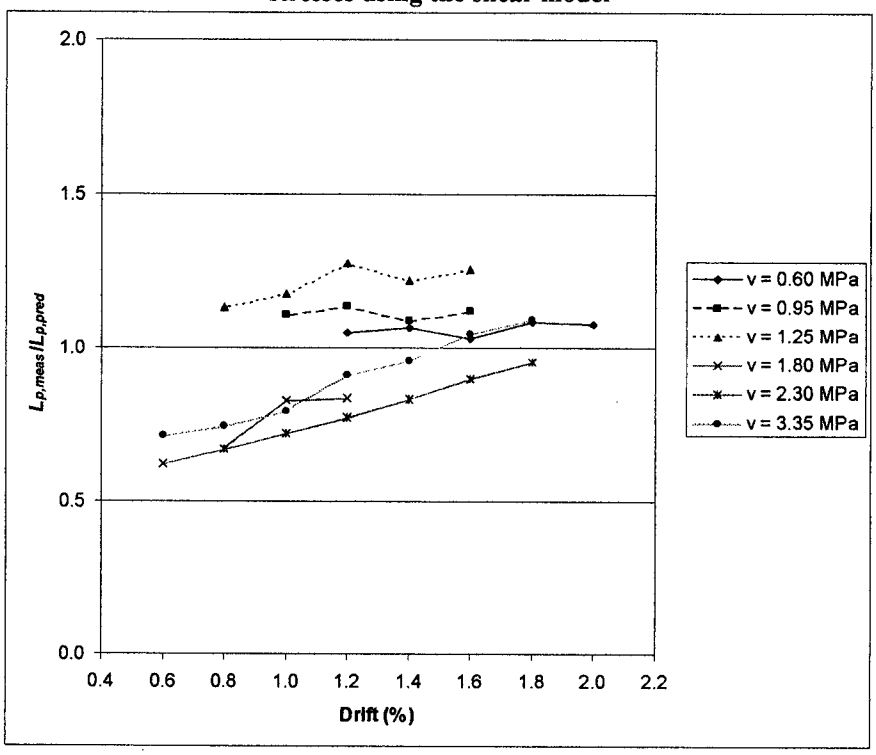

Although the predictions are now very large for low drifts (which is conservative), they are good for high drifts, which are of more interest. Considering the simplicity of the model used, the results are satisfactory. The reason why this shear model does not work for low drifts is because at this point, there are not many diagonal cracks formed in the wall, so their influence is still not significant.

It can be concluded that the diagonal cracking in walls has a significant influence in the plastic hinge length. For high shear stresses, the actual plastic hinge length is larger than the one predicted using a pure flexural prediction. The effect of shear needs to be included to estimate the length of the plastic hinge.

5.9 Influence of axial load

The fourth parameter studied was the axial load. As seen in Chapter 2, the axial load was also considered in some of the models developed for plastic hinge length. Different conclusions were made regarding the influence of axial load. Some researchers concluded that it has a significant influence in the plastic hinge length, while others did not find any significant dependence.

Studying the influence of axial load is of particular importance for coupled walls, which are subjected to high tensile and compressive axial loads. Previous studies presented in Chapter 2 were done

for compressive axial loads only, not tensile axial loads. In this study, the influence of both tensile and compressive axial loads was investigated.

The first analysis made for Wall 1 and 2, for a shear span equal to the wall height and a web thickness of 508mm, described in Section 5.3, were performed for a compressive axial load ratio (P/f'_cA_g) of 0.1. To study the influence of compressive axial loads, three new analyses for each wall were performed in VecTor2 for the following axial load ratios:

- 0.3 (46452 kN for Wall 1 and 23226 kN for Wall 2).
- 0.2 (30968 kN for Wall 1 and 15484 kN for Wall 2).
- Zero.

To study the influence of tensile axial loads, two additional analyses for each wall were performed. The tensile axial load applied cannot exceed the pure tension capacity of the walls (f_yA_s), equal to 15200 kN for Wall 1 and 7680 kN for Wall 2. The following axial load ratios were selected:

- 0.02 (3800 kN for Wall 1 and 1920 kN for Wall 2), which is equal to 1/4 of the pure tension capacity.
- 0.05 (7600 kN for Wall 1 and 3840 kN for Wall 2), which is equal to 1/2 of the pure tension capacity.

The models used for these analyses had the same characteristics as the previous ones, described in Section 5.3. The only difference was the magnitude of the constant axial loads; these loads were also equally distributed among all the six nodes at the top of each wall. The results from the analysis were used to determine the curvatures and bending moments for different drift levels, using the same procedure described in Section 5.4 and 5.6.

Since the axial load was different for all these analyses, the moment-curvature relationship was also different in all cases. The yield curvature and yield moment were also different; these were determined using the same procedures described in Section 5.4. Figure 5.25 shows the moment-curvature relationship for Wall 1 for the six axial load ratios considered (the negative sign indicates compression):

Figure 5.25 Moment-curvature relationships of Wall 1 for different axial load ratios

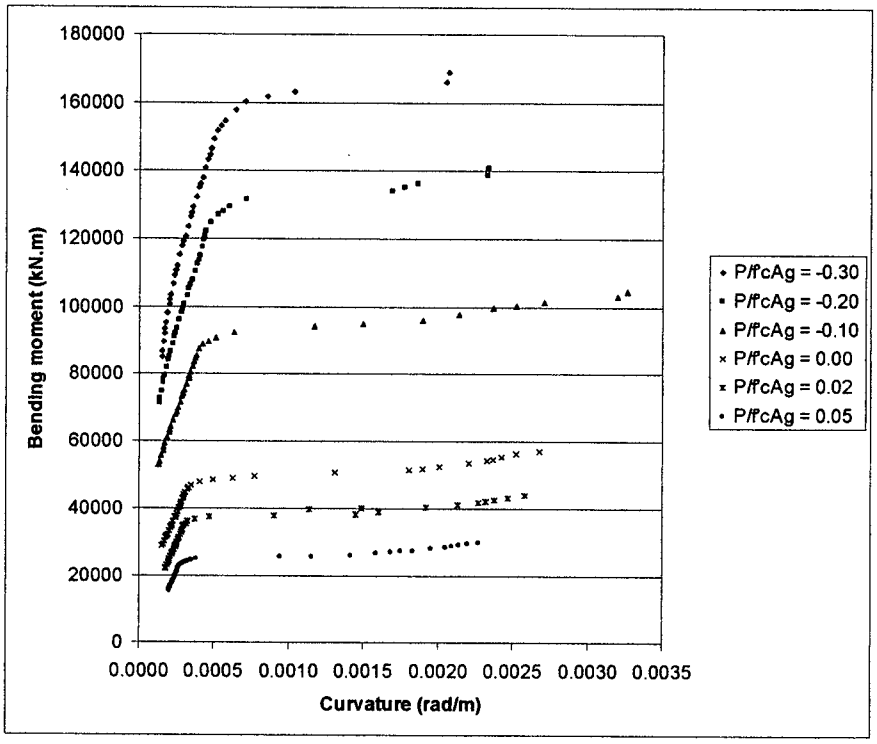

Figure 5.26 shows the moment-curvature relationship for Wall 2 for the six axial load ratios considered:

Figure 5.26 Moment-curvature relationships of Wall 2 for different axial load ratios

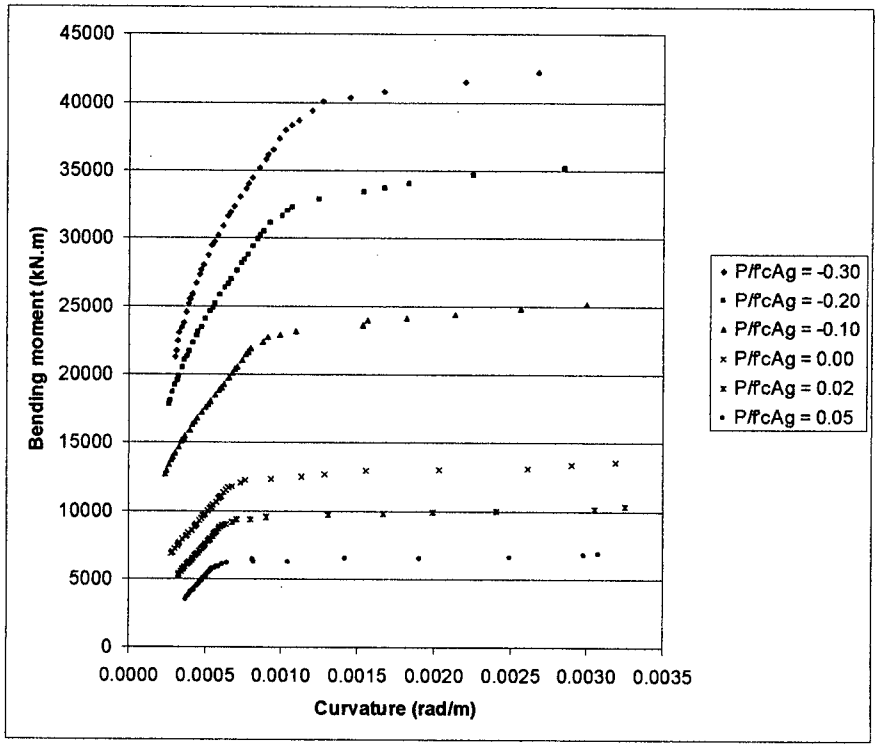

Table 5.19 shows the yield curvature and yield moment for each of the cases analyzed:

Table 5.19 Yield curvature and yield moment of Wall 1 and 2 for different axial load ratios

P/f'_cA_g	P (kN)		ϕ_y (rad/m)		M_y (kN.m)	
	Wall 1	Wall 2	Wall 1	Wall 2	Wall 1	Wall 2
-0.30	-46452.0	-23226.0	0.00062	0.00120	157840.0	39480.0
-0.20	-30968.0	-15484.0	0.00053	0.00104	127380.0	31800.0
-0.10	-15484.0	-7742.0	0.00045	0.00090	90680.0	22740.0
0.00	0.0	0.0	0.00037	0.00075	47910.0	12150.0
0.02	3800.0	1920.0	0.00035	0.00070	36270.0	9300.0
0.05	7600.0	3840.0	0.00032	0.00064	23900.0	6040.0

Table 5.20 to 5.29 show the measured (from curvature distribution) and predicted (using Equation 5.1) plastic hinge lengths for different drift levels. The results for Wall 1 and 2 for a compressive axial load ratio of 0.1 were presented in Table 5.2 and 5.3, respectively:

Table 5.20 Predicted and measured plastic hinge lengths for Wall 1 for a compressive axial load ratio of 0.3

Drift (%)	M_{max} (kN.m)	M_y (kN.m)	L_s (m)	L_p (m)	
				W1 Predicted	W1 Measured
1.2	170170.2	157840.0	54.860	3.98	4.28
1.0	168431.2	157840.0	54.860	3.45	3.43
0.8	160306.4	157840.0	54.860	0.84	0.78

Table 5.21 Predicted and measured plastic hinge lengths for Wall 2 for a compressive axial load ratio of 0.3

Drift (%)	M_{max} (kN.m)	M_y (kN.m)	L_s (m)	L_p (m)	
				W2 Predicted	W2 Measured
2.0	42522.0	39480.0	54.860	3.92	3.94
1.8	41781.4	39480.0	54.860	3.02	3.03
1.6	40722.6	39480.0	54.860	1.67	1.30

Table 5.22 Predicted and measured plastic hinge lengths for Wall 1 for a compressive axial load ratio of 0.2

Drift (%)	M_{max} (kN.m)	M_y (kN.m)	L_s (m)	L_p (m)	
				W1 Predicted	W1 Measured
1.4	141950.3	127380.0	54.860	5.63	5.93
1.2	141741.8	127380.0	54.860	5.56	5.64
1.0	139481.6	127380.0	54.860	4.76	4.71
0.8	134066.9	127380.0	54.860	2.74	2.61

Table 5.23 Predicted and measured plastic hinge lengths for Wall 2 for a compressive axial load ratio of 0.2

Drift (%)	M_{max} (kN.m)	M_y (kN.m)	L_s (m)	L_p (m)	
				W2 Predicted	W2 Measured
2.0	35472.5	31800.0	54.860	5.68	5.38
1.8	34781.2	31800.0	54.860	4.70	4.50
1.6	33826.7	31800.0	54.860	3.29	3.17
1.4	32614.3	31800.0	54.860	1.37	1.23

Table 5.24 Predicted and measured plastic hinge lengths for Wall 1 for no axial load

Drift (%)	M_{max} (kN.m)	M_y (kN.m)	L_s (m)	L_p (m)	
				W1 Predicted	W1 Measured
2.0	57690.8	47910.0	54.860	9.30	10.10
1.8	56730.7	47910.0	54.860	8.53	9.32
1.6	55929.8	47910.0	54.860	7.87	8.59
1.4	55145.3	47910.0	54.860	7.20	7.87
1.2	54278.5	47910.0	54.860	6.44	6.97

Table 5.25 Predicted and measured plastic hinge lengths for Wall 2 for no axial load

Drift (%)	M_{max} (kN.m)	M_y (kN.m)	L_s (m)	L_p (m)	
				W2 Predicted	W2 Measured
2.0	13720.5	12150.0	54.860	6.28	6.24
1.8	13391.3	12150.0	54.860	5.09	5.78
1.6	13314.5	12150.0	54.860	4.80	4.99
1.4	12957.9	12150.0	54.860	3.42	4.00
1.2	12683.6	12150.0	54.860	2.31	2.21

Table 5.26 Predicted and measured plastic hinge lengths for Wall 1 for a tensile axial load ratio of 0.02

Drift (%)	M_{max} (kN.m)	M_y (kN.m)	L_s (m)	L_p (m)	
				W1 Predicted	W1 Measured
2.0	44381.7	36270.0	54.860	10.03	10.01
1.8	43778.3	36270.0	54.860	9.41	9.73
1.6	42906.0	36270.0	54.860	8.48	8.86
1.4	42116.0	36270.0	54.860	7.61	8.06
1.2	41260.2	36270.0	54.860	6.64	6.84

Table 5.27 Predicted and measured plastic hinge lengths for Wall 2 for a tensile axial load ratio of 0.02

Drift (%)	M_{max} (kN.m)	M_y (kN.m)	L_s (m)	L_p (m)	
				W2 Predicted	W2 Measured
2.0	10461.8	9300.0	54.860	6.09	6.18
1.8	10275.3	9300.0	54.860	5.21	5.65
1.6	10209.4	9300.0	54.860	4.89	5.05
1.4	9918.7	9300.0	54.860	3.42	3.82
1.2	9627.9	9300.0	54.860	1.87	2.17

Table 5.28 Predicted and measured plastic hinge lengths for Wall 1 for a tensile axial load ratio of 0.05

Drift (%)	M_{max} (kN.m)	M_y (kN.m)	L_s (m)	L_p (m)	
				W1 Predicted	W1 Measured
2.0	30381.5	23900.0	54.860	11.70	11.19
1.8	29778.0	23900.0	54.860	10.83	10.29
1.6	29031.9	23900.0	54.860	9.70	9.17
1.4	28423.0	23900.0	54.860	8.73	8.35
1.2	27792.1	23900.0	54.860	7.68	7.03

Table 5.29 Predicted and measured plastic hinge lengths for Wall 2 for a tensile axial load ratio of 0.05

Drift (%)	M_{max} (kN.m)	M_y (kN.m)	L_s (m)	L_p (m)	
				W2 Predicted	W2 Measured
2.0	6906.9	6040.0	54.860	6.89	6.04
1.8	6868.5	6040.0	54.860	6.62	5.87
1.6	6665.5	6040.0	54.860	5.15	5.14
1.4	6616.1	6040.0	54.860	4.78	3.79
1.2	6292.4	6040.0	54.860	2.20	1.18

It can be observed that the flexural prediction provides good results for the different axial load ratios and drift levels. Figure 5.27 shows the measured plastic hinge lengths for Wall 1 as a function of the total drift:

Figure 5.27 Measured plastic hinge lengths vs. total drift for Wall 1 for different axial load ratios

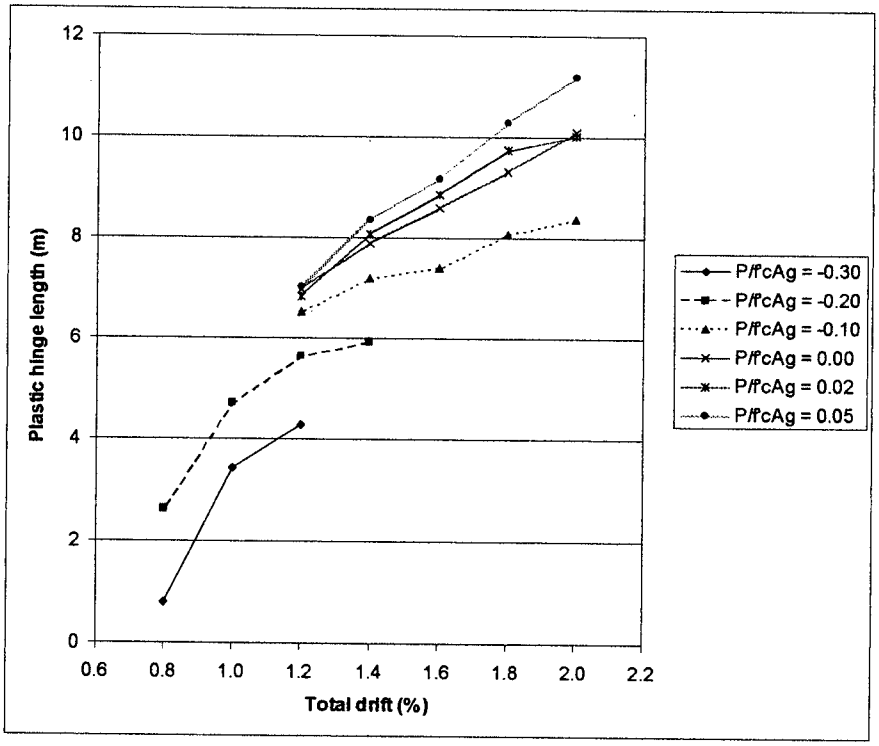

Figure 5.28 shows the measured plastic hinge lengths for Wall 2 as a function of the total drift:

Figure 5.28 Measured plastic hinge lengths vs. total drift for Wall 2 for different axial load ratios

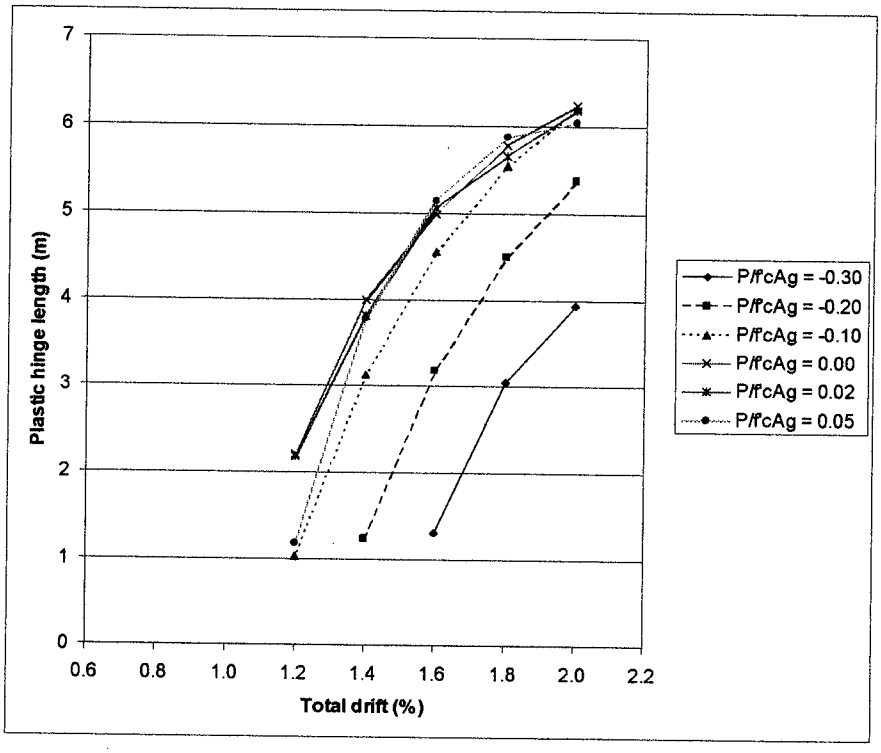

These plots show that the plastic hinge length of the wall reduces when it is subjected to compressive axial forces, and increases when it is subjected to tensile axial forces. This is because the compression load reduces the length in which the inelastic curvatures occur, and so, the length of the plastic hinge. The tension load has the opposite effect.

The quality of the predictions was evaluated by plotting the ratio of the measured to predicted plastic hinge length for different drift levels and axial loads. This is shown in Figure 5.29 and 5.30:

Figure 5.29 Ratio of measured to predicted plastic hinge lengths vs. drift for Wall 1 for different axial load ratios

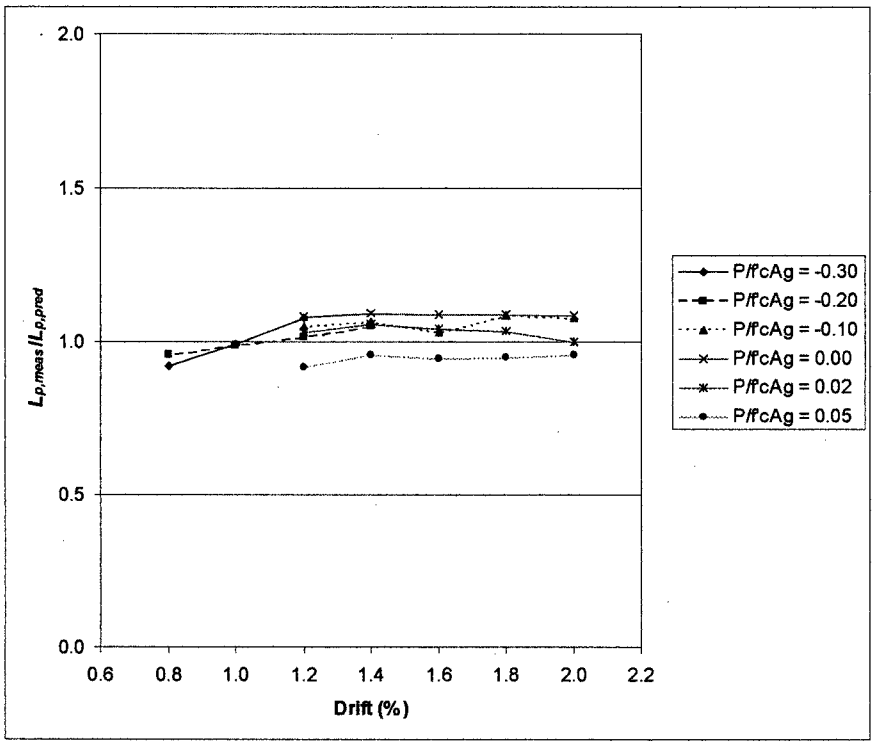

Figure 5.30 Ratio of measured to predicted plastic hinge lengths vs. drift for Wall 2 for different axial load ratios

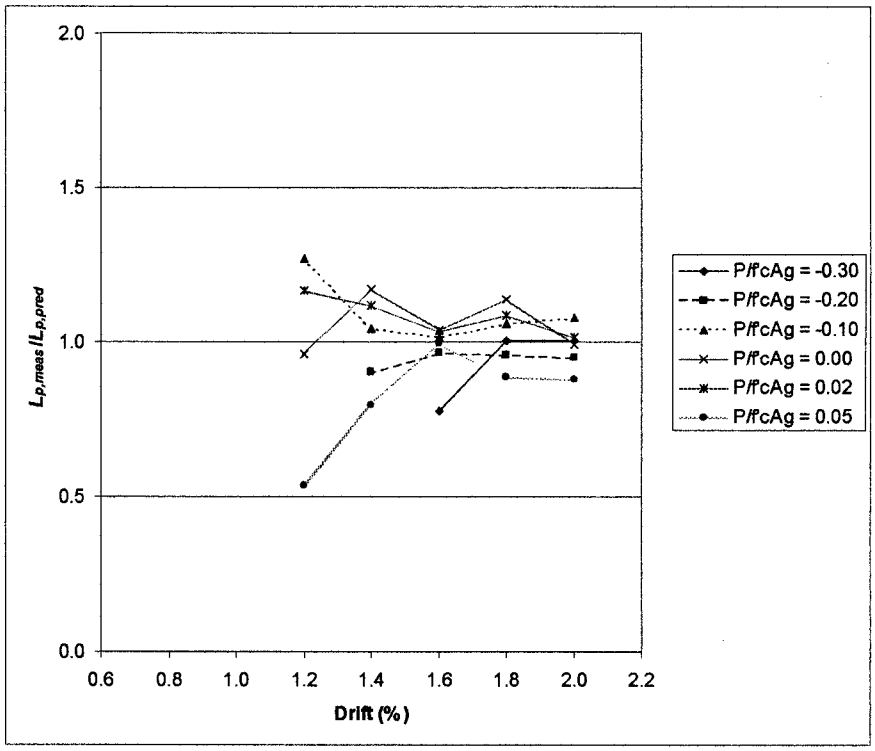

Most of the predictions shown in these figures are good. Some of the predictions for Wall 2 are not very good for the lowest drifts. This is because the wall at these drifts has just started yielding, the plastic hinge length is very small, and the ratio of measured to predicted becomes either too large or too small. For large drifts, all the predictions are good.

It can be concluded that the length of the plastic hinge reduces with the addition of compression and increases with the addition of tension. The flexural prediction can be used to estimate the plastic hinge length in walls subjected to compressive and tensile axial loads.

5.10 Summary

Table 5.30 shows the measured plastic hinge lengths at maximum drift as a function of the parameters studied for the 22 analyses presented in this chapter. These are measured plastic hinge lengths considering a linearly varying inelastic curvature:

Table 5.30 Measured plastic hinge lengths at maximum drift

Wall	L_s (m)	v (MPa)	P/f'_cA_g	L_p (m)	L_p/l_w	L_p/L_s
Wall 1	54.860	0.60	-0.10	8.39	1.10	0.15
Wall 2	54.860	0.30	-0.10	6.21	1.63	0.11
Wall 1	35.659	0.95	-0.10	6.06	0.80	0.17
Wall 2	35.659	0.45	-0.10	4.74	1.25	0.13
Wall 1	27.430	1.25	-0.10	5.55	0.73	0.20
Wall 2	27.430	0.60	-0.10	4.28	1.12	0.16
Wall 1	19.201	1.80	-0.10	4.45	0.58	0.23
Wall 2	19.201	0.85	-0.10	3.16	0.83	0.16
Wall 1	27.430	2.30	-0.10	6.26	0.82	0.23
Wall 2	27.430	1.15	-0.10	4.42	1.16	0.16
Wall 1	19.201	3.35	-0.10	5.86	0.77	0.30
Wall 2	19.201	1.65	-0.10	3.68	0.97	0.19
Wall 1	54.860	1.00	-0.30	4.28	0.56	0.08
Wall 2	54.860	0.50	-0.30	3.94	1.04	0.07
Wall 1	54.860	0.80	-0.20	5.93	0.78	0.11
Wall 2	54.860	0.40	-0.20	5.38	1.41	0.10
Wall 1	54.860	0.32	0.00	10.10	1.33	0.18
Wall 2	54.860	0.16	0.00	6.24	1.64	0.11
Wall 1	54.860	0.25	0.02	10.01	1.31	0.18
Wall 2	54.860	0.12	0.02	6.18	1.62	0.11
Wall 1	54.860	0.17	0.05	11.19	1.47	0.20
Wall 2	54.860	0.08	0.05	6.04	1.59	0.11

CHAPTER 6: SYSTEMS OF WALLS OF DIFFERENT LENGTHS CONNECTED TOGETHER BY RIGID SLABS

6.1 Scope of analysis

Program VecTor2 was used to investigate plastic hinge lengths in a system of walls of different lengths interconnected by rigid slabs at various levels. The parametric study in Chapter 5 was performed for Wall 1 and 2 separately. A new analysis for these two walls was performed, being under the same conditions as the ones described in Section 5.2, except that they were now combined together, to see how this influences the length of the plastic hinge. Additional analyses with walls of other lengths were also performed.

In high-rise buildings, it is common to have parallel walls of different lengths providing lateral resistance. These walls, as well as the gravity columns, are interconnected by rigid slabs at numerous floor levels. As a result, the lateral displacement of all these elements is the same at these levels.

To study how the plastic hinge length in walls of different lengths is influenced when they are connected together, three new analyses were performed in VecTor2 for the following wall systems:

- The first system consisted of Wall 1 and 2 combined together. Wall 1 was two times longer than Wall 2.
- The second system consisted of Wall 1 combined together with a wall that was four times shorter. This wall will be referred to as Wall 3.
- The third system consisted of Wall 1 combined together with a column that was eight times shorter. This column will be referred to as Column 1.

6.2 Wall 1 combined with Wall 2

The description of Wall 1 and 2 and their individual analytical models have already been given in Section 5.2 and 5.3, respectively. The description of the analytical model for these two walls combined together and the results obtained will be presented in the following sections.

6.2.1 Description of wall system model

The model used to analyze Wall 1 and 2 combined is presented in Figure 6.1. The slabs were provided every 2743mm, resulting in a 20 storey building. The thickness of the slabs was 203mm.

Figure 6.1 Model of Wall 1 and 2 combined

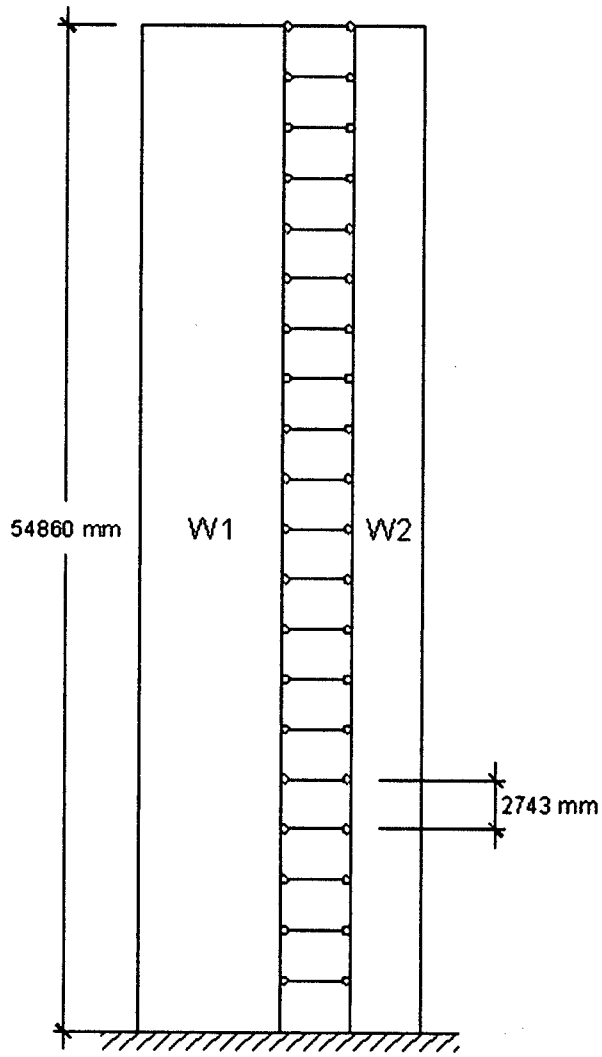

6.2.2 Analytical model of wall system

Wall 1 and 2 were modeled and analyzed together using program VecTor2. The finite element mesh used for each wall, as well as the boundary conditions, material properties and loads, were the same as the ones described in Section 5.3.

The slabs interconnecting the walls at each floor level were modeled using truss bar elements. This type of element in VecTor2 is typically used to model the reinforcing steel as discrete bars (see Section 3.3), so reinforcement properties have to be assigned to it. These elements were provided with a very high strength and stiffness, so that they do not yield and do not deform axially, in order to force the lateral displacements in both walls to be the same. A new material type was created to represent this region of the wall system.

Since the slabs are very stiff, the strains in the transverse direction of the wall at the floor levels are very small. To simulate that effect in VecTor2, the rectangular elements located at each storey level were also provided with very stiff properties. These elements had a height equal to the slab thickness (203mm). These were only provided up to half the height of the wall, where the mesh was more refined. A new material type was created to represent this region of the wall system.

All nodes and elements were numbered in the horizontal (short) direction of the wall system. The complete mesh consisted of 3357 nodes, 3066 rectangular elements, 116 triangular elements and 20 truss elements.

A monotonic lateral load was applied at the top of the Wall 1. This load was applied in a displacement-control mode, in increments of 1mm. Additionally, a constant axial load of 15484 kN in Wall 1 and 7742 kN in Wall 2 was applied; these loads were equally distributed among the six nodes at the top of each wall. The self-weight of the walls was not considered.

Figure 6.2 shows the finite element model of Wall 1 and 2, created in the pre-processor FormWorks:

Figure 6.2 Finite element model of Wall 1 and 2 in FormWorks

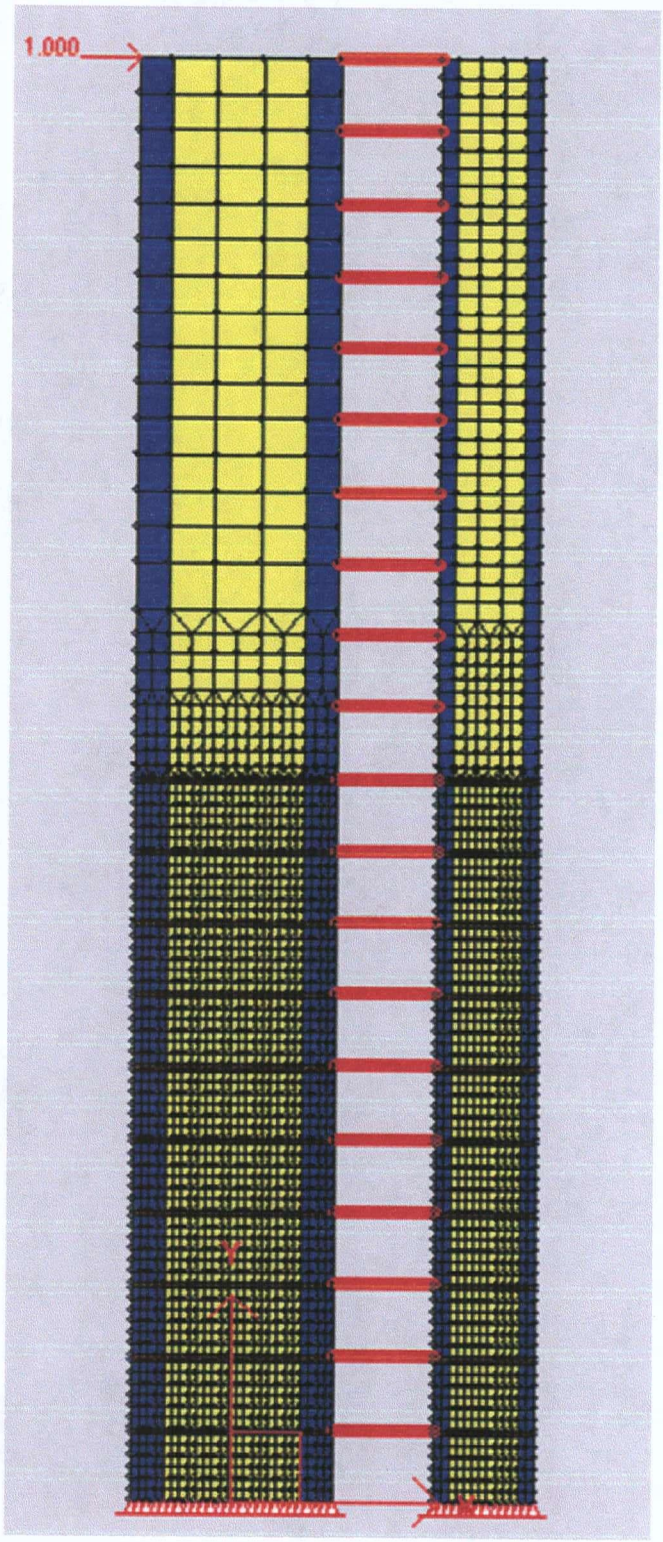

Figure 6.3 shows a more detailed view of the elements representing the slabs at each storey in the finite element model:

Figure 6.3 Detail of elements representing the slabs at each storey in finite element model of Wall 1 and 2

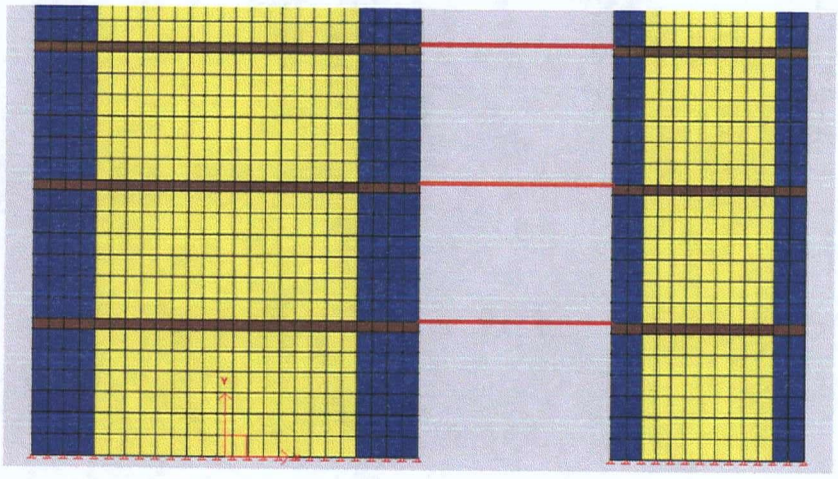

Table 6.1 and 6.2 show the material properties in the different regions of the wall system:

Table 6.1 Material properties in rectangular and triangular elements of Wall 1 and 2

Concrete properties	**Material 1**		**Material 2**		**Material 3**	
Color						
Thickness (mm)	508		508		2000	
Cylinder compressive strength (MPa)	40		40		40	
Reinforcement component properties	***x*-direction**	***y*-direction**	***x*-direction**	***y*-direction**	***x*-direction**	***y*-direction**
Reinforcement ratio (%)	0.8	2.0	0.5	0.5	0.5	0.5
Reinforcement diameter (mm)	15	25	15	15	15	15
Yield strength (MPa)	400	400	400	400	400	400
Ultimate strength (MPa)	650	650	650	650	650	650
Elastic modulus (MPa)	200000	200000	200000	200000	200000	200000
Strain hardening modulus (MPa)	4875	4875	4875	4875	4875	4875
Strain hardening strain (mm/m)	10	10	10	10	10	10

Table 6.2 Material properties in truss elements of Wall 1 and 2

Reinforcement properties	**Material 4**
Color	
Cross-sectional area (mm^2)	2500000
Reinforcement diameter (mm)	55
Yield strength (MPa)	4000
Ultimate strength (MPa)	4000
Elastic modulus (MPa)	1000000
Strain hardening modulus (MPa)	1
Strain hardening strain (mm/m)	80

6.2.3 Analytical results

The results from the analysis were used to determine the curvatures, using the same procedure described in Section 5.4 and 5.6.

The ultimate drift for the wall system was 2%. Figure 6.4 shows the curvature distribution up to the mid-height of both walls for this drift, when they are alone and combined:

Figure 6.4 Curvatures up to the mid-height of Wall 1 and 2 alone and combined for a drift of 2%

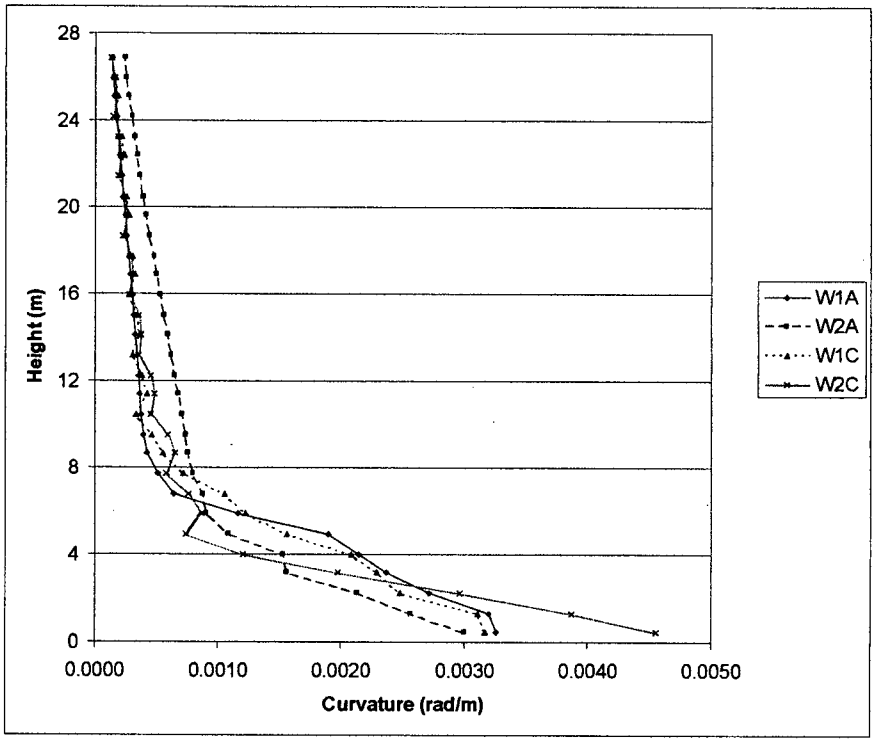

Several observations can be made for this figure. Wall 1 is pulling Wall 2 along, resulting in equal curvatures in the elastic range. After yielding, a more complex phenomenon is occurring. The curvature distribution in Wall 1 remains approximately the same, while the curvatures in Wall 2 at the base have increased considerably. The curvature distribution will be examined in more detail in the next section.

The influence of the interconnection in the moment-curvature relationship of the walls was analyzed. To develop this relationship, the bending moment diagram along the height of the wall must be calculated. The truss elements representing the slabs forced Wall 1 and 2 to displace the same at the storey levels, resulting in high axial forces in these elements. Therefore, both walls were now subjected to a system of lateral forces at each storey level, and Wall 1 is additionally subjected to the lateral load

acting at the top. The axial forces in the truss elements obtained from program VecTor2 were used to determine the system of lateral forces. Then, the bending moment diagram was calculated. Figure 6.5 shows the bending moments along the height of both walls for a drift of 2%:

Figure 6.5 Bending moments along the height of Wall 1 and 2 alone and combined for a drift of 2%

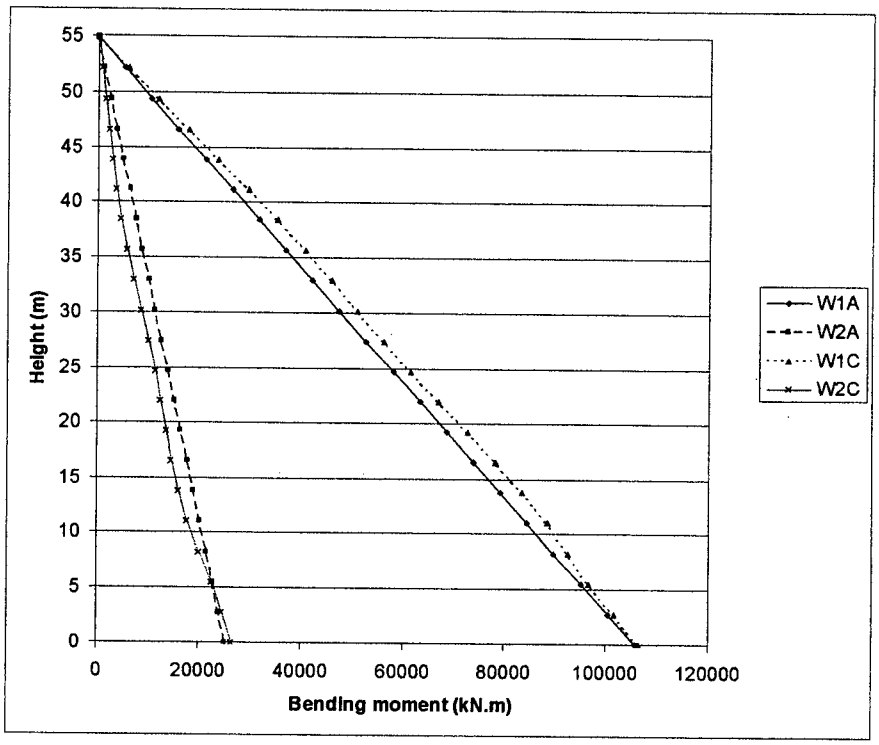

Figure 6.6 shows the moment-curvature relationship of Wall 1:

Figure 6.6 Moment-curvature relationship of Wall 1 alone and combined

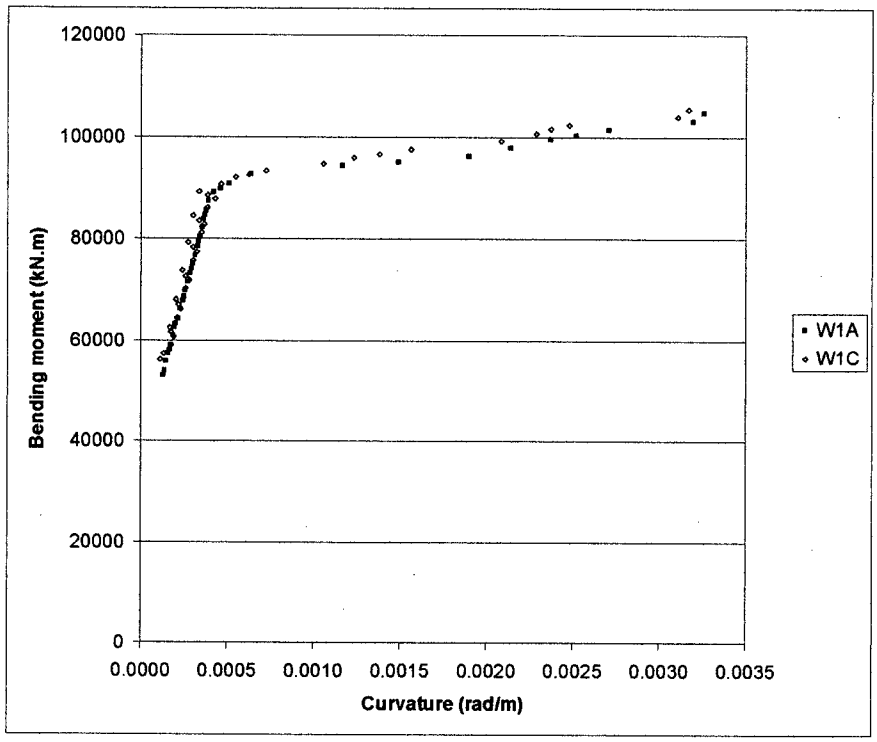

Figure 6.7 shows the moment-curvature relationship of Wall 2:

Figure 6.7 Moment-curvature relationship of Wall 2 alone and combined

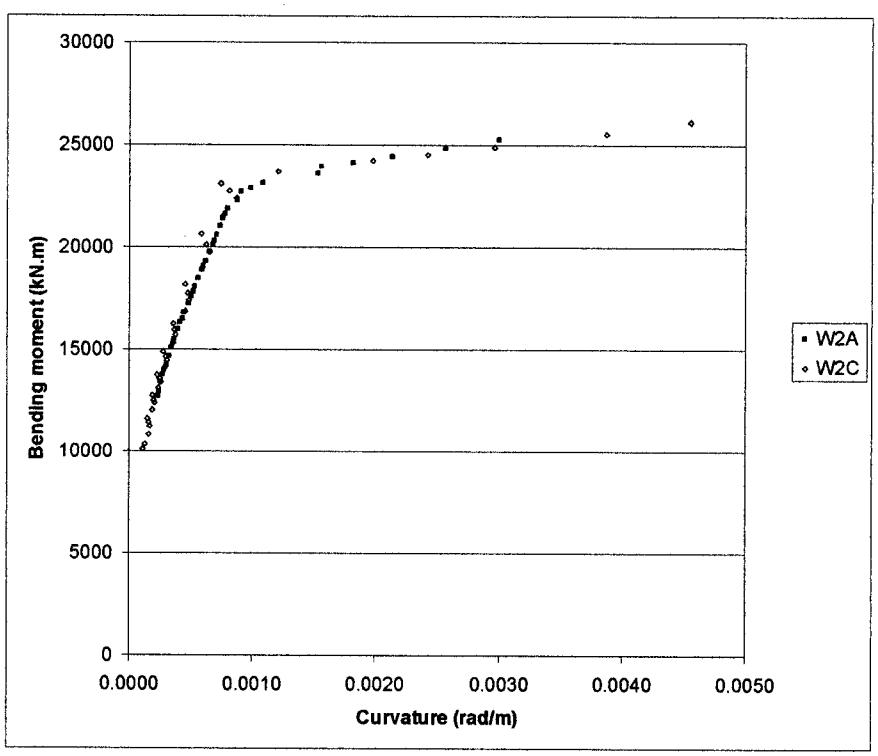

It can be seen that the moment-curvature relationship does not change when the walls are connected, so this is not causing the differences in the curvature distributions shown in Figure 6.4. Therefore, as seen in Section 5.4, the yield curvature and yield moment for Wall 1 were 0.00045 rad/m and 90680 kN.m, respectively; and for Wall 2 they were 0.0009 rad/m and 22740 kN.m.

The deflected shapes and slopes of both walls were also investigated. The total displacement at each storey, as well as its flexural and shear displacement components, were determined. The total horizontal displacements at any level or location were obtained directly from program VecTor2. The flexural displacement at a particular storey was calculated by integrating the curvatures along the height up to that level, using the second moment-area theorem:

$$\Delta_f = \int \phi(x) x dx \tag{6.1}$$

This integral was solved with the following numerical scheme:

Figure 6.8 Numerical scheme for curvature integration

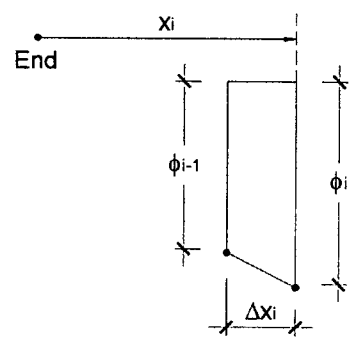

Then:

$$\Delta_f = \sum_i \left(\frac{\phi_{i-1} + \phi_i}{2} \right) \left(x_i + \frac{\Delta x_i}{2} \right) \Delta x_i \tag{6.2}$$

The shear displacement at a particular storey was then calculated as the difference between the total and flexural displacement:

$$\Delta_v = \Delta - \Delta_f \tag{6.3}$$

The slopes were calculated at the same location as the curvatures, by integrating the curvatures along the height using the first moment-area theorem:

$$\theta = \int \phi(x) dx \tag{6.4}$$

Using the numerical scheme from Figure 6.8:

$$\theta = \sum_i \left(\frac{\phi_{i-1} + \phi_i}{2} \right) \Delta x_i \tag{6.5}$$

6.2.4 Discussion of analytical results

The curvature distribution in Figure 6.4 shows that the curvatures in Wall 1 remain almost the same when it is connected with Wall 2, and its plastic hinge length has increased slightly. In Wall 2, the curvatures have increased considerably at the base, and its plastic hinge has been reduced. Using the yield curvature to measure the plastic hinge length for a drift of 2% from the curvature distribution when the walls are connected together, it was equal to 9.60m for Wall 1 and 4.64m for Wall 2. The change in the plastic hinge lengths can also be observed from the distribution of tensile steel strains in the wall. The average vertical steel strains in the elements along the height of the walls obtained from program VecTor2 were studied for this. The steel strains were observed in the exterior and interior steel layer in the boundary zones, which were shown in Figure 5.14. Figure 6.9 shows the steel strains up to the mid-height of Wall 1, alone and combined, for a drift of 2%:

Figure 6.9 Steel strains up to the mid-height of Wall 1 alone and combined for a drift of 2%

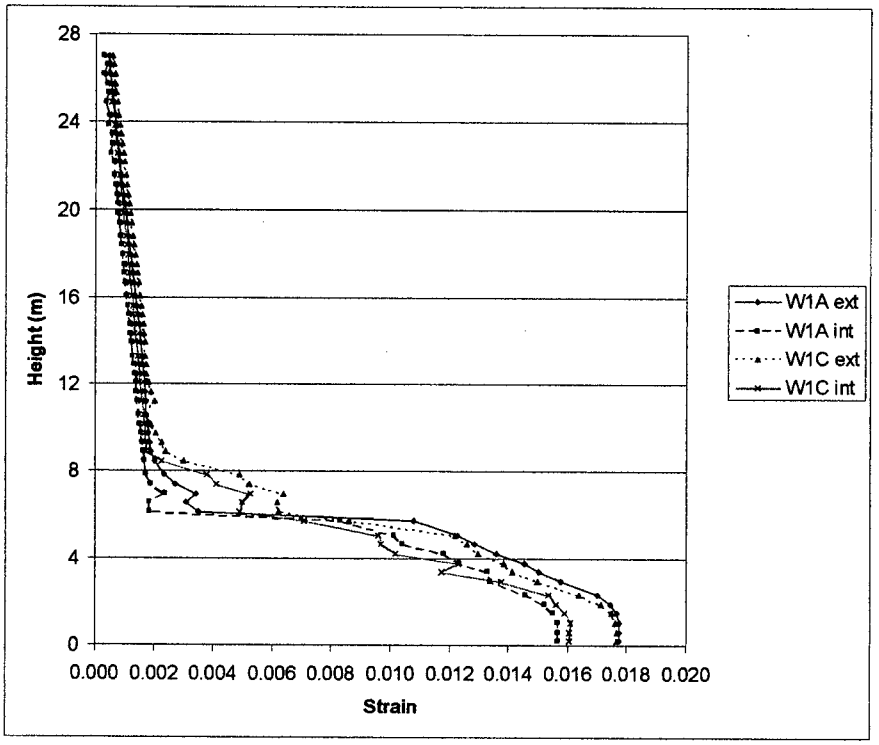

Figure 6.10 shows the steel strains up to the mid-height of Wall 2, alone and combined, for a drift of 2%:

Figure 6.10 Steel strains up to the mid-height of Wall 2 alone and combined for a drift of 2%

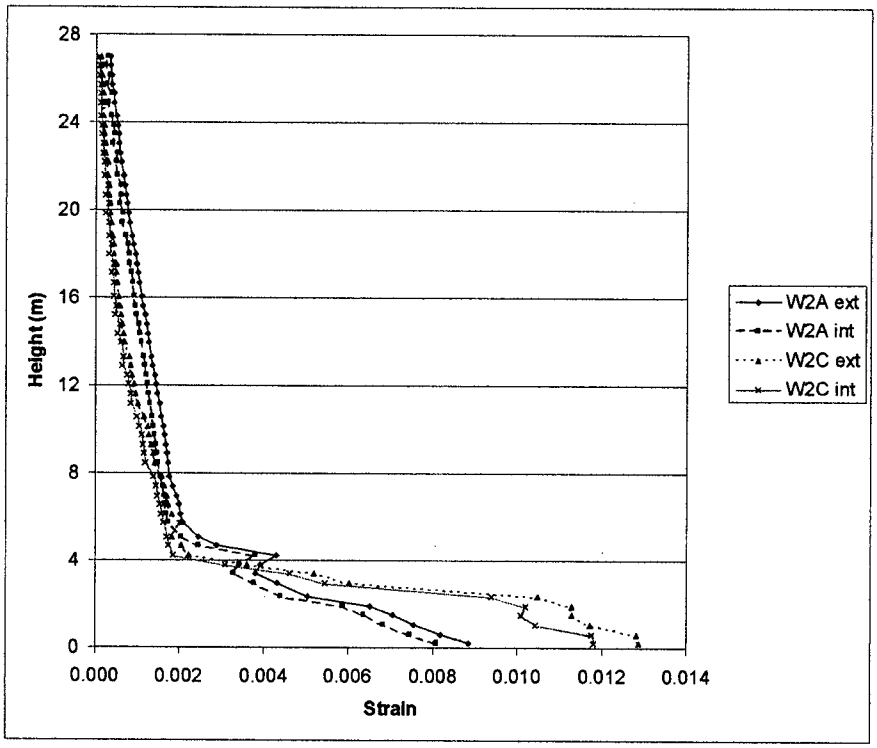

For Wall 1, the steel strains in both layers are approximately the same, but they exceed the yield strain (0.002 for these walls) at a slightly larger distance from the base when it is combined. For Wall 2, the steel strains are larger for the combined case, and they exceed the yield strain at a slightly smaller distance from the base.

All these observations are revealing that the curvature distributions and plastic hinge lengths in both walls are different, even when they are combined together by rigid slabs. In order to understand this phenomenon, the deflected shapes and slopes of both walls were studied.

Figure 6.11 shows the total lateral displacements at the faces of both walls (right face for Wall 1 and left face for Wall 2) up to the fourth storey when they are combined, for a drift of 2%; these were obtained directly from program VecTor2:

Figure 6.11 Displacements at wall faces up to the fourth storey of Wall 1 and 2 combined for a drift of 2%

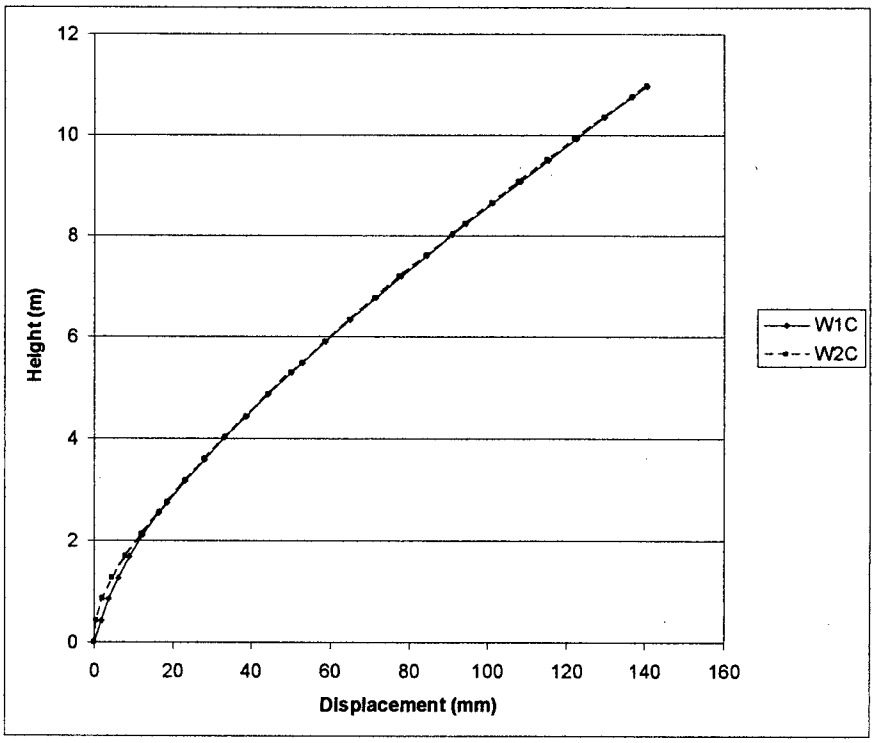

Although the lateral displacements in both walls are equal at the storey levels, these are different between these levels. So, the deflected shapes are not strictly the same. The bigger differences between the displacements in both walls are located at the bottom. Figure 6.12 shows a more detailed view of the lateral displacements at the faces of both walls up to the first storey when they are combined, for a drift of 2%:

Figure 6.12 Displacements at wall faces up to the first storey of Wall 1 and 2 combined for a drift of 2%

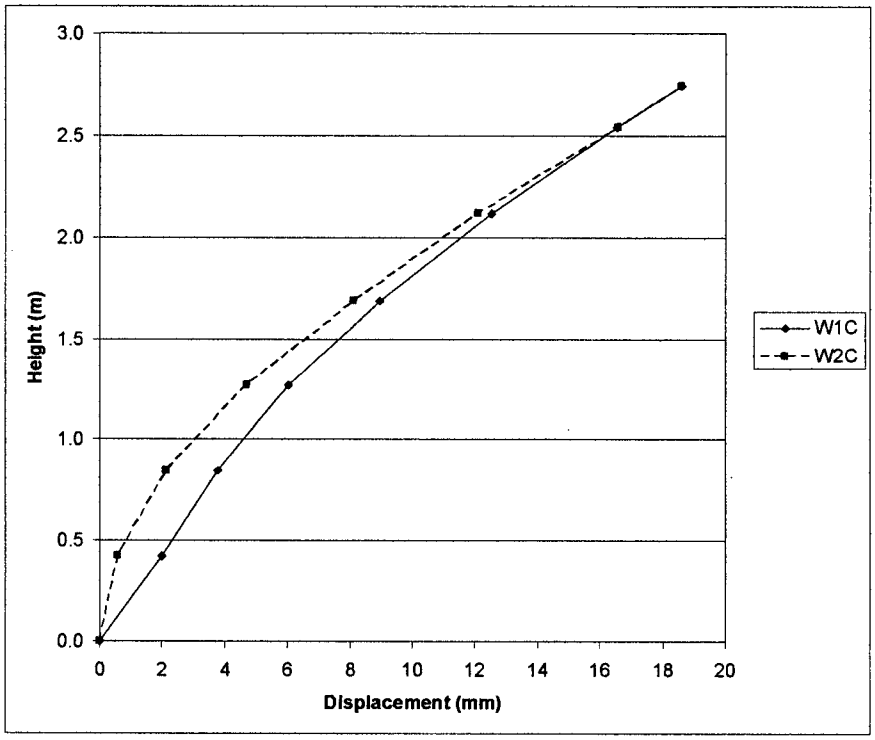

The displacements are not the same between storey levels. Wall 1 has larger displacements than Wall 2. It can also be seen that Wall 2 ends up having bigger slopes. The variation of the slope in Wall 2 is larger than in Wall 1, which is the reason why the curvatures are larger in this wall for the combined case.

Table 6.3 shows the displacement components up to the fourth storey of both walls when they are combined for a drift of 2%:

Table 6.3 Displacement components up to the fourth storey of Wall 1 and 2 combined for a drift of 2%

Storey	Height (m)	Wall 1			Wall 2		
		Δ_f (mm)	Δ_v (mm)	Δ (mm)	Δ_f (mm)	Δ_v (mm)	Δ (mm)
0	0.00	0.00	0.00	0.00	0.00	0.00	0.00
1	2.74	8.02	10.59	18.61	10.38	8.23	18.61
2	5.49	34.02	18.84	52.87	38.88	13.99	52.87
3	8.23	70.91	23.46	94.37	74.26	20.11	94.37
4	10.97	112.96	27.48	140.44	114.45	25.99	140.44

Figure 6.13 shows these results graphically:

Figure 6.13 Displacement components up to the fourth storey of Wall 1 and 2 combined for a drift of 2%

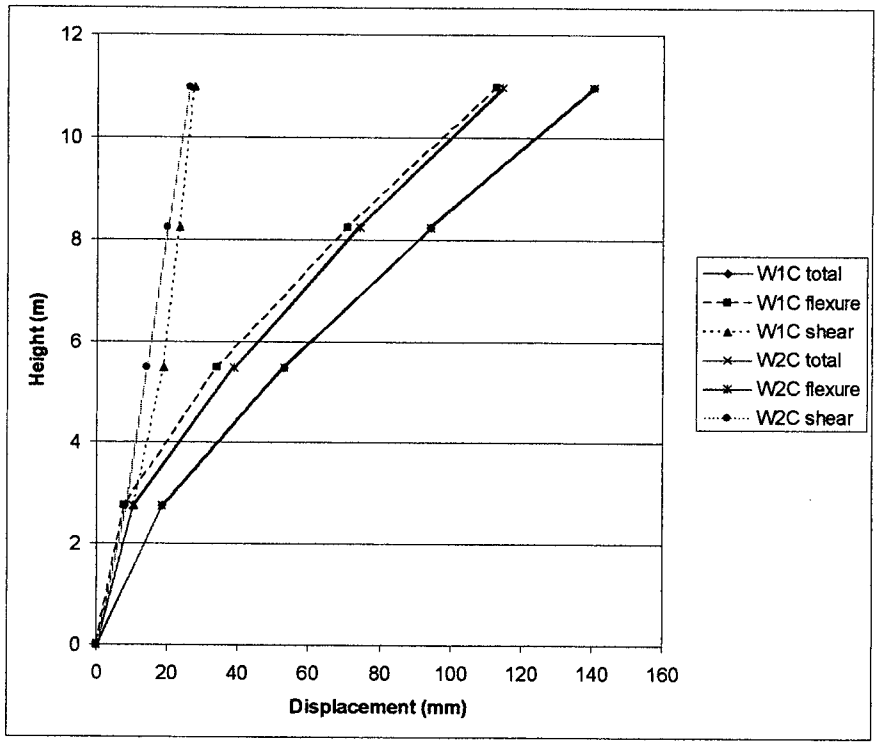

The total displacements are the same at the storey heights, but the flexural displacement is larger in Wall 2 at the lower levels. Wall 1 has higher shear displacements at the lower levels. Therefore, the displacements in Figure 6.12 in this wall up to the first storey are mostly due to shear. Although Wall 1 has larger total displacements at the bottom, Wall 2 has larger flexural displacements. The difference in shear displacements is causing the slopes to be different, as shown in Figure 6.14:

Figure 6.14 Slopes up to the mid-height of Wall 1 and 2 combined for a drift of 2%

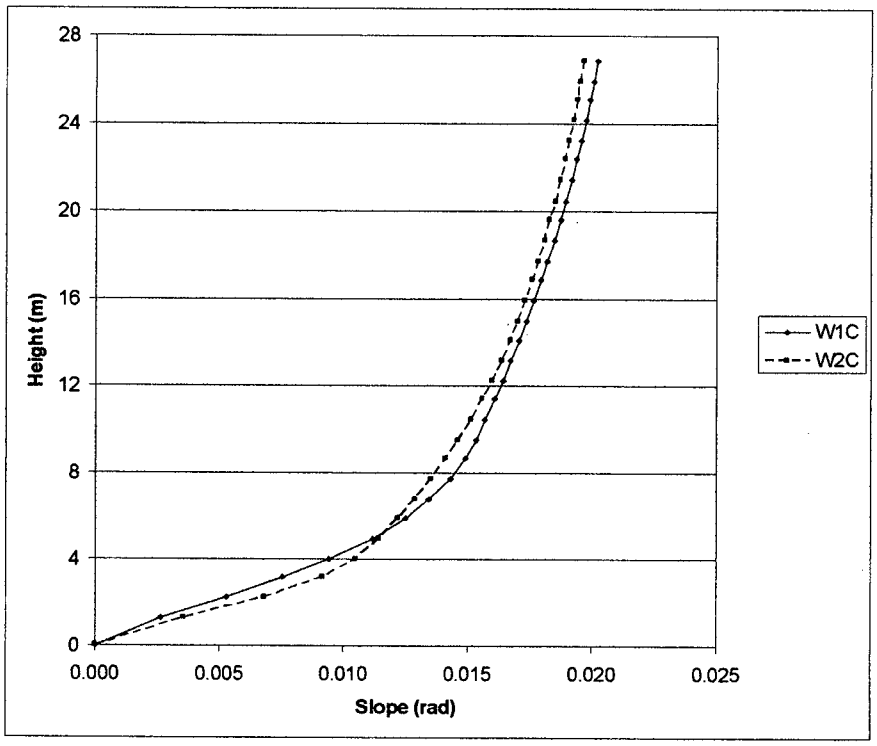

The slopes in Wall 2 are larger at the lower levels; this was also deduced by looking at Figure 6.12. The inelastic rotation in Wall 2 is concentrated in a shorter height than in Wall 1.

It can be concluded that the curvature distribution of Wall 1 and 2 when they are connected are different because of two reasons. First, the displacements between storey levels are different in both walls, so the deflected shapes are not the same. Second, the shear displacements at the lower levels are larger in Wall 1 than in Wall 2 when they are connected; resulting in lower flexural displacements, lower slopes, and lower curvatures for Wall 1. Since the curvatures are not the same, the plastic hinge lengths are also different.

Another important conclusion is that when walls of different lengths are combined together, the curvature demand for the shorter wall is much larger than when it is alone. This wall has to be able to sustain that demand.

In order to predict the maximum curvature in Wall 2 for the combined case, a very simple model was developed, based on the observations made from this study. It is shown in figure 6.15:

Figure 6.15 Proposed model to determine maximum curvature in shorter wall

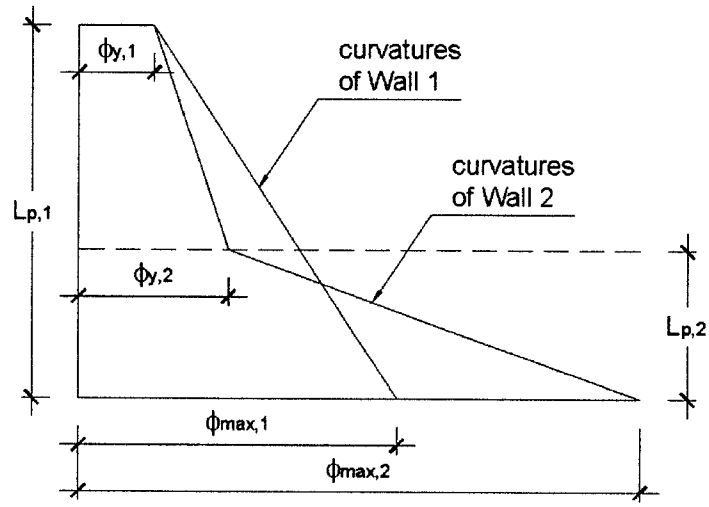

The following assumptions were made regarding this model:

- The inelastic curvatures are linearly varying.
- The plastic hinge length and the maximum curvature in Wall 1 (longer wall) do not change when it is combined with Wall 2 (shorter wall).
- The rotations or slopes in both walls at a distance equal to the plastic hinge length of Wall 1 from the section of maximum curvature are the same.

Based on these assumptions, the maximum curvature in Wall 2 can be estimated. From Figure 6.15, the total rotation in Wall 1 is determined by integrating the curvatures:

$$\theta_1 = \left(\frac{\phi_{y,1} + \phi_{\max,1}}{2}\right) L_{p,1} \tag{6.6}$$

The total rotation in Wall 2 is determined similarly:

$$\theta_2 = \left(\frac{\phi_{y,1} + \phi_{y,2}}{2}\right)\left(L_{p,1} - L_{p,2}\right) + \left(\frac{\phi_{y,2} + \phi_{\max,2}}{2}\right) L_{p,2} \tag{6.7}$$

Since we are considering that the rotations are the same:

$$\theta_1 = \theta_2 \tag{6.8}$$

Replacing Equation 6.6 and 6.7 in Equation 6.8, and solving for $\phi_{max,2}$, we finally get:

$$\phi_{\max,2} = \left(\phi_{\max,1} + \phi_{y,2}\right)\left(\frac{L_{p,1}}{L_{p,2}}\right) + \phi_{y,1} \tag{6.9}$$

The measured values of the parameters in Equation 6.9 were used to predict the maximum curvature in Wall 2, and then it was compared with the measured value, obtained from Figure 6.4. The maximum curvature, yield curvature and plastic hinge length for Wall 1 when it is alone are already known. The yield curvature of Wall 2 is also known. The plastic hinge length used for Wall 2 was the one measured in the combined case, that is, 4.64m. The result is shown in Table 6.4:

Table 6.4 Predicted and measured maximum curvature for Wall 2 combined

Drift (%)	$L_{p,1}$ (m)	$L_{p,2}$ (m)	$\phi_{y,1}$ (rad/m)	$\phi_{y,2}$ (rad/m)	$\phi_{max,1}$ (rad/m)	$\phi_{max,2}$ (rad/m)	
						Predicted	Measured
2.0	8.39	4.64	0.00045	0.00090	0.00326	0.00472	0.00456

The proposed model provides a good prediction of the maximum curvature in Wall 2.

6.3 Wall 1 combined with Wall 3

Wall 1 was then combined with a wall that was four times shorter. This wall will be referred to as Wall 3 throughout this chapter. Wall 3 was first analyzed individually, and then it was connected together with Wall 1 to compare the results obtained. The description of the analytical model for Wall 3 alone and combined together with Wall 1, and the results obtained, will be presented in the following sections.

6.3.1 Description of wall system model

Wall 3 was first analyzed alone as a cantilever element. It had a rectangular cross-section, and it was 54860mm high, 508mm thick and 1905mm long. The boundary zones were 305mm long, the vertical reinforcement in these consisted of 6-25M reinforcing bars enclosed by 15M ties spaced at 100mm. The clear cover of the ties was 40mm. The web had 15M reinforcing bars spaced at 150mm vertically and horizontally. The cross-section of Wall 3 is shown in Figure 6.16:

Figure 6.16 Cross-section details of Wall 3

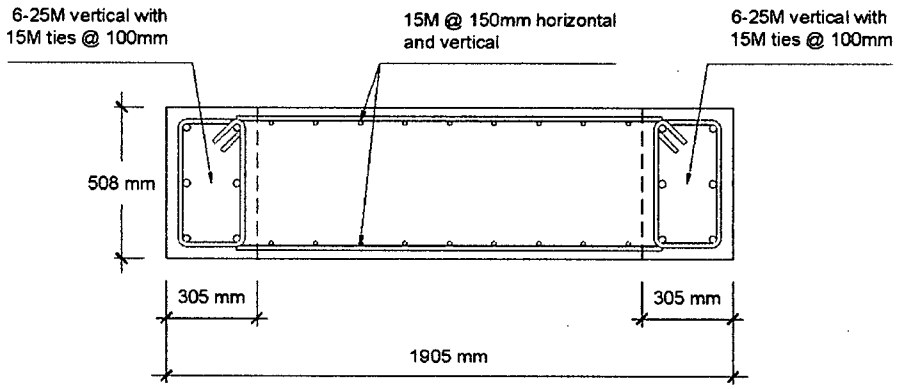

The material properties of Wall 3 were the same ones used for Wall 1 and 2, described in Section 5.2. The wall was fixed at the base. It was subjected to a monotonically increasing lateral load at the top; as well as a constant compressive axial load of $0.2A_g f'_c$, equal to 7742 kN. This is the same axial load used for Wall 2. Smaller walls usually have a larger tributary area, so the axial load ratio was increased for Wall 3.

The model used to analyze walls 1 and 3 combined was the same as the one presented in Figure 6.1, except that Wall 2 was replaced by Wall 3. The slabs were provided every 2743mm, resulting in a 20 storey building. The thickness of the slabs was 203mm.

6.3.2 Analytical model of wall system

Wall 3 was first modeled and analyzed individually using program VecTor2. The model was very similar to the one created for Wall 1 and 2, described in Section 5.3. Low-powered rectangular and triangular elements were used to model the concrete, with smeared steel to account for the presence of reinforcement. The constitutive models for concrete and steel described in Chapter 3 were used in the analysis. The same two material types from Wall 1 and 2 were used to represent the confined boundaries and the web of Wall 3 in the finite element model.

The analytical model was fixed at the bottom; both the horizontal and vertical displacements were restrained. The finite element mesh was more refined near the base (critical section). Wall 3 had the same refinement as Wall 1 in the vertical direction up to a half of the height, so that the curvatures could be calculated over the same average length.

Meshes of 305×423, 305×203, 324×423 and 324×203 rectangular elements were used; six elements (seven nodes) were used in the transverse direction of the wall. This level of refinement was

maintained up to half the height of the wall. Up from this point, five elements (six nodes) were used in the transverse direction. The transitions were made using triangular elements. All nodes and elements were numbered in the horizontal (short) direction. The complete mesh consisted of 857 nodes, 717 rectangular elements and seven triangular elements.

The material properties used in the analysis were the same ones used for Wall 1 and 2, presented in Section 5.3.

A monotonic lateral load was applied at the top of the wall. This load was applied in a displacement-control mode, in increments of 1mm. Additionally, a constant axial load of 7742 kN was applied; this load was equally distributed among the six nodes at the top of the wall. The self-weight of the wall was not considered.

Figure 6.17 shows the finite element model of Wall 3, created in the pre-processor FormWorks:

Figure 6.17 Finite element model of Wall 3 in FormWorks

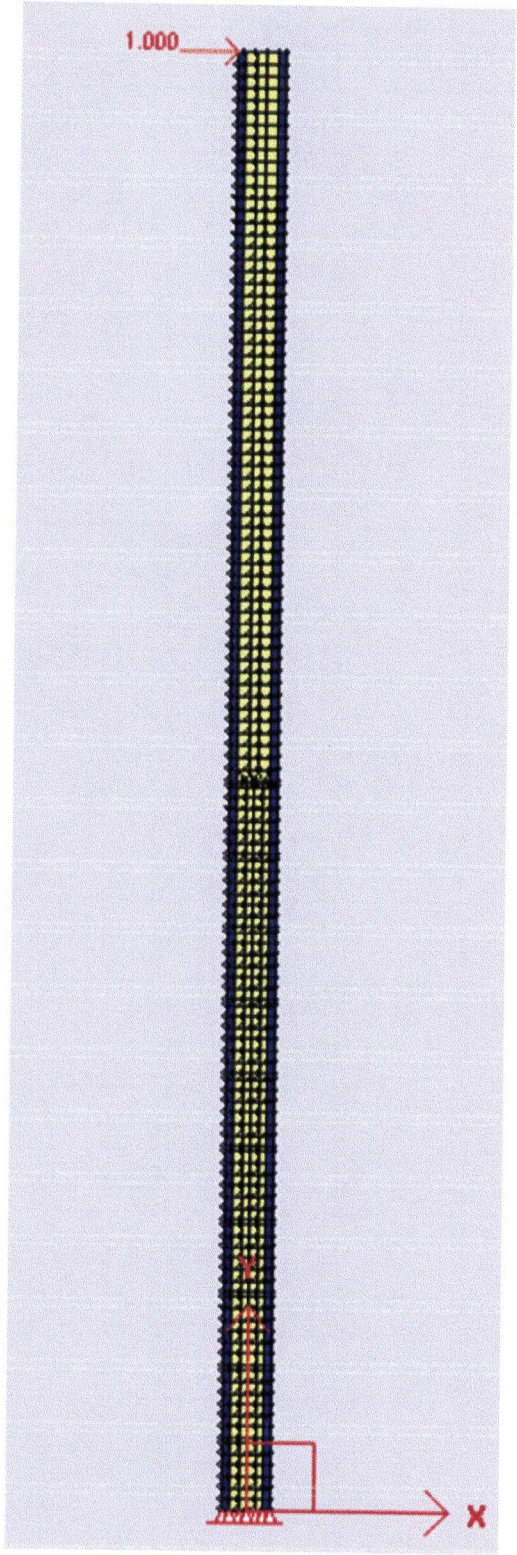

The material properties in the different regions of the wall were the same ones used for Wall 1 and 2 alone, presented in Table 5.1.

Wall 1 and 3 were then modeled and analyzed together using program VecTor2. The finite element mesh used for each wall, as well as the boundary conditions, material properties and loads, were the same as the ones described in Section 5.3 and this section.

As it was done for the model of Wall 1 and 2 combined together, described in Section 6.2.2, the slabs interconnecting the walls at each floor level were modeled using truss bar elements with very stiff properties. The rectangular elements located at each storey level, which had a height equal to the slab thickness, were also provided with very stiff properties. The same material types were used for these elements.

All nodes and elements were numbered in the horizontal (short) direction of the wall system. The complete mesh consisted of 2938 nodes, 2644 rectangular elements, 93 triangular elements and 20 truss elements.

A monotonic lateral load was applied at the top of the Wall 1. This load was applied in a displacement-control mode, in increments of 1mm. Additionally, a constant axial load of 15484 kN in Wall 1 and 7742 kN in Wall 3 was applied; these loads were equally distributed among the six nodes at the top of each wall. The self-weight of the walls was not considered.

Figure 6.18 shows the finite element model of Wall 1 and 3, created in the pre-processor FormWorks:

Figure 6.18 Finite element model of Wall 1 and 3 in FormWorks

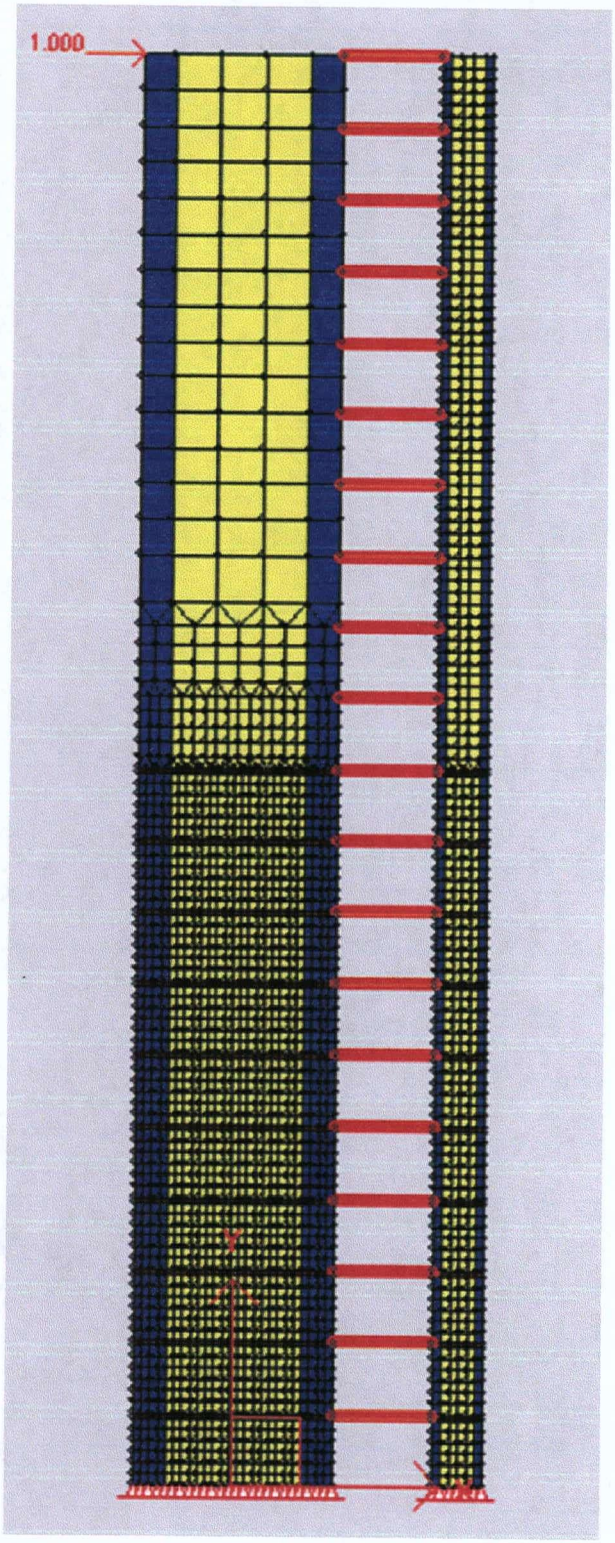

The detail of the elements representing the slabs at each storey level in the finite element model was the same as the one shown in Figure 6.3. The material properties in the different regions of the wall system were the same ones used for Wall 1 and 2 combined, presented in Table 6.1 and 6.2.

6.3.3 Analytical results

The results from the analysis were used to determine the curvatures, using the same procedure described in Section 5.4 and 5.6.

The ultimate drift for the wall system was 2%. Figure 6.19 shows the curvature distribution up to the mid-height of both walls for this drift, when they are alone and combined:

Figure 6.19 Curvatures up to the mid-height of Wall 1 and 3 alone and combined for a drift of 2%

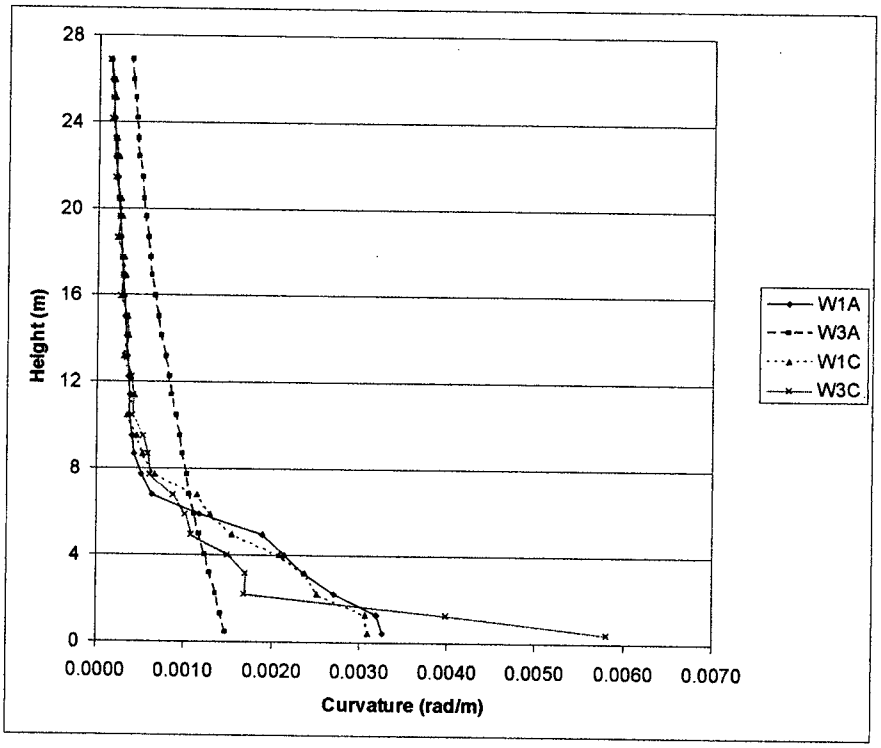

The same phenomenon observed for Wall 1 and 2, presented in Section 6.2.3, is seen here. The curvature distribution in Wall 1 remains approximately the same, while the curvatures in Wall 3 at the base have increased considerably.

The moment-curvature relationship of Wall 3 was also determined, using the procedure described in Section 5.4 when it is alone, and the procedure described in Section 6.2.3 when it is combined. It is presented in Figure 6.20:

Figure 6.20 Moment-curvature relationship of Wall 3 alone and combined

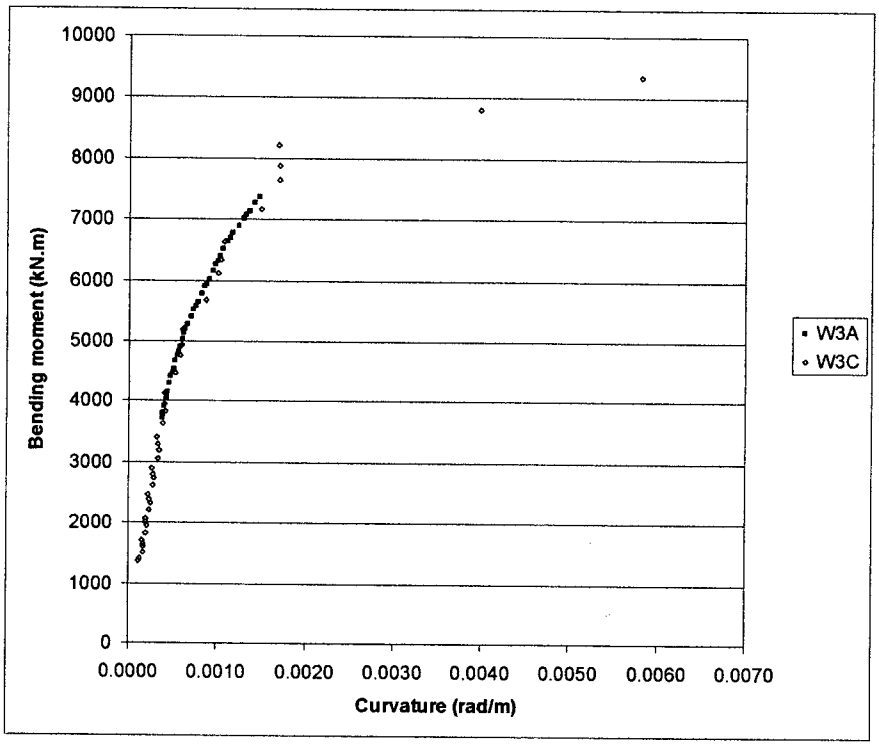

It can be seen that the moment-curvature relationship does not change when the walls are connected. The yield curvature for Wall 3 is 0.00207 rad/m.

6.3.4 Discussion of analytical results

The curvature distribution in Figure 6.19 shows that the curvatures in Wall 1 remain almost the same when it is connected with Wall 3, and its plastic hinge length has increased slightly. In Wall 3, the curvatures have increased considerably at the base. This is the same phenomenon observed for Wall 1 and 2 combined together. However, when Wall 3 is alone, the curvatures at 2% drift do not reach the yield curvature. Therefore, it is not yielding, so no plastic hinge is formed. When combined with Wall 1, the curvatures in Wall 3 increase, causing it to yield and develop a plastic hinge. This can also be observed from the distribution of tensile steel strains in the wall. The average vertical steel strains in the elements along the height of the walls obtained from program VecTor2 were studied for this. The steel strains were observed in the exterior steel layer in the boundary zones. Figure 6.21 shows the steel strains up to the mid-height of Wall 3, alone and combined, for a drift of 2%:

Figure 6.21 Steel strains up to the mid-height of Wall 3 alone and combined for a drift of 2%

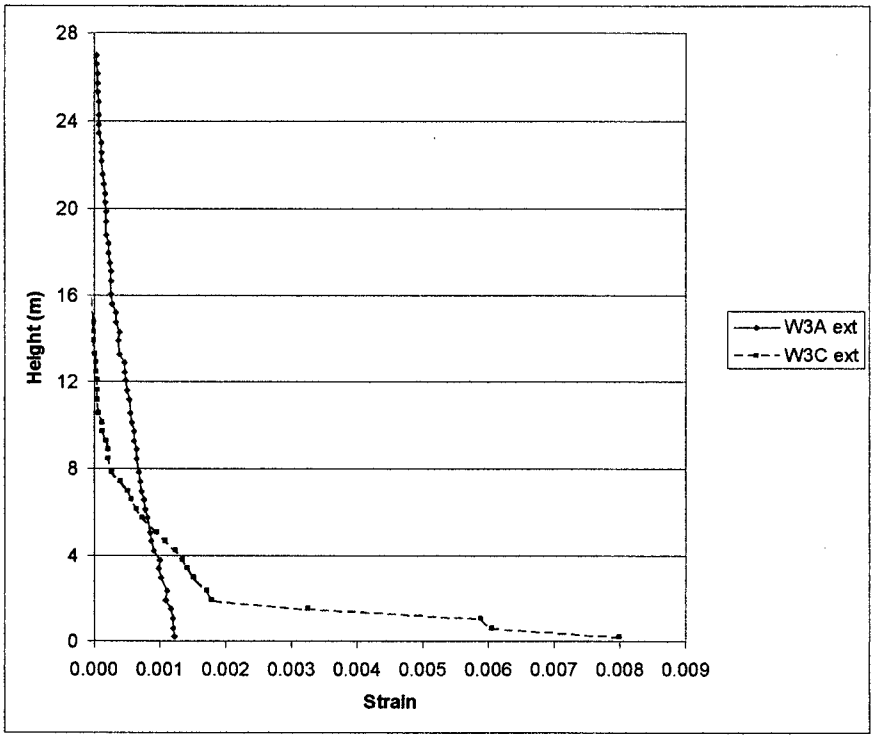

The steel strains do not reach the yield strain when Wall 3 is alone, but they do when it is combined.

Using the yield curvature to measure the plastic hinge length for a drift of 2% from the curvature distribution when the walls are connected together, it was equal to 9.58m for Wall 1 and 2.06m for Wall 3.

In conclusion, the curvature distribution and plastic hinge length of Wall 1 and 3 when they are connected are different, as it was observed for Wall 1 and 2 connected, for the same reasons explained in Section 6.2.4. Also, the curvature demand for the shorter wall is much larger when it is combined than when it is alone, and it has to be able to sustain that demand.

The maximum curvature in Wall 3 was predicted using the model presented in Figure 6.15. The measured values of the parameters in Equation 6.9 were used in the prediction, and then it was compared with the measured value, obtained from Figure 6.19. The maximum curvature, yield curvature and plastic hinge length for Wall 1 when it is alone are already known. The yield curvature of Wall 3 is also known. The plastic hinge length used for Wall 3 was the one measured in the combined case, that is, 2.06m. The result is shown in Table 6.5:

Table 6.5 Predicted and measured maximum curvature for Wall 3 combined

Drift (%)	$L_{p,1}$ (m)	$L_{p,2}$ (m)	$\phi_{y,1}$ (rad/m)	$\phi_{y,2}$ (rad/m)	$\phi_{max,1}$ (rad/m)	$\phi_{max,2}$ (rad/m)	
						Predicted	Measured
2.0	8.39	2.06	0.00045	0.00207	0.00326	0.00530	0.00581

The proposed model provides a good prediction of the maximum curvature in Wall 3.

6.4 Wall 1 combined with Column 1

Wall 1 was finally combined with a column that was eight times shorter. This column will be referred to as Column 1 throughout this chapter. Column 1 was first analyzed individually, and then it was connected together with Wall 1 to compare the results obtained. The description of the analytical model for Column 1 alone and combined together with Wall 1, and the results obtained, will be presented in the following sections.

6.4.1 Description of wall system model

Column 1 was first analyzed alone as a cantilever element. It had a rectangular cross-section, and it was 54860mm high, 508mm thick and 953mm long. The vertical reinforcement consisted of 20-25M reinforcing bars enclosed by 15M ties spaced at 100mm. The clear cover of the ties was 40mm. The cross-section of Column 1 is shown in Figure 6.22:

Figure 6.22 Cross-section details of Column 1

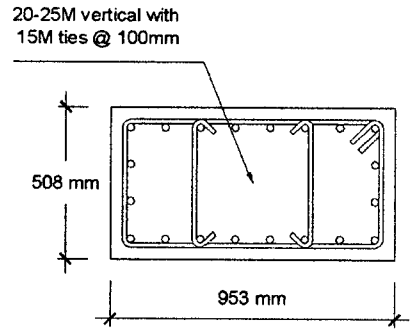

The material properties of Column 1 were the same ones used for Wall 1 and 2, described in Section 5.2. The wall was fixed at the base. It was subjected to a monotonically increasing lateral load at the top; as well as a constant compressive axial load of $0.4A_g f'_c$, equal to 7742 kN. This is the same axial load used for Wall 2 and 3. Gravity columns typically have a larger tributary area compared to walls, so the axial load ratio was increased for Column 1.

The model used to analyze Wall 1 and Column 1 combined was the same as the one presented in Figure 6.1, except that Wall 2 was replaced by Column 1. The slabs were provided every 2743mm, resulting in a 20 storey building. The thickness of the slabs was 203mm.

6.4.2 Analytical model of wall system

Column 1 was first modeled and analyzed individually using program VecTor2. The model was very similar to the one created for Wall 1 and 2, described in Section 5.3. Low-powered rectangular and triangular elements were used to model the concrete, with smeared steel to account for the presence of reinforcement. The constitutive models for concrete and steel described in Chapter 3 were used in the analysis. Only one material type was used to represent the whole column in the finite element model, it was the same one used to represent the confined boundaries of Wall 1 and 2.

The analytical model was fixed at the bottom; both the horizontal and vertical displacements were restrained. The finite element mesh was more refined near the base (critical section). Column 1 had the same refinement as Wall 1 in the vertical direction up to a half of the height, so that the curvatures could be calculated over the same average length.

Meshes of 318×423 and 318×203 rectangular elements were used; three elements (four nodes) were used in the transverse direction of the wall. This level of refinement was maintained up to half the height of the wall. Up from this point, two elements (three nodes) were used in the transverse direction, and then it was further reduced to one element (two nodes) up to the top of the wall. The transitions were made using triangular elements. All nodes and elements were numbered in the horizontal (short) direction. The complete mesh consisted of 345 nodes, 242 rectangular elements and eight triangular elements.

The material properties used in the analysis were the same ones used for Wall 1 and 2, presented in Section 5.3.

A monotonic lateral load was applied at the top of the column. This load was applied in a displacement-control mode, in increments of 1mm. Additionally, a constant axial load of 7742 kN was applied; this load was equally distributed in the two nodes at the top of the column. The self-weight of the column was not considered.

Figure 6.23 shows the finite element model of Column 1, created in the pre-processor FormWorks:

Figure 6.23 Finite element model of Column 1 in FormWorks

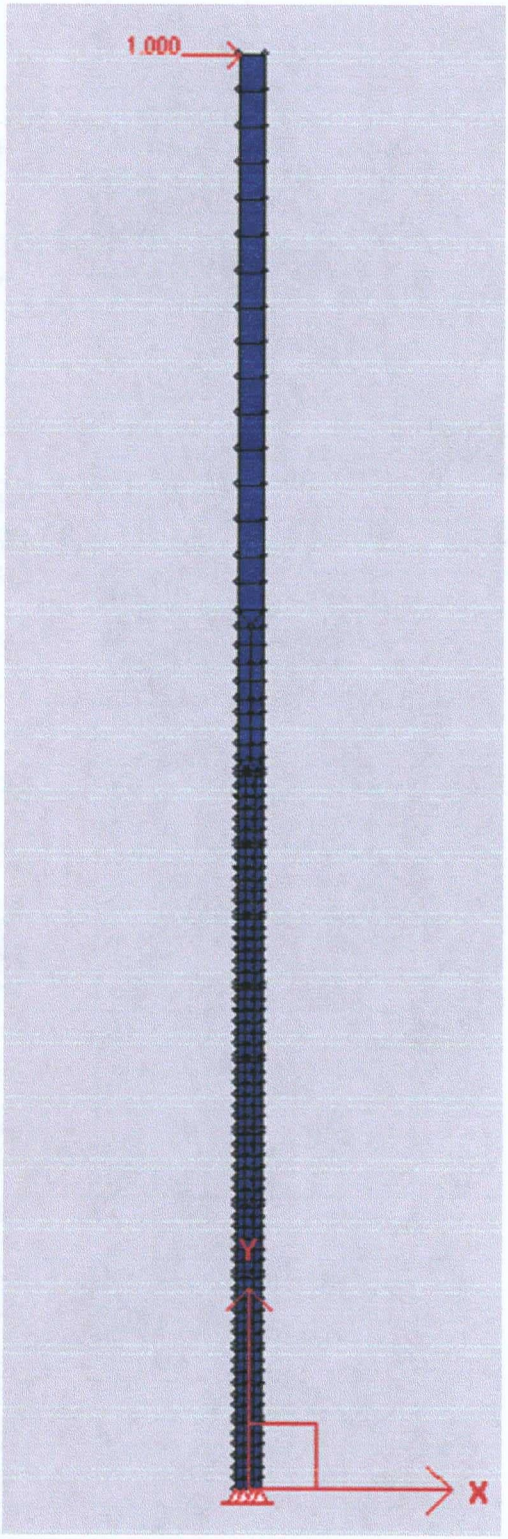

The material properties of the column were the same ones used for the material 1 in Wall 1 and 2 alone, presented in Table 5.1.

Wall 1 and Column 1 were then modeled and analyzed together using program VecTor2. The finite element mesh used for each of them, as well as the boundary conditions, material properties and loads, were the same as the ones described in Section 5.3 and this section.

As it was done for the model of Wall 1 and 2 combined together, described in Section 6.2.2, the slabs interconnecting the wall and the column at each floor level were modeled using truss bar elements with very stiff properties. The rectangular elements located at each storey level, which had a height equal to the slab thickness, were also provided with very stiff properties. The same material types were used for these elements.

All nodes and elements were numbered in the horizontal (short) direction of the wall system. The complete mesh consisted of 2426 nodes, 2169 rectangular elements, 94 triangular elements and 20 truss elements.

A monotonic lateral load was applied at the top of the Wall 1. This load was applied in a displacement-control mode, in increments of 1mm. Additionally, a constant axial load of 15484 kN in Wall 1 and 7742 kN in Column 1 was applied; these loads were equally distributed among the six nodes at the top of the wall and the two nodes at the top of the column. The self-weight of the wall and the column was not considered.

Figure 6.24 shows the finite element model of Wall 1 and Column 1, created in the pre-processor FormWorks:

Figure 6.24 Finite element model of Wall 1 and Column 1 in FormWorks

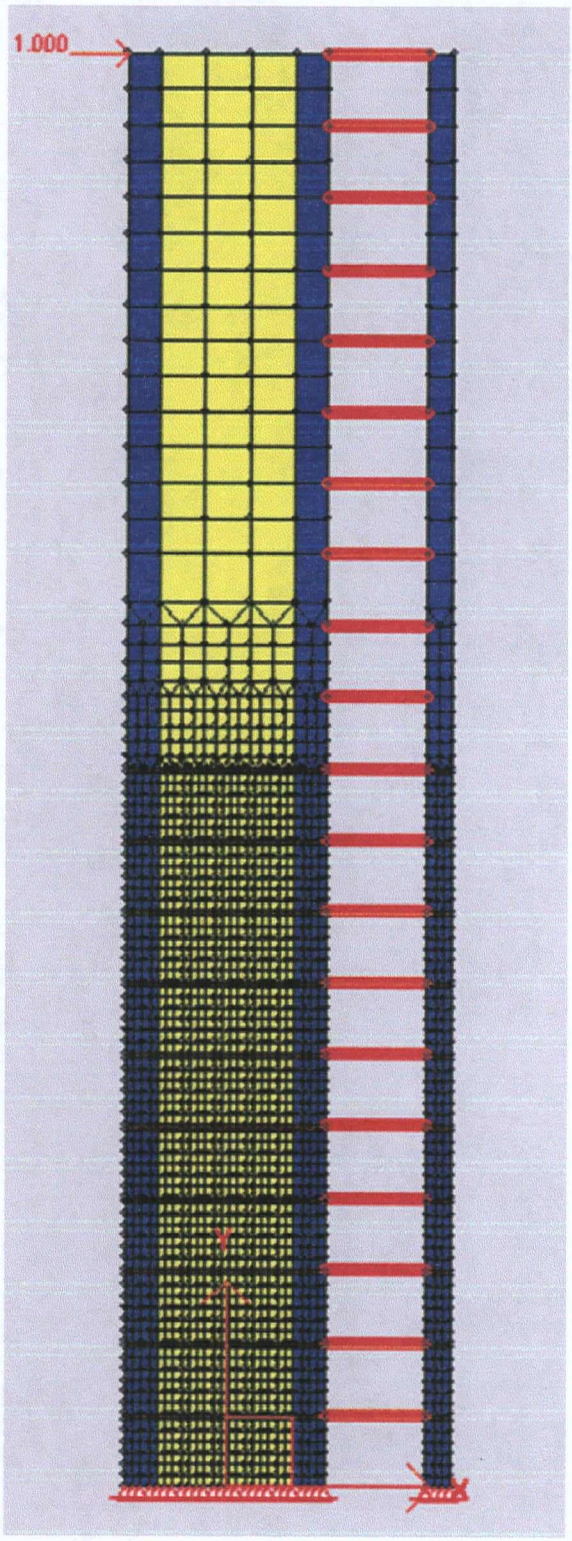

The detail of the elements representing the slabs at each storey level in the finite element model was the same as the one shown in Figure 6.3. The material properties in the different regions of the wall system were the same ones used for Wall 1 and 2 combined, presented in Table 6.1 and 6.2.

6.4.3 Analytical results

The results from the analysis were used to determine the curvatures, using the same procedure described in Section 5.4 and 5.6.

The ultimate drift for the wall system was 2%. Figure 6.25 shows the curvature distribution up to the mid-height of the wall and the column for this drift, when they are alone and combined:

Figure 6.25 Curvatures up to the mid-height of Wall 1 and Column 1 alone and combined for a drift of 2%

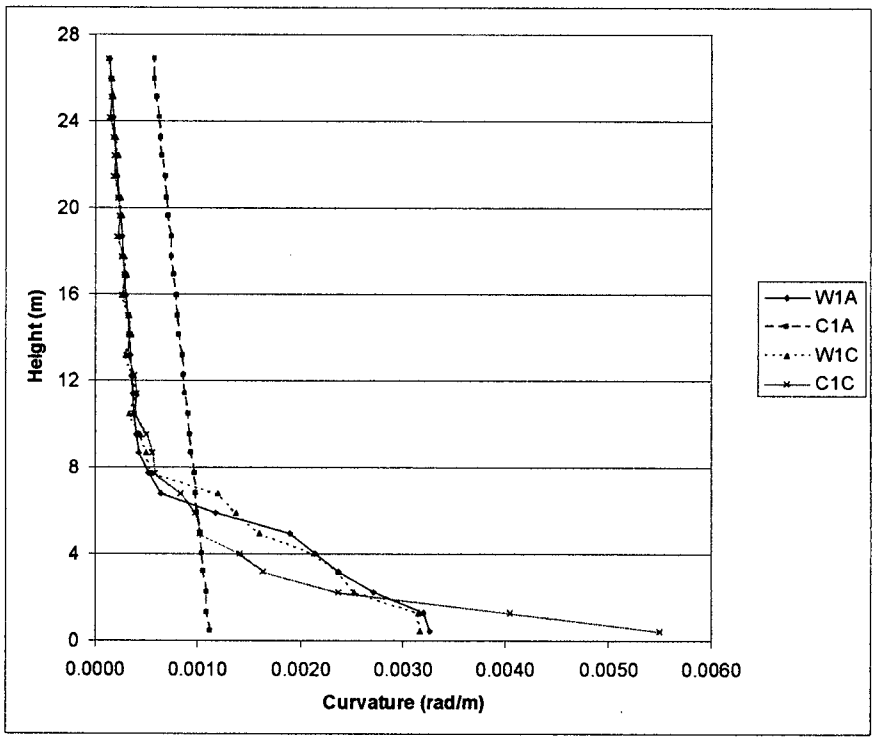

The same phenomenon observed for the previous wall systems, presented in Section 6.2.3 and 6.3.3, is seen here. The curvature distribution in Wall 1 remains approximately the same, while the curvatures in Column 1 at the base have increased considerably.

6.4.4 Discussion of analytical results

The curvature distribution in Figure 6.25 shows that the curvatures in Wall 1 remain almost the same when it is connected with Column 1, and its plastic hinge length has increased slightly. In Column 1, the curvatures have increased considerably at the base. This is the same phenomenon observed for Wall 1 and 2 and Wall 1 and 3 combined together. However, when Column 1 is alone, the curvatures at 2% drift do not reach the curvature at cracking. The column remains uncracked, so no plastic hinge is formed.

This is due to the high axial load applied to it. When combined with Wall 1, the curvatures in Column 1 increase, causing it to crack, but they are not large enough to make the column yield and develop a plastic hinge. This can also be observed from the distribution of tensile steel strains in the wall. The average vertical steel strains in the elements along the height of the walls obtained from program VecTor2 were studied for this. The steel strains were observed in the exterior steel layer. Figure 6.26 shows the steel strains up to the mid-height of Column 1, alone and combined, for a drift of 2%:

Figure 6.26 Steel strains up to the mid-height of Column 1 alone and combined for a drift of 2%

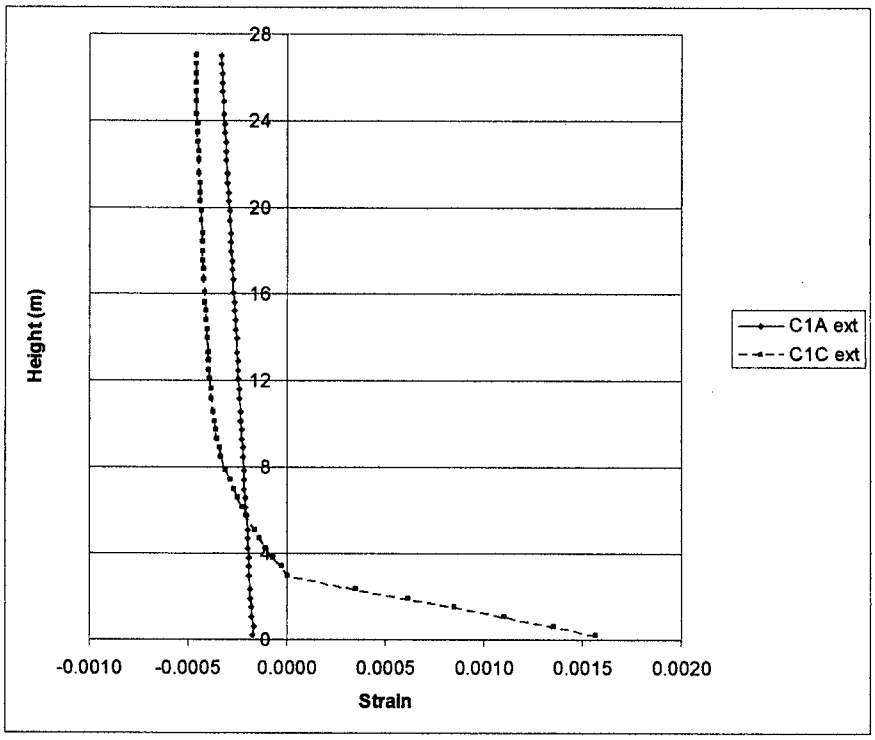

The steel strains are of compression when Column 1 is alone, but they are of tension when it is combined. The tensile strains in the combined case do not reach the yield strain.

In conclusion, as seen for the previous wall systems in Sections 6.2.4 and 6.3.4, the curvature distributions of Wall 1 and Column 1 when they are connected are different. Also, the curvature demand for the column is much larger when it is combined than when it is alone, and it has to be able to sustain that demand. It is important to consider this effect in the design of gravity columns in high-rise buildings.

CHAPTER 7: CONCLUSIONS

The plastic hinge length is a function of several parameters. Past research has focused primarily on the influence of member depth, member span and longitudinal reinforcement properties. Some studies have also considered the influence of axial load ratio and strain hardening. Many researchers arrived to the conclusion that a good lower bound approximation for the plastic hinge length is $0.5h$ or $0.5l_w$, which is the value given in many concrete codes, including CSA A23.3.

Several empirical models have been developed to predict the length of the plastic hinge. These expressions provide very different results because they have been derived from tests for different types of concrete members and consider different parameters. Past research has focused mainly on beams and columns, not walls.

Program VecTor2 is a powerful analysis tool that provides good predictions of the response of reinforced concrete members. Analytical predictions of curvatures distributions and strain profiles obtained from VecTor2 have been verified with experimental results from tests performed on wall specimens.

The curvature distribution along the height of walls, determined experimentally and analytically, has been investigated. The results indicate that the distribution of inelastic curvatures can be well approximated as linearly varying.

The concept of curvature is based on the hypothesis that plane sections remain plane after bending, which is commonly assumed for slender concrete members. The strain profile along the length of walls has also been investigated to verify this assumption. The results indicate that before cracking, the strain profile remains linear. However, after cracking, the shape of the strain profile depends on the amount of reinforcement. As the amount of reinforcement increases, the strain profile is closer to have a linear variation. Also, the linearity of the strain profile degrades as the wall goes further into the nonlinear range.

The effect of the length of the wall in the plastic hinge length is more related to the magnitude of the steel strains than to the effect of diagonal cracking. Longer walls have larger plastic hinge lengths because they have larger steel strains than shorter walls. There is a bigger difference between the yield and ultimate moment for longer walls, which increases the slope of the post-yielding phase of the moment-curvature relationship.

For low shear stresses, a pure flexural prediction can be used to estimate the plastic hinge length. When the shear stresses are high, the actual plastic hinge length is longer due to the effect of diagonal cracking. The effect of shear has to be included to estimate the length of the plastic hinge for these cases. A simple shear model has been proposed, which provides reasonable results for high drifts.

The length of the plastic hinge reduces with the addition of axial compression, and increases with the addition of axial tension.

In a system of two walls of different lengths interconnected by rigid slabs at numerous floor levels, the curvature distributions along the height of the walls are different because of two reasons. First, the displacements between storey levels are different in both walls, specially at the lower levels, so the deflected shapes are not the strictly the same. Second, the shear displacements at the lower levels are larger in the longer wall; resulting in lower flexural displacements, lower slopes, and lower curvatures for this wall. Since the curvatures are not the same, the plastic hinge lengths are also different.

When two walls of different lengths are combined together, the curvature demand of the shorter wall is much larger than when it is alone for the same drift level. The curvature distribution in the longer wall remains the same. The shorter wall has to be designed to sustain that larger curvature demand. A simple model to predict the maximum curvature in the shorter wall has been proposed. This effect is of particular importance in the design of gravity columns in high-rise buildings, which may be subjected to tensile strains and also have to sustain larger curvature demands, even if they do not provide lateral resistance.

REFERENCES

ACI-ASCE Committee 428, 1968. "Progress Report on Code Clauses for Limit Design". ACI Journal, 65(9): 713 – 715.

Adebar, P., 2005. "High-Rise Concrete Wall Buildings: Utilizing Unconfined Concrete for Seismic Resistance". CONMAT'05: Third International Conference on Construction Materials: Performance, Innovations and Structural Implications, Vancouver, B.C., 13 pp.

Adebar, P., and Ibrahim, A.M.M., 2002. "Simple Nonlinear Flexural Stiffness Model for Concrete Structural Walls". Earthquake Spectra, 18(3): 407 – 426.

Adebar, P., and Ibrahim, A.M.M., 2004. "Effective Flexural Stiffness for Linear Seismic Analysis of Concrete Walls". Canadian Journal of Civil Engineering, 31: 597 – 607.

Adebar, P., Ibrahim, A.M.M., and Bryson, M., 2004. "Test of a High-Rise Shear Wall: Effective Stiffness for Seismic Analysis". ACI Structural Journal. In press (to be published in 2007).

Adebar, P., Mutrie, J., and DeVall, R., 2005. "Ductility of Concrete Walls: The Canadian Seismic Design Provisions 1984 to 2004". Canadian Journal of Civil Engineering, 32: 1124 – 1137.

Baker, A.L.L., 1956. "The Ultimate Load Theory Applied to the Design of Reinforced and Prestressed Concrete Frames". Concrete Publications Ltd, London.

Baker, A.L.L., and Amarakone, A.M.N., 1964. "Inelastic Hyperstatic Frames Analysis". Proceedings of the International Symposium on the Flexural Mechanics of Reinforced Concrete, ASCE-ACI, Miami: 85 – 142.

Bentz, E.C., 2000. "Sectional Analysis of Reinforced Concrete Members". Ph.D. Thesis, Department of Civil Engineering, University of Toronto.

Bentz, E.C., 2001. "Response-2000, Shell-2000, Triax-2000, Membrane-2000 User Manual". Department of Civil Engineering, University of Toronto.

Bentz, E.C., 2005. "Explaining the Riddle of Tension Stiffening Models for Shear Panel Experiments". Journal of Structural Engineering, ASCE, 131(9): 1422 – 1425.

Berry, M.P., and Eberhard, M.O., 2003. "Performance Models for Flexural Damage in Reinforced Concrete Columns". Pacific Earthquake Engineering Research Center Report 2003/18, University of California, Berkeley, California.

Berry, M.P., and Eberhard, M.O., 2005. "Practical Performance Models for Bar Buckling". Journal of Structural Engineering, ASCE, 131(7): 1060 – 1070.

Bryson, M., 2000. "Testing of the Lateral Stiffness of a Slender Concrete Shear Wall". Department of Civil Engineering, University of British Columbia, Vancouver, B.C.

Cement Association of Canada, 2006. "Concrete Design Handbook: 3rd. Edition". Ottawa, Ontario.

Chan, W.W.L., 1955. "The Ultimate Strength and Deformation of Plastic Hinges in Reinforced Concrete Frameworks". Magazine of Concrete Research, 7(21): 121 – 132.

Cohn, M.Z., and Petcu, V.A., 1963. "Moment Redistribution and Rotation Capacity of Plastic Hinges in Redundant Reinforced Concrete Beams". Indian Concrete Journal, 37(8): 282 – 290.

Corley, W.G., 1966. "Rotational Capacity of Reinforced Concrete Beams". Journal of the Structural Division, ASCE, 92(ST5): 121 – 146.

David, S., 2004. "Plastic Hinge Length in Isolated Walls". Department of Civil Engineering, University of British Columbia, Vancouver, B.C.

Duong, K.V., 2006. "Seismic Behaviour of a Shear-Critical Reinforced Concrete Frame: An Experimental and Numerical Investigation". M.A.Sc. Thesis, Department of Civil Engineering, University of Toronto.

Federal Emergency Management Agency, 1997. "NEHRP Guidelines for the Seismic Rehabilitation of Buildings, FEMA 273". Washington, D.C.

Federal Emergency Management Agency, 1998. "Evaluation of Earthquake Damaged Concrete and Masonry Wall Buildings: Basic Procedures Manual, FEMA 306". Washington, D.C.

Ibrahim, A.M.M., 2000. "Linear and Nonlinear Flexural Stiffness Models for Concrete Walls in High-Rise Buildings". Ph.D. Thesis, Department of Civil Engineering, University of British Columbia, Vancouver, B.C.

Institution of Civil Engineers, 1964. "Ultimate Load Design of Concrete Structures". Research Report, William Clowes & Sons Ltd, London.

Kowalsky, M.J., 2001. "RC Structural Walls Designed According to UBC and Displacement-Based Methods". Journal of Structural Engineering, ASCE, 127(5): 506 – 516.

Lehman, D.E., and Moehle, J.P, 2000. "Seismic Performance of Well-Confined Concrete Bridge Columns". Pacific Earthquake Engineering Research Center Report 1998/01, University of California, Berkeley, California.

Mattock, A.H., 1964. "Rotational Capacity of Hinging Regions in Reinforced Concrete Beams". Proceedings of the International Symposium on the Flexural Mechanics of Reinforced Concrete, ASCE-ACI, Miami: 143 – 181.

Mattock, A.H., 1967. "Discussion of 'Rotational Capacity of Reinforced Concrete Beams', by W.G. Corley". Journal of the Structural Division, ASCE, 93(ST2): 519 – 522.

Mendis, P., 2001. "Plastic Hinge Lengths of Normal and High-Strength Concrete in Flexure". Advances in Structural Engineering, 4(4): 189 – 195.

Moehle, J.P., 1992. "Displacement-Based Design of RC Structures Subjected to Earthquakes". Earthquake Spectra, 8(3): 403 – 428.

Montoya, E., Vecchio, F.J., and Sheikh, S.A., 2001. "Compression Field Modeling of Confined Concrete". Structural Engineering and Mechanics, 12(3): 231 – 248.

Oesterle, R.G., Aristizabal-Ochoa, J.D., Shiu K.N., and Corley, W.G., 1984. "Web Crushing of Reinforced Concrete Structural Walls". ACI Journal, 81(3): 231 – 241.

Panagiotakos, T.B., and Fardis, M.N., 2001. "Deformations of Reinforced Concrete Members at Yielding and Ultimate". ACI Structural Journal, 98(2): 135 – 148.

Park, R., and Paulay, T., 1975. "Reinforced Concrete Structures". John Wiley & Sons, New York.

Park, R., Priestly, M.J.N., and Gill, W.D., 1982. "Ductility of Square-Confined Concrete Columns". Journal of the Structural Division, ASCE, 108(ST4): 929 – 950.

Paulay, T., 1986. "The Design of Ductile Reinforced Concrete Structural Walls for Earthquake Resistance". Earthquake Spectra, 2(4): 783 – 823.

Paulay, T., 2001. "Seismic Response of Structural Walls: Recent Developments". Canadian Journal of Civil Engineering, 28: 922 – 937.

Paulay, T., and Priestly, M.J.N., 1992. "Seismic Design of Reinforced Concrete and Masonry Buildings". John Wiley & Sons, New York.

Paulay, T., and Priestly, M.J.N., 1993. "Stability of Ductile Structural Walls". ACI Structural Journal, 90(4): 385 – 392.

Paulay, T., and Uzumeri, S.M., 1975. "A Critical Review of the Seismic Design Provisions for Ductile Shear Walls of the Canadian Code and Commentary". Canadian Journal of Civil Engineering, 2: 592 – 601.

Priestly, M.J.N., and Park, R., 1987. "Strength and Ductility of Concrete Bridge Columns Under Seismic Loading". ACI Structural Journal, 84(1): 61 – 76.

Priestly, M.J.N., Park, R., and Potangaroa, R.T., 1981. "Ductility and Spirally-Confined Concrete Columns". Journal of the Structural Division, ASCE, 107(ST1): 181 – 202.

Priestly, M.J.N., Seible, F., and Calvi, G.M., 1996. "Seismic Design and Retrofit of Bridges". John Wiley & Sons, New York.

Sasani, M., and Der Kiureghian, A., 2001. "Seismic Fragility of RC Structural Walls: Displacement Approach". Journal of Structural Engineering, ASCE, 127(2): 219 – 228.

Sawyer, H.A., 1964. "Design of Concrete Frames for Two Failure Stages". Proceedings of the International Symposium on the Flexural Mechanics of Reinforced Concrete, ASCE-ACI, Miami: 405 – 431.

Selby, R.G., Vecchio, F.J., and Collins, M.P., 1996. "Analysis of Reinforced Concrete Members Subject to Shear and Axial Compression". ACI Structural Journal, 93(3): 306 – 315.

Thomsen, J.H., and Wallace, J.W., 1995. "Displacement-Based Design of Reinforced Concrete Structural Walls: An Experimental Investigation of Walls with Rectangular and T-Shaped Cross-Sections". Report No. CU/CEE-95-06, Department of Civil and Environmental Engineering, Clarkson University, Postdam, New York.

Thomsen, J.H., and Wallace, J.W., 2004. "Displacement-Based Design of Slender Reinforced Concrete Structural Walls: Experimental Verification". Journal of Structural Engineering, ASCE, 130(4): 618 – 630.

Vecchio, F.J., 1989. "Nonlinear Finite Element Analysis of Reinforced Concrete Membranes". ACI Structural Journal, 86(1): 26 – 35.

Vecchio, F.J., 2000. "Disturbed Stress Field Model for Reinforced Concrete: Formulation". Journal of Structural Engineering, ASCE, 126(9): 1070 – 1077.

Vecchio, F.J., and Collins, M.P., 1986. "The Modified Compression-Field Theory for Reinforced Concrete Elements Subjected to Shear". ACI Journal, 83(2): 219 – 231.

Vecchio, F.J., and Shim, W., 2004. "Experimental and Analytical Reexamination of Classic Concrete Beam Tests". Journal of Structural Engineering, ASCE, 130(3): 460 – 469.

VecTor Analysis Group Website, University of Toronto: www.civ.utoronto.ca/vector/

Wallace, J.W., 1998. "A Designer's Guide to Displacement-Based Design of RC Structural Walls". Department of Civil Engineering, University of California, Los Angeles, California.

Wallace, J.W., and Moehle, J.P., 1992. "Ductility and Detailing Requirements of Bearing Wall Buildings". Journal of Structural Engineering, ASCE, 118(6): 1625 – 1644.

Wong, P.S., and Vecchio, F.J., 2002. "VecTor2 and FormWorks User's Manual". Department of Civil Engineering, University of Toronto.

Zahn, F.A., Park, R., and Priestly, M.J.N., 1986. "Design of Reinforced Concrete Bridge Columns for Strength and Ductility". Research Report 86-7, Department of Civil Engineering, University of Canterbury, Christchurch, New Zealand.

APPENDIX A: UBC WALL TEST

Table A.1 List of zero readings

Target		Reading 1 (mm)	Reading 2 (mm)	Reading 3 (mm)	Reading 4 (mm)	Reading 5 (mm)	Reading 6 (mm)
First	Second						
TW1	TW2	288.37	289.53	289.71	289.55	289.57	289.63
TW2	TW3	194.74	194.08	193.95	194.01	193.83	193.84
TW3	TW4	521.09	521.15	521.12	521.04	521.00	521.03
TW4	TW5	521.06	521.08	521.08	521.04	521.04	521.04
TW5	TW6	520.93	520.91	520.77	520.70	520.65	520.61
TW6	TW7	521.51	521.33	521.42	521.28	521.00	521.23
TW7	TW8	520.11	521.20	520.10	520.03	521.30	519.83
TW8	TW9	520.40	520.82	520.42	520.34	520.05	520.28
TW9	TW10	520.62	520.52	520.56	520.49	520.48	520.44
TW10	TW11	520.52	520.50	520.44	521.74	521.00	521.20
TW11	TW12	520.59	520.40	520.42	520.78	521.00	521.82
TE1	TE2	291.37	294.36	294.78	294.73	294.80	294.82
TE2	TE3	191.04	191.61	191.24	191.98	190.92	191.12
TE3	TE4	521.10	521.10	521.28	521.30	521.09	521.00
TE4	TE5	521.06	520.89	521.07	520.90	520.95	520.89
TE5	TE6	521.25	521.07	521.26	521.02	521.04	520.97
TE6	TE7	521.06	521.12	521.08	521.06	521.09	521.03
TE7	TE8	521.03	521.46	521.16	520.99	520.95	521.08
TE8	TE9	521.06	521.07	521.34	520.98	521.05	521.26
TE9	TE10	521.33	521.16	521.14	521.02	521.11	521.16
TE10	TE11	521.16	521.24	521.13	521.05	521.10	521.22
TE11	TE12	521.33	521.28	521.15	521.25	521.41	521.07

Marked cells show measurements out of range, these were neglected.

Table A.2 Mean values of zero readings

Target		Reading 1 (mm)	Reading 2 (mm)	Reading 3 (mm)	Reading 4 (mm)	Reading 5 (mm)	Reading 6 (mm)	Mean value (mm)
First	Second							
TW1	TW2		289.53	289.71	289.55	289.57	289.63	289.60
TW2	TW3		194.08	193.95	194.01	193.83	193.84	193.94
TW3	TW4	521.09	521.15	521.12	521.04	521.00	521.03	521.07
TW4	TW5	521.06	521.08	521.08	521.04	521.04	521.04	521.06
TW5	TW6	520.93	520.91	520.77	520.70	520.65	520.61	520.76
TW6	TW7	521.51	521.33	521.42	521.28		521.23	521.35
TW7	TW8	520.11		520.10	520.03		519.83	520.02
TW8	TW9	520.40		520.42	520.34		520.28	520.36
TW9	TW10	520.62	520.52	520.56	520.49	520.48	520.44	520.52
TW10	TW11	520.52	520.50	520.44		521.00	521.20	520.73
TW11	TW12	520.59	520.40	520.42	520.78	521.00		520.64
TE1	TE2		294.36	294.78	294.73	294.80	294.82	294.70
TE2	TE3	191.04	191.61	191.24		190.92	191.12	191.19
TE3	TE4	521.10	521.10	521.28	521.30	521.09	521.00	521.15
TE4	TE5	521.06	520.89	521.07	520.90	520.95	520.89	520.96
TE5	TE6	521.25	521.07	521.26	521.02	521.04	520.97	521.10
TE6	TE7	521.06	521.12	521.08	521.06	521.09	521.03	521.07
TE7	TE8	521.03		521.16	520.99	520.95	521.08	521.04
TE8	TE9	521.06	521.07	521.34	520.98	521.05	521.26	521.13
TE9	TE10	521.33	521.16	521.14	521.02	521.11	521.16	521.15
TE10	TE11	521.16	521.24	521.13	521.05	521.10	521.22	521.15
TE11	TE12	521.33	521.28	521.15	521.25	521.41	521.07	521.25

Table A.3 Experimental (pushing east) curvatures for a wall displacement of 105mm

Target		Reading (mm)	Zero reading (mm)	Cumulative (mm)	Height (mm)	Strain	Curvature (rad/m)
First	Second						
TW1	TW2	290.24	289.60	289.60	146.07	0.0022	0.00228
TW2	TW3	196.22	193.94	483.54	388.43	0.0117	0.00821
TW3	TW4	524.50	521.07	1004.61	745.27	0.0066	0.00476
TW4	TW5	523.21	521.06	1525.67	1266.32	0.0041	0.00305
TW5	TW6	521.96	520.76	2046.43	1787.29	0.0023	0.00190
TW6	TW7	521.92	521.35	2567.78	2308.37	0.0011	0.00106
TW7	TW8	520.78	520.02	3087.80	2829.24	0.0015	0.00129
TW8	TW9	520.52	520.36	3608.16	3349.88	0.0003	0.00029
TW9	TW10	520.75	520.52	4128.68	3870.67	0.0004	0.00038
TW10	TW11	521.16	520.73	4649.41	4391.55	0.0008	0.00069
TW11	TW12	520.97	520.64	5170.05	4912.50	0.0006	0.00072
Top of wall		-	-	-	11760.00	0.0000	0.00000
TE1	TE2	294.26	294.70	294.70	146.07	-0.0015	0.00228
TE2	TE3	190.88	191.19	485.88	388.43	-0.0016	0.00821
TE3	TE4	520.54	521.15	1007.03	745.27	-0.0012	0.00476
TE4	TE5	520.53	520.96	1527.99	1266.32	-0.0008	0.00305
TE5	TE6	520.69	521.10	2049.09	1787.29	-0.0008	0.00190
TE6	TE7	520.74	521.07	2570.16	2308.37	-0.0006	0.00106
TE7	TE8	520.71	521.04	3091.21	2829.24	-0.0006	0.00129
TE8	TE9	521.04	521.13	3612.33	3349.88	-0.0002	0.00029
TE9	TE10	521.06	521.15	4133.49	3870.67	-0.0002	0.00038
TE10	TE11	520.99	521.15	4654.64	4391.55	-0.0003	0.00069
TE11	TE12	520.97	521.25	5175.88	4912.50	-0.0005	0.00072
Top of wall		-	-	-	11760.00	0.0000	0.00000

Wall length: 1625 mm

Table A.4 Experimental (pushing west) curvatures for a wall displacement of 104mm

Target		Reading (mm)	Zero reading (mm)	Cumulative (mm)	Height (mm)	Strain	Curvature (rad/m)
First	Second						
TW1	TW2	288.76	289.60	289.60	146.07	-0.0029	0.00433
TW2	TW3	193.67	193.94	483.54	388.43	-0.0014	0.01050
TW3	TW4	520.59	521.07	1004.61	745.27	-0.0009	0.00364
TW4	TW5	520.65	521.06	1525.67	1266.32	-0.0008	0.00259
TW5	TW6	520.38	520.76	2046.43	1787.29	-0.0007	0.00149
TW6	TW7	521.02	521.35	2567.78	2308.37	-0.0006	0.00052
TW7	TW8	519.50	520.02	3087.80	2829.24	-0.0010	0.00155
TW8	TW9	520.11	520.36	3608.16	3349.88	-0.0005	0.00039
TW9	TW10	520.28	520.52	4128.68	3870.67	-0.0005	0.00031
TW10	TW11	520.87	520.73	4649.41	4391.55	0.0003	0.00010
TW11	TW12	520.58	520.64	5170.05	4912.50	-0.0001	0.00006
Top of wall		-	-	-	11760.00	0.0000	0.00000
TE1	TE2	295.92	294.70	294.70	146.07	0.0041	0.00433
TE2	TE3	194.18	191.19	485.88	388.43	0.0157	0.01050
TE3	TE4	523.75	521.15	1007.03	745.27	0.0050	0.00364
TE4	TE5	522.75	520.96	1527.99	1266.32	0.0034	0.00259
TE5	TE6	521.98	521.10	2049.09	1787.29	0.0017	0.00149
TE6	TE7	521.18	521.07	2570.16	2308.37	0.0002	0.00052
TE7	TE8	521.84	521.04	3091.21	2829.24	0.0015	0.00155
TE8	TE9	521.21	521.13	3612.33	3349.88	0.0002	0.00039
TE9	TE10	521.18	521.15	4133.49	3870.67	0.0001	0.00031
TE10	TE11	521.20	521.15	4654.64	4391.55	0.0001	0.00010
TE11	TE12	521.24	521.25	5175.88	4912.50	0.0000	0.00006
Top of wall		-	-	-	11760.00	0.0000	0.00000

Wall length: 1625 mm

Table A.5 Experimental (pushing east) curvatures for a wall displacement of 132mm

Target		Reading (mm)	Zero reading (mm)	Cumulative (mm)	Height (mm)	Strain	Curvature (rad/m)
First	Second						
TW1	TW2	288.10	289.60	289.60	146.07	-0.0052	0.00214
TW2	TW3	196.79	193.94	483.54	388.43	0.0147	0.01028
TW3	TW4	526.00	521.07	1004.61	745.27	0.0095	0.00659
TW4	TW5	524.08	521.06	1525.67	1266.32	0.0058	0.00413
TW5	TW6	522.34	520.76	2046.43	1787.29	0.0030	0.00235
TW6	TW7	522.00	521.35	2567.78	2308.37	0.0012	0.00114
TW7	TW8	520.86	520.02	3087.80	2829.24	0.0016	0.00138
TW8	TW9	520.45	520.36	3608.16	3349.88	0.0002	0.00048
TW9	TW10	520.84	520.52	4128.68	3870.67	0.0006	0.00073
TW10	TW11	521.14	520.73	4649.41	4391.55	0.0008	0.00077
TW11	TW12	520.86	520.64	5170.05	4912.50	0.0004	0.00060
Top of wall		-	-	-	11760.00	0.0000	0.00000
TE1	TE2	294.20	294.70	294.70	146.07	-0.0017	0.00214
TE2	TE3	190.80	191.19	485.88	388.43	-0.0020	0.01028
TE3	TE4	520.49	521.15	1007.03	745.27	-0.0013	0.00659
TE4	TE5	520.49	520.96	1527.99	1266.32	-0.0009	0.00413
TE5	TE6	520.69	521.10	2049.09	1787.29	-0.0008	0.00235
TE6	TE7	520.75	521.07	2570.16	2308.37	-0.0006	0.00114
TE7	TE8	520.72	521.04	3091.21	2829.24	-0.0006	0.00138
TE8	TE9	520.81	521.13	3612.33	3349.88	-0.0006	0.00048
TE9	TE10	520.86	521.15	4133.49	3870.67	-0.0006	0.00073
TE10	TE11	520.91	521.15	4654.64	4391.55	-0.0005	0.00077
TE11	TE12	520.96	521.25	5175.88	4912.50	-0.0006	0.00060
Top of wall		-	-	-	11760.00	0.0000	0.00000

Wall length: 1625 mm

Table A.6 Experimental (pushing west) curvatures for a wall displacement of 138mm

Target		Reading (mm)	Zero reading (mm)	Cumulative (mm)	Height (mm)	Strain	Curvature (rad/m)
First	Second						
TW1	TW2	288.95	289.60	289.60	146.07	-0.0022	0.00307
TW2	TW3	193.70	193.94	483.54	388.43	-0.0012	0.01472
TW3	TW4	520.47	521.07	1004.61	745.27	-0.0012	0.00557
TW4	TW5	520.74	521.06	1525.67	1266.32	-0.0006	0.00375
TW5	TW6	520.35	520.76	2046.43	1787.29	-0.0008	0.00191
TW6	TW7	520.98	521.35	2567.78	2308.37	-0.0007	0.00048
TW7	TW8	519.61	520.02	3087.80	2829.24	-0.0008	0.00172
TW8	TW9	520.12	520.36	3608.16	3349.88	-0.0005	0.00055
TW9	TW10	520.44	520.52	4128.68	3870.67	-0.0002	0.00012
TW10	TW11	521.11	520.73	4649.41	4391.55	0.0007	0.00041
TW11	TW12	520.65	520.64	5170.05	4912.50	0.0000	0.00013
Top of wall		-	-	-	11760.00	0.0000	0.00000
TE1	TE2	295.51	294.70	294.70	146.07	0.0028	0.00307
TE2	TE3	195.52	191.19	485.88	388.43	0.0227	0.01472
TE3	TE4	525.26	521.15	1007.03	745.27	0.0079	0.00557
TE4	TE5	523.82	520.96	1527.99	1266.32	0.0055	0.00375
TE5	TE6	522.31	521.10	2049.09	1787.29	0.0023	0.00191
TE6	TE7	521.11	521.07	2570.16	2308.37	0.0001	0.00048
TE7	TE8	522.09	521.04	3091.21	2829.24	0.0020	0.00172
TE8	TE9	521.35	521.13	3612.33	3349.88	0.0004	0.00055
TE9	TE10	521.18	521.15	4133.49	3870.67	0.0001	0.00012
TE10	TE11	521.18	521.15	4654.64	4391.55	0.0001	0.00041
TE11	TE12	521.15	521.25	5175.88	4912.50	-0.0002	0.00013
Top of wall		-	-	-	11760.00	0.0000	0.00000

Wall length: 1625 mm

Table A.7 Experimental (pushing east) curvatures for a wall displacement of 182mm

Target		Reading (mm)	Zero reading (mm)	Cumulative (mm)	Height (mm)	Strain	Curvature (rad/m)
First	Second						
TW1	TW2	289.65	289.60	289.60	146.07	0.0002	0.00151
TW2	TW3	198.00	193.94	483.54	388.43	0.0209	0.01402
TW3	TW4	528.79	521.07	1004.61	745.27	0.0148	0.01021
TW4	TW5	525.59	521.06	1525.67	1266.32	0.0087	0.00600
TW5	TW6	523.16	520.76	2046.43	1787.29	0.0046	0.00340
TW6	TW7	522.12	521.35	2567.78	2308.37	0.0015	0.00132
TW7	TW8	520.98	520.02	3087.80	2829.24	0.0019	0.00157
TW8	TW9	520.45	520.36	3608.16	3349.88	0.0002	0.00053
TW9	TW10	521.09	520.52	4128.68	3870.67	0.0011	0.00108
TW10	TW11	521.15	520.73	4649.41	4391.55	0.0008	0.00080
TW11	TW12	520.87	520.64	5170.05	4912.50	0.0004	0.00071
Top of wall		-	-	-	11760.00	0.0000	0.00000
TE1	TE2	294.03	294.70	294.70	146.07	-0.0023	0.00151
TE2	TE3	190.83	191.19	485.88	388.43	-0.0019	0.01402
TE3	TE4	520.22	521.15	1007.03	745.27	-0.0018	0.01021
TE4	TE5	520.41	520.96	1527.99	1266.32	-0.0011	0.00600
TE5	TE6	520.62	521.10	2049.09	1787.29	-0.0009	0.00340
TE6	TE7	520.72	521.07	2570.16	2308.37	-0.0007	0.00132
TE7	TE8	520.68	521.04	3091.21	2829.24	-0.0007	0.00157
TE8	TE9	520.77	521.13	3612.33	3349.88	-0.0007	0.00053
TE9	TE10	520.81	521.15	4133.49	3870.67	-0.0007	0.00108
TE10	TE11	520.89	521.15	4654.64	4391.55	-0.0005	0.00080
TE11	TE12	520.88	521.25	5175.88	4912.50	-0.0007	0.00071
Top of wall		-	-	-	11760.00	0.0000	0.00000

Wall length: 1625 mm

Table A.8 Experimental (pushing west) curvatures for a wall displacement of 187mm

Target		Reading (mm)	Zero reading (mm)	Cumulative (mm)	Height (mm)	Strain	Curvature (rad/m)
First	Second						
TW1	TW2	288.86	289.60	289.60	146.07	-0.0025	0.00341
TW2	TW3	193.53	193.94	483.54	388.43	-0.0021	0.02253
TW3	TW4	520.33	521.07	1004.61	745.27	-0.0014	0.00808
TW4	TW5	520.52	521.06	1525.67	1266.32	-0.0010	0.00577
TW5	TW6	520.29	520.76	2046.43	1787.29	-0.0009	0.00278
TW6	TW7	520.95	521.35	2567.78	2308.37	-0.0008	0.00125
TW7	TW8	519.67	520.02	3087.80	2829.24	-0.0007	0.00159
TW8	TW9	520.07	520.36	3608.16	3349.88	-0.0006	0.00061
TW9	TW10	520.28	520.52	4128.68	3870.67	-0.0005	0.00034
TW10	TW11	520.86	520.73	4649.41	4391.55	0.0002	0.00008
TW11	TW12	520.96	520.64	5170.05	4912.50	0.0006	0.00034
Top of wall		-	-	-	11760.00	0.0000	0.00000
TE1	TE2	295.58	294.70	294.70	146.07	0.0030	0.00341
TE2	TE3	197.78	191.19	485.88	388.43	0.0345	0.02253
TE3	TE4	527.25	521.15	1007.03	745.27	0.0117	0.00808
TE4	TE5	525.31	520.96	1527.99	1266.32	0.0083	0.00577
TE5	TE6	522.98	521.10	2049.09	1787.29	0.0036	0.00278
TE6	TE7	521.73	521.07	2570.16	2308.37	0.0013	0.00125
TE7	TE8	522.04	521.04	3091.21	2829.24	0.0019	0.00159
TE8	TE9	521.35	521.13	3612.33	3349.88	0.0004	0.00061
TE9	TE10	521.20	521.15	4133.49	3870.67	0.0001	0.00034
TE10	TE11	521.21	521.15	4654.64	4391.55	0.0001	0.00008
TE11	TE12	521.28	521.25	5175.88	4912.50	0.0001	0.00034
Top of wall		-	-	-	11760.00	0.0000	0.00000

Wall length: 1625 mm

Table A.9 Analytical curvatures for a wall displacement of 105mm

Node		Node 1 y-displ (mm)	Node 2 y-displ (mm)	Node 2 y-coord (mm)	Difference (mm)	Height (mm)	Strain	Curvature (rad/m)
First	Second							
1	22	0.00	0.78	58.71	58.71	29.36	0.0134	0.00985
22	148	0.78	6.87	579.63	520.92	319.17	0.0117	0.00822
148	274	6.87	9.51	1100.55	520.92	840.09	0.0051	0.00375
274	400	9.51	10.27	1621.47	520.92	1361.01	0.0015	0.00139
400	526	10.27	10.90	2142.39	520.92	1881.93	0.0012	0.00118
526	652	10.90	11.35	2663.31	520.92	2402.85	0.0009	0.00091
652	778	11.35	11.62	3184.23	520.92	2923.77	0.0005	0.00066
778	904	11.62	11.75	3705.15	520.92	3444.69	0.0002	0.00046
904	1030	11.75	11.86	4226.07	520.92	3965.61	0.0002	0.00041
1030	1156	11.86	11.91	4746.99	520.92	4486.53	0.0001	0.00033
Top of wall		-	-	-	-	11330.00	0.0000	0.00000
21	42	0.00	-0.16	58.71	58.71	29.36	-0.0027	0.00985
42	168	-0.16	-1.03	579.63	520.92	319.17	-0.0017	0.00822
168	294	-1.03	-1.57	1100.55	520.92	840.09	-0.0010	0.00375
294	420	-1.57	-1.98	1621.47	520.92	1361.01	-0.0008	0.00139
420	546	-1.98	-2.34	2142.39	520.92	1881.93	-0.0007	0.00118
546	672	-2.34	-2.67	2663.31	520.92	2402.85	-0.0006	0.00091
672	798	-2.67	-2.96	3184.23	520.92	2923.77	-0.0006	0.00066
798	924	-2.96	-3.22	3705.15	520.92	3444.69	-0.0005	0.00046
924	1050	-3.22	-3.46	4226.07	520.92	3965.61	-0.0005	0.00041
1050	1176	-3.46	-3.68	4746.99	520.92	4486.53	-0.0004	0.00033
Top of wall		-	-	-	-	11330.00	0.0000	0.00000

Wall length: 1625 mm

Table A.10 Analytical curvatures for a wall displacement of 104mm

Node		Node 1 y-displ (mm)	Node 2 y-displ (mm)	Node 2 y-coord (mm)	Difference (mm)	Height (mm)	Strain	Curvature (rad/m)
First	Second							
1	22	0.00	0.78	58.71	58.71	29.36	0.0133	0.00981
22	148	0.78	6.82	579.63	520.92	319.17	0.0116	0.00816
148	274	6.82	9.37	1100.55	520.92	840.09	0.0049	0.00365
274	400	9.37	10.13	1621.47	520.92	1361.01	0.0015	0.00139
400	526	10.13	10.77	2142.39	520.92	1881.93	0.0012	0.00118
526	652	10.77	11.21	2663.31	520.92	2402.85	0.0009	0.00091
652	778	11.21	11.49	3184.23	520.92	2923.77	0.0005	0.00067
778	904	11.49	11.61	3705.15	520.92	3444.69	0.0002	0.00046
904	1030	11.61	11.72	4226.07	520.92	3965.61	0.0002	0.00041
1030	1156	11.72	11.77	4746.99	520.92	4486.53	0.0001	0.00033
Top of wall		-	-	-	-	11330.00	0.0000	0.00000
21	42	0.00	-0.16	58.71	58.71	29.36	-0.0026	0.00981
42	168	-0.16	-1.02	579.63	520.92	319.17	-0.0017	0.00816
168	294	-1.02	-1.56	1100.55	520.92	840.09	-0.0010	0.00365
294	420	-1.56	-1.97	1621.47	520.92	1361.01	-0.0008	0.00139
420	546	-1.97	-2.33	2142.39	520.92	1881.93	-0.0007	0.00118
546	672	-2.33	-2.66	2663.31	520.92	2402.85	-0.0006	0.00091
672	798	-2.66	-2.95	3184.23	520.92	2923.77	-0.0006	0.00067
798	924	-2.95	-3.21	3705.15	520.92	3444.69	-0.0005	0.00046
924	1050	-3.21	-3.45	4226.07	520.92	3965.61	-0.0005	0.00041
1050	1176	-3.45	-3.67	4746.99	520.92	4486.53	-0.0004	0.00033
Top of wall		-	-	-	-	11330.00	0.0000	0.00000

Wall length: 1625 mm

Table A.11 Analytical curvatures for a wall displacement of 132mm

Node		Node 1 y-displ (mm)	Node 2 y-displ (mm)	Node 2 y-coord (mm)	Difference (mm)	Height (mm)	Strain	Curvature (rad/m)
First	Second							
1	22	0.00	0.93	58.71	58.71	29.36	0.0158	0.01171
22	148	0.93	8.10	579.63	520.92	319.17	0.0138	0.00967
148	274	8.10	12.41	1100.55	520.92	840.09	0.0083	0.00580
274	400	12.41	13.80	1621.47	520.92	1361.01	0.0027	0.00217
400	526	13.80	14.47	2142.39	520.92	1881.93	0.0013	0.00123
526	652	14.47	15.01	2663.31	520.92	2402.85	0.0010	0.00103
652	778	15.01	15.28	3184.23	520.92	2923.77	0.0005	0.00067
778	904	15.28	15.47	3705.15	520.92	3444.69	0.0004	0.00054
904	1030	15.47	15.58	4226.07	520.92	3965.61	0.0002	0.00042
1030	1156	15.58	15.63	4746.99	520.92	4486.53	0.0001	0.00033
Top of wall		-	-	-	-	11330.00	0.0000	0.00000
21	42	0.00	-0.19	58.71	58.71	29.36	-0.0032	0.01171
42	168	-0.19	-1.20	579.63	520.92	319.17	-0.0020	0.00967
168	294	-1.20	-1.81	1100.55	520.92	840.09	-0.0012	0.00580
294	420	-1.81	-2.25	1621.47	520.92	1361.01	-0.0009	0.00217
420	546	-2.25	-2.63	2142.39	520.92	1881.93	-0.0007	0.00123
546	672	-2.63	-2.96	2663.31	520.92	2402.85	-0.0006	0.00103
672	798	-2.96	-3.26	3184.23	520.92	2923.77	-0.0006	0.00067
798	924	-3.26	-3.53	3705.15	520.92	3444.69	-0.0005	0.00054
924	1050	-3.53	-3.77	4226.07	520.92	3965.61	-0.0005	0.00042
1050	1176	-3.77	-4.00	4746.99	520.92	4486.53	-0.0004	0.00033
Top of wall		-	-	-	-	11330.00	0.0000	0.00000

Wall length: 1625 mm

Table A.12 Analytical curvatures for a wall displacement of 138mm

Node		Node 1 y-displ (mm)	Node 2 y-displ (mm)	Node 2 y-coord (mm)	Difference (mm)	Height (mm)	Strain	Curvature (rad/m)
First	Second							
1	22	0.00	0.97	58.71	58.71	29.36	0.0165	0.01221
22	148	0.97	8.56	579.63	520.92	319.17	0.0146	0.01021
148	274	8.56	13.17	1100.55	520.92	840.09	0.0089	0.00617
274	400	13.17	14.62	1621.47	520.92	1361.01	0.0028	0.00225
400	526	14.62	15.29	2142.39	520.92	1881.93	0.0013	0.00124
526	652	15.29	15.84	2663.31	520.92	2402.85	0.0010	0.00104
652	778	15.84	16.11	3184.23	520.92	2923.77	0.0005	0.00067
778	904	16.11	16.29	3705.15	520.92	3444.69	0.0004	0.00054
904	1030	16.29	16.41	4226.07	520.92	3965.61	0.0002	0.00042
1030	1156	16.41	16.46	4746.99	520.92	4486.53	0.0001	0.00033
Top of wall		-	-	-	-	11330.00	0.0000	0.00000
21	42	0.00	-0.20	58.71	58.71	29.36	-0.0034	0.01221
42	168	-0.20	-1.25	579.63	520.92	319.17	-0.0020	0.01021
168	294	-1.25	-1.86	1100.55	520.92	840.09	-0.0012	0.00617
294	420	-1.86	-2.30	1621.47	520.92	1361.01	-0.0009	0.00225
420	546	-2.30	-2.68	2142.39	520.92	1881.93	-0.0007	0.00124
546	672	-2.68	-3.02	2663.31	520.92	2402.85	-0.0006	0.00104
672	798	-3.02	-3.32	3184.23	520.92	2923.77	-0.0006	0.00067
798	924	-3.32	-3.58	3705.15	520.92	3444.69	-0.0005	0.00054
924	1050	-3.58	-3.83	4226.07	520.92	3965.61	-0.0005	0.00042
1050	1176	-3.83	-4.06	4746.99	520.92	4486.53	-0.0004	0.00033
Top of wall		-	-	-	-	11330.00	0.0000	0.00000

Wall length: 1625 mm

Table A.13 Analytical curvatures for a wall displacement of 182mm

Node		Node 1 y-displ (mm)	Node 2 y-displ (mm)	Node 2 y-coord (mm)	Difference (mm)	Height (mm)	Strain	Curvature (rad/m)
First	Second							
1	22	0.00	1.14	58.71	58.71	29.36	0.0193	0.01458
22	148	1.14	10.31	579.63	520.92	319.17	0.0176	0.01235
148	274	10.31	17.78	1100.55	520.92	840.09	0.0143	0.00965
274	400	17.78	20.51	1621.47	520.92	1361.01	0.0052	0.00380
400	526	20.51	21.23	2142.39	520.92	1881.93	0.0014	0.00132
526	652	21.23	21.82	2663.31	520.92	2402.85	0.0011	0.00111
652	778	21.82	22.18	3184.23	520.92	2923.77	0.0007	0.00078
778	904	22.18	22.37	3705.15	520.92	3444.69	0.0004	0.00056
904	1030	22.37	22.49	4226.07	520.92	3965.61	0.0002	0.00044
1030	1156	22.49	22.55	4746.99	520.92	4486.53	0.0001	0.00034
Top of wall		-	-	-	-	11330.00	0.0000	0.00000
21	42	0.00	-0.26	58.71	58.71	29.36	-0.0044	0.01458
42	168	-0.26	-1.54	579.63	520.92	319.17	-0.0025	0.01235
168	294	-1.54	-2.24	1100.55	520.92	840.09	-0.0013	0.00965
294	420	-2.24	-2.72	1621.47	520.92	1361.01	-0.0009	0.00380
420	546	-2.72	-3.12	2142.39	520.92	1881.93	-0.0008	0.00132
546	672	-3.12	-3.46	2663.31	520.92	2402.85	-0.0007	0.00111
672	798	-3.46	-3.77	3184.23	520.92	2923.77	-0.0006	0.00078
798	924	-3.77	-4.05	3705.15	520.92	3444.69	-0.0005	0.00056
924	1050	-4.05	-4.30	4226.07	520.92	3965.61	-0.0005	0.00044
1050	1176	-4.30	-4.53	4746.99	520.92	4486.53	-0.0004	0.00034
Top of wall		-	-	-	-	11330.00	0.0000	0.00000

Wall length: 1625 mm

Table A.14 Analytical curvatures for a wall displacement of 187mm

Node		Node 1 y-displ (mm)	Node 2 y-displ (mm)	Node 2 y-coord (mm)	Difference (mm)	Height (mm)	Strain	Curvature (rad/m)
First	Second							
1	22	0.00	1.16	58.71	58.71	29.36	0.0197	0.01487
22	148	1.16	10.52	579.63	520.92	319.17	0.0180	0.01260
148	274	10.52	18.15	1100.55	520.92	840.09	0.0147	0.00986
274	400	18.15	21.17	1621.47	520.92	1361.01	0.0058	0.00414
400	526	21.17	21.91	2142.39	520.92	1881.93	0.0014	0.00134
526	652	21.91	22.50	2663.31	520.92	2402.85	0.0011	0.00112
652	778	22.50	22.86	3184.23	520.92	2923.77	0.0007	0.00079
778	904	22.86	23.06	3705.15	520.92	3444.69	0.0004	0.00056
904	1030	23.06	23.18	4226.07	520.92	3965.61	0.0002	0.00044
1030	1156	23.18	23.24	4746.99	520.92	4486.53	0.0001	0.00035
Top of wall		-	-	-	-	11330.00	0.0000	0.00000
21	42	0.00	-0.26	58.71	58.71	29.36	-0.0045	0.01487
42	168	-0.26	-1.57	579.63	520.92	319.17	-0.0025	0.01260
168	294	-1.57	-2.28	1100.55	520.92	840.09	-0.0014	0.00986
294	420	-2.28	-2.77	1621.47	520.92	1361.01	-0.0009	0.00414
420	546	-2.77	-3.17	2142.39	520.92	1881.93	-0.0008	0.00134
546	672	-3.17	-3.51	2663.31	520.92	2402.85	-0.0007	0.00112
672	798	-3.51	-3.82	3184.23	520.92	2923.77	-0.0006	0.00079
798	924	-3.82	-4.10	3705.15	520.92	3444.69	-0.0005	0.00056
924	1050	-4.10	-4.35	4226.07	520.92	3965.61	-0.0005	0.00044
1050	1176	-4.35	-4.58	4746.99	520.92	4486.53	-0.0004	0.00035
Top of wall		-	-	-	-	11330.00	0.0000	0.00000

Wall length: 1625 mm

Table A.15 Plane sections analysis to determine ultimate curvature

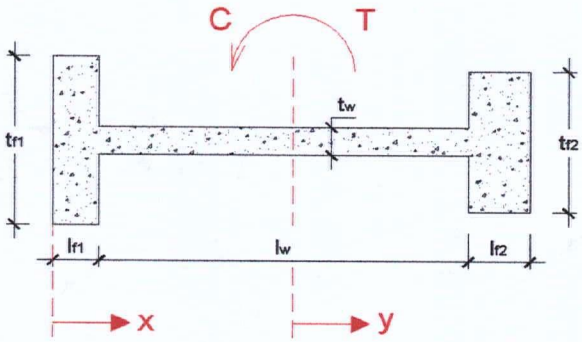

Concrete properties		Wall dimensions	
f'_c (MPa)	49.0	l_{f1} (mm)	203.0
ε_{cu}	0.0035	t_{f1} (mm)	380.0
ϕ_c	1.00	l_{f2} (mm)	203.0
Reinforcement properties		t_{f2} (mm)	380.0
		l_w (mm)	1219.0
f_y (MPa)	455.0	t_w (mm)	127.0
E_s (MPa)	200000.0	**Axial load**	
ϕ_s	1.00	P (kN)	-1500.0

Stress block factors		Yield strain		Section centroid		Forces in concrete	
α_1	0.777	ε_y	0.0023	x (mm)	812.50	c (mm)	148.23
β_1	0.848					a (mm)	125.62
						P_c (kN)	-1816.31
						M_c (kN.m)	1361.67

Forces in reinforcement							
Layer	x (mm)	A_s (mm^2)	ε_s	f_s (MPa)	P_s (kN)	y (mm)	M_s (kN.m)
1	21.00	300.0	-0.0030	-455.00	-125.09	-791.50	99.01
2	182.00	200.0	0.0008	159.49	31.90	-630.50	-20.11
3	355.00	100.0	0.0049	455.00	45.50	-457.50	-20.82
4	660.00	100.0	0.0121	455.00	45.50	-152.50	-6.94
5	965.00	100.0	0.0193	455.00	45.50	152.50	6.94
6	1270.00	100.0	0.0265	455.00	45.50	457.50	20.82
7	1443.00	200.0	0.0306	455.00	91.00	630.50	57.38
8	1604.00	300.0	0.0344	455.00	136.50	791.50	108.04
				Total	316.31	**Total**	244.31

Results	
P_r (kN)	-1500.00
M_r (kN.m)	1605.98
ϕ_u (rad/m)	0.0236

APPENDIX B: CLARKSON UNIVERSITY WALL TEST

Table B.1 Analytical strain profile at base for a drift of 1.5%

Node		Node 1 y-displ (mm)	Node 2 y-displ (mm)	Distance along wall length (mm)	Distance between nodes (mm)	Strain (mm/m)
First	Second					
1	27	0.00	5.71	0.00	228.60	24.96
3	29	0.00	5.07	177.80	228.60	22.20
5	31	0.00	4.92	381.00	228.60	21.52
7	33	0.00	3.26	609.60	228.60	14.27
9	35	0.00	1.59	838.20	228.60	6.93
11	37	0.00	0.27	1041.40	228.60	1.18
13	39	0.00	-1.48	1219.20	228.60	-6.47

Table B.2 Analytical strain profile at base for a drift of 2%

Node		Node 1 y-displ (mm)	Node 2 y-displ (mm)	Distance along wall length (mm)	Distance between nodes (mm)	Strain (mm/m)
First	Second					
1	27	0.00	6.56	0.00	228.60	28.67
3	29	0.00	5.60	177.80	228.60	24.49
5	31	0.00	5.14	381.00	228.60	22.48
7	33	0.00	3.64	609.60	228.60	15.93
9	35	0.00	2.39	838.20	228.60	10.45
11	37	0.00	0.39	1041.40	228.60	1.69
13	39	0.00	-2.15	1219.20	228.60	-9.41

Table B.3 Analytical strain profile accounting for cover spalling at base for a drift of 1.5%

Node		Node 1 y-displ (mm)	Node 2 y-displ (mm)	Distance along wall length (mm)	Distance between nodes (mm)	Strain (mm/m)
First	Second					
1	27	0.00	5.49	0.00	228.60	24.02
3	29	0.00	4.52	177.80	228.60	19.77
5	31	0.00	3.18	381.00	228.60	13.89
7	33	0.00	3.03	609.60	228.60	13.23
9	35	0.00	1.48	838.20	228.60	6.48
11	37	0.00	-0.23	1041.40	228.60	-0.99
13	39	0.00	-1.76	1219.20	228.60	-7.69

Table B.4 Analytical strain profile accounting for cover spalling at base for a drift of 2%

Node		Node 1 y-displ (mm)	Node 2 y-displ (mm)	Distance along wall length (mm)	Distance between nodes (mm)	Strain (mm/m)
First	Second					
1	27	0.00	6.40	0.00	228.60	27.98
3	29	0.00	5.18	177.80	228.60	22.66
5	31	0.00	3.41	381.00	228.60	14.90
7	33	0.00	3.47	609.60	228.60	15.18
9	35	0.00	2.26	838.20	228.60	9.88
11	37	0.00	-0.35	1041.40	228.60	-1.54
13	39	0.00	-2.33	1219.20	228.60	-10.20

APPENDIX C: CALCULATIONS FOR PARAMETRIC STUDY

Table C.1 Curvatures up to the mid-height of Wall 1 for a drift of 2%

Node		Node 1 y-displ (mm)	Node 2 y-displ (mm)	Node 2 y-coord (mm)	Difference (mm)	Height (mm)	Strain	Curvature (rad/m)
First	Second							
1	53	0.00	15.39	846.60	846.60	423.30	0.0182	0.00326
53	105	15.39	30.70	1693.20	846.60	1269.90	0.0181	0.00320
105	183	30.70	49.08	2743.00	1049.80	2218.10	0.0175	0.00271
183	235	49.08	62.44	3589.60	846.60	3166.30	0.0158	0.00237
235	287	62.44	74.59	4436.20	846.60	4012.90	0.0143	0.00214
287	365	74.59	87.95	5486.00	1049.80	4961.10	0.0127	0.00190
365	417	87.95	94.19	6332.60	846.60	5909.30	0.0074	0.00117
417	469	94.19	97.11	7179.20	846.60	6755.90	0.0035	0.00064
469	547	97.11	99.87	8229.00	1049.80	7704.10	0.0026	0.00052
547	599	99.87	101.58	9075.60	846.60	8652.30	0.0020	0.00042
599	651	101.58	103.17	9922.20	846.60	9498.90	0.0019	0.00040
651	729	103.17	105.05	10972.00	1049.80	10447.10	0.0018	0.00038
729	781	105.05	106.53	11818.60	846.60	11395.30	0.0018	0.00037
781	833	106.53	107.97	12665.20	846.60	12241.90	0.0017	0.00036
833	911	107.97	109.70	13715.00	1049.80	13190.10	0.0016	0.00034
911	963	109.70	111.03	14561.60	846.60	14138.30	0.0016	0.00033
963	1015	111.03	112.30	15408.20	846.60	14984.90	0.0015	0.00032
1015	1093	112.30	113.79	16458.00	1049.80	15933.10	0.0014	0.00030
1093	1145	113.79	114.92	17304.60	846.60	16881.30	0.0013	0.00029
1145	1197	114.92	115.99	18151.20	846.60	17727.90	0.0013	0.00027
1197	1275	115.99	117.22	19201.00	1049.80	18676.10	0.0012	0.00026
1275	1327	117.22	118.14	20047.60	846.60	19624.30	0.0011	0.00024
1327	1379	118.14	118.99	20894.20	846.60	20470.90	0.0010	0.00023
1379	1457	118.99	119.96	21944.00	1049.80	21419.10	0.0009	0.00022
1457	1509	119.96	120.67	22790.60	846.60	22367.30	0.0008	0.00020
1509	1561	120.67	121.31	23637.20	846.60	23213.90	0.0008	0.00019
1561	1639	121.31	122.03	24687.00	1049.80	24162.10	0.0007	0.00017
1639	1691	122.03	122.55	25533.60	846.60	25110.30	0.0006	0.00016
1691	1743	122.55	123.01	26380.20	846.60	25956.90	0.0005	0.00015
1743	1821	123.01	123.52	27430.00	1049.80	26905.10	0.0005	0.00014
26	78	0.00	-5.66	846.60	846.60	423.30	-0.0067	0.00326
78	130	-5.66	-10.98	1693.20	846.60	1269.90	-0.0063	0.00320
130	208	-10.98	-14.31	2743.00	1049.80	2218.10	-0.0032	0.00271
208	260	-14.31	-16.24	3589.60	846.60	3166.30	-0.0023	0.00237
260	312	-16.24	-17.93	4436.20	846.60	4012.90	-0.0020	0.00214
312	390	-17.93	-19.76	5486.00	1049.80	4961.10	-0.0017	0.00190
390	442	-19.76	-21.07	6332.60	846.60	5909.30	-0.0015	0.00117
442	494	-21.07	-22.26	7179.20	846.60	6755.90	-0.0014	0.00064
494	572	-22.26	-23.63	8229.00	1049.80	7704.10	-0.0013	0.00052
572	624	-23.63	-24.65	9075.60	846.60	8652.30	-0.0012	0.00042
624	676	-24.65	-25.63	9922.20	846.60	9498.90	-0.0012	0.00040
676	754	-25.63	-26.78	10972.00	1049.80	10447.10	-0.0011	0.00038
754	806	-26.78	-27.67	11818.60	846.60	11395.30	-0.0011	0.00037
806	858	-27.67	-28.53	12665.20	846.60	12241.90	-0.0010	0.00036
858	936	-28.53	-29.56	13715.00	1049.80	13190.10	-0.0010	0.00034
936	988	-29.56	-30.36	14561.60	846.60	14138.30	-0.0009	0.00033
988	1040	-30.36	-31.13	15408.20	846.60	14984.90	-0.0009	0.00032
1040	1118	-31.13	-32.06	16458.00	1049.80	15933.10	-0.0009	0.00030

Node		Node 1 y-displ (mm)	Node 2 y-displ (mm)	Node 2 y-coord (mm)	Difference (mm)	Height (mm)	Strain	Curvature (rad/m)
First	Second							
1118	1170	-32.06	-32.78	17304.60	846.60	16881.30	-0.0009	0.00029
1170	1222	-32.78	-33.48	18151.20	846.60	17727.90	-0.0008	0.00027
1222	1300	-33.48	-34.31	19201.00	1049.80	18676.10	-0.0008	0.00026
1300	1352	-34.31	-34.96	20047.60	846.60	19624.30	-0.0008	0.00024
1352	1404	-34.96	-35.59	20894.20	846.60	20470.90	-0.0007	0.00023
1404	1482	-35.59	-36.34	21944.00	1049.80	21419.10	-0.0007	0.00022
1482	1534	-36.34	-36.93	22790.60	846.60	22367.30	-0.0007	0.00020
1534	1586	-36.93	-37.49	23637.20	846.60	23213.90	-0.0007	0.00019
1586	1664	-37.49	-38.16	24687.00	1049.80	24162.10	-0.0006	0.00017
1664	1716	-38.16	-38.68	25533.60	846.60	25110.30	-0.0006	0.00016
1716	1768	-38.68	-39.18	26380.20	846.60	25956.90	-0.0006	0.00015
1768	1846	-39.18	-39.78	27430.00	1049.80	26905.10	-0.0006	0.00014

Wall length: 7620 mm

Table C.2 Interpolation of curvatures at storey heights of Wall 1 for a drift of 2%

Storey	Height (mm)	Curvature (rad/m)
	423.30	0.00326
	1269.90	0.00320
	2218.10	0.00271
1	2743.00	0.00252
	3166.30	0.00237
	4012.90	0.00214
	4961.10	0.00190
2	5486.00	0.00150
	5909.30	0.00117
	6755.90	0.00064
	7704.10	0.00052
3	8229.00	0.00047
	8652.30	0.00042
	9498.90	0.00040
	10447.10	0.00038
4	10972.00	0.00037
	11395.30	0.00037
	12241.90	0.00036
	13190.10	0.00034
5	13715.00	0.00034
	14138.30	0.00033
	14984.90	0.00032
	15933.10	0.00030
6	16458.00	0.00029
	16881.30	0.00029
	17727.90	0.00027
	18676.10	0.00026
7	19201.00	0.00025
	19624.30	0.00024
	20470.90	0.00023
	21419.10	0.00022
8	21944.00	0.00021
	22367.30	0.00020
	23213.90	0.00019
	24162.10	0.00017
9	24687.00	0.00017
	25110.30	0.00016
	25956.90	0.00015
	26905.10	0.00014
10	27430.00	0.00013

Table C.3 Bending moments along the height of Wall 1 for a drift of 2%

Storey	Height (m)	Force (kN)	Shear (kN)	Moment incr. (kN.m)	Moment (kN.m)
0	0.00	0.0	1925.5	815.1	105632.9
	0.42	0.0	1925.5	1630.1	104817.9
	1.27	0.0	1925.5	1825.8	103187.7
	2.22	0.0	1925.5	1010.7	101362.0
1	2.74	0.0	1925.5	815.1	100351.3
	3.17	0.0	1925.5	1630.1	99536.2
	4.01	0.0	1925.5	1825.8	97906.1
	4.96	0.0	1925.5	1010.7	96080.3
2	5.49	0.0	1925.5	815.1	95069.6
	5.91	0.0	1925.5	1630.1	94254.6
	6.76	0.0	1925.5	1825.8	92624.4
	7.70	0.0	1925.5	1010.7	90798.7
3	8.23	0.0	1925.5	815.1	89788.0
	8.65	0.0	1925.5	1630.1	88972.9
	9.50	0.0	1925.5	1825.8	87342.8
	10.45	0.0	1925.5	1010.7	85517.0
4	10.97	0.0	1925.5	815.1	84506.3
	11.40	0.0	1925.5	1630.1	83691.3
	12.24	0.0	1925.5	1825.8	82061.2
	13.19	0.0	1925.5	1010.7	80235.4
5	13.72	0.0	1925.5	815.1	79224.7
	14.14	0.0	1925.5	1630.1	78409.6
	14.98	0.0	1925.5	1825.8	76779.5
	15.93	0.0	1925.5	1010.7	74953.7
6	16.46	0.0	1925.5	815.1	73943.1
	16.88	0.0	1925.5	1630.1	73128.0
	17.73	0.0	1925.5	1825.8	71497.9
	18.68	0.0	1925.5	1010.7	69672.1
7	19.20	0.0	1925.5	815.1	68661.4
	19.62	0.0	1925.5	1630.1	67846.3
	20.47	0.0	1925.5	1825.8	66216.2
	21.42	0.0	1925.5	1010.7	64390.5
8	21.94	0.0	1925.5	815.1	63379.8
	22.37	0.0	1925.5	1630.1	62564.7
	23.21	0.0	1925.5	1825.8	60934.6
	24.16	0.0	1925.5	1010.7	59108.8
9	24.69	0.0	1925.5	815.1	58098.1
	25.11	0.0	1925.5	1630.1	57283.0
	25.96	0.0	1925.5	1825.8	55652.9
	26.91	0.0	1925.5	1010.7	53827.2
10	27.43	0.0	1925.5	5281.6	52816.5
11	30.17	0.0	1925.5	5281.6	47534.8
12	32.92	0.0	1925.5	5281.6	42253.2
13	35.66	0.0	1925.5	5281.6	36971.5
14	38.40	0.0	1925.5	5281.6	31689.9
15	41.15	0.0	1925.5	5281.6	26408.2
16	43.89	0.0	1925.5	5281.6	21126.6
17	46.63	0.0	1925.5	5281.6	15844.9
18	49.37	0.0	1925.5	5281.6	10563.3
19	52.12	0.0	1925.5	5281.6	5281.6
20	54.86	1925.5	1925.5	0.0	0.0

Table C.4 Curvatures up to the mid-height of Wall 2 for a drift of 2%

Node		Node 1 y-displ (mm)	Node 2 y-displ (mm)	Node 2 y-coord (mm)	Difference (mm)	Height (mm)	Strain	Curvature (rad/m)
First	Second							
1	29	0.00	7.52	846.60	846.60	423.30	0.0089	0.00300
29	57	7.52	14.01	1693.20	846.60	1269.90	0.0077	0.00257
57	99	14.01	20.58	2743.00	1049.80	2218.10	0.0063	0.00214
99	127	20.58	24.25	3589.60	846.60	3166.30	0.0043	0.00157
127	155	24.25	27.94	4436.20	846.60	4012.90	0.0044	0.00153
155	197	27.94	30.86	5486.00	1049.80	4961.10	0.0028	0.00109
197	225	30.86	32.74	6332.60	846.60	5909.30	0.0022	0.00091
225	253	32.74	34.56	7179.20	846.60	6755.90	0.0021	0.00088
253	295	34.56	36.55	8229.00	1049.80	7704.10	0.0019	0.00080
295	323	36.55	38.09	9075.60	846.60	8652.30	0.0018	0.00076
323	351	38.09	39.58	9922.20	846.60	9498.90	0.0018	0.00074
351	393	39.58	41.34	10972.00	1049.80	10447.10	0.0017	0.00071
393	421	41.34	42.69	11818.60	846.60	11395.30	0.0016	0.00068
421	449	42.69	43.98	12665.20	846.60	12241.90	0.0015	0.00065
449	491	43.98	45.49	13715.00	1049.80	13190.10	0.0014	0.00062
491	519	45.49	46.63	14561.60	846.60	14138.30	0.0014	0.00059
519	547	46.63	47.71	15408.20	846.60	14984.90	0.0013	0.00057
547	589	47.71	48.96	16458.00	1049.80	15933.10	0.0012	0.00054
589	617	48.96	49.90	17304.60	846.60	16881.30	0.0011	0.00051
617	645	49.90	50.77	18151.20	846.60	17727.90	0.0010	0.00048
645	687	50.77	51.76	19201.00	1049.80	18676.10	0.0009	0.00045
687	715	51.76	52.49	20047.60	846.60	19624.30	0.0009	0.00042
715	743	52.49	53.16	20894.20	846.60	20470.90	0.0008	0.00040
743	785	53.16	53.92	21944.00	1049.80	21419.10	0.0007	0.00037
785	813	53.92	54.47	22790.60	846.60	22367.30	0.0007	0.00034
813	841	54.47	54.98	23637.20	846.60	23213.90	0.0006	0.00032
841	883	54.98	55.54	24687.00	1049.80	24162.10	0.0005	0.00030
883	911	55.54	55.94	25533.60	846.60	25110.30	0.0005	0.00028
911	939	55.94	56.30	26380.20	846.60	25956.90	0.0004	0.00026
939	981	56.30	56.71	27430.00	1049.80	26905.10	0.0004	0.00024
14	42	0.00	-2.16	846.60	846.60	423.30	-0.0025	0.00300
42	70	-2.16	-3.96	1693.20	846.60	1269.90	-0.0021	0.00257
70	112	-3.96	-5.93	2743.00	1049.80	2218.10	-0.0019	0.00214
112	140	-5.93	-7.31	3589.60	846.60	3166.30	-0.0016	0.00157
140	168	-7.31	-8.57	4436.20	846.60	4012.90	-0.0015	0.00153
168	210	-8.57	-10.00	5486.00	1049.80	4961.10	-0.0014	0.00109
210	238	-10.00	-11.07	6332.60	846.60	5909.30	-0.0013	0.00091
238	266	-11.07	-12.08	7179.20	846.60	6755.90	-0.0012	0.00088
266	308	-12.08	-13.28	8229.00	1049.80	7704.10	-0.0011	0.00080
308	336	-13.28	-14.21	9075.60	846.60	8652.30	-0.0011	0.00076
336	364	-14.21	-15.10	9922.20	846.60	9498.90	-0.0011	0.00074
364	406	-15.10	-16.18	10972.00	1049.80	10447.10	-0.0010	0.00071
406	434	-16.18	-17.01	11818.60	846.60	11395.30	-0.0010	0.00068
434	462	-17.01	-17.82	12665.20	846.60	12241.90	-0.0010	0.00065
462	504	-17.82	-18.81	13715.00	1049.80	13190.10	-0.0009	0.00062
504	532	-18.81	-19.58	14561.60	846.60	14138.30	-0.0009	0.00059
532	560	-19.58	-20.32	15408.20	846.60	14984.90	-0.0009	0.00057
560	602	-20.32	-21.22	16458.00	1049.80	15933.10	-0.0009	0.00054

Node		Node 1 y-displ (mm)	Node 2 y-displ (mm)	Node 2 y-coord (mm)	Difference (mm)	Height (mm)	Strain	Curvature (rad/m)
First	Second							
602	630	-21.22	-21.91	17304.60	846.60	16881.30	-0.0008	0.00051
630	658	-21.91	-22.59	18151.20	846.60	17727.90	-0.0008	0.00048
658	700	-22.59	-23.40	19201.00	1049.80	18676.10	-0.0008	0.00045
700	728	-23.40	-24.02	20047.60	846.60	19624.30	-0.0007	0.00042
728	756	-24.02	-24.62	20894.20	846.60	20470.90	-0.0007	0.00040
756	798	-24.62	-25.35	21944.00	1049.80	21419.10	-0.0007	0.00037
798	826	-25.35	-25.90	22790.60	846.60	22367.30	-0.0007	0.00034
826	854	-25.90	-26.44	23637.20	846.60	23213.90	-0.0006	0.00032
854	896	-26.44	-27.09	24687.00	1049.80	24162.10	-0.0006	0.00030
896	924	-27.09	-27.58	25533.60	846.60	25110.30	-0.0006	0.00028
924	952	-27.58	-28.06	26380.20	846.60	25956.90	-0.0006	0.00026
952	994	-28.06	-28.63	27430.00	1049.80	26905.10	-0.0005	0.00024

Wall length: 3810 mm

Table C.5 Interpolation of curvatures at storey heights of Wall 2 for a drift of 2%

Storey	Height (mm)	Curvature (rad/m)
	423.30	0.00300
	1269.90	0.00257
	2218.10	0.00214
1	2743.00	0.00182
	3166.30	0.00157
	4012.90	0.00153
	4961.10	0.00109
2	5486.00	0.00099
	5909.30	0.00091
	6755.90	0.00088
	7704.10	0.00080
3	8229.00	0.00078
	8652.30	0.00076
	9498.90	0.00074
	10447.10	0.00071
4	10972.00	0.00069
	11395.30	0.00068
	12241.90	0.00065
	13190.10	0.00062
5	13715.00	0.00061
	14138.30	0.00059
	14984.90	0.00057
	15933.10	0.00054
6	16458.00	0.00052
	16881.30	0.00051
	17727.90	0.00048
	18676.10	0.00045
7	19201.00	0.00043
	19624.30	0.00042
	20470.90	0.00040
	21419.10	0.00037
8	21944.00	0.00036
	22367.30	0.00034
	23213.90	0.00032
	24162.10	0.00030
9	24687.00	0.00029
	25110.30	0.00028
	25956.90	0.00026
	26905.10	0.00024
10	27430.00	0.00024

Table C.6 Bending moments along the height of Wall 2 for a drift of 2%

Storey	Height (m)	Force (kN)	Shear (kN)	Moment incr. (kN.m)	Moment (kN.m)
0	0.00	0.0	463.1	196.0	25405.7
	0.42	0.0	463.1	392.1	25209.6
	1.27	0.0	463.1	439.1	24817.6
	2.22	0.0	463.1	243.1	24378.5
1	2.74	0.0	463.1	196.0	24135.4
	3.17	0.0	463.1	392.1	23939.4
	4.01	0.0	463.1	439.1	23547.3
	4.96	0.0	463.1	243.1	23108.2
2	5.49	0.0	463.1	196.0	22865.1
	5.91	0.0	463.1	392.1	22669.1
	6.76	0.0	463.1	439.1	22277.0
	7.70	0.0	463.1	243.1	21837.9
3	8.23	0.0	463.1	196.0	21594.8
	8.65	0.0	463.1	392.1	21398.8
	9.50	0.0	463.1	439.1	21006.7
	10.45	0.0	463.1	243.1	20567.6
4	10.97	0.0	463.1	196.0	20324.5
	11.40	0.0	463.1	392.1	20128.5
	12.24	0.0	463.1	439.1	19736.4
	13.19	0.0	463.1	243.1	19297.3
5	13.72	0.0	463.1	196.0	19054.2
	14.14	0.0	463.1	392.1	18858.2
	14.98	0.0	463.1	439.1	18466.2
	15.93	0.0	463.1	243.1	18027.0
6	16.46	0.0	463.1	196.0	17784.0
	16.88	0.0	463.1	392.1	17587.9
	17.73	0.0	463.1	439.1	17195.9
	18.68	0.0	463.1	243.1	16756.8
7	19.20	0.0	463.1	196.0	16513.7
	19.62	0.0	463.1	392.1	16317.7
	20.47	0.0	463.1	439.1	15925.6
	21.42	0.0	463.1	243.1	15486.5
8	21.94	0.0	463.1	196.0	15243.4
	22.37	0.0	463.1	392.1	15047.4
	23.21	0.0	463.1	439.1	14655.3
	24.16	0.0	463.1	243.1	14216.2
9	24.69	0.0	463.1	196.0	13973.1
	25.11	0.0	463.1	392.1	13777.1
	25.96	0.0	463.1	439.1	13385.0
	26.91	0.0	463.1	243.1	12945.9
10	27.43	0.0	463.1	1270.3	12702.8
11	30.17	0.0	463.1	1270.3	11432.5
12	32.92	0.0	463.1	1270.3	10162.3
13	35.66	0.0	463.1	1270.3	8892.0
14	38.40	0.0	463.1	1270.3	7621.7
15	41.15	0.0	463.1	1270.3	6351.4
16	43.89	0.0	463.1	1270.3	5081.1
17	46.63	0.0	463.1	1270.3	3810.8
18	49.37	0.0	463.1	1270.3	2540.6
19	52.12	0.0	463.1	1270.3	1270.3
20	54.86	463.1	463.1	0.0	0.0

Table C.7 Average shear stress in Wall 1

Drift (%)	Yield drift (%)	Plastic drift (%)	V (kN)	l_w (mm)	b_w (mm)	v (MPa)
2.0	0.61	1.39	1925.5	7620.0	508.0	0.62
1.8	0.61	1.19	1912.3	7620.0	508.0	0.62
1.6	0.61	0.99	1901.5	7620.0	508.0	0.61
1.4	0.61	0.79	1883.8	7620.0	508.0	0.61
1.2	0.61	0.59	1864.4	7620.0	508.0	0.60

Table C.8 Average shear stress in Wall 2

Drift (%)	Yield drift (%)	Plastic drift (%)	V (kN)	l_w (mm)	b_w (mm)	v (MPa)
2.0	1.18	0.82	463.1	3810.0	508.0	0.30
1.8	1.18	0.62	458.2	3810.0	508.0	0.30
1.6	1.18	0.42	451.5	3810.0	508.0	0.29
1.4	1.18	0.22	438.4	3810.0	508.0	0.28
1.2	1.18	0.02	420.7	3810.0	508.0	0.27

Table C.9 Average shear stress in Wall 1 for a shear span of 35659mm

Drift (%)	Yield drift (%)	Plastic drift (%)	V (kN)	l_w (mm)	b_w (mm)	v (MPa)
1.6	0.43	1.17	2996.5	7620.0	508.0	0.97
1.4	0.43	0.97	2982.1	7620.0	508.0	0.96
1.2	0.43	0.77	2962.8	7620.0	508.0	0.96
1.0	0.43	0.57	2911.0	7620.0	508.0	0.94

Table C.10 Average shear stress in Wall 2 for a shear span of 35659mm

Drift (%)	Yield drift (%)	Plastic drift (%)	V (kN)	l_w (mm)	b_w (mm)	v (MPa)
1.6	0.79	0.81	727.5	3810.0	508.0	0.47
1.4	0.79	0.61	722.8	3810.0	508.0	0.47
1.2	0.79	0.41	708.8	3810.0	508.0	0.46
1.0	0.79	0.21	686.9	3810.0	508.0	0.44

Table C.11 Average shear stress in Wall 1 for a shear span of 27430mm

Drift (%)	Yield drift (%)	Plastic drift (%)	V (kN)	l_w (mm)	b_w (mm)	v (MPa)
1.6	0.35	1.25	3941.8	7620.0	508.0	1.27
1.4	0.35	1.05	3936.7	7620.0	508.0	1.27
1.2	0.35	0.85	3897.4	7620.0	508.0	1.26
1.0	0.35	0.65	3855.8	7620.0	508.0	1.25
0.8	0.35	0.45	3794.0	7620.0	508.0	1.23

Table C.12 Average shear stress in Wall 2 for a shear span of 27430mm

Drift (%)	Yield drift (%)	Plastic drift (%)	V (kN)	l_w (mm)	b_w (mm)	v (MPa)
1.6	0.63	0.97	969.2	3810.0	508.0	0.63
1.4	0.63	0.77	958.4	3810.0	508.0	0.62
1.2	0.63	0.57	948.8	3810.0	508.0	0.61
1.0	0.63	0.37	933.4	3810.0	508.0	0.60
0.8	0.63	0.17	897.2	3810.0	508.0	0.58

Table C.13 Average shear stress in Wall 1 for a shear span of 19201mm

Drift (%)	Yield drift (%)	Plastic drift (%)	V (kN)	l_w (mm)	b_w (mm)	v (MPa)
1.2	0.28	0.92	5644.1	7620.0	508.0	1.82
1.0	0.28	0.72	5591.5	7620.0	508.0	1.81
0.8	0.28	0.52	5550.1	7620.0	508.0	1.79
0.6	0.28	0.32	5448.5	7620.0	508.0	1.76

Table C.14 Average shear stress in Wall 2 for a shear span of 19201mm

Drift (%)	Yield drift (%)	Plastic drift (%)	V (kN)	l_w (mm)	b_w (mm)	v (MPa)
1.2	0.47	0.73	1394.0	3810.0	508.0	0.90
1.0	0.47	0.53	1368.8	3810.0	508.0	0.88
0.8	0.47	0.33	1349.5	3810.0	508.0	0.87
0.6	0.47	0.13	1293.7	3810.0	508.0	0.84

Table C.15 Average shear stress in Wall 1 for a web thickness of 254mm and a shear span of 27430mm

Drift (%)	Yield drift (%)	Plastic drift (%)	V (kN)	l_w (mm)	b_w (mm)	v (MPa)
1.8	0.37	1.43	3656.3	7620.0	254.0	2.36
1.6	0.37	1.23	3639.7	7620.0	254.0	2.35
1.4	0.37	1.03	3571.7	7620.0	254.0	2.31
1.2	0.37	0.83	3580.1	7620.0	254.0	2.31
1.0	0.37	0.63	3565.5	7620.0	254.0	2.30
0.8	0.37	0.43	3524.0	7620.0	254.0	2.28

Table C.16 Average shear stress in Wall 2 for a web thickness of 254mm and a shear span of 27430mm

Drift (%)	Yield drift (%)	Plastic drift (%)	V (kN)	l_w (mm)	b_w (mm)	v (MPa)
1.8	0.65	1.15	915.5	3810.0	254.0	1.18
1.6	0.65	0.95	904.7	3810.0	254.0	1.17
1.4	0.65	0.75	890.7	3810.0	254.0	1.15
1.2	0.65	0.55	880.4	3810.0	254.0	1.14
1.0	0.65	0.35	864.6	3810.0	254.0	1.12
0.8	0.65	0.15	844.4	3810.0	254.0	1.09

Table C.17 Average shear stress in Wall 1 for a web thickness of 254mm and a shear span of 19201mm

Drift (%)	Yield drift (%)	Plastic drift (%)	V (kN)	l_w (mm)	b_w (mm)	v (MPa)
1.8	0.30	1.50	5274.6	7620.0	254.0	3.41
1.6	0.30	1.30	5260.4	7620.0	254.0	3.40
1.4	0.30	1.10	5220.3	7620.0	254.0	3.37
1.2	0.30	0.90	5179.0	7620.0	254.0	3.34
1.0	0.30	0.70	5162.1	7620.0	254.0	3.33
0.8	0.30	0.50	5064.5	7620.0	254.0	3.27
0.6	0.30	0.30	5035.1	7620.0	254.0	3.25

Table C.18 Average shear stress in Wall 2 for a web thickness of 254mm and a shear span of 19201mm

Drift (%)	Yield drift (%)	Plastic drift (%)	V (kN)	l_w (mm)	b_w (mm)	v (MPa)
1.8	0.49	1.31	1343.5	3810.0	254.0	1.74
1.6	0.49	1.11	1328.1	3810.0	254.0	1.72
1.4	0.49	0.91	1321.6	3810.0	254.0	1.71
1.2	0.49	0.71	1299.2	3810.0	254.0	1.68
1.0	0.49	0.51	1272.9	3810.0	254.0	1.64
0.8	0.49	0.31	1255.6	3810.0	254.0	1.62
0.6	0.49	0.11	1213.3	3810.0	254.0	1.57

Table C.19 Average shear stress in Wall 1 for a compressive axial load ratio of 0.3

Drift (%)	Yield drift (%)	Plastic drift (%)	V (kN)	l_w (mm)	b_w (mm)	v (MPa)
1.2	0.78	0.42	3101.9	7620.0	508.0	1.00
1.0	0.78	0.22	3070.2	7620.0	508.0	0.99
0.8	0.78	0.02	2922.1	7620.0	508.0	0.94

Table C.20 Average shear stress in Wall 2 for a compressive axial load ratio of 0.3

Drift (%)	Yield drift (%)	Plastic drift (%)	V (kN)	l_w (mm)	b_w (mm)	v (MPa)
2.0	1.51	0.49	775.1	3810.0	508.0	0.50
1.8	1.51	0.29	761.6	3810.0	508.0	0.49
1.6	1.51	0.09	742.3	3810.0	508.0	0.48

Table C.21 Average shear stress in Wall 1 for a compressive axial load ratio of 0.2

Drift (%)	Yield drift (%)	Plastic drift (%)	V (kN)	l_w (mm)	b_w (mm)	v (MPa)
1.4	0.69	0.71	2587.5	7620.0	508.0	0.84
1.2	0.69	0.51	2583.7	7620.0	508.0	0.83
1.0	0.69	0.31	2542.5	7620.0	508.0	0.82
0.8	0.69	0.11	2443.8	7620.0	508.0	0.79

Table C.22 Average shear stress in Wall 2 for a compressive axial load ratio of 0.2

Drift (%)	Yield drift (%)	Plastic drift (%)	V (kN)	l_w (mm)	b_w (mm)	v (MPa)
2.0	1.34	0.66	646.6	3810.0	508.0	0.42
1.8	1.34	0.46	634.0	3810.0	508.0	0.41
1.6	1.34	0.26	616.6	3810.0	508.0	0.40
1.4	1.34	0.06	594.5	3810.0	508.0	0.38

Table C.23 Average shear stress in Wall 1 for no axial load

Drift (%)	Yield drift (%)	Plastic drift (%)	V (kN)	l_w (mm)	b_w (mm)	v (MPa)
2.0	0.55	1.45	1051.6	7620.0	508.0	0.34
1.8	0.55	1.25	1034.1	7620.0	508.0	0.33
1.6	0.55	1.05	1019.5	7620.0	508.0	0.33
1.4	0.55	0.85	1005.2	7620.0	508.0	0.32
1.2	0.55	0.65	989.4	7620.0	508.0	0.32

Table C.24 Average shear stress in Wall 2 for no axial load

Drift (%)	Yield drift (%)	Plastic drift (%)	V (kN)	l_w (mm)	b_w (mm)	v (MPa)
2.0	1.08	0.92	250.1	3810.0	508.0	0.16
1.8	1.08	0.72	244.1	3810.0	508.0	0.16
1.6	1.08	0.52	242.7	3810.0	508.0	0.16
1.4	1.08	0.32	236.2	3810.0	508.0	0.15
1.2	1.08	0.12	231.2	3810.0	508.0	0.15

Table C.25 Average shear stress in Wall 1 for a tensile axial load ratio of 0.02

Drift (%)	Yield drift (%)	Plastic drift (%)	V (kN)	l_w (mm)	b_w (mm)	v (MPa)
2.0	0.55	1.45	809.0	7620.0	508.0	0.26
1.8	0.55	1.25	798.0	7620.0	508.0	0.26
1.6	0.55	1.05	782.1	7620.0	508.0	0.25
1.4	0.55	0.85	767.7	7620.0	508.0	0.25
1.2	0.55	0.65	752.1	7620.0	508.0	0.24

Table C.26 Average shear stress in Wall 2 for a tensile axial load ratio of 0.02

Drift (%)	Yield drift (%)	Plastic drift (%)	V (kN)	l_w (mm)	b_w (mm)	v (MPa)
2.0	1.11	0.89	190.7	3810.0	508.0	0.12
1.8	1.11	0.69	187.3	3810.0	508.0	0.12
1.6	1.11	0.49	186.1	3810.0	508.0	0.12
1.4	1.11	0.29	180.8	3810.0	508.0	0.12
1.2	1.11	0.09	175.5	3810.0	508.0	0.11

Table C.27 Average shear stress in Wall 1 for a tensile axial load ratio of 0.05

Drift (%)	Yield drift (%)	Plastic drift (%)	V (kN)	l_w (mm)	b_w (mm)	v (MPa)
2.0	0.58	1.42	553.8	7620.0	508.0	0.18
1.8	0.58	1.22	542.8	7620.0	508.0	0.18
1.6	0.58	1.02	529.2	7620.0	508.0	0.17
1.4	0.58	0.82	518.1	7620.0	508.0	0.17
1.2	0.58	0.62	506.6	7620.0	508.0	0.16

Table C.28 Average shear stress in Wall 2 for a tensile axial load ratio of 0.05

Drift (%)	Yield drift (%)	Plastic drift (%)	V (kN)	l_w (mm)	b_w (mm)	v (MPa)
2.0	1.17	0.83	125.9	3810.0	508.0	0.08
1.8	1.17	0.63	125.2	3810.0	508.0	0.08
1.6	1.17	0.43	121.5	3810.0	508.0	0.08
1.4	1.17	0.23	120.6	3810.0	508.0	0.08
1.2	1.17	0.03	114.7	3810.0	508.0	0.07

Table C.29 Curvatures up to the mid-height of Wall 1 combined with Wall 2 for a drift of 2%

Node		Node 1 y-displ (mm)	Node 2 y-displ (mm)	Node 2 y-coord (mm)	Difference (mm)	Height (mm)	Strain	Curvature (rad/m)
First	Second							
1	81	0.00	15.30	846.60	846.60	423.30	0.0181	0.00317
81	161	15.30	30.51	1693.20	846.60	1269.90	0.0180	0.00311
161	281	30.51	47.37	2743.00	1049.80	2218.10	0.0161	0.00248
281	361	47.37	59.96	3589.60	846.60	3166.30	0.0149	0.00229
361	441	59.96	71.56	4436.20	846.60	4012.90	0.0137	0.00209
441	561	71.56	82.29	5486.00	1049.80	4961.10	0.0102	0.00156
561	641	82.29	88.74	6332.60	846.60	5909.30	0.0076	0.00123
641	721	88.74	94.21	7179.20	846.60	6755.90	0.0065	0.00106
721	841	94.21	98.66	8229.00	1049.80	7704.10	0.0042	0.00073
841	921	98.66	101.03	9075.60	846.60	8652.30	0.0028	0.00055
921	1001	101.03	102.93	9922.20	846.60	9498.90	0.0022	0.00046
1001	1121	102.93	104.52	10972.00	1049.80	10447.10	0.0015	0.00034
1121	1201	104.52	106.27	11818.60	846.60	11395.30	0.0021	0.00043
1201	1281	106.27	107.81	12665.20	846.60	12241.90	0.0018	0.00038
1281	1401	107.81	109.28	13715.00	1049.80	13190.10	0.0014	0.00031
1401	1481	109.28	110.77	14561.60	846.60	14138.30	0.0018	0.00037
1481	1561	110.77	112.19	15408.20	846.60	14984.90	0.0017	0.00035
1561	1681	112.19	113.52	16458.00	1049.80	15933.10	0.0013	0.00028
1681	1761	113.52	114.82	17304.60	846.60	16881.30	0.0015	0.00033
1761	1841	114.82	116.04	18151.20	846.60	17727.90	0.0014	0.00031
1841	1961	116.04	117.17	19201.00	1049.80	18676.10	0.0011	0.00024
1961	2041	117.17	118.26	20047.60	846.60	19624.30	0.0013	0.00028
2041	2121	118.26	119.27	20894.20	846.60	20470.90	0.0012	0.00026
2121	2241	119.27	120.18	21944.00	1049.80	21419.10	0.0009	0.00020
2241	2321	120.18	121.06	22790.60	846.60	22367.30	0.0010	0.00023
2321	2401	121.06	121.85	23637.20	846.60	23213.90	0.0009	0.00021
2401	2521	121.85	122.56	24687.00	1049.80	24162.10	0.0007	0.00017
2521	2601	122.56	123.21	25533.60	846.60	25110.30	0.0008	0.00019
2601	2681	123.21	123.79	26380.20	846.60	25956.90	0.0007	0.00017
2681	2801	123.79	124.32	27430.00	1049.80	26905.10	0.0005	0.00014
26	106	0.00	-5.17	846.60	846.60	423.30	-0.0061	0.00317
106	186	-5.17	-10.01	1693.20	846.60	1269.90	-0.0057	0.00311
186	306	-10.01	-12.98	2743.00	1049.80	2218.10	-0.0028	0.00248
306	386	-12.98	-15.18	3589.60	846.60	3166.30	-0.0026	0.00229
386	466	-15.18	-17.04	4436.20	846.60	4012.90	-0.0022	0.00209
466	586	-17.04	-18.81	5486.00	1049.80	4961.10	-0.0017	0.00156
586	666	-18.81	-20.30	6332.60	846.60	5909.30	-0.0018	0.00123
666	746	-20.30	-21.65	7179.20	846.60	6755.90	-0.0016	0.00106
746	866	-21.65	-23.00	8229.00	1049.80	7704.10	-0.0013	0.00073
866	946	-23.00	-24.18	9075.60	846.60	8652.30	-0.0014	0.00055
946	1026	-24.18	-25.26	9922.20	846.60	9498.90	-0.0013	0.00046
1026	1146	-25.26	-26.38	10972.00	1049.80	10447.10	-0.0011	0.00034
1146	1226	-26.38	-27.38	11818.60	846.60	11395.30	-0.0012	0.00043
1226	1306	-27.38	-28.32	12665.20	846.60	12241.90	-0.0011	0.00038
1306	1426	-28.32	-29.30	13715.00	1049.80	13190.10	-0.0009	0.00031
1426	1506	-29.30	-30.19	14561.60	846.60	14138.30	-0.0011	0.00037
1506	1586	-30.19	-31.03	15408.20	846.60	14984.90	-0.0010	0.00035
1586	1706	-31.03	-31.90	16458.00	1049.80	15933.10	-0.0008	0.00028

Node		Node 1 y-displ (mm)	Node 2 y-displ (mm)	Node 2 y-coord (mm)	Difference (mm)	Height (mm)	Strain	Curvature (rad/m)
First	Second							
1706	1786	-31.90	-32.70	17304.60	846.60	16881.30	-0.0009	0.00033
1786	1866	-32.70	-33.45	18151.20	846.60	17727.90	-0.0009	0.00031
1866	1986	-33.45	-34.24	19201.00	1049.80	18676.10	-0.0007	0.00024
1986	2066	-34.24	-34.95	20047.60	846.60	19624.30	-0.0008	0.00028
2066	2146	-34.95	-35.62	20894.20	846.60	20470.90	-0.0008	0.00026
2146	2266	-35.62	-36.32	21944.00	1049.80	21419.10	-0.0007	0.00020
2266	2346	-36.32	-36.96	22790.60	846.60	22367.30	-0.0007	0.00023
2346	2426	-36.96	-37.56	23637.20	846.60	23213.90	-0.0007	0.00021
2426	2546	-37.56	-38.18	24687.00	1049.80	24162.10	-0.0006	0.00017
2546	2626	-38.18	-38.74	25533.60	846.60	25110.30	-0.0007	0.00019
2626	2706	-38.74	-39.28	26380.20	846.60	25956.90	-0.0006	0.00017
2706	2826	-39.28	-39.84	27430.00	1049.80	26905.10	-0.0005	0.00014

Wall length: 7620 mm

Table C.30 Interpolation of curvatures at storey heights of Wall 1 combined with Wall 2 for a drift of 2%

Storey	Height (mm)	Curvature (rad/m)
	423.30	0.00317
	1269.90	0.00311
	2218.10	0.00248
1	2743.00	0.00238
	3166.30	0.00229
	4012.90	0.00209
	4961.10	0.00156
2	5486.00	0.00138
	5909.30	0.00123
	6755.90	0.00106
	7704.10	0.00073
3	8229.00	0.00063
	8652.30	0.00055
	9498.90	0.00046
	10447.10	0.00034
4	10972.00	0.00039
	11395.30	0.00043
	12241.90	0.00038
	13190.10	0.00031
5	13715.00	0.00034
	14138.30	0.00037
	14984.90	0.00035
	15933.10	0.00028
6	16458.00	0.00030
	16881.30	0.00033
	17727.90	0.00031
	18676.10	0.00024
7	19201.00	0.00026
	19624.30	0.00028
	20470.90	0.00026
	21419.10	0.00020
8	21944.00	0.00022
	22367.30	0.00023
	23213.90	0.00021
	24162.10	0.00017
9	24687.00	0.00018
	25110.30	0.00019
	25956.90	0.00017
	26905.10	0.00014
10	27430.00	0.00011

Table C.31 Displacement components at the first storey of Wall 1 combined with Wall 2 for a drift of 2%

Storey	1			
Height (m)	2.74			
Height (m)	Curvature (rad/m)	Δx (m)	x (m)	Flexural displ (mm)
0.42	0.00317		2.32	
1.27	0.00311	0.85	1.47	5.04
2.22	0.00248	0.95	0.52	2.65
2.74	0.00238	0.52	0.00	0.33
			Total	8.02
			Total displacement (mm)	18.61
			Shear displacement (mm)	10.59

Table C.32 Displacement components at the second storey of Wall 1 combined with Wall 2 for a drift of 2%

Storey	2			
Height (m)	5.49			
Height (m)	Curvature (rad/m)	Δx (m)	x (m)	Flexural displ (mm)
0.42	0.00317		5.06	
1.27	0.00311	0.85	4.22	12.33
2.22	0.00248	0.95	3.27	9.91
2.74	0.00238	0.52	2.74	3.83
3.17	0.00229	0.42	2.32	2.50
4.01	0.00209	0.85	1.47	3.52
4.96	0.00156	0.95	0.52	1.73
5.49	0.00138	0.52	0.00	0.20
			Total	34.02
			Total displacement (mm)	52.87
			Shear displacement (mm)	18.84

Table C.33 Displacement components at the third storey of Wall 1 combined with Wall 2 for a drift of 2%

Storey	3			
Height (m)	8.23			
Height (m)	Curvature (rad/m)	Δx (m)	x (m)	Flexural displ (mm)
0.42	0.00317		7.81	
1.27	0.00311	0.85	6.96	19.63
2.22	0.00248	0.95	6.01	17.18
2.74	0.00238	0.52	5.49	7.32
3.17	0.00229	0.42	5.06	5.21
4.01	0.00209	0.85	4.22	8.60
4.96	0.00156	0.95	3.27	6.47
5.49	0.00138	0.52	2.74	2.32
5.91	0.00123	0.42	2.32	1.40
6.76	0.00106	0.85	1.47	1.84
7.70	0.00073	0.95	0.52	0.84
8.23	0.00063	0.52	0.00	0.09
			Total	70.91
		Total displacement (mm)		94.37
		Shear displacement (mm)		23.46

Table C.34 Displacement components at the fourth storey of Wall 1 combined with Wall 2 for a drift of 2%

Storey	4			
Height (m)	10.97			
Height (m)	Curvature (rad/m)	Δx (m)	x (m)	Flexural displ (mm)
0.42	0.00317		10.55	
1.27	0.00311	0.85	9.70	26.92
2.22	0.00248	0.95	8.75	24.44
2.74	0.00238	0.52	8.23	10.82
3.17	0.00229	0.42	7.81	7.92
4.01	0.00209	0.85	6.96	13.69
4.96	0.00156	0.95	6.01	11.22
5.49	0.00138	0.52	5.49	4.44
5.91	0.00123	0.42	5.06	2.91
6.76	0.00106	0.85	4.22	4.49
7.70	0.00073	0.95	3.27	3.16
8.23	0.00063	0.52	2.74	1.07
8.65	0.00055	0.42	2.32	0.63
9.50	0.00046	0.85	1.47	0.81
10.45	0.00034	0.95	0.52	0.38
10.97	0.00039	0.52	0.00	0.05
			Total	112.96
		Total displacement (mm)		140.44
		Shear displacement (mm)		27.48

Table C.35 Slopes up to the mid-height of Wall 1 combined with Wall 2 for a drift of 2%

Height (m)	Curvature (rad/m)	Δx (m)	Slope incr. (rad)	Slope (rad)
0.42	0.00317			
1.27	0.00311	0.85	0.0027	0.0027
2.22	0.00248	0.95	0.0026	0.0053
3.17	0.00229	0.95	0.0023	0.0076
4.01	0.00209	0.85	0.0019	0.0094
4.96	0.00156	0.95	0.0017	0.0112
5.91	0.00123	0.95	0.0013	0.0125
6.76	0.00106	0.85	0.0010	0.0134
7.70	0.00073	0.95	0.0008	0.0143
8.65	0.00055	0.95	0.0006	0.0149
9.50	0.00046	0.85	0.0004	0.0153
10.45	0.00034	0.95	0.0004	0.0157
11.40	0.00043	0.95	0.0004	0.0161
12.24	0.00038	0.85	0.0003	0.0164
13.19	0.00031	0.95	0.0003	0.0167
14.14	0.00037	0.95	0.0003	0.0171
14.98	0.00035	0.85	0.0003	0.0174
15.93	0.00028	0.95	0.0003	0.0177
16.88	0.00033	0.95	0.0003	0.0179
17.73	0.00031	0.85	0.0003	0.0182
18.68	0.00024	0.95	0.0003	0.0185
19.62	0.00028	0.95	0.0002	0.0187
20.47	0.00026	0.85	0.0002	0.0189
21.42	0.00020	0.95	0.0002	0.0192
22.37	0.00023	0.95	0.0002	0.0194
23.21	0.00021	0.85	0.0002	0.0196
24.16	0.00017	0.95	0.0002	0.0197
25.11	0.00019	0.95	0.0002	0.0199
25.96	0.00017	0.85	0.0002	0.0201
26.91	0.00014	0.95	0.0001	0.0202

Table C.36 Bending moments along the height of Wall 1 combined with Wall 2 for a drift of 2%

Storey	Height (m)	Force (kN)	Shear (kN)	Moment incr. (kN.m)	Moment (kN.m)
0	0.00	0.0	1726.0	730.6	106307.1
	0.42	0.0	1726.0	1461.2	105576.5
	1.27	0.0	1726.0	1636.6	104115.3
	2.22	0.0	1726.0	906.0	102478.7
1	2.74	-44.9	1726.0	740.1	101572.7
	3.17	0.0	1770.9	1499.2	100832.6
	4.01	0.0	1770.9	1679.2	99333.4
	4.96	0.0	1770.9	929.5	97654.2
2	5.49	321.0	1770.9	681.7	96724.6
	5.91	0.0	1449.9	1227.5	96043.0
	6.76	0.0	1449.9	1374.8	94815.5
	7.70	0.0	1449.9	761.1	93440.7
3	8.23	-90.4	1449.9	632.9	92679.6
	8.65	0.0	1540.3	1304.0	92046.8
	9.50	0.0	1540.3	1460.5	90742.7
	10.45	0.0	1540.3	808.5	89282.2
4	10.97	-252.7	1540.3	705.5	88473.7
	11.40	0.0	1793.0	1518.0	87768.2
	12.24	0.0	1793.0	1700.1	86250.3
	13.19	0.0	1793.0	941.1	84550.2
5	13.72	-166.0	1793.0	794.1	83609.0
	14.14	0.0	1959.0	1658.5	82814.9
	14.98	0.0	1959.0	1857.5	81156.4
	15.93	0.0	1959.0	1028.3	79298.9
6	16.46	-69.8	1959.0	844.0	78270.6
	16.88	0.0	2028.8	1717.6	77426.6
	17.73	0.0	2028.8	1923.7	75709.0
	18.68	0.0	2028.8	1064.9	73785.3
7	19.20	-14.2	2028.8	861.8	72720.4
	19.62	0.0	2043.0	1729.6	71858.6
	20.47	0.0	2043.0	1937.2	70129.0
	21.42	0.0	2043.0	1072.4	68191.8
8	21.94	30.5	2043.0	858.3	67119.4
	22.37	0.0	2012.5	1703.8	66261.1
	23.21	0.0	2012.5	1908.3	64557.3
	24.16	0.0	2012.5	1056.4	62649.1
9	24.69	67.4	2012.5	837.6	61592.7
	25.11	0.0	1945.1	1646.7	60755.1
	25.96	0.0	1945.1	1844.3	59108.3
	26.91	0.0	1945.1	1021.0	57264.0
10	27.43	112.5	1945.1	5181.1	56243.0
11	30.17	-42.1	1832.6	5084.6	51061.9
12	32.92	-89.7	1874.7	5265.3	45977.3
13	35.66	-89.4	1964.4	5511.0	40712.0
14	38.40	-52.8	2053.8	5706.0	35201.1
15	41.15	-22.6	2106.6	5809.4	29495.1
16	43.89	-11.9	2129.2	5856.7	23685.7
17	46.63	-26.6	2141.1	5909.5	17829.0
18	49.37	-48.3	2167.7	6012.2	11919.4
19	52.12	124.9	2216.0	5907.2	5907.2
20	54.86	2091.1	2091.1	0.0	0.0

Table C.37 Curvatures up to the mid-height of Wall 2 combined with Wall 1 for a drift of 2%

Node		Node 1 y-displ (mm)	Node 2 y-displ (mm)	Node 2 y-coord (mm)	Difference (mm)	Height (mm)	Strain	Curvature (rad/m)
First	Second							
27	107	0.00	11.38	846.60	846.60	423.30	0.0134	0.00456
107	187	11.38	21.65	1693.20	846.60	1269.90	0.0121	0.00388
187	307	21.65	31.63	2743.00	1049.80	2218.10	0.0095	0.00296
307	387	31.63	36.59	3589.60	846.60	3166.30	0.0059	0.00198
387	467	36.59	39.24	4436.20	846.60	4012.90	0.0031	0.00121
467	587	39.24	41.02	5486.00	1049.80	4961.10	0.0017	0.00074
587	667	41.02	42.80	6332.60	846.60	5909.30	0.0021	0.00086
667	747	42.80	44.34	7179.20	846.60	6755.90	0.0018	0.00076
747	867	44.34	45.78	8229.00	1049.80	7704.10	0.0014	0.00059
867	947	45.78	47.08	9075.60	846.60	8652.30	0.0015	0.00065
947	1027	47.08	48.26	9922.20	846.60	9498.90	0.0014	0.00060
1027	1147	48.26	49.35	10972.00	1049.80	10447.10	0.0010	0.00046
1147	1227	49.35	50.25	11818.60	846.60	11395.30	0.0011	0.00049
1227	1307	50.25	51.07	12665.20	846.60	12241.90	0.0010	0.00045
1307	1427	51.07	51.83	13715.00	1049.80	13190.10	0.0007	0.00035
1427	1507	51.83	52.45	14561.60	846.60	14138.30	0.0007	0.00037
1507	1587	52.45	53.03	15408.20	846.60	14984.90	0.0007	0.00035
1587	1707	53.03	53.56	16458.00	1049.80	15933.10	0.0005	0.00028
1707	1787	53.56	54.03	17304.60	846.60	16881.30	0.0005	0.00031
1787	1867	54.03	54.45	18151.20	846.60	17727.90	0.0005	0.00029
1867	1987	54.45	54.85	19201.00	1049.80	18676.10	0.0004	0.00023
1987	2067	54.85	55.20	20047.60	846.60	19624.30	0.0004	0.00025
2067	2147	55.20	55.51	20894.20	846.60	20470.90	0.0004	0.00024
2147	2267	55.51	55.81	21944.00	1049.80	21419.10	0.0003	0.00019
2267	2347	55.81	56.06	22790.60	846.60	22367.30	0.0003	0.00021
2347	2427	56.06	56.28	23637.20	846.60	23213.90	0.0003	0.00019
2427	2547	56.28	56.47	24687.00	1049.80	24162.10	0.0002	0.00015
2547	2627	56.47	56.64	25533.60	846.60	25110.30	0.0002	0.00017
2627	2707	56.64	56.79	26380.20	846.60	25956.90	0.0002	0.00016
2707	2827	56.79	56.91	27430.00	1049.80	26905.10	0.0001	0.00013
40	120	0.00	-3.32	846.60	846.60	423.30	-0.0039	0.00456
120	200	-3.32	-5.55	1693.20	846.60	1269.90	-0.0026	0.00388
200	320	-5.55	-7.42	2743.00	1049.80	2218.10	-0.0018	0.00296
320	400	-7.42	-8.84	3589.60	846.60	3166.30	-0.0017	0.00198
400	480	-8.84	-10.08	4436.20	846.60	4012.90	-0.0015	0.00121
480	600	-10.08	-11.28	5486.00	1049.80	4961.10	-0.0011	0.00074
600	680	-11.28	-12.28	6332.60	846.60	5909.30	-0.0012	0.00086
680	760	-12.28	-13.19	7179.20	846.60	6755.90	-0.0011	0.00076
760	880	-13.19	-14.10	8229.00	1049.80	7704.10	-0.0009	0.00059
880	960	-14.10	-14.90	9075.60	846.60	8652.30	-0.0009	0.00065
960	1040	-14.90	-15.64	9922.20	846.60	9498.90	-0.0009	0.00060
1040	1160	-15.64	-16.39	10972.00	1049.80	10447.10	-0.0007	0.00046
1160	1240	-16.39	-17.05	11818.60	846.60	11395.30	-0.0008	0.00049
1240	1320	-17.05	-17.69	12665.20	846.60	12241.90	-0.0007	0.00045
1320	1440	-17.69	-18.34	13715.00	1049.80	13190.10	-0.0006	0.00035
1440	1520	-18.34	-18.92	14561.60	846.60	14138.30	-0.0007	0.00037
1520	1600	-18.92	-19.48	15408.20	846.60	14984.90	-0.0007	0.00035
1600	1720	-19.48	-20.06	16458.00	1049.80	15933.10	-0.0006	0.00028

Node		Node 1 y-displ (mm)	Node 2 y-displ (mm)	Node 2 y-coord (mm)	Difference (mm)	Height (mm)	Strain	Curvature (rad/m)
First	Second							
1720	1800	-20.06	-20.58	17304.60	846.60	16881.30	-0.0006	0.00031
1800	1880	-20.58	-21.08	18151.20	846.60	17727.90	-0.0006	0.00029
1880	2000	-21.08	-21.61	19201.00	1049.80	18676.10	-0.0005	0.00023
2000	2080	-21.61	-22.08	20047.60	846.60	19624.30	-0.0006	0.00025
2080	2160	-22.08	-22.53	20894.20	846.60	20470.90	-0.0005	0.00024
2160	2280	-22.53	-23.00	21944.00	1049.80	21419.10	-0.0004	0.00019
2280	2360	-23.00	-23.42	22790.60	846.60	22367.30	-0.0005	0.00021
2360	2440	-23.42	-23.82	23637.20	846.60	23213.90	-0.0005	0.00019
2440	2560	-23.82	-24.24	24687.00	1049.80	24162.10	-0.0004	0.00015
2560	2640	-24.24	-24.62	25533.60	846.60	25110.30	-0.0004	0.00017
2640	2720	-24.62	-24.98	26380.20	846.60	25956.90	-0.0004	0.00016
2720	2840	-24.98	-25.36	27430.00	1049.80	26905.10	-0.0004	0.00013

Wall length: 3810 mm

Table C.38 Interpolation of curvatures at storey heights of Wall 2 combined with Wall 1 for a drift of 2%

Storey	Height (mm)	Curvature (rad/m)
	423.30	0.00456
	1269.90	0.00388
	2218.10	0.00296
1	2743.00	0.00242
	3166.30	0.00198
	4012.90	0.00121
	4961.10	0.00074
2	5486.00	0.00081
	5909.30	0.00086
	6755.90	0.00076
	7704.10	0.00059
3	8229.00	0.00062
	8652.30	0.00065
	9498.90	0.00060
	10447.10	0.00046
4	10972.00	0.00047
	11395.30	0.00049
	12241.90	0.00045
	13190.10	0.00035
5	13715.00	0.00036
	14138.30	0.00037
	14984.90	0.00035
	15933.10	0.00028
6	16458.00	0.00029
	16881.30	0.00031
	17727.90	0.00029
	18676.10	0.00023
7	19201.00	0.00024
	19624.30	0.00025
	20470.90	0.00024
	21419.10	0.00019
8	21944.00	0.00020
	22367.30	0.00021
	23213.90	0.00019
	24162.10	0.00015
9	24687.00	0.00016
	25110.30	0.00017
	25956.90	0.00016
	26905.10	0.00013
10	27430.00	0.00011

Table C.39 Displacement components at the first storey of Wall 2 combined with Wall 1 for a drift of 2%

Storey	1			
Height (m)	2.74			
Height (m)	Curvature (rad/m)	Δx (m)	x (m)	Flexural displ (mm)
0.42	0.00456		2.32	
1.27	0.00388	0.85	1.47	6.77
2.22	0.00296	0.95	0.52	3.24
2.74	0.00242	0.52	0.00	0.37
			Total	10.38
		Total displacement (mm)		18.61
		Shear displacement (mm)		8.23

Table C.40 Displacement components at the second storey of Wall 2 combined with Wall 1 for a drift of 2%

Storey	2			
Height (m)	5.49			
Height (m)	Curvature (rad/m)	Δx (m)	x (m)	Flexural displ (mm)
0.42	0.00456		5.06	
1.27	0.00388	0.85	4.22	16.56
2.22	0.00296	0.95	3.27	12.13
2.74	0.00242	0.52	2.74	4.24
3.17	0.00198	0.42	2.32	2.36
4.01	0.00121	0.85	1.47	2.56
4.96	0.00074	0.95	0.52	0.92
5.49	0.00081	0.52	0.00	0.11
			Total	38.88
		Total displacement (mm)		52.87
		Shear displacement (mm)		13.99

Table C.41 Displacement components at the third storey of Wall 2 combined with Wall 1 for a drift of 2%

Storey	3			
Height (m)	8.23			
Height (m)	Curvature (rad/m)	Δx (m)	x (m)	Flexural displ (mm)
0.42	0.00456		7.81	
1.27	0.00388	0.85	6.96	26.35
2.22	0.00296	0.95	6.01	21.03
2.74	0.00242	0.52	5.49	8.12
3.17	0.00198	0.42	5.06	4.91
4.01	0.00121	0.85	4.22	6.26
4.96	0.00074	0.95	3.27	3.46
5.49	0.00081	0.52	2.74	1.23
5.91	0.00086	0.42	2.32	0.90
6.76	0.00076	0.85	1.47	1.30
7.70	0.00059	0.95	0.52	0.64
8.23	0.00062	0.52	0.00	0.08
			Total	74.26
		Total displacement (mm)		94.37
		Shear displacement (mm)		20.11

Table C.42 Displacement components at the fourth storey of Wall 2 combined with Wall 1 for a drift of 2%

Storey	4			
Height (m)	10.97			
Height (m)	Curvature (rad/m)	Δx (m)	x (m)	Flexural displ (mm)
0.42	0.00456		10.55	
1.27	0.00388	0.85	9.70	36.14
2.22	0.00296	0.95	8.75	29.92
2.74	0.00242	0.52	8.23	11.99
3.17	0.00198	0.42	7.81	7.46
4.01	0.00121	0.85	6.96	9.95
4.96	0.00074	0.95	6.01	5.99
5.49	0.00081	0.52	5.49	2.34
5.91	0.00086	0.42	5.06	1.87
6.76	0.00076	0.85	4.22	3.19
7.70	0.00059	0.95	3.27	2.39
8.23	0.00062	0.52	2.74	0.95
8.65	0.00065	0.42	2.32	0.68
9.50	0.00060	0.85	1.47	1.00
10.45	0.00046	0.95	0.52	0.50
10.97	0.00047	0.52	0.00	0.06
			Total	114.45
		Total displacement (mm)		140.44
		Shear displacement (mm)		25.99

Table C.43 Slopes up to the mid-height of Wall 2 combined with Wall 1 for a drift of 2%

Height (m)	Curvature (rad/m)	Δx (m)	Slope incr. (rad)	Slope (rad)
0.42	0.00456			
1.27	0.00388	0.85	0.0036	0.0036
2.22	0.00296	0.95	0.0032	0.0068
3.17	0.00198	0.95	0.0023	0.0092
4.01	0.00121	0.85	0.0013	0.0105
4.96	0.00074	0.95	0.0009	0.0114
5.91	0.00086	0.95	0.0008	0.0122
6.76	0.00076	0.85	0.0007	0.0129
7.70	0.00059	0.95	0.0006	0.0135
8.65	0.00065	0.95	0.0006	0.0141
9.50	0.00060	0.85	0.0005	0.0146
10.45	0.00046	0.95	0.0005	0.0151
11.40	0.00049	0.95	0.0004	0.0156
12.24	0.00045	0.85	0.0004	0.0160
13.19	0.00035	0.95	0.0004	0.0164
14.14	0.00037	0.95	0.0003	0.0167
14.98	0.00035	0.85	0.0003	0.0170
15.93	0.00028	0.95	0.0003	0.0173
16.88	0.00031	0.95	0.0003	0.0176
17.73	0.00029	0.85	0.0003	0.0178
18.68	0.00023	0.95	0.0002	0.0181
19.62	0.00025	0.95	0.0002	0.0183
20.47	0.00024	0.85	0.0002	0.0185
21.42	0.00019	0.95	0.0002	0.0187
22.37	0.00021	0.95	0.0002	0.0189
23.21	0.00019	0.85	0.0002	0.0191
24.16	0.00015	0.95	0.0002	0.0192
25.11	0.00017	0.95	0.0002	0.0194
25.96	0.00016	0.85	0.0001	0.0195
26.91	0.00013	0.95	0.0001	0.0197

Table C.44 Bending moments along the height of Wall 2 combined with Wall 1 for a drift of 2%

Storey	Height (m)	Force (kN)	Shear (kN)	Moment incr. (kN.m)	Moment (kN.m)
0	0.00	0.0	693.4	293.5	26421.1
	0.42	0.0	693.4	587.0	26127.6
	1.27	0.0	693.4	657.5	25540.6
	2.22	0.0	693.4	364.0	24883.1
1	2.74	44.9	693.4	284.0	24519.1
	3.17	0.0	648.5	549.0	24235.1
	4.01	0.0	648.5	614.9	23686.1
	4.96	0.0	648.5	340.4	23071.2
2	5.49	-321.0	648.5	342.4	22730.8
	5.91	0.0	969.5	820.8	22388.4
	6.76	0.0	969.5	919.3	21567.6
	7.70	0.0	969.5	508.9	20648.3
3	8.23	90.4	969.5	391.3	20139.4
	8.65	0.0	879.1	744.2	19748.2
	9.50	0.0	879.1	833.6	19003.9
	10.45	0.0	879.1	461.4	18170.3
4	10.97	252.7	879.1	318.6	17708.9
	11.40	0.0	626.4	530.3	17390.3
	12.24	0.0	626.4	594.0	16860.0
	13.19	0.0	626.4	328.8	16266.0
5	13.72	166.0	626.4	230.0	15937.2
	14.14	0.0	460.4	389.8	15707.2
	14.98	0.0	460.4	436.6	15317.4
	15.93	0.0	460.4	241.7	14880.9
6	16.46	69.8	460.4	180.1	14639.2
	16.88	0.0	390.6	330.7	14459.1
	17.73	0.0	390.6	370.4	14128.4
	18.68	0.0	390.6	205.0	13758.0
7	19.20	14.2	390.6	162.3	13553.0
	19.62	0.0	376.4	318.7	13390.7
	20.47	0.0	376.4	356.9	13072.0
	21.42	0.0	376.4	197.6	12715.1
8	21.94	-30.5	376.4	165.8	12517.5
	22.37	0.0	406.9	344.5	12351.7
	23.21	0.0	406.9	385.8	12007.3
	24.16	0.0	406.9	213.6	11621.4
9	24.69	-67.4	406.9	186.5	11407.9
	25.11	0.0	474.3	401.5	11221.4
	25.96	0.0	474.3	449.7	10819.8
	26.91	0.0	474.3	249.0	10370.1
10	27.43	-112.5	474.3	1455.3	10121.1
11	30.17	42.1	586.8	1551.9	8665.8
12	32.92	89.7	544.7	1371.1	7114.0
13	35.66	89.4	455.0	1125.5	5742.9
14	38.40	52.8	365.6	930.4	4617.4
15	41.15	22.6	312.8	827.0	3687.0
16	43.89	11.9	290.2	779.7	2860.0
17	46.63	26.6	278.3	726.9	2080.3
18	49.37	48.3	251.7	624.2	1353.4
19	52.12	-124.9	203.4	729.2	729.2
20	54.86	328.3	328.3	0.0	0.0

Table C.45 Curvatures up to the mid-height of Wall 3 for a drift of 2%

Node		Node 1 y-displ (mm)	Node 2 y-displ (mm)	Node 2 y-coord (mm)	Difference (mm)	Height (mm)	Strain	Curvature (rad/m)
First	Second							
1	15	0.00	1.21	846.60	846.60	423.30	0.0014	0.00148
15	29	1.21	2.39	1693.20	846.60	1269.90	0.0014	0.00143
29	50	2.39	3.76	2743.00	1049.80	2218.10	0.0013	0.00137
50	64	3.76	4.80	3589.60	846.60	3166.30	0.0012	0.00130
64	78	4.80	5.76	4436.20	846.60	4012.90	0.0011	0.00124
78	99	5.76	6.86	5486.00	1049.80	4961.10	0.0011	0.00118
99	113	6.86	7.69	6332.60	846.60	5909.30	0.0010	0.00112
113	127	7.69	8.45	7179.20	846.60	6755.90	0.0009	0.00107
127	148	8.45	9.35	8229.00	1049.80	7704.10	0.0009	0.00103
148	162	9.35	10.03	9075.60	846.60	8652.30	0.0008	0.00098
162	176	10.03	10.66	9922.20	846.60	9498.90	0.0008	0.00095
176	197	10.66	11.41	10972.00	1049.80	10447.10	0.0007	0.00092
197	211	11.41	11.96	11818.60	846.60	11395.30	0.0006	0.00086
211	225	11.96	12.47	12665.20	846.60	12241.90	0.0006	0.00083
225	246	12.47	13.06	13715.00	1049.80	13190.10	0.0006	0.00079
246	260	13.06	13.47	14561.60	846.60	14138.30	0.0005	0.00074
260	274	13.47	13.84	15408.20	846.60	14984.90	0.0004	0.00070
274	295	13.84	14.25	16458.00	1049.80	15933.10	0.0004	0.00066
295	309	14.25	14.55	17304.60	846.60	16881.30	0.0003	0.00062
309	323	14.55	14.82	18151.20	846.60	17727.90	0.0003	0.00060
323	344	14.82	15.14	19201.00	1049.80	18676.10	0.0003	0.00059
344	358	15.14	15.37	20047.60	846.60	19624.30	0.0003	0.00055
358	372	15.37	15.58	20894.20	846.60	20470.90	0.0002	0.00053
372	393	15.58	15.83	21944.00	1049.80	21419.10	0.0002	0.00052
393	407	15.83	15.98	22790.60	846.60	22367.30	0.0002	0.00047
407	421	15.98	16.11	23637.20	846.60	23213.90	0.0002	0.00046
421	442	16.11	16.26	24687.00	1049.80	24162.10	0.0001	0.00044
442	456	16.26	16.37	25533.60	846.60	25110.30	0.0001	0.00042
456	470	16.37	16.46	26380.20	846.60	25956.90	0.0001	0.00041
470	491	16.46	16.56	27430.00	1049.80	26905.10	0.0001	0.00039
7	21	0.00	-1.18	846.60	846.60	423.30	-0.0014	0.00148
21	35	-1.18	-2.30	1693.20	846.60	1269.90	-0.0013	0.00143
35	56	-2.30	-3.67	2743.00	1049.80	2218.10	-0.0013	0.00137
56	70	-3.67	-4.73	3589.60	846.60	3166.30	-0.0013	0.00130
70	84	-4.73	-5.77	4436.20	846.60	4012.90	-0.0012	0.00124
84	105	-5.77	-7.03	5486.00	1049.80	4961.10	-0.0012	0.00118
105	119	-7.03	-8.01	6332.60	846.60	5909.30	-0.0012	0.00112
119	133	-8.01	-8.96	7179.20	846.60	6755.90	-0.0011	0.00107
133	154	-8.96	-10.13	8229.00	1049.80	7704.10	-0.0011	0.00103
154	168	-10.13	-11.03	9075.60	846.60	8652.30	-0.0011	0.00098
168	182	-11.03	-11.93	9922.20	846.60	9498.90	-0.0011	0.00095
182	203	-11.93	-13.01	10972.00	1049.80	10447.10	-0.0010	0.00092
203	217	-13.01	-13.86	11818.60	846.60	11395.30	-0.0010	0.00086
217	231	-13.86	-14.68	12665.20	846.60	12241.90	-0.0010	0.00083
231	252	-14.68	-15.68	13715.00	1049.80	13190.10	-0.0010	0.00079
252	266	-15.68	-16.46	14561.60	846.60	14138.30	-0.0009	0.00074
266	280	-16.46	-17.21	15408.20	846.60	14984.90	-0.0009	0.00070
280	301	-17.21	-18.12	16458.00	1049.80	15933.10	-0.0009	0.00066

Node		Node 1 y-displ (mm)	Node 2 y-displ (mm)	Node 2 y-coord (mm)	Difference (mm)	Height (mm)	Strain	Curvature (rad/m)
First	Second							
301	315	-18.12	-18.83	17304.60	846.60	16881.30	-0.0008	0.00062
315	329	-18.83	-19.53	18151.20	846.60	17727.90	-0.0008	0.00060
329	350	-19.53	-20.37	19201.00	1049.80	18676.10	-0.0008	0.00059
350	364	-20.37	-21.04	20047.60	846.60	19624.30	-0.0008	0.00055
364	378	-21.04	-21.69	20894.20	846.60	20470.90	-0.0008	0.00053
378	399	-21.69	-22.47	21944.00	1049.80	21419.10	-0.0008	0.00052
399	413	-22.47	-23.09	22790.60	846.60	22367.30	-0.0007	0.00047
413	427	-23.09	-23.69	23637.20	846.60	23213.90	-0.0007	0.00046
427	448	-23.69	-24.42	24687.00	1049.80	24162.10	-0.0007	0.00044
448	462	-24.42	-24.99	25533.60	846.60	25110.30	-0.0007	0.00042
462	476	-24.99	-25.55	26380.20	846.60	25956.90	-0.0007	0.00041
476	497	-25.55	-26.24	27430.00	1049.80	26905.10	-0.0007	0.00039

Wall length: 1905 mm

Table C.46 Interpolation of curvatures at storey heights of Wall 3 for a drift of 2%

Storey	Height (mm)	Curvature (rad/m)
	423.30	0.00148
	1269.90	0.00143
	2218.10	0.00137
1	2743.00	0.00133
	3166.30	0.00130
	4012.90	0.00124
	4961.10	0.00118
2	5486.00	0.00115
	5909.30	0.00112
	6755.90	0.00107
	7704.10	0.00103
3	8229.00	0.00100
	8652.30	0.00098
	9498.90	0.00095
	10447.10	0.00092
4	10972.00	0.00089
	11395.30	0.00086
	12241.90	0.00083
	13190.10	0.00079
5	13715.00	0.00076
	14138.30	0.00074
	14984.90	0.00070
	15933.10	0.00066
6	16458.00	0.00064
	16881.30	0.00062
	17727.90	0.00060
	18676.10	0.00059
7	19201.00	0.00057
	19624.30	0.00055
	20470.90	0.00053
	21419.10	0.00052
8	21944.00	0.00049
	22367.30	0.00047
	23213.90	0.00046
	24162.10	0.00044
9	24687.00	0.00043
	25110.30	0.00042
	25956.90	0.00041
	26905.10	0.00039
10	27430.00	0.00039

Table C.47 Bending moments along the height of Wall 3 for a drift of 2%

Storey	Height (m)	Force (kN)	Shear (kN)	Moment incr. (kN.m)	Moment (kN.m)
0	0.00	0.0	135.4	57.3	7428.0
	0.42	0.0	135.4	114.6	7370.7
	1.27	0.0	135.4	128.4	7256.1
	2.22	0.0	135.4	71.1	7127.7
1	2.74	0.0	135.4	57.3	7056.6
	3.17	0.0	135.4	114.6	6999.3
	4.01	0.0	135.4	128.4	6884.7
	4.96	0.0	135.4	71.1	6756.3
2	5.49	0.0	135.4	57.3	6685.2
	5.91	0.0	135.4	114.6	6627.9
	6.76	0.0	135.4	128.4	6513.3
	7.70	0.0	135.4	71.1	6384.9
3	8.23	0.0	135.4	57.3	6313.8
	8.65	0.0	135.4	114.6	6256.5
	9.50	0.0	135.4	128.4	6141.9
	10.45	0.0	135.4	71.1	6013.5
4	10.97	0.0	135.4	57.3	5942.4
	11.40	0.0	135.4	114.6	5885.1
	12.24	0.0	135.4	128.4	5770.5
	13.19	0.0	135.4	71.1	5642.1
5	13.72	0.0	135.4	57.3	5571.0
	14.14	0.0	135.4	114.6	5513.7
	14.98	0.0	135.4	128.4	5399.1
	15.93	0.0	135.4	71.1	5270.7
6	16.46	0.0	135.4	57.3	5199.6
	16.88	0.0	135.4	114.6	5142.3
	17.73	0.0	135.4	128.4	5027.7
	18.68	0.0	135.4	71.1	4899.3
7	19.20	0.0	135.4	57.3	4828.2
	19.62	0.0	135.4	114.6	4770.9
	20.47	0.0	135.4	128.4	4656.3
	21.42	0.0	135.4	71.1	4527.9
8	21.94	0.0	135.4	57.3	4456.8
	22.37	0.0	135.4	114.6	4399.5
	23.21	0.0	135.4	128.4	4284.9
	24.16	0.0	135.4	71.1	4156.5
9	24.69	0.0	135.4	57.3	4085.4
	25.11	0.0	135.4	114.6	4028.1
	25.96	0.0	135.4	128.4	3913.5
	26.91	0.0	135.4	71.1	3785.1
10	27.43	0.0	135.4	371.4	3714.0
11	30.17	0.0	135.4	371.4	3342.6
12	32.92	0.0	135.4	371.4	2971.2
13	35.66	0.0	135.4	371.4	2599.8
14	38.40	0.0	135.4	371.4	2228.4
15	41.15	0.0	135.4	371.4	1857.0
16	43.89	0.0	135.4	371.4	1485.6
17	46.63	0.0	135.4	371.4	1114.2
18	49.37	0.0	135.4	371.4	742.8
19	52.12	0.0	135.4	371.4	371.4
20	54.86	135.4	135.4	0.0	0.0

Table C.48 Curvatures up to the mid-height of Wall 1 combined with Wall 3 for a drift of 2%

Node		Node 1 y-displ (mm)	Node 2 y-displ (mm)	Node 2 y-coord (mm)	Difference (mm)	Height (mm)	Strain	Curvature (rad/m)
First	Second							
1	67	0.00	15.02	846.60	846.60	423.30	0.0177	0.00310
67	133	15.02	29.99	1693.20	846.60	1269.90	0.0177	0.00307
133	232	29.99	47.07	2743.00	1049.80	2218.10	0.0163	0.00251
232	298	47.07	60.20	3589.60	846.60	3166.30	0.0155	0.00238
298	364	60.20	71.74	4436.20	846.60	4012.90	0.0136	0.00209
364	463	71.74	82.30	5486.00	1049.80	4961.10	0.0101	0.00155
463	529	82.30	89.14	6332.60	846.60	5909.30	0.0081	0.00130
529	595	89.14	95.15	7179.20	846.60	6755.90	0.0071	0.00114
595	694	95.15	99.06	8229.00	1049.80	7704.10	0.0037	0.00066
694	760	99.06	101.27	9075.60	846.60	8652.30	0.0026	0.00053
760	826	101.27	103.17	9922.20	846.60	9498.90	0.0022	0.00046
826	925	103.17	104.79	10972.00	1049.80	10447.10	0.0015	0.00034
925	991	104.79	106.54	11818.60	846.60	11395.30	0.0021	0.00042
991	1057	106.54	108.08	12665.20	846.60	12241.90	0.0018	0.00038
1057	1156	108.08	109.54	13715.00	1049.80	13190.10	0.0014	0.00030
1156	1222	109.54	111.02	14561.60	846.60	14138.30	0.0017	0.00036
1222	1288	111.02	112.43	15408.20	846.60	14984.90	0.0017	0.00035
1288	1387	112.43	113.74	16458.00	1049.80	15933.10	0.0013	0.00027
1387	1453	113.74	115.03	17304.60	846.60	16881.30	0.0015	0.00032
1453	1519	115.03	116.24	18151.20	846.60	17727.90	0.0014	0.00030
1519	1618	116.24	117.35	19201.00	1049.80	18676.10	0.0011	0.00024
1618	1684	117.35	118.43	20047.60	846.60	19624.30	0.0013	0.00028
1684	1750	118.43	119.42	20894.20	846.60	20470.90	0.0012	0.00026
1750	1849	119.42	120.33	21944.00	1049.80	21419.10	0.0009	0.00020
1849	1915	120.33	121.19	22790.60	846.60	22367.30	0.0010	0.00023
1915	1981	121.19	121.97	23637.20	846.60	23213.90	0.0009	0.00021
1981	2080	121.97	122.68	24687.00	1049.80	24162.10	0.0007	0.00017
2080	2146	122.68	123.34	25533.60	846.60	25110.30	0.0008	0.00019
2146	2212	123.34	123.92	26380.20	846.60	25956.90	0.0007	0.00017
2212	2311	123.92	124.44	27430.00	1049.80	26905.10	0.0005	0.00013
26	92	0.00	-4.98	846.60	846.60	423.30	-0.0059	0.00310
92	158	-4.98	-9.82	1693.20	846.60	1269.90	-0.0057	0.00307
158	257	-9.82	-12.86	2743.00	1049.80	2218.10	-0.0029	0.00251
257	323	-12.86	-15.11	3589.60	846.60	3166.30	-0.0027	0.00238
323	389	-15.11	-17.04	4436.20	846.60	4012.90	-0.0023	0.00209
389	488	-17.04	-18.86	5486.00	1049.80	4961.10	-0.0017	0.00155
488	554	-18.86	-20.40	6332.60	846.60	5909.30	-0.0018	0.00130
554	620	-20.40	-21.77	7179.20	846.60	6755.90	-0.0016	0.00114
620	719	-21.77	-23.13	8229.00	1049.80	7704.10	-0.0013	0.00066
719	785	-23.13	-24.30	9075.60	846.60	8652.30	-0.0014	0.00053
785	851	-24.30	-25.37	9922.20	846.60	9498.90	-0.0013	0.00046
851	950	-25.37	-26.47	10972.00	1049.80	10447.10	-0.0010	0.00034
950	1016	-26.47	-27.46	11818.60	846.60	11395.30	-0.0012	0.00042
1016	1082	-27.46	-28.37	12665.20	846.60	12241.90	-0.0011	0.00038
1082	1181	-28.37	-29.34	13715.00	1049.80	13190.10	-0.0009	0.00030
1181	1247	-29.34	-30.21	14561.60	846.60	14138.30	-0.0010	0.00036
1247	1313	-30.21	-31.03	15408.20	846.60	14984.90	-0.0010	0.00035
1313	1412	-31.03	-31.90	16458.00	1049.80	15933.10	-0.0008	0.00027

Node		Node 1 y-displ (mm)	Node 2 y-displ (mm)	Node 2 y-coord (mm)	Difference (mm)	Height (mm)	Strain	Curvature (rad/m)
First	Second							
1412	1478	-31.90	-32.68	17304.60	846.60	16881.30	-0.0009	0.00032
1478	1544	-32.68	-33.43	18151.20	846.60	17727.90	-0.0009	0.00030
1544	1643	-33.43	-34.21	19201.00	1049.80	18676.10	-0.0007	0.00024
1643	1709	-34.21	-34.91	20047.60	846.60	19624.30	-0.0008	0.00028
1709	1775	-34.91	-35.58	20894.20	846.60	20470.90	-0.0008	0.00026
1775	1874	-35.58	-36.29	21944.00	1049.80	21419.10	-0.0007	0.00020
1874	1940	-36.29	-36.92	22790.60	846.60	22367.30	-0.0007	0.00023
1940	2006	-36.92	-37.52	23637.20	846.60	23213.90	-0.0007	0.00021
2006	2105	-37.52	-38.14	24687.00	1049.80	24162.10	-0.0006	0.00017
2105	2171	-38.14	-38.71	25533.60	846.60	25110.30	-0.0007	0.00019
2171	2237	-38.71	-39.24	26380.20	846.60	25956.90	-0.0006	0.00017
2237	2336	-39.24	-39.80	27430.00	1049.80	26905.10	-0.0005	0.00013

Wall length: 7620 mm

Table C.49 Curvatures up to the mid-height of Wall 3 combined with Wall 1 for a drift of 2%

Node		Node 1 y-displ (mm)	Node 2 y-displ (mm)	Node 2 y-coord (mm)	Difference (mm)	Height (mm)	Strain	Curvature (rad/m)
First	Second							
27	93	0.00	6.60	846.60	846.60	423.30	0.0078	0.00581
93	159	6.60	11.04	1693.20	846.60	1269.90	0.0052	0.00399
159	258	11.04	12.83	2743.00	1049.80	2218.10	0.0017	0.00169
258	324	12.83	14.30	3589.60	846.60	3166.30	0.0017	0.00170
324	390	14.30	15.56	4436.20	846.60	4012.90	0.0015	0.00149
390	489	15.56	16.65	5486.00	1049.80	4961.10	0.0010	0.00108
489	555	16.65	17.37	6332.60	846.60	5909.30	0.0009	0.00101
555	621	17.37	17.95	7179.20	846.60	6755.90	0.0007	0.00087
621	720	17.95	18.36	8229.00	1049.80	7704.10	0.0004	0.00060
720	786	18.36	18.62	9075.60	846.60	8652.30	0.0003	0.00059
786	852	18.62	18.82	9922.20	846.60	9498.90	0.0002	0.00052
852	951	18.82	18.96	10972.00	1049.80	10447.10	0.0001	0.00040
951	1017	18.96	19.07	11818.60	846.60	11395.30	0.0001	0.00042
1017	1083	19.07	19.15	12665.20	846.60	12241.90	0.0001	0.00039
1083	1182	19.15	19.22	13715.00	1049.80	13190.10	0.0001	0.00032
1182	1248	19.22	19.27	14561.60	846.60	14138.30	0.0001	0.00035
1248	1314	19.27	19.31	15408.20	846.60	14984.90	0.0000	0.00033
1314	1413	19.31	19.33	16458.00	1049.80	15933.10	0.0000	0.00027
1413	1479	19.33	19.33	17304.60	846.60	16881.30	0.0000	0.00029
1479	1545	19.33	19.32	18151.20	846.60	17727.90	0.0000	0.00028
1545	1644	19.32	19.30	19201.00	1049.80	18676.10	0.0000	0.00023
1644	1710	19.30	19.27	20047.60	846.60	19624.30	0.0000	0.00025
1710	1776	19.27	19.23	20894.20	846.60	20470.90	0.0000	0.00023
1776	1875	19.23	19.17	21944.00	1049.80	21419.10	-0.0001	0.00019
1875	1941	19.17	19.10	22790.60	846.60	22367.30	-0.0001	0.00021
1941	2007	19.10	19.03	23637.20	846.60	23213.90	-0.0001	0.00019
2007	2106	19.03	18.94	24687.00	1049.80	24162.10	-0.0001	0.00016
2106	2172	18.94	18.85	25533.60	846.60	25110.30	-0.0001	0.00017
2172	2238	18.85	18.75	26380.20	846.60	25956.90	-0.0001	0.00016
2238	2337	18.75	18.63	27430.00	1049.80	26905.10	-0.0001	0.00013
33	99	0.00	-2.77	846.60	846.60	423.30	-0.0033	0.00581
99	165	-2.77	-4.76	1693.20	846.60	1269.90	-0.0024	0.00399
165	264	-4.76	-6.36	2743.00	1049.80	2218.10	-0.0015	0.00169
264	330	-6.36	-7.64	3589.60	846.60	3166.30	-0.0015	0.00170
330	396	-7.64	-8.77	4436.20	846.60	4012.90	-0.0013	0.00149
396	495	-8.77	-9.85	5486.00	1049.80	4961.10	-0.0010	0.00108
495	561	-9.85	-10.76	6332.60	846.60	5909.30	-0.0011	0.00101
561	627	-10.76	-11.59	7179.20	846.60	6755.90	-0.0010	0.00087
627	726	-11.59	-12.39	8229.00	1049.80	7704.10	-0.0008	0.00060
726	792	-12.39	-13.08	9075.60	846.60	8652.30	-0.0008	0.00059
792	858	-13.08	-13.72	9922.20	846.60	9498.90	-0.0008	0.00052
858	957	-13.72	-14.36	10972.00	1049.80	10447.10	-0.0006	0.00040
957	1023	-14.36	-14.93	11818.60	846.60	11395.30	-0.0007	0.00042
1023	1089	-14.93	-15.48	12665.20	846.60	12241.90	-0.0006	0.00039
1089	1188	-15.48	-16.05	13715.00	1049.80	13190.10	-0.0005	0.00032
1188	1254	-16.05	-16.56	14561.60	846.60	14138.30	-0.0006	0.00035
1254	1320	-16.56	-17.06	15408.20	846.60	14984.90	-0.0006	0.00033
1320	1419	-17.06	-17.57	16458.00	1049.80	15933.10	-0.0005	0.00027

Node		Node 1 y-displ (mm)	Node 2 y-displ (mm)	Node 2 y-coord (mm)	Difference (mm)	Height (mm)	Strain	Curvature (rad/m)
First	Second							
1419	1485	-17.57	-18.04	17304.60	846.60	16881.30	-0.0006	0.00029
1485	1551	-18.04	-18.50	18151.20	846.60	17727.90	-0.0005	0.00028
1551	1650	-18.50	-18.98	19201.00	1049.80	18676.10	-0.0005	0.00023
1650	1716	-18.98	-19.41	20047.60	846.60	19624.30	-0.0005	0.00025
1716	1782	-19.41	-19.83	20894.20	846.60	20470.90	-0.0005	0.00023
1782	1881	-19.83	-20.27	21944.00	1049.80	21419.10	-0.0004	0.00019
1881	1947	-20.27	-20.67	22790.60	846.60	22367.30	-0.0005	0.00021
1947	2013	-20.67	-21.05	23637.20	846.60	23213.90	-0.0005	0.00019
2013	2112	-21.05	-21.46	24687.00	1049.80	24162.10	-0.0004	0.00016
2112	2178	-21.46	-21.83	25533.60	846.60	25110.30	-0.0004	0.00017
2178	2244	-21.83	-22.19	26380.20	846.60	25956.90	-0.0004	0.00016
2244	2343	-22.19	-22.57	27430.00	1049.80	26905.10	-0.0004	0.00013

Wall length: 1905 mm

Table C.50 Interpolation of curvatures at storey heights of Wall 3 combined with Wall 1 for a drift of 2%

Storey	Height (mm)	Curvature (rad/m)
	423.30	0.00581
	1269.90	0.00399
	2218.10	0.00169
1	2743.00	0.00170
	3166.30	0.00170
	4012.90	0.00149
	4961.10	0.00108
2	5486.00	0.00104
	5909.30	0.00101
	6755.90	0.00087
	7704.10	0.00060
3	8229.00	0.00059
	8652.30	0.00059
	9498.90	0.00052
	10447.10	0.00040
4	10972.00	0.00041
	11395.30	0.00042
	12241.90	0.00039
	13190.10	0.00032
5	13715.00	0.00034
	14138.30	0.00035
	14984.90	0.00033
	15933.10	0.00027
6	16458.00	0.00028
	16881.30	0.00029
	17727.90	0.00028
	18676.10	0.00023
7	19201.00	0.00024
	19624.30	0.00025
	20470.90	0.00023
	21419.10	0.00019
8	21944.00	0.00020
	22367.30	0.00021
	23213.90	0.00019
	24162.10	0.00016
9	24687.00	0.00017
	25110.30	0.00017
	25956.90	0.00016
	26905.10	0.00013
10	27430.00	0.00011

Table C.51 Bending moments along the height of Wall 3 combined with Wall 1 for a drift of 2%

Storey	Height (m)	Force (kN)	Shear (kN)	Moment incr. (kN.m)	Moment (kN.m)
0	0.00	0.0	632.3	267.7	9621.2
	0.42	0.0	632.3	535.3	9353.6
	1.27	0.0	632.3	599.5	8818.2
	2.22	0.0	632.3	331.9	8218.7
1	2.74	70.3	632.3	252.8	7886.8
	3.17	0.0	562.0	475.8	7634.0
	4.01	0.0	562.0	532.9	7158.2
	4.96	0.0	562.0	295.0	6625.4
2	5.49	58.8	562.0	225.4	6330.4
	5.91	0.0	503.2	426.0	6104.9
	6.76	0.0	503.2	477.1	5678.9
	7.70	0.0	503.2	264.1	5201.8
3	8.23	155.3	503.2	180.1	4937.6
	8.65	0.0	347.9	294.5	4757.5
	9.50	0.0	347.9	329.9	4463.0
	10.45	0.0	347.9	182.6	4133.1
4	10.97	114.7	347.9	123.0	3950.5
	11.40	0.0	233.2	197.4	3827.5
	12.24	0.0	233.2	221.1	3630.1
	13.19	0.0	233.2	122.4	3408.9
5	13.72	62.5	233.2	85.5	3286.5
	14.14	0.0	170.7	144.5	3201.1
	14.98	0.0	170.7	161.9	3056.5
	15.93	0.0	170.7	89.6	2894.7
6	16.46	19.8	170.7	68.1	2805.1
	16.88	0.0	150.9	127.8	2737.0
	17.73	0.0	150.9	143.1	2609.3
	18.68	0.0	150.9	79.2	2466.2
7	19.20	9.7	150.9	61.8	2387.0
	19.62	0.0	141.2	119.5	2325.1
	20.47	0.0	141.2	133.9	2205.6
	21.42	0.0	141.2	74.1	2071.7
8	21.94	15.1	141.2	56.6	1997.6
	22.37	0.0	126.1	106.8	1941.0
	23.21	0.0	126.1	119.6	1834.3
	24.16	0.0	126.1	66.2	1714.7
9	24.69	24.5	126.1	48.2	1648.5
	25.11	0.0	101.6	86.0	1600.3
	25.96	0.0	101.6	96.3	1514.3
	26.91	0.0	101.6	53.3	1418.0
10	27.43	-30.9	101.6	321.1	1364.6
11	30.17	51.3	132.5	293.1	1043.6
12	32.92	27.9	81.2	184.5	750.5
13	35.66	13.9	53.3	127.1	566.0
14	38.40	4.9	39.4	101.4	438.9
15	41.15	2.5	34.5	91.2	337.5
16	43.89	-3.0	32.0	91.9	246.3
17	46.63	12.8	35.0	78.4	154.4
18	49.37	55.0	22.2	-14.5	76.0
19	52.12	-131.6	-32.8	90.5	90.5
20	54.86	98.8	98.8	0.0	0.0

Table C.52 Curvatures up to the mid-height of Column 1 for a drift of 2%

Node		Node 1 y-displ (mm)	Node 2 y-displ (mm)	Node 2 y-coord (mm)	Difference (mm)	Height (mm)	Strain	Curvature (rad/m)
First	Second							
1	9	0.00	0.01	846.60	846.60	423.30	0.0000	0.00113
9	17	0.01	0.00	1693.20	846.60	1269.90	0.0000	0.00109
17	29	0.00	0.00	2743.00	1049.80	2218.10	0.0000	0.00109
29	37	0.00	-0.02	3589.60	846.60	3166.30	0.0000	0.00105
37	45	-0.02	-0.05	4436.20	846.60	4012.90	0.0000	0.00104
45	57	-0.05	-0.08	5486.00	1049.80	4961.10	0.0000	0.00103
57	65	-0.08	-0.13	6332.60	846.60	5909.30	0.0000	0.00099
65	73	-0.13	-0.17	7179.20	846.60	6755.90	-0.0001	0.00098
73	85	-0.17	-0.24	8229.00	1049.80	7704.10	-0.0001	0.00097
85	93	-0.24	-0.30	9075.60	846.60	8652.30	-0.0001	0.00094
93	101	-0.30	-0.37	9922.20	846.60	9498.90	-0.0001	0.00092
101	113	-0.37	-0.46	10972.00	1049.80	10447.10	-0.0001	0.00092
113	121	-0.46	-0.54	11818.60	846.60	11395.30	-0.0001	0.00088
121	129	-0.54	-0.63	12665.20	846.60	12241.90	-0.0001	0.00087
129	141	-0.63	-0.75	13715.00	1049.80	13190.10	-0.0001	0.00086
141	149	-0.75	-0.86	14561.60	846.60	14138.30	-0.0001	0.00082
149	157	-0.86	-0.97	15408.20	846.60	14984.90	-0.0001	0.00081
157	169	-0.97	-1.11	16458.00	1049.80	15933.10	-0.0001	0.00080
169	177	-1.11	-1.24	17304.60	846.60	16881.30	-0.0002	0.00077
177	185	-1.24	-1.38	18151.20	846.60	17727.90	-0.0002	0.00075
185	197	-1.38	-1.55	19201.00	1049.80	18676.10	-0.0002	0.00074
197	205	-1.55	-1.70	20047.60	846.60	19624.30	-0.0002	0.00071
205	213	-1.70	-1.86	20894.20	846.60	20470.90	-0.0002	0.00069
213	225	-1.86	-2.06	21944.00	1049.80	21419.10	-0.0002	0.00069
225	233	-2.06	-2.23	22790.60	846.60	22367.30	-0.0002	0.00066
233	241	-2.23	-2.41	23637.20	846.60	23213.90	-0.0002	0.00064
241	253	-2.41	-2.64	24687.00	1049.80	24162.10	-0.0002	0.00063
253	261	-2.64	-2.83	25533.60	846.60	25110.30	-0.0002	0.00060
261	269	-2.83	-3.03	26380.20	846.60	25956.90	-0.0002	0.00059
269	281	-3.03	-3.28	27430.00	1049.80	26905.10	-0.0002	0.00058
4	12	0.00	-0.90	846.60	846.60	423.30	-0.0011	0.00113
12	20	-0.90	-1.79	1693.20	846.60	1269.90	-0.0010	0.00109
20	32	-1.79	-2.89	2743.00	1049.80	2218.10	-0.0010	0.00109
32	40	-2.89	-3.76	3589.60	846.60	3166.30	-0.0010	0.00105
40	48	-3.76	-4.62	4436.20	846.60	4012.90	-0.0010	0.00104
48	60	-4.62	-5.69	5486.00	1049.80	4961.10	-0.0010	0.00103
60	68	-5.69	-6.53	6332.60	846.60	5909.30	-0.0010	0.00099
68	76	-6.53	-7.37	7179.20	846.60	6755.90	-0.0010	0.00098
76	88	-7.37	-8.40	8229.00	1049.80	7704.10	-0.0010	0.00097
88	96	-8.40	-9.22	9075.60	846.60	8652.30	-0.0010	0.00094
96	104	-9.22	-10.04	9922.20	846.60	9498.90	-0.0010	0.00092
104	116	-10.04	-11.04	10972.00	1049.80	10447.10	-0.0010	0.00092
116	124	-11.04	-11.84	11818.60	846.60	11395.30	-0.0009	0.00088
124	132	-11.84	-12.63	12665.20	846.60	12241.90	-0.0009	0.00087
132	144	-12.63	-13.60	13715.00	1049.80	13190.10	-0.0009	0.00086
144	152	-13.60	-14.37	14561.60	846.60	14138.30	-0.0009	0.00082
152	160	-14.37	-15.14	15408.20	846.60	14984.90	-0.0009	0.00081
160	172	-15.14	-16.08	16458.00	1049.80	15933.10	-0.0009	0.00080

Node		Node 1 y-displ (mm)	Node 2 y-displ (mm)	Node 2 y-coord (mm)	Difference (mm)	Height (mm)	Strain	Curvature (rad/m)
First	Second							
172	180	-16.08	-16.83	17304.60	846.60	16881.30	-0.0009	0.00077
180	188	-16.83	-17.57	18151.20	846.60	17727.90	-0.0009	0.00075
188	200	-17.57	-18.48	19201.00	1049.80	18676.10	-0.0009	0.00074
200	208	-18.48	-19.21	20047.60	846.60	19624.30	-0.0009	0.00071
208	216	-19.21	-19.92	20894.20	846.60	20470.90	-0.0008	0.00069
216	228	-19.92	-20.81	21944.00	1049.80	21419.10	-0.0008	0.00069
228	236	-20.81	-21.51	22790.60	846.60	22367.30	-0.0008	0.00066
236	244	-21.51	-22.20	23637.20	846.60	23213.90	-0.0008	0.00064
244	256	-22.20	-23.06	24687.00	1049.80	24162.10	-0.0008	0.00063
256	264	-23.06	-23.74	25533.60	846.60	25110.30	-0.0008	0.00060
264	272	-23.74	-24.41	26380.20	846.60	25956.90	-0.0008	0.00059
272	284	-24.41	-25.24	27430.00	1049.80	26905.10	-0.0008	0.00058

Col. length: 952.5 mm

Table C.53 Curvatures up to the mid-height of Wall 1 combined with Column 1 for a drift of 2%

Node		Node 1 y-displ (mm)	Node 2 y-displ (mm)	Node 2 y-coord (mm)	Difference (mm)	Height (mm)	Strain	Curvature (rad/m)
First	Second							
1	61	0.00	15.45	846.60	846.60	423.30	0.0182	0.00316
61	121	15.45	30.84	1693.20	846.60	1269.90	0.0182	0.00315
121	211	30.84	47.94	2743.00	1049.80	2218.10	0.0163	0.00253
211	271	47.94	60.94	3589.60	846.60	3166.30	0.0154	0.00237
271	331	60.94	72.75	4436.20	846.60	4012.90	0.0140	0.00213
331	421	72.75	83.68	5486.00	1049.80	4961.10	0.0104	0.00160
421	481	83.68	91.00	6332.60	846.60	5909.30	0.0086	0.00137
481	541	91.00	97.35	7179.20	846.60	6755.90	0.0075	0.00120
541	631	97.35	100.38	8229.00	1049.80	7704.10	0.0029	0.00055
631	691	100.38	102.43	9075.60	846.60	8652.30	0.0024	0.00050
691	751	102.43	104.19	9922.20	846.60	9498.90	0.0021	0.00044
751	841	104.19	105.72	10972.00	1049.80	10447.10	0.0015	0.00033
841	901	105.72	107.38	11818.60	846.60	11395.30	0.0020	0.00041
901	961	107.38	108.89	12665.20	846.60	12241.90	0.0018	0.00037
961	1051	108.89	110.33	13715.00	1049.80	13190.10	0.0014	0.00030
1051	1111	110.33	111.76	14561.60	846.60	14138.30	0.0017	0.00035
1111	1171	111.76	113.12	15408.20	846.60	14984.90	0.0016	0.00033
1171	1261	113.12	114.38	16458.00	1049.80	15933.10	0.0012	0.00026
1261	1321	114.38	115.62	17304.60	846.60	16881.30	0.0015	0.00031
1321	1381	115.62	116.77	18151.20	846.60	17727.90	0.0014	0.00029
1381	1471	116.77	117.82	19201.00	1049.80	18676.10	0.0010	0.00023
1471	1531	117.82	118.84	20047.60	846.60	19624.30	0.0012	0.00026
1531	1591	118.84	119.78	20894.20	846.60	20470.90	0.0011	0.00025
1591	1681	119.78	120.63	21944.00	1049.80	21419.10	0.0008	0.00019
1681	1741	120.63	121.44	22790.60	846.60	22367.30	0.0010	0.00022
1741	1801	121.44	122.16	23637.20	846.60	23213.90	0.0009	0.00020
1801	1891	122.16	122.82	24687.00	1049.80	24162.10	0.0006	0.00016
1891	1951	122.82	123.41	25533.60	846.60	25110.30	0.0007	0.00018
1951	2011	123.41	123.95	26380.20	846.60	25956.90	0.0006	0.00016
2011	2101	123.95	124.42	27430.00	1049.80	26905.10	0.0005	0.00013
26	86	0.00	-4.96	846.60	846.60	423.30	-0.0059	0.00316
86	146	-4.96	-9.92	1693.20	846.60	1269.90	-0.0059	0.00315
146	236	-9.92	-13.06	2743.00	1049.80	2218.10	-0.0030	0.00253
236	296	-13.06	-15.36	3589.60	846.60	3166.30	-0.0027	0.00237
296	356	-15.36	-17.29	4436.20	846.60	4012.90	-0.0023	0.00213
356	446	-17.29	-19.12	5486.00	1049.80	4961.10	-0.0017	0.00160
446	506	-19.12	-20.67	6332.60	846.60	5909.30	-0.0018	0.00137
506	566	-20.67	-22.02	7179.20	846.60	6755.90	-0.0016	0.00120
566	656	-22.02	-23.36	8229.00	1049.80	7704.10	-0.0013	0.00055
656	716	-23.36	-24.52	9075.60	846.60	8652.30	-0.0014	0.00050
716	776	-24.52	-25.57	9922.20	846.60	9498.90	-0.0012	0.00044
776	866	-25.57	-26.64	10972.00	1049.80	10447.10	-0.0010	0.00033
866	926	-26.64	-27.60	11818.60	846.60	11395.30	-0.0011	0.00041
926	986	-27.60	-28.50	12665.20	846.60	12241.90	-0.0011	0.00037
986	1076	-28.50	-29.45	13715.00	1049.80	13190.10	-0.0009	0.00030
1076	1136	-29.45	-30.30	14561.60	846.60	14138.30	-0.0010	0.00035
1136	1196	-30.30	-31.10	15408.20	846.60	14984.90	-0.0009	0.00033
1196	1286	-31.10	-31.95	16458.00	1049.80	15933.10	-0.0008	0.00026

Node		Node 1 y-displ (mm)	Node 2 y-displ (mm)	Node 2 y-coord (mm)	Difference (mm)	Height (mm)	Strain	Curvature (rad/m)
First	Second							
1286	1346	-31.95	-32.71	17304.60	846.60	16881.30	-0.0009	0.00031
1346	1406	-32.71	-33.43	18151.20	846.60	17727.90	-0.0009	0.00029
1406	1496	-33.43	-34.19	19201.00	1049.80	18676.10	-0.0007	0.00023
1496	1556	-34.19	-34.88	20047.60	846.60	19624.30	-0.0008	0.00026
1556	1616	-34.88	-35.53	20894.20	846.60	20470.90	-0.0008	0.00025
1616	1706	-35.53	-36.21	21944.00	1049.80	21419.10	-0.0006	0.00019
1706	1766	-36.21	-36.82	22790.60	846.60	22367.30	-0.0007	0.00022
1766	1826	-36.82	-37.40	23637.20	846.60	23213.90	-0.0007	0.00020
1826	1916	-37.40	-38.00	24687.00	1049.80	24162.10	-0.0006	0.00016
1916	1976	-38.00	-38.55	25533.60	846.60	25110.30	-0.0006	0.00018
1976	2036	-38.55	-39.06	26380.20	846.60	25956.90	-0.0006	0.00016
2036	2126	-39.06	-39.60	27430.00	1049.80	26905.10	-0.0005	0.00013

Wall length: 7620 mm

Table C.54 Curvatures up to the mid-height of Column 1 combined with Wall 1 for a drift of 2%

Node		Node 1 y-displ (mm)	Node 2 y-displ (mm)	Node 2 y-coord (mm)	Difference (mm)	Height (mm)	Strain	Curvature (rad/m)
First	Second							
27	87	0.00	1.91	846.60	846.60	423.30	0.0023	0.00550
87	147	1.91	3.31	1693.20	846.60	1269.90	0.0017	0.00404
147	237	3.31	4.16	2743.00	1049.80	2218.10	0.0008	0.00238
237	297	4.16	4.37	3589.60	846.60	3166.30	0.0002	0.00164
297	357	4.37	4.49	4436.20	846.60	4012.90	0.0001	0.00141
357	447	4.49	4.52	5486.00	1049.80	4961.10	0.0000	0.00102
447	507	4.52	4.47	6332.60	846.60	5909.30	-0.0001	0.00097
507	567	4.47	4.37	7179.20	846.60	6755.90	-0.0001	0.00083
567	657	4.37	4.19	8229.00	1049.80	7704.10	-0.0002	0.00059
657	717	4.19	3.98	9075.60	846.60	8652.30	-0.0002	0.00055
717	777	3.98	3.75	9922.20	846.60	9498.90	-0.0003	0.00050
777	867	3.75	3.48	10972.00	1049.80	10447.10	-0.0003	0.00039
867	927	3.48	3.21	11818.60	846.60	11395.30	-0.0003	0.00040
927	987	3.21	2.93	12665.20	846.60	12241.90	-0.0003	0.00038
987	1077	2.93	2.63	13715.00	1049.80	13190.10	-0.0003	0.00031
1077	1137	2.63	2.33	14561.60	846.60	14138.30	-0.0004	0.00033
1137	1197	2.33	2.03	15408.20	846.60	14984.90	-0.0004	0.00032
1197	1287	2.03	1.69	16458.00	1049.80	15933.10	-0.0003	0.00026
1287	1347	1.69	1.38	17304.60	846.60	16881.30	-0.0004	0.00028
1347	1407	1.38	1.05	18151.20	846.60	17727.90	-0.0004	0.00027
1407	1497	1.05	0.70	19201.00	1049.80	18676.10	-0.0003	0.00022
1497	1557	0.70	0.37	20047.60	846.60	19624.30	-0.0004	0.00023
1557	1617	0.37	0.03	20894.20	846.60	20470.90	-0.0004	0.00022
1617	1707	0.03	-0.34	21944.00	1049.80	21419.10	-0.0004	0.00018
1707	1767	-0.34	-0.69	22790.60	846.60	22367.30	-0.0004	0.00019
1767	1827	-0.69	-1.05	23637.20	846.60	23213.90	-0.0004	0.00018
1827	1917	-1.05	-1.44	24687.00	1049.80	24162.10	-0.0004	0.00015
1917	1977	-1.44	-1.80	25533.60	846.60	25110.30	-0.0004	0.00016
1977	2037	-1.80	-2.17	26380.20	846.60	25956.90	-0.0004	0.00016
2037	2127	-2.17	-2.56	27430.00	1049.80	26905.10	-0.0004	0.00014
30	90	0.00	-2.53	846.60	846.60	423.30	-0.0030	0.00550
90	150	-2.53	-4.38	1693.20	846.60	1269.90	-0.0022	0.00404
150	240	-4.38	-5.91	2743.00	1049.80	2218.10	-0.0015	0.00238
240	300	-5.91	-7.03	3589.60	846.60	3166.30	-0.0013	0.00164
300	360	-7.03	-8.04	4436.20	846.60	4012.90	-0.0012	0.00141
360	450	-8.04	-9.03	5486.00	1049.80	4961.10	-0.0009	0.00102
450	510	-9.03	-9.86	6332.60	846.60	5909.30	-0.0010	0.00097
510	570	-9.86	-10.63	7179.20	846.60	6755.90	-0.0009	0.00083
570	660	-10.63	-11.39	8229.00	1049.80	7704.10	-0.0007	0.00059
660	720	-11.39	-12.05	9075.60	846.60	8652.30	-0.0008	0.00055
720	780	-12.05	-12.68	9922.20	846.60	9498.90	-0.0007	0.00050
780	870	-12.68	-13.34	10972.00	1049.80	10447.10	-0.0006	0.00039
870	930	-13.34	-13.93	11818.60	846.60	11395.30	-0.0007	0.00040
930	990	-13.93	-14.51	12665.20	846.60	12241.90	-0.0007	0.00038
990	1080	-14.51	-15.13	13715.00	1049.80	13190.10	-0.0006	0.00031
1080	1140	-15.13	-15.69	14561.60	846.60	14138.30	-0.0007	0.00033
1140	1200	-15.69	-16.25	15408.20	846.60	14984.90	-0.0007	0.00032
1200	1290	-16.25	-16.84	16458.00	1049.80	15933.10	-0.0006	0.00026

Node		Node 1 y-displ (mm)	Node 2 y-displ (mm)	Node 2 y-coord (mm)	Difference (mm)	Height (mm)	Strain	Curvature (rad/m)
First	Second							
1290	1350	-16.84	-17.38	17304.60	846.60	16881.30	-0.0006	0.00028
1350	1410	-17.38	-17.92	18151.20	846.60	17727.90	-0.0006	0.00027
1410	1500	-17.92	-18.49	19201.00	1049.80	18676.10	-0.0005	0.00022
1500	1560	-18.49	-19.01	20047.60	846.60	19624.30	-0.0006	0.00023
1560	1620	-19.01	-19.53	20894.20	846.60	20470.90	-0.0006	0.00022
1620	1710	-19.53	-20.08	21944.00	1049.80	21419.10	-0.0005	0.00018
1710	1770	-20.08	-20.59	22790.60	846.60	22367.30	-0.0006	0.00019
1770	1830	-20.59	-21.09	23637.20	846.60	23213.90	-0.0006	0.00018
1830	1920	-21.09	-21.63	24687.00	1049.80	24162.10	-0.0005	0.00015
1920	1980	-21.63	-22.12	25533.60	846.60	25110.30	-0.0006	0.00016
1980	2040	-22.12	-22.61	26380.20	846.60	25956.90	-0.0006	0.00016
2040	2130	-22.61	-23.14	27430.00	1049.80	26905.10	-0.0005	0.00014

Col. length: 952.5 mm

UBC Civil Engineering Grad Students, 2004/2005

(Contains some students who graduated in 2003/04. Many students did not have their photo taken)

LEGEND: SPECIALIZATION GROUP ID

CM	Construction Management	**H**	Hydrotechnical Engineering
EF	Environmental Fluid Mechanics	**M**	Materials Engineering
EQ	Earthquake Engineering	**PC**	Pollution Control
G	Geotechnical Engineering	**S**	Structural Engineering
GE	Environmental Geotechnics	**T**	Transportation Engineering

Reem Hameed
Abdul-Hafidh
MEng CM

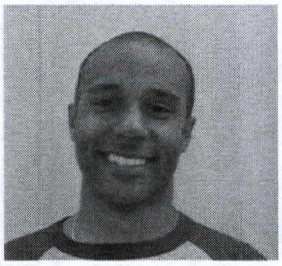

Yapo
Alle-Ando
MASc EF

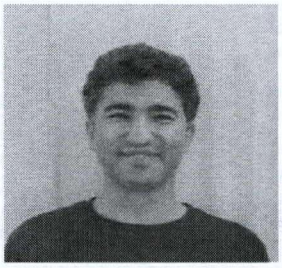

Ali
Amini Asalemi
PhD G

Parmeshwaree
Bahadoorsingh
PhD PC

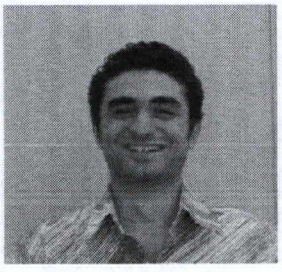

Armin
Bebamzadeh
MASc S

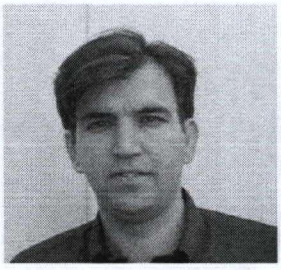

Alireza
Biparva
MASc M

Cynthia Evelyn
Bluteau
MASc EF

Alfredo Guillermo
Bohl
MASc S

Chrisopher
Borstad
MASc EF

Christian
Brumpton
MEng PC

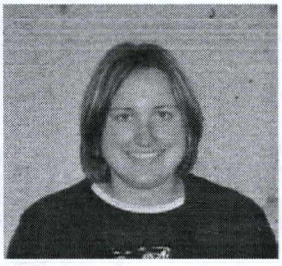

Kelly Lynn
Bush
MASc PC

Jessica Erin
Campbell
MASc G

100 to match his preferance
245 ~~#c~~ to match title page
OK per Danielle